UNIVERSITY OF CAPE TOWN
IYUNIVESITHI YASEKAPA • UNIVERSITEIT VAN KAAPSTAD

MSc (Eng) in Civil Engineering

The effect of cyclic wetting and drying on the corrosion rate of steel in reinforced concrete

By
Gavin Golden

Supervisor: Professor Mark Alexander

Co-supervisor: Associate Professor Hans Beushausen

A Dissertation submitted to the Faculty of Engineering and the Built Environment, University of Cape Town, in partial fulfilment of the requirements for the degree of Master of Science in Engineering

Submission Date: 23/01/2015

PLAGIARISM DECLARATION

1. I know that plagiarism is wrong. Plagiarism is to use another's work and to pretend that it is one's own.
2. I have used the Harvard Convention for citation and referencing. Each significant contribution to and quotation in this report from the work or works of other people has been attributed and has been cited and referenced.
3. This dissertation is my own work
4. I have not allowed and will not allow anyone to copy my work with the intension of passing it as his or her own work.

GLDGAV005 GOLDEN, G.C. Signed by candidate

SUBMISSION DATE: 23 January 2015

ABSTRACT

Preventing chloride-induced reinforcement corrosion in marine concrete structures remains a concern for structural engineers. Marine structures are typically exposed to high chloride concentrations through direct exposure to sea water, which provides the primary conditions required for reinforcement corrosion. The progress of corrosion can be controlled through anodic, cathodic or resistivity processes. However, high chloride concentrations tend to prevent anodic control from governing the corrosion rate, while direct exposure to moisture generally prevents resistivity control. Consequently, cathodic control remains an important process in the marine environment to restrict the progress of corrosion. The primary cathodic reaction in reinforcement corrosion is the reduction of oxygen, and as a result the availability of oxygen is a key factor when considering reinforcement corrosion in the marine tidal zone. The corrosion rate may be effectively reduced if the drying time of the concrete during tidal cycles is sufficiently short, thereby reducing the oxygen supply at the level of the embedded steel.

A laboratory-based testing programme was designed to investigate the influence of different cycles of wetting and drying on the corrosion of embedded reinforcing steel. A total of 72 prism specimens (100 x 100 x 240 mm) were cast from concretes with two different water-binder ratios (0.40 and 0.65) and three different binder types (100% PC, 50% PC/50% GGBS and 70% PC/30% FA). A 10 mm diameter high yield steel reinforcing bar was imbedded in each specimen at a cover of 20 mm. An impressed current was applied to each specimen to accelerate active corrosion conditions, after which the specimens were exposed to cyclic wetting and drying. The wetting period remained constant throughout at 2 days; while the drying time was varied at 1, 3, 5 and 7 days. The wetting period was applied by submerging the samples in a 5% NaCl solution, while accelerated drying conditions were applied by exposing the samples in an environmental room at 30 ± 1°C and 50 ± 5% RH. The prism specimens were monitored for half-cell potential, resistivity and corrosion rate at the end of each cycle of wetting. At the end of the monitoring phase (approximately 180 days), chloride concentrations were measured at the level of the steel in each specimen. Additionally, companion cubes were cast from each mix and tested for durability indices and compressive strength.

At first the impressed current technique was unsuccessful at accelerating corrosion and the specimens were monitored for five weeks in this condition. This phase highlighted the early-age effect of the sulphides and thiosulphates in slag-bearing concretes. Relatively high corrosion rates were measured in the GGBS specimens while the FA and PC specimens remained passive. The high early-age corrosion rates in slag-bearing concretes were attributed to low dissolved oxygen concentrations. The sulphides and thiosulphates have oxygen-reducing characteristics which lower the dissolved oxygen concentration and prevent the formation of a passive protective layer at an early age. This passive protective layer ordinarily prevents corrosion of the embedded reinforcing steel, but is only formed at a later stage in slag-bearing concretes. The GGBS specimens were expected to revert to a

passive state over time, however monitoring in this state ended before this was achieved. An additional impressed current was applied at the end of the five week period to accelerate corrosion.

The additional impressed current was successful and caused active corrosion in all of the specimens. However, the applied cycles of wetting and drying did not cause a noticeable effect on the corrosion rate at a w/b ratio of 0.40, irrespective of the binder type. Additionally, no significant difference was measured between the performance of the different binder types, at a w/b ratio of 0.40. The relatively high resistivity in the 0.40 FA and 0.40 GGBS mixes was considered to be the dominant effect in limiting the progress of corrosion; while the low corrosion rates in the 0.40 PC specimens was attributed to an inferred oxygen deprived condition where the drying time was sufficiently short to prevent drying to the level of the embedded steel.

An increase in the w/b ratio from 0.40 to 0.65 caused a significant increase in the corrosion rates. A mixed effects model for a continuous response was fitted to the data which identified the w/b ratio as the primary influencing factor on the corrosion rate. Additionally, at a w/b ratio of 0.65, the corrosion rate fluctuated more readily due to changes in the binder type and the applied drying time. At the higher w/b ratio, an increase in the drying time generally caused an increase in the corrosion rate, irrespective of the binder type. However, the effect of the drying time was more noticeable in the PC specimens which illustrated the controlling effect of the inferred oxygen availability in PC concrete. The varied drying durations appeared to have a secondary influence on the corrosion rate in the FA and GGBS specimens and were not able to prevent corrosion even under permanently submerged conditions.

The results of this experimental work suggest that the corrosion rate can be effectively controlled by limiting the w/b ratio alone, provided the cover is sufficiently high. The benefits of including FA and GGBS in the marine tidal zone were evident for a high w/b ratio. The SCMs did reduce the Chloride Conductivity Index values as well as the final measured chloride content, but this did not cause a noticeable change in the corrosion rate at a w/b ratio of 0.40. The benefit of including FA and GGBS was noted for a w/b ratio of 0.65, but the European Standard EN 206 (2013) stipulates a maximum w/b ratio of 0.45 for the marine tidal and splash zone. As a result, it is evident that the corrosion rate can be reduced or controlled if drying to the level of the steel can be prevented. This conclusion requires further verification through in-situ corrosion rate monitoring of specimens exposed directly to the marine tidal zone. The benefits of this knowledge can only be realised if adequate concrete drying models are established which will guide the selection of an appropriate cover depth and concrete quality.

ACKNOWLEDGEMENTS

I would like to express my sincere gratitude towards my supervisor Prof. Mark Alexander, as well as my co-supervisor A/Prof. Hans Beushausen. Without their support and guidance, this research project would not have come together. I must also express my gratitude to Dr. Mike Otieno for his assistance. Thanks must also be attributed to Nooredien Hassen, Charles Nicholas and all the laboratory staff for their assistance while completing my laboratory work.

I would like to thank the National Research Foundation (NRF) and CoMSIRU for funding this research project and to Sika and PPC for their donations of required materials. Lastly, I would like to thank my family and friends for their continued support during this project.

TABLE OF CONTENTS

LIST OF FIGURES

LIST OF TABLES

GLOSSARY

w/b	Water-binder ratio (cement and binder used interchangeably)
SCM	Supplementary cementitious material (also referred to as a cement extender)
PC	Portland cement
FA	Fly ash
GGBS	Ground granulated blastfurnace slag
CSF	Condensed silica fume
SANS	South African National Standards
BS	British Standards
HCP	Half-cell potential
LPR	Linear polarisation resistance
SHE	Standard hydrogen electrode
ITZ	Interfacial transition zone
OPI	Oxygen Permeability Index
CCI	Chloride Conductivity Index
WSI	Water Sorptivity Index
CR1	First set of data (sample one in each batch)
CR2	Second set of data (sample two and sample three in each batch)
0.1 µA/cm²	Theoretical active corrosion threshold
200 µA/cm²	Experimental limit for the impressed current technique

CHAPTER 1: INTRODUCTION

1.1 Background

Reinforced concrete as a composite construction material provides an electro-chemically stable environment for embedded reinforcing steel. The steel is protected by the highly alkaline concrete and develops a gamma ferric oxide protective layer on the surface of the steel. The robust nature of reinforced concrete, as well as certain construction benefits, has resulted in an abundance of reinforced concrete structures worldwide. However, in certain aggressive environments, these structures are exposed to conditions that lead to premature deterioration. Consequently, reinforced concrete deterioration has become of paramount concern in an attempt to avoid the excessive costs associated with repair, rehabilitation or possible decommissioning of damaged structures.

Reinforcement corrosion is the primary degradation mechanism of most reinforced concrete structures. The initiation of reinforcement corrosion is triggered by the ingress of deleterious substances through the cover concrete. Consequently, the thickness and quality of the cover concrete are essential in influencing the transport mechanisms and the associated deterioration. Corrosion of the reinforcing steel leads to a loss in steel cross-sectional area, with an associated structural deficiency. Additionally, the products of corrosion are expansive and may cause delamination or spalling of the cover concrete, with consequences for structural deficiency, integrity and safety.

Chloride-induced and carbonation-induced corrosion are the most common forms of reinforcement corrosion. Carbonation-induced corrosion is initiated by the ingress of CO_2, in the presence of moisture, which reacts with calcium hydroxide to form calcium carbonate. This process results in a reduction of the internal pH and depassivates the steel. Carbonation proceeds as a front and generally results in micro-cell corrosion (closely-spaced adjacent anodes and cathodes).

Chloride-induced corrosion (the focus of this study) is initiated through the ingress of chlorides to the level of the reinforcing steel. Chlorides, commonly in solution, permeate through the cover concrete and destroy the gamma ferric oxide layer which protects the reinforcing steel. The initiation phase of chloride-induced corrosion is controlled by the rate of chloride ingress and the chloride threshold. Chloride threshold values are normally case-specific and depend on a number of environmental and material factors. However, a conservative chloride content of 0.4% by weight of binder is generally accepted as a threshold to initiate corrosion.

Chloride induced corrosion is generally a macro-cell reaction with a large cathode separated from a comparatively small anode. Chloride-induced corrosion can be classified by high local or pitting corrosion which causes a localised loss in cross-sectional area, illustrated in Figure 1.1.

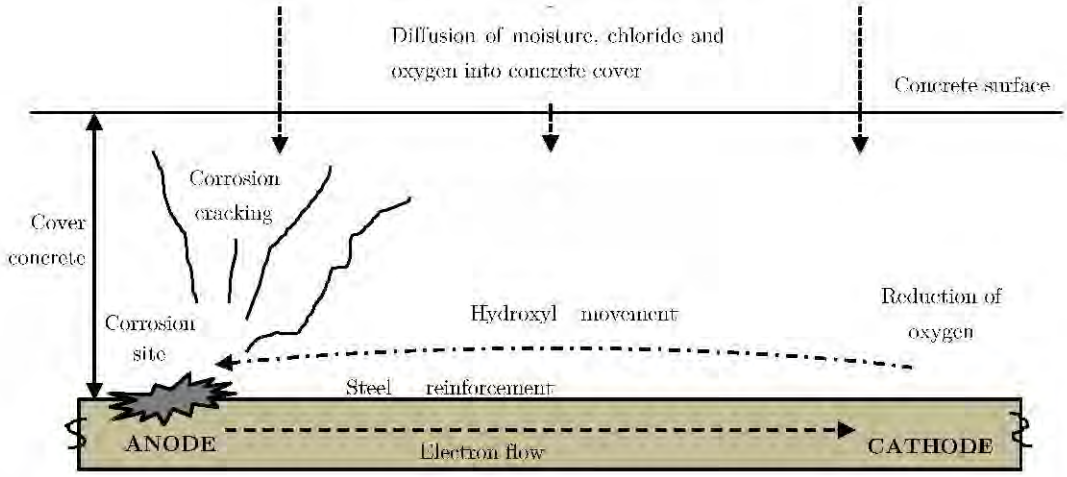

Figure 1.1: Schematic of corrosion of reinforcement (after Mackechnie, 2001)

Chloride ions commonly enter into concrete through the application of de-icing salts or through exposure to the marine environment. This research focuses on chloride-induced reinforcement corrosion in the marine environment, but the findings and general processes of corrosion may also be applicable to corrosion caused by the introduction of de-icing salts. Further discussions regarding chloride-induced corrosion are assumed to relate to exposure to the marine environment.

The general marine environment includes structures exposed directly to sea water (marine tidal and splash zones) and structures exposed to air-borne chlorides in the marine spray zone. These zones have been further classified by Mackechnie (2001) and consider direct exposure to sea water as the most severe case (Table 1.1). The severity of the exposure condition is further exacerbated by abrasion damage caused by direct wave action.

Table 1.1: Classification of marine exposure categories (Mackechnie, 2001)

Marine exposure category	Marine tidal and splash zones	Marine spray zone
Extreme	Structure exposed directly to sea water with heavy wave action and/or abrasion	N/A
Very severe	Structure exposed directly to sea water under sheltered conditions with little wave action	Structure within 500 m of shore exposed to heavy wave action and onshore wind
Severe	N/A	Structure located near shore (> 500 m) in an exposed marine location
Moderate	N/A	Structure in a sheltered location within 1 km of shore or anywhere within 30 km of coast

These environmental classifications have been simplified into three distinct marine environment exposure conditions. For example BS EN 206 (2013) provides details for the use of reinforced concrete in these environmental exposure classes. It details limitations for the composition and properties of concrete for their respective environments. Table 1.2 presents the environmental exposure classes with further details discussed in Section 2.7.1.1.

Table 1.2: Exposure classes according to BS EN 206-1 (2013)

Class designation	Description of the environment	Informative examples where exposure classes may occur
XS1	Exposed to airborne salt but not in direct contact with sea water	Structures near to or on the coast
XS2	Permanently submerged	Parts of marine structures
XS3	Tidal, splash and spray zones	Parts of marine structures

The current marine classifications apply a blanket exposure class for all structures exposed directly to wave action (XS3). However, recent studies completed by the University of Cape Town in Namibia (West Coast of Southern Africa) have shown that jetties in the area have high chloride contents at the level of the reinforcement but minimal corrosion damage in the tidal zone. This finding challenges the existing knowledge of expected corrosion damage in the marine tidal and splash zone, which is classified as the most severe exposure condition. The findings in these studies have been justified by relating the corrosion damage to the availability of oxygen at the level of the reinforcing steel. If the cover concrete is of sufficient quality and thickness, concrete exposed in the tidal zone may not have sufficient time to dry out to the level of the reinforcement. As a result, insufficient oxygen is available for the corrosion reaction to proceed at an appreciable rate. This phenomenon requires further investigation for its potential benefits to reduce the rate of reinforcement corrosion.

Therefore, a better understanding of corrosion under cyclic wetting and drying is required to assess the exposure conditions in the marine tidal and splash zone. Considering the tidal fluctuations and variations in drying times may assist in improving the durability of marine structures. As a result, the fundamentals of corrosion under cyclic wetting and drying require investigation and possible correlation to laboratory experimental work.

The electrochemical reaction of corrosion can be simplified into an equivalent electric circuit presented by Raupach (1996a). This model considers a combined system resistance based on the four components of the reaction:

- $R_{electrolyte}$ – Resistance of the electrolyte
- R_{anode} – Resistance of the anode
- $R_{cathode}$ – Resistance of the cathode
- R_{steel} – Resistance of the steel

The component with the largest resistance will govern the rate at which the reaction proceeds. In cases of limited oxygen availability, the cathodic resistance is sufficiently large that it governs the rate at which corrosion proceeds. Consequently, the cathodic resistance of the corrosion cycle will be the focal point throughout this dissertation.

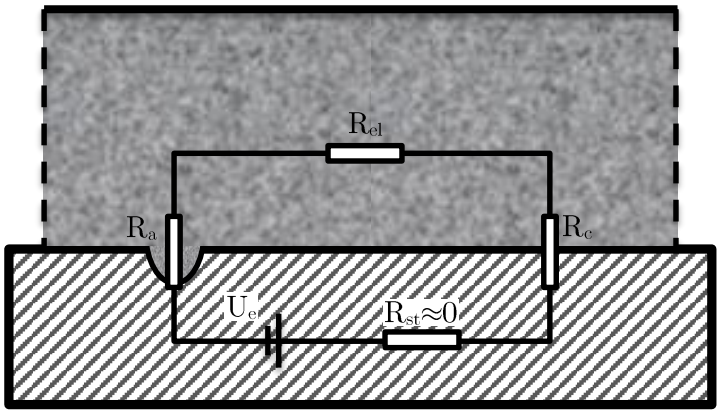

Figure 1.2: Simplified model showing the equivalent electric circuit for the electrochemical processes related to chloride-induced corrosion of steel in concrete (after Raupach, 1996a)

1.2 Subject and Motivation for Research

This research investigates corrosion under cyclic wetting and drying of simulated marine environment conditions. This constitutes an investigation into the fundamentals of corrosion combined with laboratory experimental work. The experimental work investigates the effect of the drying duration, binder type and water-binder ratio on the corrosion rate of embedded reinforcing steel.

The motivation for this research derives from several observations over time on existing marine structures. These observations presented a surprising phenomenon of limited corrosion damage in the tidal zone, despite measured high chloride concentrations. Consequently, this investigation will look to combine the fundamentals of corrosion with an experimental programme to both quantify and qualify the tidal zone in the marine environment. The expectation of this thesis is that the reduced corrosion damage in the tidal zone is a result of a reduction in the availability of oxygen, which is an integral component of the corrosion reaction.

There is limited literature available on the influence of oxygen availability on the corrosion rate of embedded reinforcing steel. Andrade, Alonso & Garcia (1990), Hussain & Ishida (2012) and Raupach (1996a & 1996b) have completed some investigations, with limited consistency between their findings. However, the findings of Raupach (1996a) present results which best represent the expectations of this research project. This primarily focusses on the individual resistance of each component of corrosion, with the limiting factor for corrosion being provided by the component with the highest resistance. With limited oxygen availability, this assumes cathodic control of the system and can result in the corrosion rate being effectively stifled.

It is likely that the theoretical distribution of chlorides with depth in the tidal zone is valid, but it is not the governing factor for corrosion due to the limited availability of oxygen. It is also expected that the concrete cover depth, quality, binder type and the water-binder ratio are critical factors in determining oxygen penetration. With sufficient concrete cover depth and quality, reinforcement in the tidal zone will effectively become submerged with a significant reduction in the corrosion rate.

1.3 Problem Statement

Current standards and guidelines do not provide sufficient protection for reinforced concrete structures in the marine environment and classify the marine tidal zone as a region of high corrosion potential. BS EN 206 (2013) specifies a maximum w/c ratio, minimum strength class and a minimum cement content for each exposure condition in the marine environment. However, these guidelines do not consider the primary influencing factors for reinforcement corrosion and, as a result, do not consider the selection of an appropriate binder type or a minimum cover depth. These factors are an integral component when considering reinforcement corrosion under cyclic wetting and drying and have not been adequately considered.

1.4 Objective

This research investigates the effect of the drying duration on the corrosion rate of reinforcing steel embedded in concrete and exposed to cyclic wetting and drying. Varying the drying duration is expected to cause an inferred change in the oxygen availability, which requires investigation for its influence on the corrosion rate. The intention of the experimental work is to test and/or validate observations of limited corrosion damage in the tidal zone, which is in direct contrast to the expectations of design guidelines. The findings of this research could be included in service life models and could be used to further classify the marine tidal zone and suggest more suitable design guidelines.

It was not practically possible to simulate natural marine cycles of wetting and drying due to the imposed time constraints. Cycles of 6.25 hours were not suitable for laboratory work with the available instrumentation. As a result, a laboratory-based study was developed to investigate the influence of an inferred change in oxygen availability on the corrosion rate. This will provide an indication of the influence of the duration of cyclic wetting and drying on the corrosion of steel embedded in concrete. Findings from this research can be used to justify the limited corrosion damage noted in the marine tidal zone in Namibia.

In the experimental testing a constant wetting period of 2 days was applied; while the duration of drying was varied between 1, 3, 5 and 7 days. It should be noted that extending the periods of wetting and drying does not adequately simulate the marine environment, but provides an indication of the influence of the inferred oxygen availability. This will provide a conservative approach that exaggerates the influence of cyclic wetting and drying on the corrosion rate.

1.5 Aims

The principal objective of this research is to determine the effect of the drying time on the corrosion rate of reinforced concrete members exposed to cyclic wetting and drying. With this primary focus in mind, the following aspects will also be considered for their influences on corrosion in the marine tidal and splash zone:

- The effect of the binder type on the corrosion rate by considering plain Portland cement and blended mixes with blastfurnace slag and fly ash.
- The effect of the water-binder (w/b) ratio on the corrosion rate by considering two different w/b ratios.
- Investigate the relationship between corrosion rate measurements and resistivity.
- Investigate the relationship between corrosion rate measurements and half-cell potential.
- Relate the experimental findings to the exposure conditions naturally experienced in the marine tidal and splash zone.

1.6 Scope of Study

This study does not consider the effects of abrasion in the tidal zone. It only considers laboratory experimental work and could be expanded to include an identical set of specimens exposed to natural sea water under cyclic wetting and drying.

The study is limited to marine environments in South Africa and materials used in South Africa. Additionally, some of the data used in the analysis of existing structures will be extracted from work by other researchers. Hence, any discussions or conclusions drawn from these data will be limited by the accuracy and scope of the data source itself. Furthermore, the experimental testing will only involve simulations for up to six months and hence the findings will be limited to their short-term applicability.

1.7 Thesis Outline

This thesis is divided into 6 chapters, as follow:

Chapter 1: Introduction – Presents a general introduction to the research topic and the significance of the research. A brief background is provided along with the motivation, objective, aims and scope of the study.

Chapter 2: Literature Review – Underlines the fundamental parameter when considering corrosion of reinforcing steel embedded in concrete.

Chapter 3: Experimental Methodology – Outlines the experimental laboratory work completed during the course of this thesis.

Chapter 4: Results and Discussion – Provides a summary of key findings and discusses the relevant trends and key parameter variations.

Chapter 5: General Discussion, Conclusions and recommendations – Provides a general discussion of the thesis findings and details relevant conclusions and recommendations based on the preceding chapters.

Appendices – Provide additional information.

References

Alexander, M. G. & Mackechnie, J., 2003. Concrete mixes for durable marine structures. *Journal of the South African Institution of Civil Engineering.* 45(2): 20-25.

Alonso, C., Andrade, C. & Garcia, A. M., 1998. The role of oxygen in the kinetic of the corrosion of reinforcements. *Proceedings of Eurocorr'98.*

Andrade, C., Alonso, C. & Garcia, A.M., 1990. Oxygen availability in the corrosion of reinforcements. *Advances in Cement Research.* 3(11): 127-132.

European Standards. 2013. *Concrete –Specification, performance, production and conformity.* (BS EN 206:2013).

Hussain, R.R. & Ishida, T. 2012. Multivariable empirical analysis of coupled oxygen and moisture for potential and rate of quantitative corrosion in concrete. *Journal of Materials in Civil Engineering.* 24(7): 950-958.

Mackechnie, J. R., 2001. *Predictions of reinforced concrete durability in the marine environment – Research Monograph No. 1 (Rev.).* South Africa: Department of Civil Engineering, University of Cape Town.

Otieno, M., 2008. Corrosion propagation in cracked and uncracked concrete. *MSc Thesis.* University of Cape Town.

Raupach, M., 1996a. Investigations on the influence of oxygen on corrosion of steel in concrete - Part 1. *Materials and Structures.* 29: 174-184.

Raupach, M., 1996b. Investigations on the influence of oxygen on corrosion of steel in concrete - Part 2. *Materials and Structures.* 29: 226-232.

CHAPTER 2: LITERATURE REVIEW

2.1 Introduction

The primary mechanism for the deterioration of reinforced concrete structures in the marine environment is corrosion of the reinforcing steel. Pig iron, the heated and processed form of iron ore, is in a higher energy state at normal temperatures than its natural form. Consequently, the laws of thermodynamics dictate that ordinary steel (made up of iron and alloying elements) will tend to its lowest energy state. The connotations of this phenomenon lead to the rusting of steel to form iron oxide, which is the lowest energy form of steel (Carino, 2004). Thus, steel will naturally corrode, provided sufficient moisture and oxygen is available. The process of rusting is further exacerbated by the presence of deleterious compounds and, in some cases, may proceed at undesirable rates.

This thesis will investigate corrosion in the marine environment, focusing on the tidal zone, where cyclic wetting and drying typically provides both moisture and oxygen in abundance. Reinforced concrete members in the tidal zone are exposed to high chloride contents and regular cycles of wetting and drying. This region is commonly perceived as the harshest environment for corrosion of reinforced concrete due to the severe environmental conditions coupled with the damaging effects of abrasion. Corrosion in the tidal zone will be studied through a literature review and an experimental programme exposing reinforced concrete specimens to different cycles of wetting and drying.

This chapter presents the fundamentals of corrosion, focusing on cyclic wetting and drying and its effects on the corrosion of reinforcing steel. This includes aspects of the marine environment that are pertinent to corrosion and the exposure conditions in the marine environment. This literature review will present an overview of the corrosion process and the fundamental aspects which concern corrosion under cyclic wetting and drying of a chloride-laden solution. Finally, relevant testing methods will be investigated for monitoring the corrosion rate and other relevant indicators.

2.2 Background

The aggressive conditions of the marine environment bring about corrosion through the high presence of chlorides and the availability of moisture. It is generally understood that the tidal zone, shown in Figure 2.1, is exposed to the harshest conditions, with physical abrasion causing additional damage to structures (Mehta, 1991). This illustrates the current understanding of the possible structural threats associated with the marine environment. Furthermore, the tidal zone is indicated simplistically by one high and one low tide mark without any indication of seasonal changes and varying exposure conditions within this region. As a result, the tidal and splash zones have been categorised in numerous standards as one environmental class. This thesis looks to investigate different cycles of wetting and drying in an attempt to further classify this region.

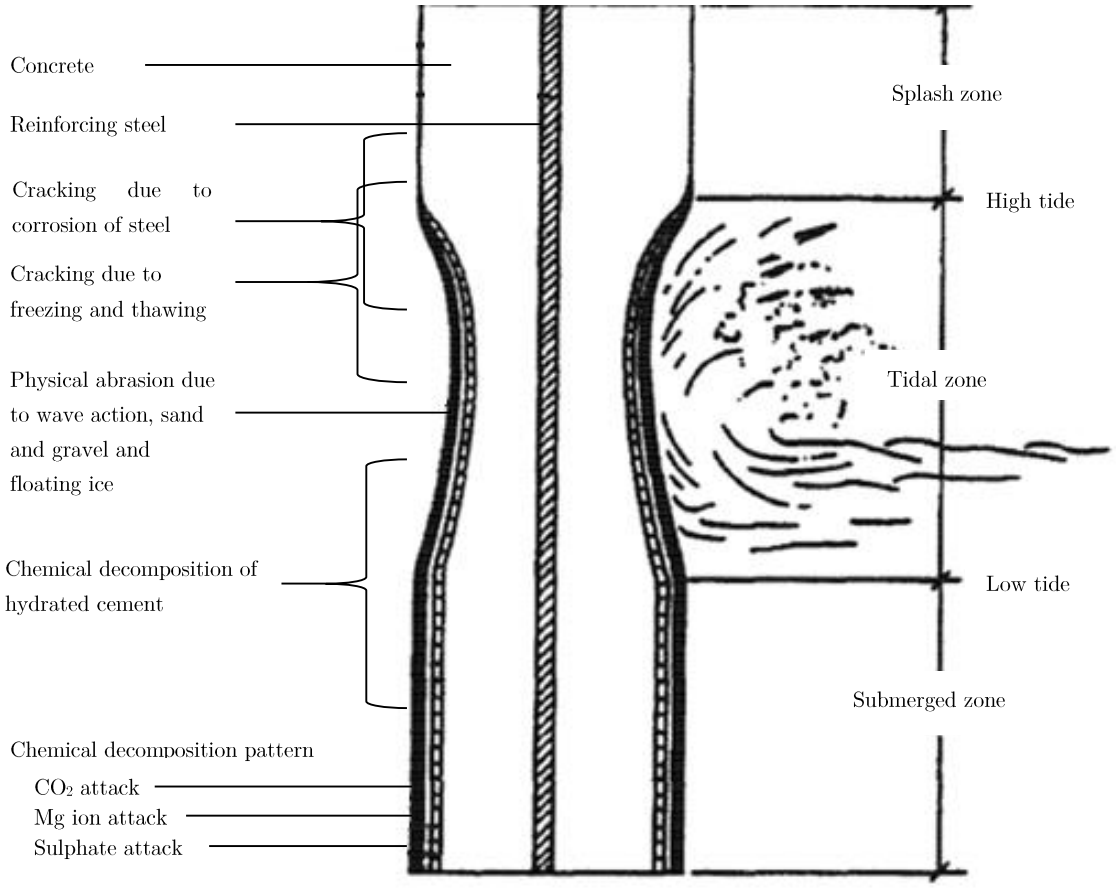

Figure 2.1: Deterioration in marine concrete (after Mehta, 1991)

2.3 Transport Mechanisms in Concrete

The deterioration of reinforced concrete structures is primarily controlled by the transport mechanisms governing the movement of gases, fluid and ions in concrete. This will determine the ease with which deleterious compounds can penetrate the concrete and, in this case, attack the embedded reinforcing steel. An in-depth understanding of the associated transport mechanisms is essential to fully categorise corrosion under cyclic wetting and drying and to understand the forces at play. This section discusses the transport mechanisms in concrete, focusing on the relevant parameters for reinforcement corrosion under cyclic wetting and drying.

2.3.1 Permeability

The permeability of concrete describes the flow of fluids under an externally applied pressure gradient, whilst the pores are saturated with the same fluid. The gas or liquid permeates through the concrete cracks and pore spaces under the externally applied pressure gradient. The rate of penetration is governed by Darcy's Law (Eq. 2.1), where the flow is along a negative pressure gradient.

$$v = \left(\frac{k}{n}\right)\left(-\frac{dh}{dx}\right) \qquad \text{(Eq. 2.1)}$$

where: v is the velocity of the fluid (m/s), k is the permeability coefficient (m/s), n is the porosity of the concrete (%), h is the hydraulic head (m) and x is the distance parameter (m).

The permeability of concrete is important in water retaining structures. It can also be used for predicting carbonation. It is primarily governed by the concrete microstructure, properties of the permeating fluid and the moisture content of the concrete (Ballim, Alexander & Beushausen, 2009).

2.3.2 Sorption

Sorption is a measure of the movement of the wetting front in dry or partially saturated concrete. The exposure to moisture leads to capillary suction and the uptake of liquids into the capillary pores. The rate of capillary suction is directly influenced by the degree of hydration, pore content, pore connectivity and the degree of saturation (Ballim, Alexander & Beushausen, 2009). Hence, curing of the surface concrete is essential to reduce capillary suction and the absorption of fluids. Sorptivity is measured using the following uni-directional equation:

$$S = \frac{Fd}{M_{sv} - M_{s0}} \qquad \text{(Eq. 2.2)}$$

where: F is the slope of the mass loss against the square root of time ($g/h^{0.5}$), d is the specimen thickness (mm), M_{sv} is the vacuum saturated mass (g) and M_{s0} is the dry mass (g) at the initial time (t_0).

2.3.3 Diffusion

Diffusion is defined as the movement of gases, ions or particles under a concentration gradient. The mechanism of diffusion governs the ingress of chlorides in saturated concrete and can be modelled using Fick's laws of diffusion. Diffusion mechanisms also govern the transport of chlorides in the interior of concrete exposed to cyclic wetting and drying. When concrete is exposed to cyclic wetting and drying, the transport of chlorides is governed by convection on the surface and diffusion in the interior region (discussed further in Sections 2.3.4 and 2.5.2).

Fick's first law can be applied to steady-state diffusion and requires constant surface concentration and a uniform concentration gradient. This can be applied to gaseous diffusion of carbon dioxide in unsaturated concrete. The transport of oxygen in concrete is also mainly governed by a diffusion process. Fick's first law contains a negative prefix which implies that the flow is along a negative concentration gradient.

$$J = -D_e\left(\frac{dC}{dx}\right) \qquad \text{(Eq. 2.3)}$$

where: J is the mass transport rate (g/m^2s), D_e is the effective diffusion coefficient (m^2/s), C is the concentration of fluid (ion or gas), x is the penetration depth (m) and dC/dx is the concentration gradient ($g/m^3/m$).

The ingress of chlorides in saturated or partially-saturated concrete is governed by ionic diffusion. Ionic diffusion can be modelled by Fick's second law of diffusion which considers the rate of change of concentration with respect to time and distance.

$$\frac{\partial C}{\partial t} = D\frac{\partial^2 C}{\partial x^2} \qquad \text{(Eq. 2.4)}$$

where: C is the concentration of the fluid (g/m^3), t is a time parameter (s), D is the diffusion coefficient (m^2/s) and x is the penetration depth (m).

Crank's error function solution to Fick's 2nd law of diffusion provides a solution to the partial differential equation (Eq. 2.4). A number of boundary constraints must be applied to achieve this solution which include $C_x=0$ at $t=0$ where $0<x<\infty$ and $C_x=C_s$ at $x=0$ where $0<t<\infty$. The effect of this solution on the ingress of chlorides is investigated further in Section 2.5.2.

$$C_{x,t} = C_s\left[1 - erf\left(\frac{x}{2\sqrt{D_\alpha t}}\right)\right] \qquad \text{(Eq. 2.5)}$$

where: $C_{x,t}$ is the concentration of chloride at depth x and time t, C_s is the surface concentration of chlorides, erf is the mathematical error function, x is the depth into the concrete cover, D_α is the apparent chloride diffusion coefficient and t is the time.

2.3.4 Convection

Convection is the process of transporting solutes and ions due to the bulk movement of water in concrete. Convection is suitable for the transport of surface chlorides in unsaturated concrete exposed to cyclic wetting and drying. An assumption of diffusion is that chlorides move within motionless water and, hence, Fick's second law is no longer applicable. Convection can be modelled in the surface layer using Eq. 2.6 below.

$$\left(\frac{\partial C}{\partial t}\right) = -v\left(\frac{\partial^2 C}{\partial x^2}\right) \qquad \text{(Eq. 2.6)}$$

where: v is the average velocity vector of fluid flow and C is the concentration of solute at depth x after time t.

In permanently submerged reinforced concrete structures convection is negligible due to the saturation of the pores. However, exposure to cyclic wetting and drying allows the surface layer to be affected by the movement of chloride ions through the bulk movement of water. This is critical for concrete structures in the marine environment (tidal and splash zones) with direct exposure to salt-laden sea water. Under cyclic wetting and drying, the ingress of chlorides is governed by a surface convection layer and an interior diffusion region, discussed further in Section 2.5.2. However, the depth of the convection layer is primarily controlled by the following factors:

- Penetrability of the concrete to water
- Drying and wetting time
- Water pressure gradient
- Time to capillary suction during wetting

2.3.5 Migration

Migration of ions is also referred to as accelerated-diffusion or electro-diffusion. Migration considers the movement of ions in solution under an electrical potential gradient. The electrical potential component can be related to diffusion through the Nernst-Einstein equation (Eq. 2.7). The concept

of accelerated-diffusion is commonly applied for laboratory-based chloride tests. In this case, the movement of ions due to migration dominates in comparison to significantly slower rates of diffusion.

$$J = \frac{DzECF}{RT} \qquad \text{(Eq. 2.7)}$$

where: J is the flux (kg/m^2/s), D is the diffusion coefficient (m^2/s), z is the valence of the ionic species (-1 for Cl^-), E is the electrical field potential (V), C is the concentration of the ionic species (mol/m^3), F is Faraday's constant (96500 $A \cdot s$), R is the universal gas constant (8.314 J/mol/K) and T is the absolute temperature (298 K).

2.3.6 Wick action

Wick action can occur when a relatively thin concrete member is exposed to drying on one face while simultaneously exposed to wetting with an ionic solution on the opposing face. The change in exposure conditions on the opposite faces causes the ionic solution to be drawn to the drying face where evaporation occurs. The evaporation leads to the deposition of the ionic species and a subsequent increase in the ionic concentration within the concrete member. The wick action causes an increase in the rate of chloride ingress beyond that predicted by diffusion alone (Hearn, Hooton & Nokken, 2006).

2.3.7 Combined transport processes

It is generally considered an over-simplification to consider transport mechanisms acting independently. At any given time a combination of a number of transport mechanisms might transpire. They may act simultaneously or within different sections with the same path direction.

2.4 Introduction to Corrosion

All metals, except gold and platinum, are thermodynamically unstable at normal atmospheric pressure and will ultimately revert to their oxides, hydroxides or sulphides (Heckroodt, 2002). In reinforced concrete structures the mechanism for this reversion is through corrosion. Corrosion is unavoidable; but the rate of corrosion can be controlled. Corrosion is an electrochemical process that involves the transfer of electrons, without the supply of an external electrical source. As a result, corrosion relies on the development of two half-cell reactions, with the anodic reaction capable of producing electrons (ACI 222, 2001). The anodic reaction is the oxidation of iron to form ferrous ions, while the cathodic reaction is the reduction of oxygen to form hydroxyl ions (discussed further in Section 2.6).

The corrosion process is commonly divided into three distinct stages; initiation, propagation and acceleration, as shown in Figure 2.2. Each of these phases is critical when assessing reinforcement corrosion in the marine environment with the initiation, propagation and acceleration phases outlined in Sections 2.5, 2.6 and 2.7, respectively.

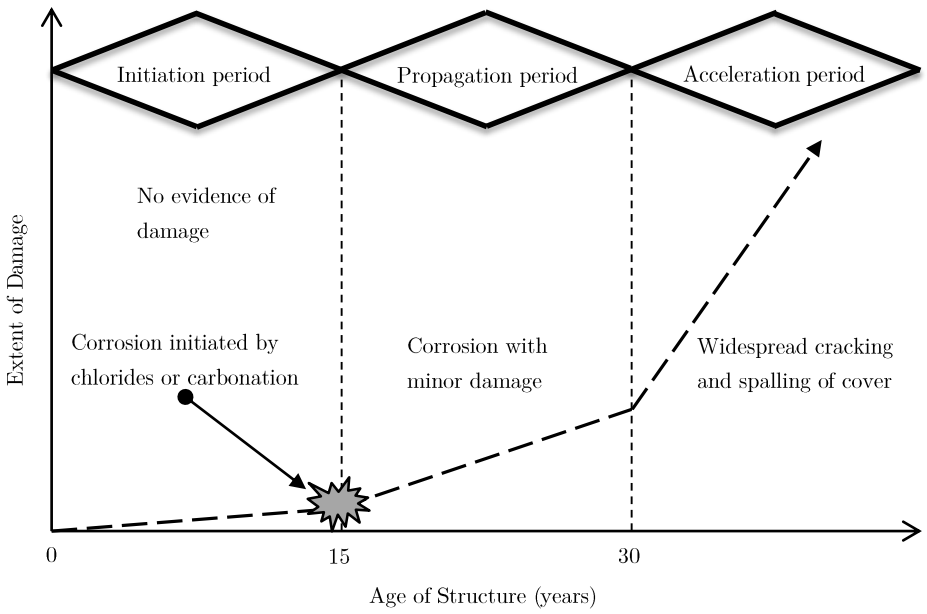

Figure 2.2: Three stage model of corrosion damage (after Heckroodt, 2002)

The corrosion rate can be determined through measuring the rate at which electrons are removed from the anode (reinforcing steel). This corrosion current can then be converted into a loss of metal via Faraday's Law (Stansbury and Buchanan, 2000).

$$M = \frac{ItA_w}{nF} \qquad \text{(Eq. 2.8)}$$

where: M is the mass of metal dissolved or converted to oxide (g), I is the current (A), t is the time (s), A_w is the atomic weight (g/mol), n is the valence and F is Faraday's constant (96500 A · s).

2.5 Initiation of Corrosion

The initiation, and subsequent propagation, of corrosion requires that certain criteria are fulfilled. The main requirements include the depassivation of the steel and a sufficient supply of oxygen and moisture. This section will include details of the initiation of corrosion, while Sections 2.6 and 2.7 will investigate the propagation and acceleration phases of corrosion.

2.5.1 Passive protection

The highly alkaline nature of the concrete pore solution protects the reinforcing steel from corrosion. This highly alkaline environment is developed through the hydration of cement which forms mainly calcium silicate hydrate and calcium hydroxide. As a result, under natural conditions concrete will develop a pH in the range of 12-13. In these conditions a passive protective layer is developed on the surface of the steel. This protective film of gamma ferric oxide (Fe_2O_3) prevents iron cations (Fe^{2+}) from entering into solution with the electrolyte (Tapan, 2007). The protective layer also prevents oxygen anions (O_2) from accessing the steel. As a result, the passive protective layer can prevent the reinforcing steel from corroding at an appreciable rate. However, a drop in the pH (below 11) or the

ingress of chlorides can destabilise the passive protective layer and expose the reinforcing steel to the possibility of corrosion (Mehta, 1991).

2.5.2 Ingress of chlorides

The marine environment supplies an abundance of chloride ions which results in the breakdown of the passive protective layer. The rate of ingress of chlorides ions is fundamentally controlled by the transport mechanisms in the concrete cover layer. In permanently submerged reinforced concrete the saturated pore condition nullifies any significant chloride transportation through bulk movement of the chloride solution. As a result, chlorides enter the concrete through diffusion under a concentration gradient. Under these conditions the rate of penetration of chlorides by diffusion can be estimated using Crank's error function solution to Fick's 2nd law of diffusion, discussed in Section 2.3.3.

The governing transport mechanisms are more complex in partially-saturated or dry concrete. The exposure to cyclic wetting and drying introduces a chloride solution to a dry or partially-dry concrete surface. This causes an inwards movement of the chloride solution by convection, which prevents the development of clear diffusion in the near surface region. This near surface layer is commonly referred to as the convection zone, where the forces of capillary absorption lead to relatively higher chloride concentrations in the convection zone. Consequently, an interior concentration gradient is developed with the further transport of chlorides being governed by diffusion. As mentioned in Section 2.3.4, the depth of the convection layer depends on a number of factors. It is worth noting that the drying and wetting time has an effect on the depth of the convection layer. Longer drying times will allow a greater drying depth and thus a larger convection layer.

The ingress of chlorides beyond the convection zone can then be modelled taking into account an initial concentration using a modification to Crank's error function solution to Fick's 2nd law (Crank, 1975). This modification is shown in Eq. 2.9 and takes into account a convection layer of depth Δx. The penetration of chlorides beyond the convection layer then proceeds as a diffusion process, with the combined convection and diffusion zones illustrated in Figure 2.3.

$$C_{x,t} = C_i + (C_{\Delta x} - C_i) \cdot erf\left[1 - \frac{x - \Delta x}{2\sqrt{(t - t_{exp})D_{app}(t)}}\right] \qquad \text{(Eq. 2.9)}$$

where: $C_{x,t}$ is the concentration of chloride at depth x and time t, C_i is the initial chloride content, $C_{\Delta x}$ is the chloride content at depth Δx, erf is a mathematical error function, x is the depth into the concrete cover (mm), Δx is the depth of the convection layer (mm), $D_{app}(t)$ is the time dependant apparent diffusion coefficient (m^2/s), t is the concrete age (seconds) and t_{exp} is the time until first exposure to chlorides (seconds).

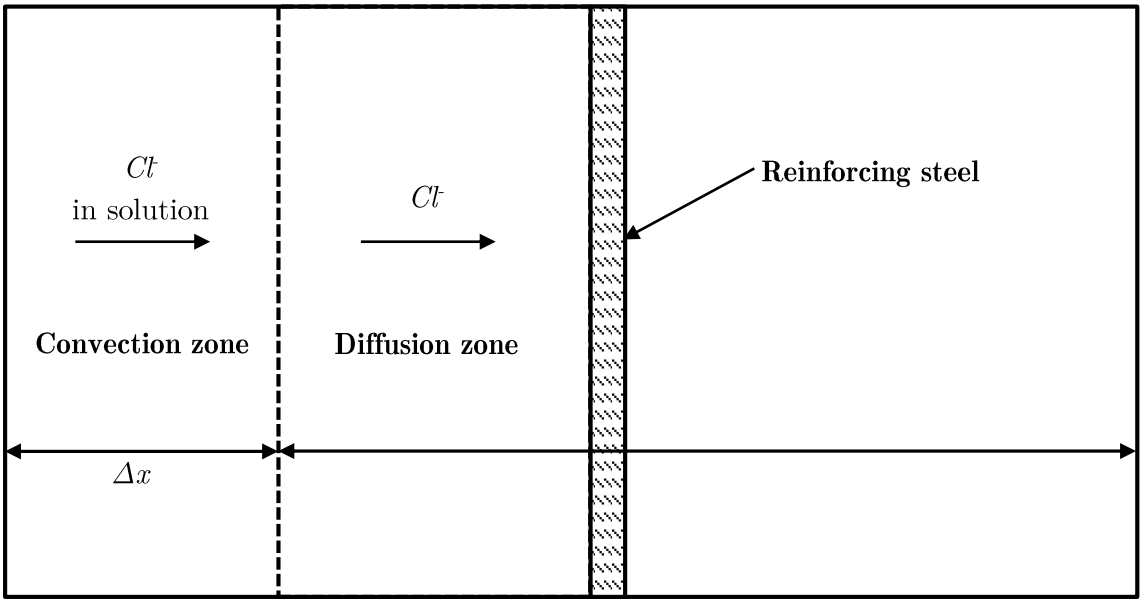

Figure 2.3: An illustration of the convection and diffusion zones controlling the ingress of chlorides under cyclic wetting and drying

2.5.2.1 Chloride content

The ingress of chlorides can be associated with chemical and/or physical reactions that oppose the rate of ingress. This process is commonly referred to as the 'binding' of chlorides to the cement hydration products, particularly the aluminates (Broomfield, 2007). The binding process can be separated into two processes, including a physical and chemical component. The large surface area of hydration gel leads to the physical adsorption of chlorides; while the chlorides also react chemically with the hydration products to form Friedel's salt. The binding of chlorides leads to a reduction in the amount of available chlorides to initiate corrosion of the reinforcing steel.

As a result, chlorides can exist in concrete as either free or bound. The bound chlorides are no longer 'free' to transport further into the concrete or take part in the depassivation of the reinforcing steel. Consequently, the development of a chloride concentration gradient only considers free chlorides (chlorides that actively participate in the depassivation of the reinforcing steel). It is also worth noting that bound chlorides can be released or desorbed due to carbonation, sulphate attack or a reduction in the free chloride concentration (Tang, Nilsson & Basheer, 2011).

The chloride binding capacity of concrete is primarily controlled by the binder content and the binder type. An increase in the binder content will result in the formation of more hydration products to bind chlorides. Additionally, it is worth noting the benefits of GGBS and FA as replacements for Portland cement. The relative decrease in free chlorides is illustrated in Figure 2.4.

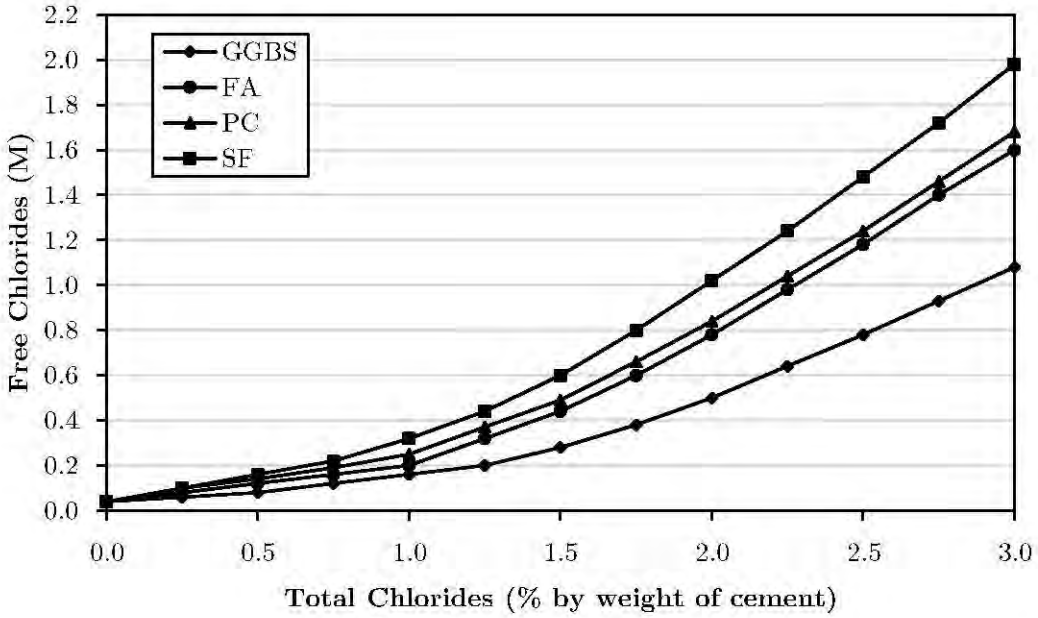

Figure 2.4: Chloride binding capacity of different binder types (Glass & Beunfeld, 1997)

Chloride profiles can be developed by measuring the chloride content at specific depths. The total chloride content is normally measured as a percentage of the mass of the binder, ignoring the effects of chloride binding. A typical chloride profile is shown in Figure 2.5, where a clear distinction is evident between the convection (white dots) and diffusion (black dots) zones. Notable features of this profile include higher chloride contents in the convection zone and the wash-out effect causing a significant reduction in surface chlorides.

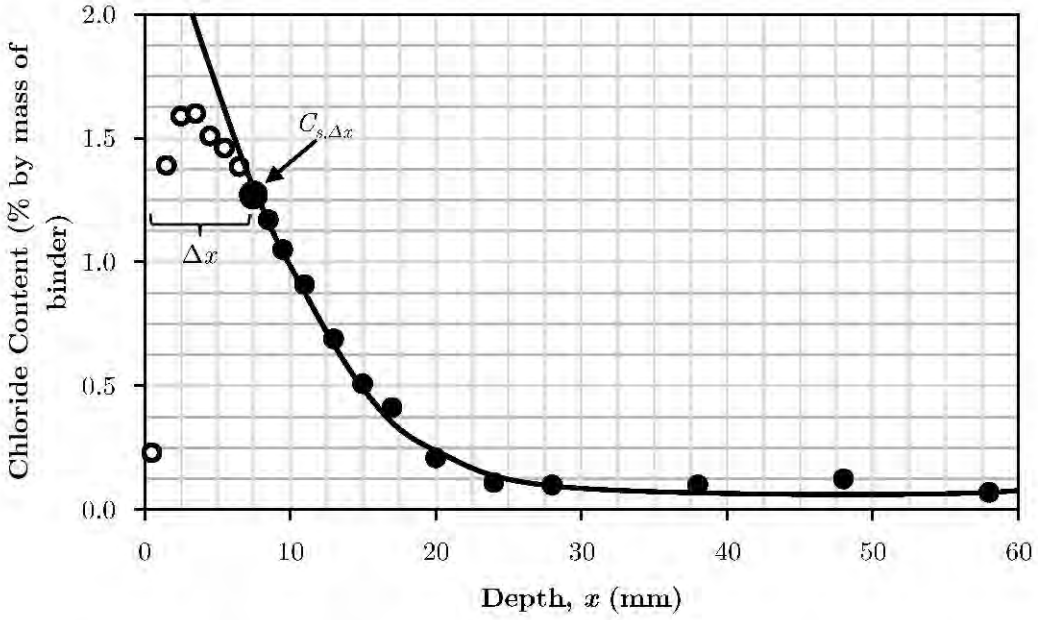

Figure 2.5: A splash zone chloride profile fitted to the error function solution of Fick's 2nd law (neglecting the convection zone) (after Schiessl & Lay, 2005)

2.5.2.2 Effect of chlorides

Chlorides in sufficient concentration can have a significant impact on the embedded reinforcing steel in reinforced concrete. Initiation of corrosion commences once the amount of chlorides exceeds a case-specific threshold (discussed later). Upon the breakdown of the passive protective layer, the local electrochemical potential becomes more negative. A corrosion cell is developed between the disparity in electrochemical potential of the local steel and the rest of the passive steel. The unprotected steel, with its greater negative electrochemical potential, becomes the anode and the remaining steel is the cathode. In these conditions corrosion can propagate at appreciable rates, provided sufficient oxygen and moisture is available. The effect of chlorides on corrosion can be summarised by the following four processes (Hunkeler, 2005):

1. Destroys the gamma ferric oxide passive protective layer on the reinforcing steel
2. Reduces the pH of the pore solution by decreasing the solubility of the calcium hydroxide
3. Increases the moisture content due to the hygroscopic properties of salts present in concrete (e.g. $CaCl_2$, NaCl)
4. Increases the electrical conductivity of concrete

Regardless of the numerous effects of the chlorides, the primary function of the chloride ions is to release ferrous ions through the formation of ferrous chloride. The remaining effects associated with chloride ingress simply promote the propagation of corrosion.

2.5.2.3 Chloride threshold

The *chloride threshold value* or *critical chloride content* is the concentration of chlorides sufficient to break down the passive protective layer covering the embedded reinforcing steel. It is generally accepted that reinforcement corrosion in non-carbonated, alkaline concrete cannot proceed unless this threshold concentration is surpassed.

A remarkable amount of research has been conducted on chloride threshold values without a general consensus being achieved. Through this work numerous chloride threshold values have been developed, which typically vary between one order of magnitude depending on the binder type and conditions. Angst and Vennesland (2009) attribute the large scatter in chloride threshold values to varying definitions of the critical chloride content and different experimental techniques, combined with other inherent properties that affect the chloride threshold value. Angst and Vennesland (2009) identify the following inherent parameters as critical factors affecting the chloride threshold value:

1. Steel-concrete interface
2. pH of the pore solution
3. Electrochemical potential of the steel

The chloride threshold is commonly measured as the total chloride content relative to the mass of binder. This is due to the relative ease with which the total chlorides can be measured. The critical chloride content can also be represented by the free chlorides only (excluding bound chlorides that generally do not contribute to the corrosion reaction) or by relating the chloride concentration with

the hydroxyl ion concentration. Glass and Beunfeld (1997) argue that measuring the total chlorides provides the best representation of the chloride threshold value based on analysis of available data in literature. A typical chloride profile is illustrated in Figure 2.6, adapted to include a conservative chloride threshold value of 0.4% chlorides by weight of cement. Typical chloride threshold values are presented in Section 2.5.3.4, taking into account the binder type.

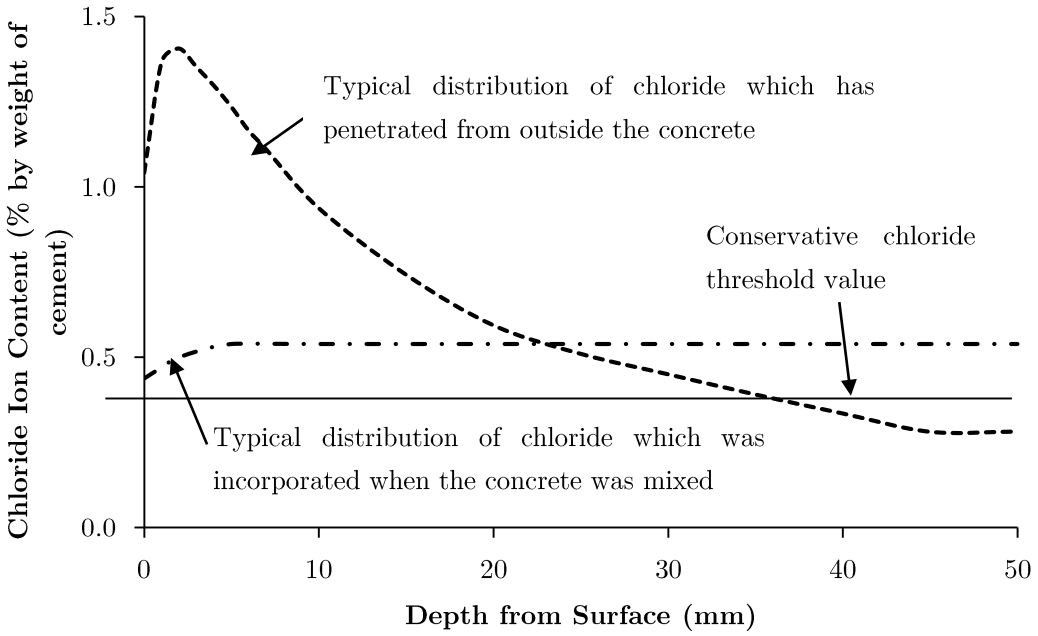

Figure 2.6: Typical chloride profile of concrete elements in the marine environment (after Pullar-Strecker, 2002)

2.5.3 Effect of binder type

The type and content of cement extender plays a vital role in corrosion initiation, but cement extenders also affect the rate of the corrosion reaction (Otieno, 2008). South African codes focus on the grade of the concrete and ignore the effect of the binder type on controlling the ingress of chlorides (Alexander & Mackechnie, 2003). With improved concrete grade, the chloride resistance does generally increase, but this simplification for ease of application ignores the superior chloride resistance that could be achieved through the implementation of supplementary cementitious materials (SCMs).

The specification of a concrete grade has its advantages in practicality and ease of implementation and verification. However, as shown in Figure 2.7, the time to corrosion activation can be significantly increased through the incorporation of an appropriate cement extender. This phenomenon could be utilised to decrease the total binder content and thus reduce the costs of manufacture. Alternatively, the superior durability of blended cements could be used to ensure extended service life of reinforced concrete structures in the marine environment.

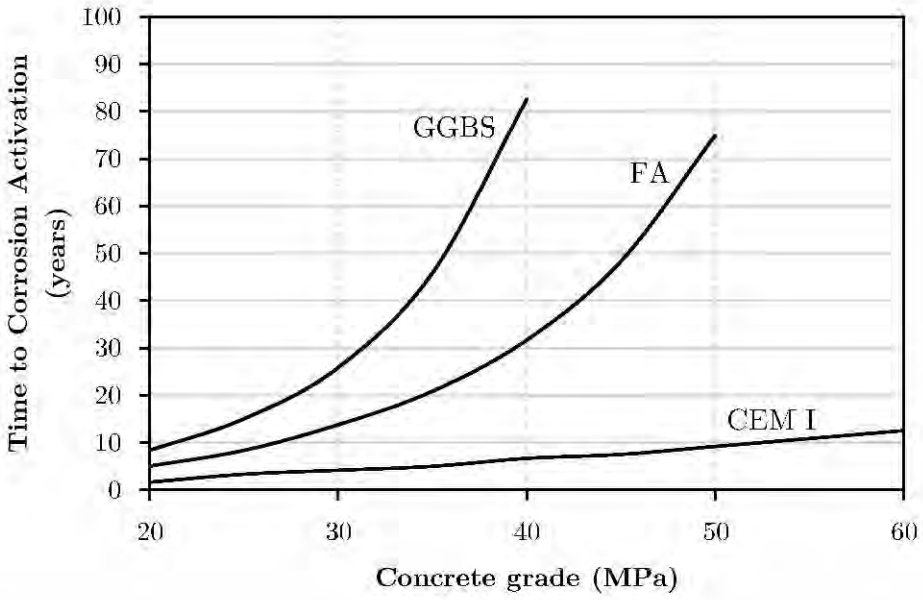

Figure 2.7: Model prediction results of the time to corrosion activation for different concrete types (after Ballim, Alexander & Beushausen, 2009)

Nevertheless, the selection of an appropriate SCM should consider the coupled effects on the concrete properties. Specifically, when considering the use of silica fume (CSF), the significant decline in chloride penetration rates might be overshadowed by a reduction in the chloride threshold level (Manera *et al.*, 2008). As a result, each case should be considered on its own merits considering all the factors involved (e.g. mix composition, effectiveness of vibration, curing, cover thickness, etc.). The effect of SCMs on the time to corrosion activation is illustrated in Figure 2.8 where Portland cement has been replaced with 50% for the slag bearing concrete, 30% for the fly ash concrete and 8-10% replacement for the silica fume concrete (Alexander & Mackechnie, 2003).

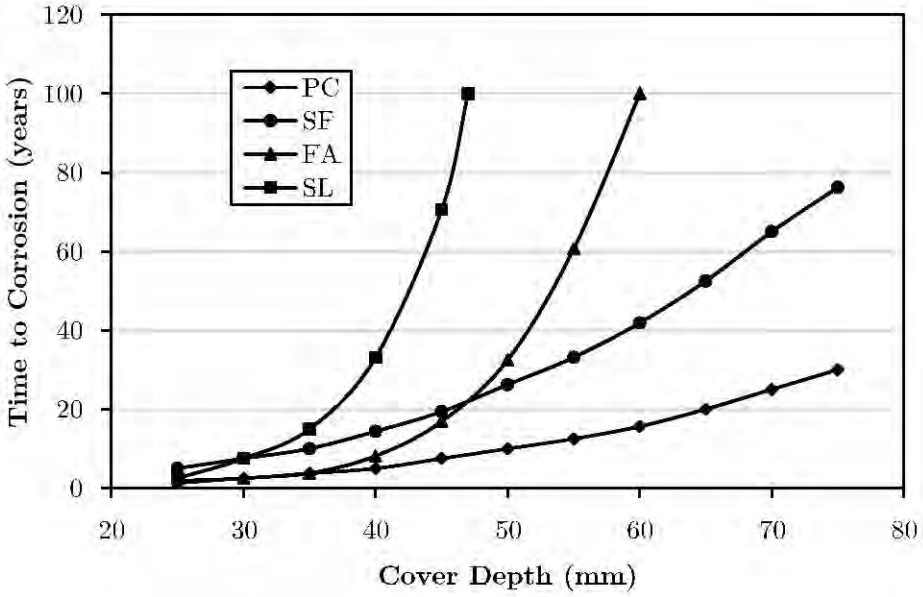

Figure 2.8: Time to corrosion activation in very severe marine environment (after Alexander & Mackechnie, 2003)

2.5.3.1 Effect on chloride transport

Various researchers have conducted chloride penetration testing in the marine environment over the past few decades (Bamforth & Chapman-Andrews, 1994; Polder, 1996; Scott, 2004). The use of SCMs has been shown to significantly reduce the rate of penetration of chloride ions through concrete (Scott, 2004). Polder (1996) reported that the inclusion of SCMs can decrease the rate of chloride penetration by 3-10 times when compared to Portland cement concrete.

Figure 2.9 provides a graphical representation of the reduced chloride penetration of chloride in blended concrete (30% fly ash mix and a 70% slag mix) compared to PC concrete. A reduction in the chloride content will lead to delayed initiation of corrosion and, hence, provide the necessary motivation for the inclusion of SCMs for reinforced concrete exposed to the marine environment.

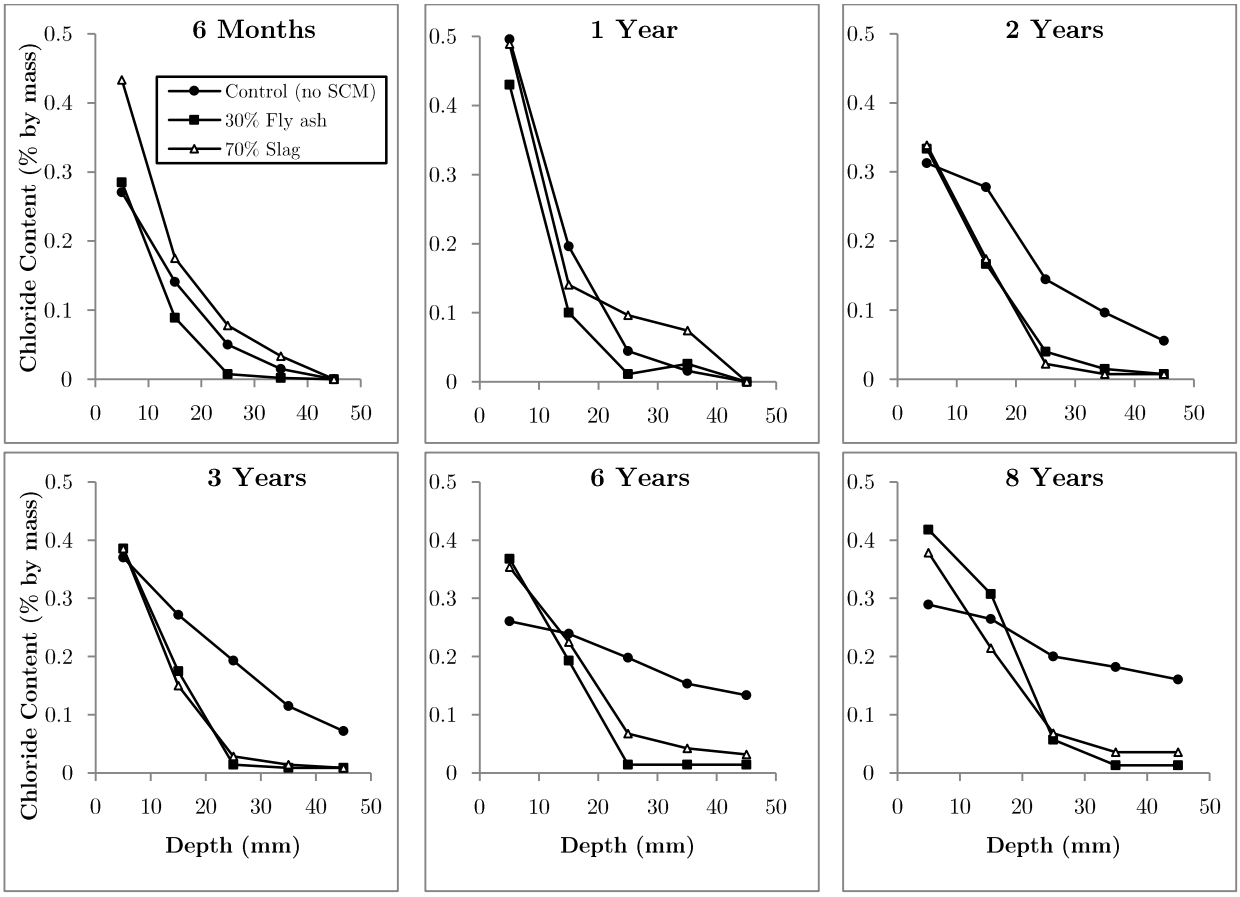

Figure 2.9: Chloride profiles in concrete blocks exposed to seawater spray (after Thomas, 2013)

2.5.3.2 Chloride binding capacity

Alonso *et al.* (2012) provide an overview of experimental work conducted on the effect of SCMs on the chloride binding capacity. It was concluded that the inclusion of CSF results in a decrease of the chloride binding capacity; while FA and GGBS were both found to increase the chloride binding capacity.

The inclusion of SCMs enhances the formation of CSH gel which offers a larger total surface area for the adsorption of chlorides. Furthermore, chemical reactions involving FA and GGBS result

in the formation of calcium aluminate hydrates which can form Friedel's salt. Both these processes allow for the removal of free chlorides from the concrete pore solution (Angst & Vennesland, 2009).

2.5.3.3 Lower alkalinity

FA and CSF are pozzolanic materials that consume calcium hydroxide to form cementing products. The consumption of calcium hydroxide will be associated with a decrease in the alkalinity. GGBS has a similar effect of lowering the alkalinity but through a different process. The latent hydraulic binder does not consume calcium hydroxide, however, the relatively high replacement levels of GGBS for PC will result in the formation of less calcium hydroxide (with commonly between 30-70% less cement).

The effect of the SCMs on the alkalinity of concrete can be expressed through the concentration of hydroxyl ions. Thomas (2013) conducted experimental pore solution tests with the results shown in Figure 2.10. It is evident that the inclusion of SCMs has significantly decreased the hydroxyl ion concentration and hence negatively impacted the alkalinity. Thomas (2013) attributes the decrease in hydroxyl ion concentration to an increased capacity for the hydration products to bind alkalis in the presence of SCMs. Consequently, the incorporation of SCMs will generally decrease the alkalinity of concrete.

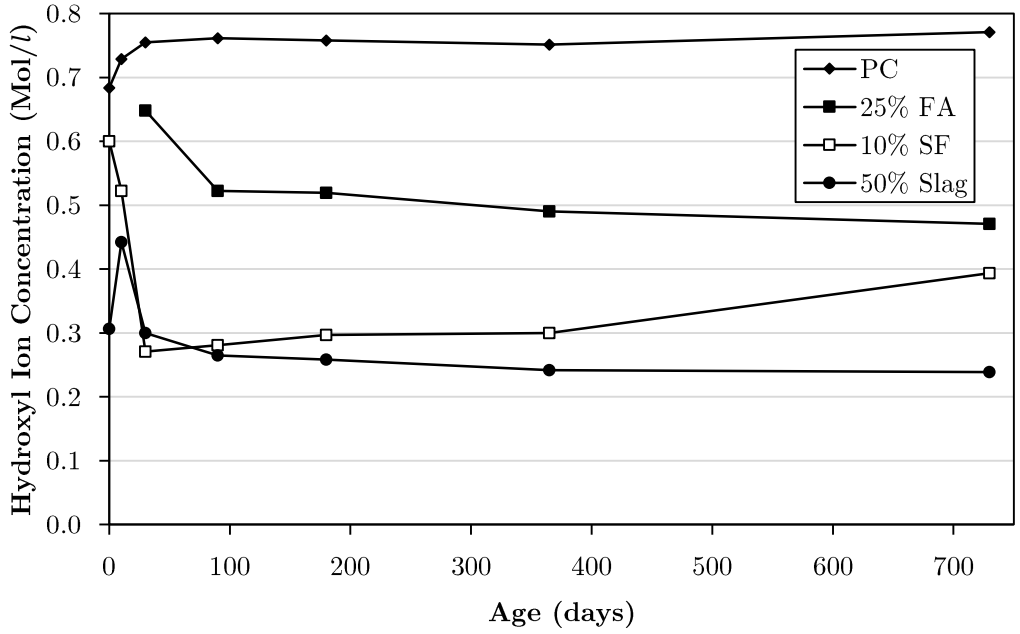

Figure 2.10: Pore solution evolution for pasts of high-alkali cement and various SCMs (Thomas, 2013)

However, it is important to note that this drop in hydroxyl ion concentration does not correspond to a pH drop of the same proportion, For example, Siddique and Khan (2011) found that including up to 30% SF did not cause the pH to drop below 12. In Figure 2.10 the inclusion of 10% SF caused the hydroxyl ion concentration to halve compared to PC, whereas this is unlikely to cause a major drop in the pH from the normal range of 12-13 to ensure passive protection of the reinforcing steel, as mentioned in Section 2.5.1.

2.5.3.4 Chloride threshold

The pH of the pore solution and the steel-concrete interface are two critical factors that influence the chloride threshold value. These factors can be directly affected by variations in the binder type (Alonso *et al.*, 2012). Nevertheless, authors commonly present a conservative chloride threshold value of 0.4% total chlorides by weight of cement based on experience with Portland cement (Alonso *et al.*, 2012). This evidently neglects the effect of the binder type on the chloride threshold value and should be considered with some reservations especially considering the high variations in measured chloride threshold values (illustrated in Figure 2.11).

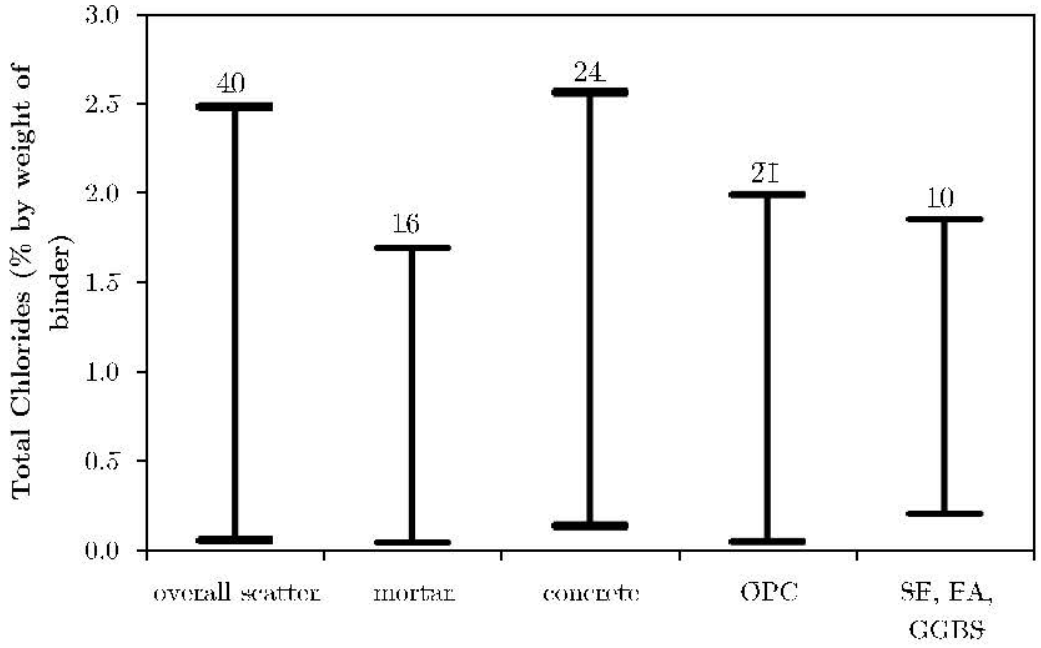

Figure 2.11: Scatter of chloride threshold values in the literature sorted by selected parameters and when excluding values obtained as potentials < -200 mV SCE. The number above each bar indicates the frequency of occurrence in literature (after Angst *et al.*, 2009)

The effect of SCMs on the chloride threshold value has been primarily investigated through experimental work due to conflicting expectations in literature. For instance, the inclusion of GGBS increases the chloride binding capacity but can also be associated with a decrease in the overall alkalinity. As a result, the amount of free chlorides may be reduced but the favourable protective conditions have also been diminished by lowering the alkalinity (Poulsen & Sørenson, 2012). The extent of the counteracting factors has thus been investigated through experimental work.

Two governing factors for the chloride threshold value have been identified as the chloride binding capacity and the alkalinity of the pore solution. However, these counteracting factors act in combination and have resulted in relatively inconclusive results. The inclusion of CSF has been found to lower the chloride threshold value, while fly ash and GGBS have shown conflicting results (Alonso *et al.*, 2012).

2.5.4 Initiation process

Reinforcement corrosion is initiated through the reduction of the gamma ferric oxide passive protective layer, which leaves the reinforcing steel unprotected. Carbonation and chloride ingress are considered the primary agents that result in the reduction of the passive protective layer. Carbonation is not the focus of this research and as a result will not be considered further, but it is worth noting that the permeation of CO_2 can result in the depassivation of the reinforcing steel by lowering the pH of concrete.

The ingress of chlorides in a sufficient concentration acts as a catalyst to initiate corrosion. Chlorides contribute to the breakdown of the passive protective layer and allow corrosion to proceed at a faster rate. Otieno (2008) elaborates further on this issue indicating a degree of uncertainty on the exact process that allows chloride ingress to contribute to the depassivation of reinforcing steel. However, this process is not essential to develop a clear understanding of the effects of chloride ingress on corrosion. Nevertheless, Figure 2.12 illustrates the perceived mechanism for the initiation of corrosion and the development of localised/pitting corrosion.

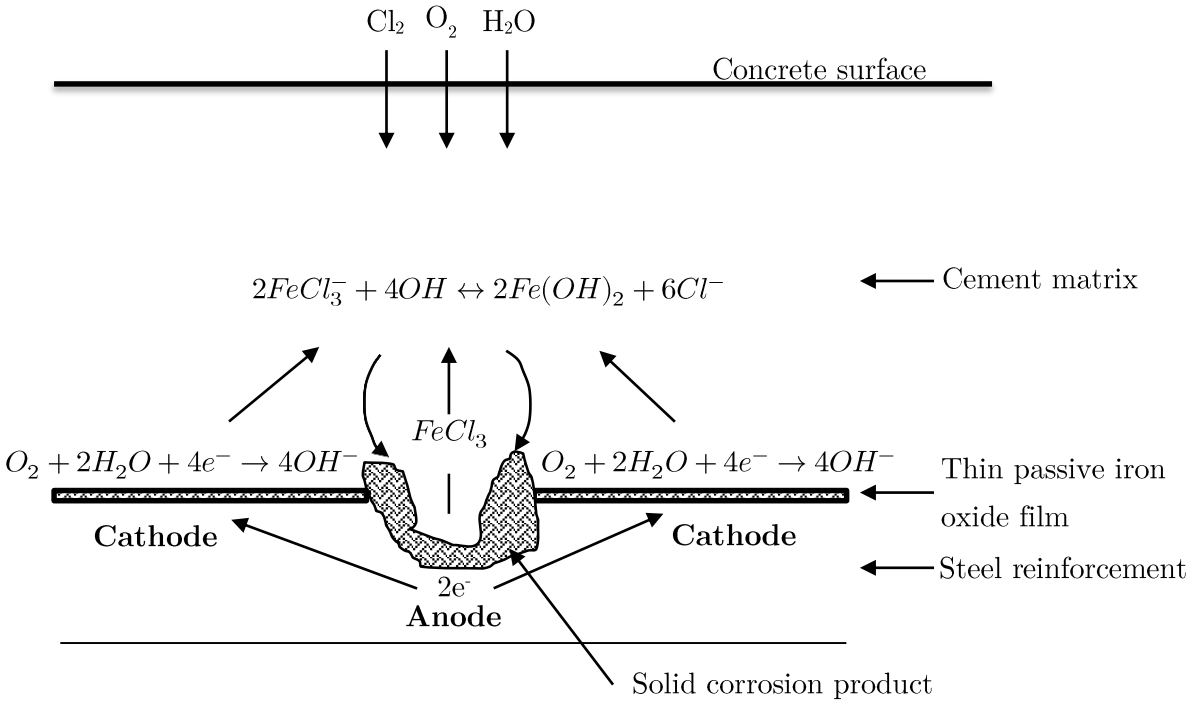

Figure 2.12: Chloride exposure initiating local corrosion (after Broomfield, 2007)

2.6 Propagation of Corrosion

The propagation phase of corrosion commences once corrosion has been initiated. This phase can be associated with minor corrosion damage to the embedded steel. The corrosion rate is initially slow and highly dependent on the oxygen and moisture availability (Hunkeler, 2005). However, as a by-product of the corrosion reaction, water is produced and develops a self-sustaining chemical reaction. With sufficient water supply and oxygen the rate of corrosion will accelerate, ultimately

leading to widespread cracking and spalling of the concrete cover. The three step process of corrosion development is shown in Figure 2.2.

The corrosion process requires certain initial conditions to initiate corrosion and ensure the continued corrosion. These conditions are summarised in Table 2.1 and are commonly fulfilled in reinforced concrete in a marine environment when sufficient chlorides and oxygen are available with a suitably conductive electrolyte. In the corrosion process, the flux of ions and electrons can be used as a measure of the corrosion rate. This corrosion rate can be presented in a number of interchangeable formats (shown for iron/steel), but is most commonly presented as a corrosion current per area of steel (Hunkeler, 2005).

$$1mA/cm^2 \cong 11.6mm/year \cong 250g/m^2/day$$
$$1\mu A/cm^2 \cong 12\mu m/year \cong 0.25g/m^2/day$$

Table 2.1: Conditions for corrosion of steel in concrete (after Hunkeler, 2005)

Condition for corrosion of steel in concrete	Condition is fulfilled, if:
An anodic reaction is possible.	The passive layer of the steel breaks down and depassivation of the steel occurs. This can be caused by carbonation of concrete and/or ingress of chloride into the concrete, reaching a critical level.
A cathodic reaction is possible.	Oxygen as the driving force of the corrosion process is available at the interface of the reinforcement in a reasonable amount.
A flux of ions between the site of the anodic reaction and the site of the cathodic reaction is possible.	The environment or electrolyte between the site of the anodic reaction and the site of the cathodic reaction permits good conduction.
A flux of electrons is possible.	There is metallic connection between the sites of anodic and cathodic reactions. For monolithic reinforced concrete structures this condition is usually fulfilled.

The expansion due to corrosion of the reinforcing steel can cause the concrete to crack or delaminate. The propensity for cracking of the cover concrete depends predominantly on the porosity of the cover concrete. The corrosion product attempts to fill void space and a lack of void space will develop a build-up in stress. Consequently, a porous concrete will be less susceptible to cracking due to reinforcement corrosion. However, this property of concrete is not normally desired, with porous concrete resulting in a shorter time to corrosion activation by allowing contaminants to dissipate to the reinforcing steel. The expansive forces within the cover concrete are also dependant on the type of corrosion products developed. Figure 2.13 illustrates the relative expansion of the possible corrosion products from reinforcing steel to indicate the propensity of corroding steel to cause cracking or delamination.

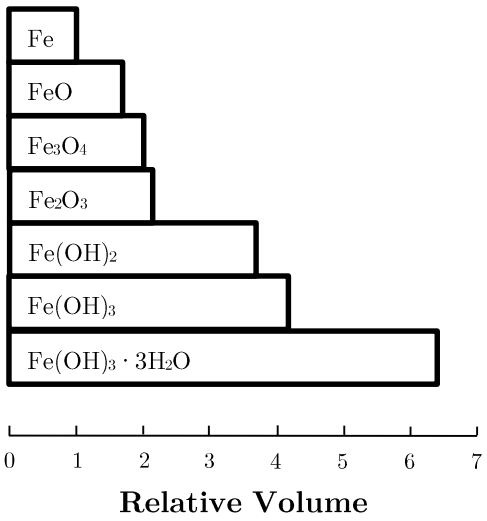

Figure 2.13: Relative size of corrosion products (after Mehta, 1991)

2.6.1 Service life

Various definitions of the service life of reinforced concrete structures exist depending on the defined required level of service for a structure. Tuutti (1982) provided one of the first interpretations of service life, with it being defined as a combination of the time to initiation and the time for propagation (sometimes divided into propagation and acceleration as in Figure 2.2). As a result, maintaining or extending the service life of a structure can be approached through either of these processes. When considering the time-to-initiation, Polder (1996) explains that the chloride diffusion and cover depth control the duration of this period, while the resistivity of the cover concrete controls the corrosion rate, and hence the propagation period.

2.6.2 Macrocell corrosion

Chloride-induced corrosion forms as a macrocell reaction, with a large cathode and a relatively small anode. The anode and the cathode are widely separated with electrolytes carrying the potential from the anode to the cathode to complete the two half-cell reactions. The two half-cell reactions consist of oxidation of the anode (iron) and the reduction of oxygen at the cathode. The two possible half-cell reactions are shown below (Eq. 2.10 and Eq. 2.11) and an illustration of the macrocell corrosion process is provided in Figure 2.14.

Anodic Half-Cell Reaction	$Fe \rightarrow Fe^{2+} + 2e$	(Eq. 2.10a)
	$2Fe^{2+} + 4OH \rightarrow 2Fe(OH)_2$	(Eq. 2.10b)
	$Fe(OH)_2 + \frac{1}{2O_2} \rightarrow 2FeOOH + H_2O$	(Eq. 2.10c)
	$Fe^{2+} + OH + H_2O \rightarrow HFeO_2 + H_2$	(Eq. 2.10d)
Cathodic Half-Cell Reaction	$2H_2O + O_2 + 4e \rightarrow 4OH$	(Eq. 2.11a)
	$H^+ + 2e \rightarrow H_2$	(Eq. 2.11b)

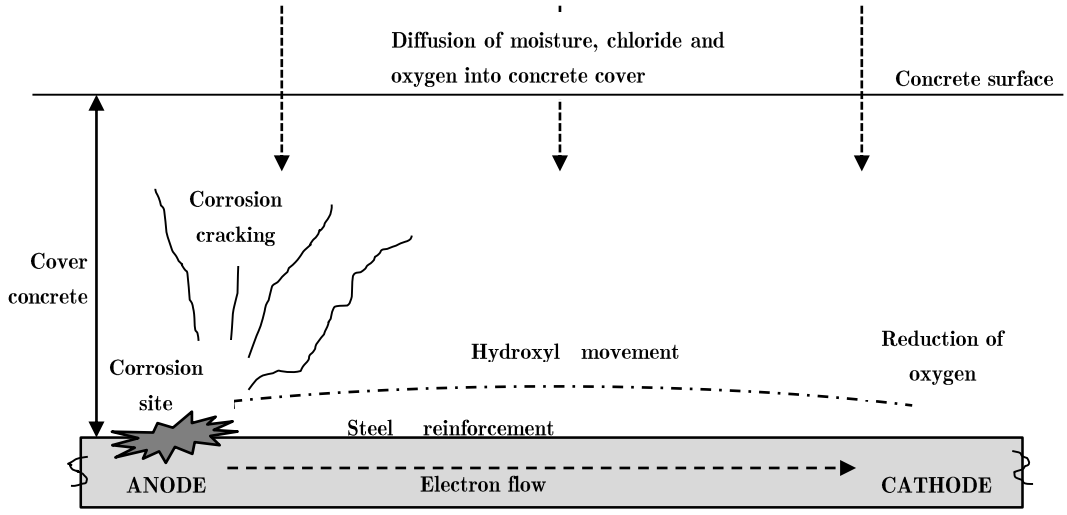

Figure 2.14: Schematic of corrosion of reinforcement (after Mackechnie, 2001)

2.6.3 Microcell corrosion

Microcell corrosion typically occurs in carbonated concrete and is characterised by having its anode and cathode adjacent to each other (Otieno, 2008). Microcell corrosion can also occur when the corroding steel is coupled with another piece of steel which is passive. The passivity in the neighbouring steel may be brought on by different environmental conditions for the neighbouring steel or from a different composition of the steel (Miyazato & Otsuki, 2010). Corrosion of the anode usually proceeds as general corrosion of the steel cross-section and is commonly a slower process than macrocell corrosion.

Figure 2.15 provides an alternative approach to differentiate between macrocell and microcell corrosion. Macrocell corrosion is presented as two distinct bars with an electrical connection provided between them. This enforces the concept that the anode and cathode must be distinctly separated while still providing electrical connectivity. On the other hand, microcell corrosion is depicted as corrosion on one bar where the anode and cathode are relatively close. Although it should be stressed that two distinct bars are not necessary for chloride-induced reinforcement corrosion to propagate.

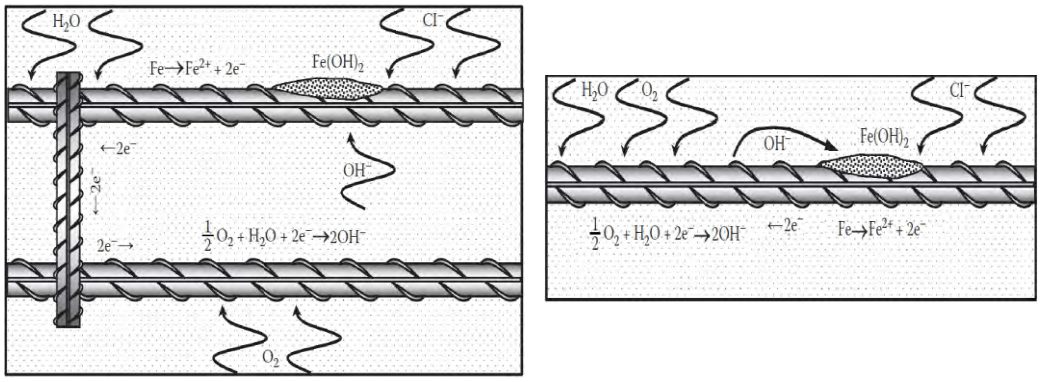

Figure 2.15: Macrocell and microcell corrosion of steel in concrete (Thomas, 2013)

2.6.4 Combined microcell and macrocell corrosion

Miyazato & Otsuki (2010) investigated the effect of macrocell and microcell corrosion and the necessity to combine these reactions for a better reflection of the actual corrosion process. They found that the macrocell corrosion process dominated for low w/b ratios. However, for high w/b ratios the microcell corrosion process prevailed. Justification for this phenomenon was provided by linking the corrosion type to the flux of oxygen and water through the concrete.

2.7 Acceleration of Corrosion

The acceleration phase of reinforcement corrosion commences after the reinforcing steel has become depassivated and is corroding at a sufficient rate to cause cracking or spalling of the cover concrete. At this point, the corrosion process contains four primary components which must all produce the same current (Bertolini *et al.*, 2013). With this constraint in place, it is evident that the system can be controlled through the reduction of the current in any one of the four components, shown in Eq. 2.12.

$$I_{anode} = I_{cathode} = I_{metal} = I_{electrolyte} = I_{corrosion} \quad \text{(Eq. 2.12)}$$

where: I_{anode} is the current of the anode, $I_{cathode}$ is the current of the cathode, I_{metal} is the current of the metal, $I_{electrolyte}$ is the current of the electrolyte and $I_{corrosion}$ is the overall corrosion current.

Generally, the resistance of the metal is negligible and thus will not be a limiting factor in the corrosion process. The other three mechanisms will control the rate of corrosion in the following cases (Bertolini *et al.*, 2013):

- Anodic control – Reinforcing steel has not been depassivated by a pH drop or chloride ingress. Hence, the anodic reaction limits the progress of corrosion.
- Cathodic control – Oxygen deprived conditions result in limited oxygen availability for reduction; otherwise known as oxygen diffusion control.
- Resistivity control – Dry or low humidity conditions do not allow easy transport of electrons for corrosion. Hence, the two half-cells cannot be completed. Also commonly referred to as ohmic control.

Sufficient chloride concentrations are available in the marine environment to ensure depassivation of the reinforcing steel. Hence, the primary focus should be cathodic and/or resistivity control. Bertolini *et al.* (2013) also describe the optimum conditions for corrosion as when the steel has been depassivated, there is sufficient oxygen at the concrete/steel interface, and the resistivity of the concrete is low. The reliance of the corrosion rate on the resistivity of concrete has also been identified by Polder (1996) through theoretical and experimental findings (Polder, 1996).

Reinforced concrete in the marine environment is often exposed to solutions of high chloride contents. Bakker *et al.* (1994) investigated the effect of the chloride content on the corrosion rate and found that the anodic process is not rate-controlling at chloride contents above 1%. Polder (1996) explains that the cathodic process is not rate-controlling in the marine tidal and splash zones since

the concrete is not completely saturated and will allow sufficient oxygen to penetrate to the level of the reinforcing steel. Macrocell corrosion experiments performed by Raupach (1996) showed that the resistivity controlled the corrosion rate in concrete with a high resistivity. However, when the resistivity was significantly lower, other factors come into play (such as cathodic and anodic control). Polder *et al.* (1994) suggest that the corrosion rate is controlled by the resistivity when it is in excess of 70 Ω.m.

2.7.1 General parameters affecting corrosion

The deterioration of reinforced concrete structures in the marine environment is primarily caused by the ingress of chlorides and the associated corrosion of the reinforcing steel (Mackechnie, 2001). This implies that for reinforced concrete, not impaired by external structural failure, durability of concrete should be the factor of most concern. Mackechnie (2001) elaborates on this point by identifying the primary factors that affect the durability of reinforced concrete. These factors include the concrete type, cover to reinforcement, site practice and the severity of exposure. This research focuses on the concrete type and severity of exposure but other general parameter will also be discussed.

2.7.1.1 Exposure classes

The marine environment offers exposure conditions that are conducive to corrosion of the reinforcing steel. Structures in the marine environment can be classified according to their exposure conditions to determine the deterioration potential based on the exposure to sea water. Mackechnie (2001) presented a guideline for the classification of marine structures (shown in Section 1.1). A similar scheme is given in the European National Standard EN 206 (Table 2.2) which incorporates a prescriptive design approach to structures exposed to the marine environment (BS EN 206, 2013). This investigation will focus on the class designations 'XS2' and 'XS3' and the sections to follow will centre on these exposure categories.

Table 2.2: Exposure classes according to European Standards (after BS EN 206, 2013)

Class designation	Description of the environment	Informative examples where exposure classes may occur
XS1	Exposed to airborne salt but not in direct contact with sea water	Structures near to or on the coast
XS2	Permanently submerged	Parts of marine structures
XS3	Tidal, splash and spray zones	Parts of marine structures

Submerged zone

The submerged zone can be classified as concrete that is permanently submerged and saturated to the level of the reinforcement, shown in Figure 2.1. These conditions provide sufficient chlorides to depassivate the steel but can also be linked to slow corrosion rates. The saturated pore structure develops pure diffusion transport mechanisms within the cover concrete which leads to relatively rapid ingress of chlorides. However, as discussed in Section 2.7.3, saturation of the cover concrete prevents the ingress of sufficient oxygen to accelerate the corrosion at an appreciable rate. As a

result, permanently submerged reinforced concrete may be exposed to high levels of chlorides but are not expected to corrode due to a lack of oxygen (Polder, 2005).

Splash zone

The splash zone is located above the high tide level where wave action causes moisture to splash onto the concrete surface, as shown in Figure 2.1. The potential for reinforcement corrosion is generally considered to be most severe in the splash zone (Polder, 2005). Both the chloride penetration and the subsequent reinforcement corrosion are relatively rapid within this region. The penetration of chlorides in the splash zone is inflated by partial drying of the cover concrete which leads to capillary absorption of sea water. This leads to greater chloride concentrations than expected in the submerged zone. Meanwhile, the availability of moisture ensures that the cover concrete develops a low resistivity, causing a relatively rapid corrosion rate. Furthermore, the unsaturated condition of the cover concrete ensures that sufficient oxygen is available (discussed further in Section 2.7.3). A combination of all these conditions leads to fairly rapid corrosion and deterioration of reinforced concrete structures.

Tidal zone

The tidal zone is defined as the region between high tide and low tide, again shown in Figure 2.1 (Mehta, 1991). This zone of consideration is thus the region between the lowest and highest water levels experienced on a coast line. High and low tides occur twice a day, separated by approximately 12 hours and 25 minutes (Mehta, 1991). As a result, marine structures experience two cycles of wetting and drying per day, which may also have an associated heating and cooling effect. The tidal range can vary from about 0.5 m to 15 m in some cases, which is also affected by the depth of the ocean (Mehta, 1991). In the Western Cape of South Africa the tidal range is approximately 0.7-1.5 m. Based on this approximate tidal range, the water may rise or fall at an approximate rate of 10-25 cm/hour.

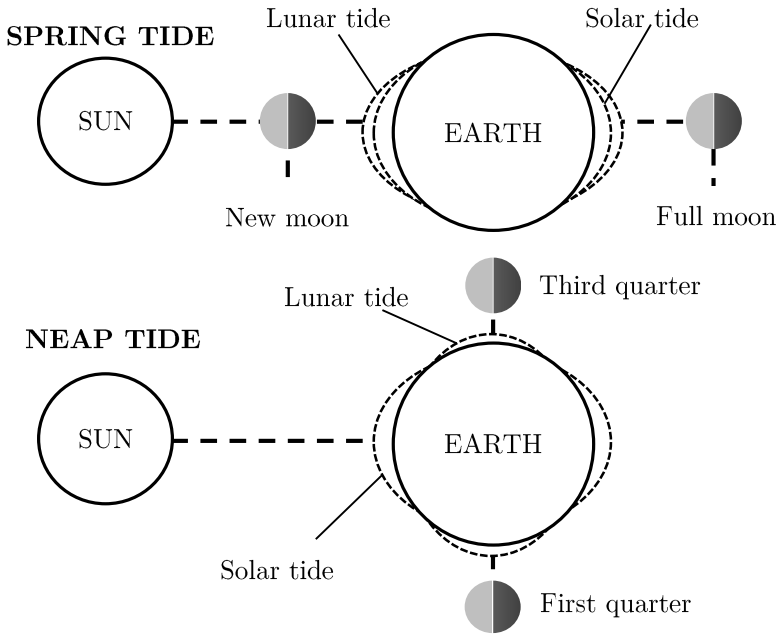

Figure 2.16: Spring and Neap tide location of the moon

The position of the low and high tide depend on the position of the moon. Spring tides (not associated with the season of spring) occur when the moon is in the same linear axis as the earth and the sun. As a result, the moon and sun have complementary pulls on the earth's surface and create higher high tides and lower low tides. Neap tides, on the other hand, occur when the sun and moon are perpendicularly aligned and create opposing gravitational pulls on the earth's surface. This phenomenon creates lower high tides and higher low tides and a subsequently smaller tidal range. The position of the sun and moon relative to the earth are shown in Figure 2.16 and illustrates how spring and neap tides are developed.

Consequently, the tidal zone is a large zone that is exposed to highly variable conditions. As a result, exposure classifications of the tidal zone will vary depending on the location in the tidal zone and the concrete cover thickness and quality. The tidal zone can be compared to either the submerged or splash zone, or even a combination at different heights within the tidal zone (Polder, 2005). The severity of the exposure conditions will depend primarily on the time taken for the concrete to dry to the level of the reinforcement. An indication of the relative drying time is presented in Figure 2.17, where it is evident that the short-term environmental exposure conditions do not affect the relative water content below 60 mm from the concrete surface. However, at concrete depths less than 40 mm, the relative moisture content may vary by as much as 30%. Good quality concrete of sufficient thickness may provide protection from rapid drying and thus drying to the level of the reinforcement will not occur before the next cycle of wetting.

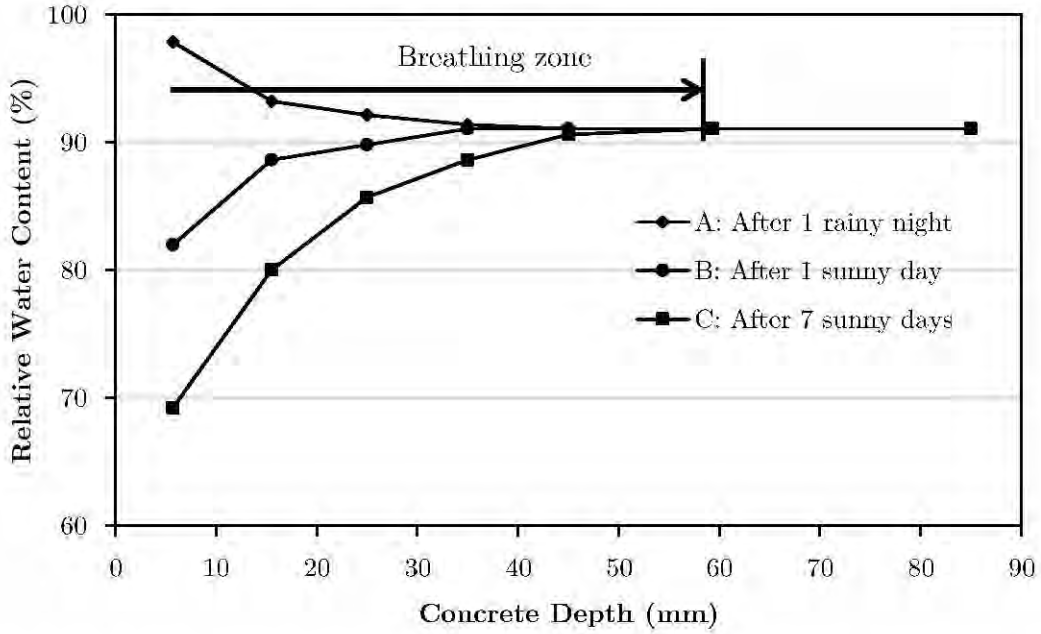

Figure 2.17: Water content in cover concrete after various exposure conditions (after Hunkeler, 2005)

Hong & Hooton (1999) also investigated chloride penetration into concrete under cyclic wetting and drying by varying the duration and the number of cycles. This problem, identified as key for marine structures, results in an accumulation of harmful materials including sulphates, alkalis, acids and

chlorides in the cover concrete (Hong & Hooton, 1999). The effect of cyclic wetting and drying is illustrated in Figure 2.18 and Figure 2.19. From these results it is evident that the chloride content increases as the number of cycles of wetting and drying increases. Additionally, from a comparison between Figure 2.18 and Figure 2.19, it is evident that the chloride penetration increases as the duration of the drying increases.

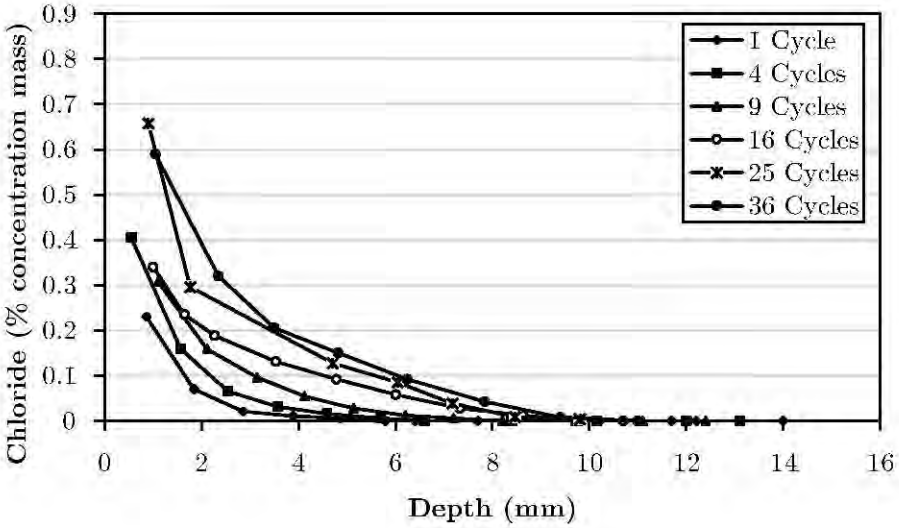

Figure 2.18: Chloride profiles for concrete (25% slag, 0.4 w/b) exposed to cycles of wetting and drying of 6 hours wetting and 18 hours drying (after Hong & Hooton, 1999)

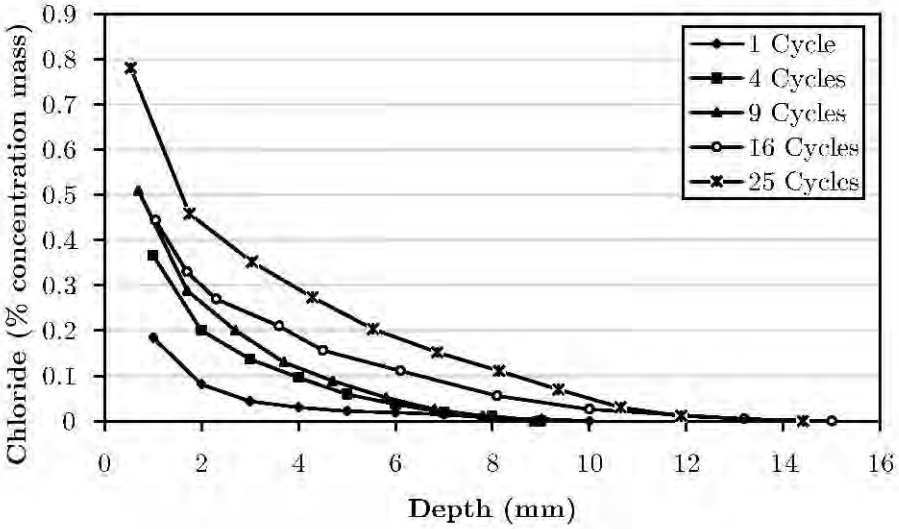

Figure 2.19: Chloride profile for concrete (25% slag, 0.4 w/b) exposed to cycles of wetting and drying of 6 hours wetting and 66 hours drying (after Hong & Hooton, 1999)

Both these phenomena can be justified by investigating the convection zone under cyclic wetting and drying, as discussed in Sections 2.3.4 and 2.5.2. Exposure to cyclic wetting and drying develops a convection zone within the cover concrete. The thickness of this convection zone depends primarily on the drying time and the concrete quality. The thickness of the convection zone increases as the drying time increases, which is also evident when comparing Figure 2.18 to Figure 2.19. A thicker

convection zone provides a larger zone for the deposition of chlorides and leads to a higher chloride concentration. Additionally, increasing the number of cycles of wetting and drying promotes the deposition of chlorides. Both of these factors can be linked to higher chloride concentrations.

2.7.1.2 Binder content and w/b ratio

The water-binder (w/b) ratio is a widely used concrete parameter which is generally considered as an indicator of strength. However, an increase in strength of concrete can be associated with a refinement of the pore structure. This refinement of the pore structure has further benefits of decreasing the permeability of concrete to moisture, oxygen and chlorides. As a result, the w/b ratio and cement content have been incorporated in the design guidelines presented in European National Standards and shown in Table 2.3 (BS EN 206, 2013).

Table 2.3: Recommended limiting values for composition and properties of concrete (BS EN 206, 2013)

Chloride-induced corrosion by exposure to sea water			
Limiting criteria	**XS1**	**XS2**	**XS3**
Maximum w/c	0.50	0.45	0.45
Minimum strength class	C30/37	C35/45	C35/45
Minimum cement content (kg/m^3)	300	320	340
Minimum air content	-	-	-

The effect of the w/b ratio on the corrosion rate of reinforcing steel was experimentally investigated by Mangat, Khatib & Molloy (1994). The results are presented in Table 2.4, where it is evident that an increase in the w/b ratio resulted in an elevated corrosion rate. This increase may be linked to the increased permeability allowing easier transport of oxygen and moisture. It is also worth noting that a higher w/b ratio can be linked to a lower concrete resistivity (Otieno, 2008). This will affect the ease of transport of hydroxyl ions and can directly affect the corrosion rate.

Table 2.4: Effect of w/b ratio on the corrosion rate (after Mangat, Khatib & Molloy, 1994)

w/b ratio	**Cement Content (kg/m^3)**	**i_{corr} (µA/cm^2)**
0.45	430	0.13
0.58	430	0.65
0.58	330	0.62
0.58	530	0.52
0.76	430	2.16

2.7.1.3 Cover thickness

The concrete cover, also known as covercrete, is an essential protection mechanism for reinforcing steel. Concrete cover of between 50 to 70 mm is recommended by Alexander & Mackechnie (2003) for reinforced concrete in the marine environment. Alexander & Mackechnie (2003) indicate that insufficient concrete cover can be detrimental even if a high quality concrete is used. It is also worth noting that excessively large cover (>75 mm) can be detrimental to corrosion of reinforcing steel and can result in cracking of the concrete surface which develops a path of ingress for chloride ions. The

effect of the cover depth on time to corrosion initiation is illustrated in Figure 2.8 (shown on page 19) for different binder types; while, Figure 2.20 shows how the cover thickness affects the oxygen diffusion flow rate in concrete.

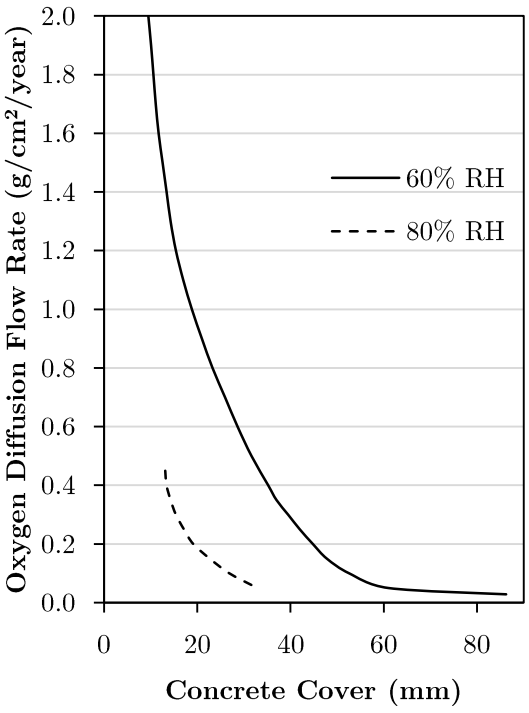

Figure 2.20: The effect of concrete cover depth on oxygen diffusion (after Bentur *et al.*, 1997)

2.7.1.4 Cracking

Cracks in concrete develop a path of ingress for moisture, oxygen and chlorides to penetrate to the reinforcing steel. This ultimately results in an acceleration of deterioration through corrosion of the embedded reinforcement (Otieno, 2008). Cracks should be differentiated based on their origin and relationship to corrosion of the reinforcing steel. There are two main crack development mechanisms which should be considered in relation to reinforcement corrosion. Cracks can develop from the tensile strength of concrete being exceeded or from corrosion of the embedded reinforcement.

Cracking of concrete by exceeding tensile strength develops a path of ingress for moisture, oxygen and chlorides. The concrete cracks as a coping mechanism and the cracks will widen with continued loading. This will lead to further ingress of deleterious compounds exposing the reinforcing steel to possible corrosion. In this case the cracking causes the reinforcing steel to corrode.

On the other hand, cracking can be caused by the corrosion of the embedded reinforcing steel. The oxidation of the anode (iron) produces a corrosion product which can have a resultant increase in volume of up to 6.5 times the volume of the original steel. This causes an inherent increase in stress in the concrete and can result in the development of cracks. These cracks then act to further accelerate the rate of ingress of chlorides and oxygen through an easier path.

Otieno (2008) investigated the effects of stress-induced cracking on the corrosion rate, including the effective depth, width, frequency and orientation of the cracks. Selected results are presented in Figure 2.21 to show the effect of cracking on the corrosion rate.

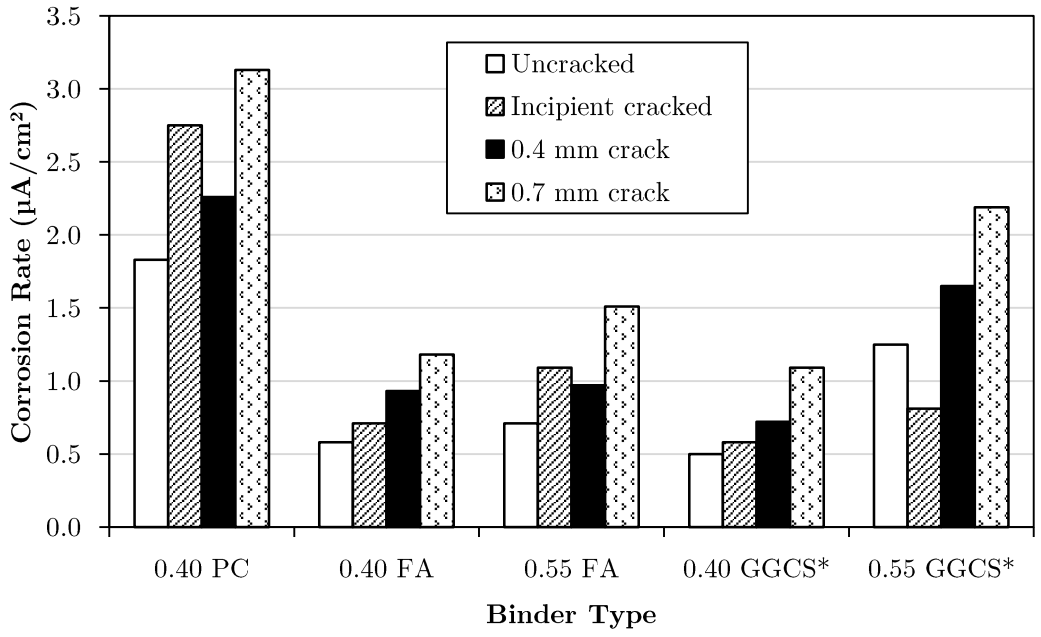

*GGCS – Ground granulated corex slag

Figure 2.21: Effect of cracking on corrosion rate for 20 mm cover (data from Otieno (2014))

2.7.1.5 Effect of chloride content

In environments of high chloride exposure, the infiltration of a deleterious amount of chlorides is inevitable; it is just a matter of time (Gjørv, 1972). The penetration of chlorides will cause the depassivation of the steel with the electrical resistivity and the oxygen availability governing the rate of reinforcement corrosion (McCarter & Vennesland, 2004). The availability of chlorides is more critical in the initiation process (discussed in Section 2.5); however, the chloride content does impact the subsequent rate of reinforcement corrosion.

The chloride content primarily affects the anodic reaction requiring that the chloride threshold value is surpassed, discussed in Section 2.5.2.3. Moreover, the chloride content has a minor influence on the actual corrosion process (Bakker *et al.*, 1994). The influence of chlorides on the initiation of corrosion is discussed in Section 2.5.2.2; however, assuming prior initiation of corrosion, the chloride content will have a notable influence on the moisture content and electrical conductivity of the concrete.

The effect of the chloride content on the moisture content and electrical resistivity was investigated experimentally by Saleem *et al.* (1996). The results were originally presented as a mass per volume of concrete which have been converted to a mass by weight of binder (assuming a binder content of 400 kg/m^3 and unit weight of concrete of 2400 kg/m^3). The adapted findings are presented in Figure 2.22 where it is evident that an increase in the chloride content will result in a decrease in the electrical resistivity.

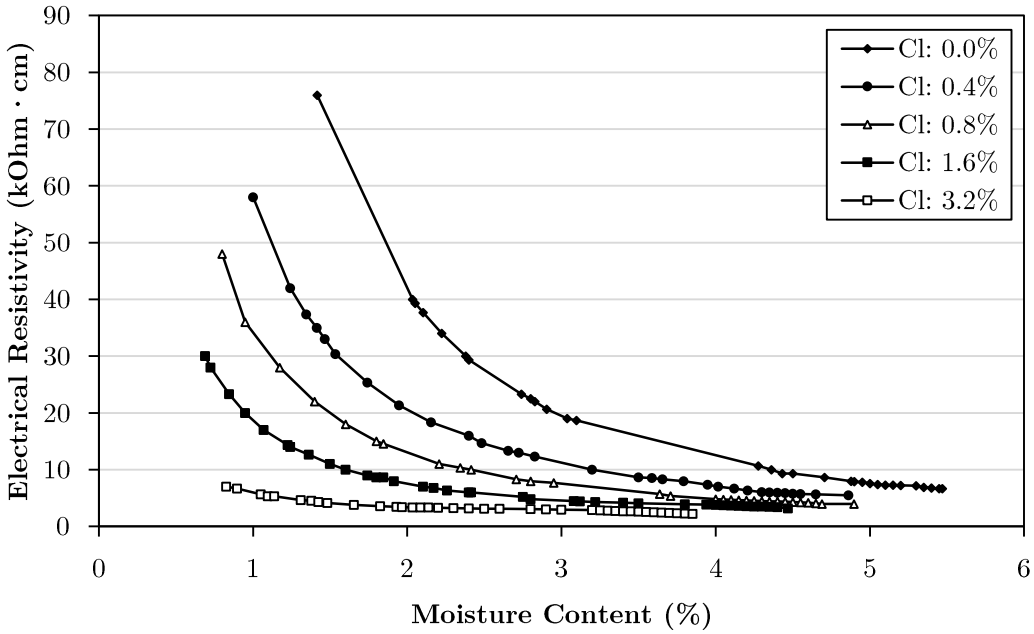

Figure 2.22: Relationship between moisture content and electrical resistivity in chloride-contaminated concrete (after Saleem *et al.*, 1996)

2.7.1.6 Marine environment chloride profiling

As discussed in Section 2.7.1.1, the marine environment is typically divided into four zones, as shown in Figure 2.23. This discussion will consider the submerged, tidal and splash zone for relevance to this research.

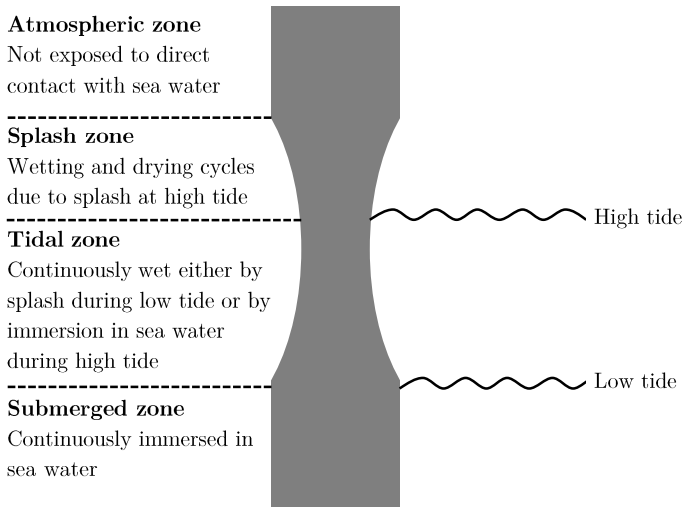

Figure 2.23: Schematic of marine environment exposure conditions (after Ghods *et al.*, 2005)

Each zone is exposed to different exposure conditions and thus chlorides will follow differing mechanisms of ingress. In the submerged zone chloride will ingress through diffusion; while chloride in the tidal and splash zones will enter through a combined convection and diffusion process. Drying of the surface zone leads to deposition of chlorides and thus a relatively higher chloride content is expected in the splash and tidal zones. Ghods *et al.* (2005) investigated this phenomenon through a

field study in the Persian Gulf. The results somewhat confirmed the expectations with Figure 2.24 showing how the chloride content varies according to the exposure conditions. The 0.40 PC specimens clearly depicts higher chloride contents in the tidal and splash zones; however at various SF replacement levels this phenomenon is not as clear.

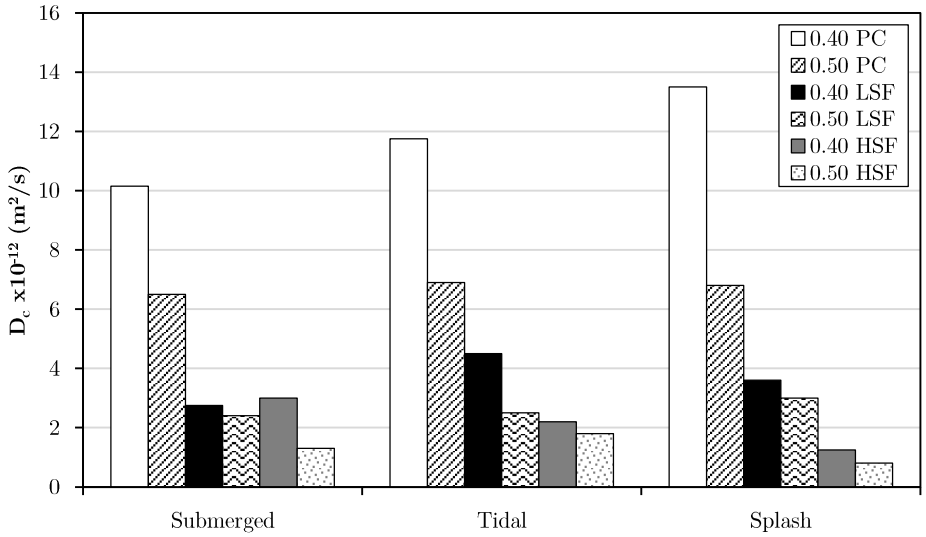

*LSF – 7.5% SF replacement

*HSF – 15% SF replacement

Figure 2.24: Diffusion coefficient at different exposure conditions (after Ghods *et al.*, 2005)

2.7.1.7 Temperature

The temperature of the environment has a direct impact on the corrosion rate. The corrosion rate generally increases as the temperature increases. However, Zivica (2003) found that this relationship between temperature and corrosion rate peaks at a temperature of about 40°C. At temperatures higher than 40°C the rate of corrosion decreases. Zivica (2003) attributes this reduction in corrosion rate to the decreased solubility of oxygen in the pore solution at higher temperatures.

2.7.2 Effect of moisture content

The moisture content of concrete is controlled through the porosity and the site-specific exposure conditions. In the marine environment, cycles of wetting and drying cause partial saturation of concrete. If the cycles of drying are sufficiently short, concrete will not have sufficient time to dry out to the level of the reinforcement and will effectively be saturated at the reinforcement. This has the consequence of ensuring sufficient moisture is available for corrosion, but may also limit the transport of oxygen to the reinforcing steel (Correia *et al.*, 2006). As discussed in Section 2.7.1.1, a region of this nature will be susceptible to relatively rapid ingress of chlorides but corrosion may not occur due to a lack of oxygen availability.

2.7.2.1 Measuring the moisture content

Direct measurements of the moisture content are complicated by the pore structure and the heterogeneous nature of concrete. It is often more practical to measure the internal relative humidity and infer a moisture condition. A relationship between the relative humidity and the moisture

content in concrete is illustrated in Figure 2.25. This relationship is presented for conditions of equilibrium and may vary due to changing environmental conditions and fluctuating moisture conditions (as found in the tidal zone). This figure is not suitable for concrete exposed to cyclic wetting and drying but it presents a basic relationship between relative humidity and the moisture content under ideal conditions.

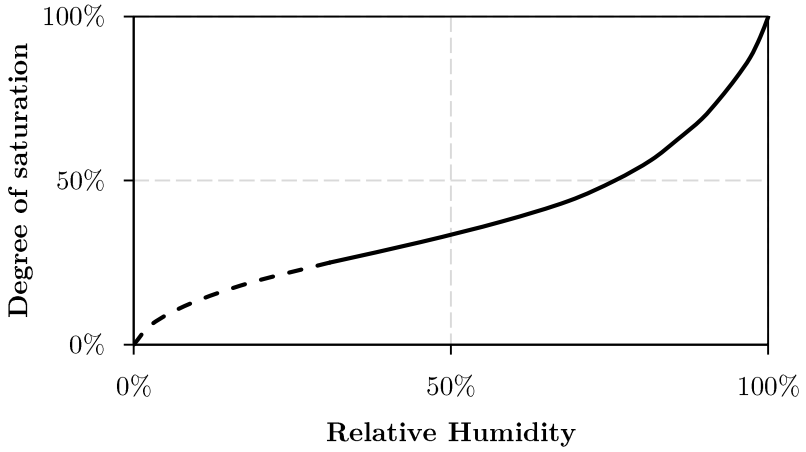

Figure 2.25: Water content as a function of relative humidity, in conditions of equilibrium (after Bertolini, 2004)

2.7.2.2 Moisture at a microscopic level

The moisture content of concrete is directly influenced by the adsorption and desorption of water to/from the surrounding conditions (Hunkeler, 2005). This process involves the transfer of moisture between the concrete and its surrounding environment. The process of moisture movement is governed by the pore structure (pore radii and distribution), pore water composition and the relative humidity of the surrounding air. The humidity of the surrounding air is a site-specific characteristic, while the pore structure and pore water composition are intrinsic properties relating to a specific concrete mix design and subsequent curing. The intrinsic properties of the concrete are primarily influenced by the binder type, w/b ratio, curing conditions and the age of the concrete (Hunkeler, 2005).

The pore structure is the primary intrinsic property of concrete that governs the moisture content of concrete in equilibrium with its external environment. Connected pores with access to the external environment will be exposed to varying saturation conditions depending on the size of the capillary pores. A threshold pore size exists whereby pores larger than this specific size will be filled with air, while smaller pores will be water filled. A lower w/b ratio and a higher degree of hydration will result in the formation of a larger volume of gel products compared to the volume of capillary pores. This is significant for the bonding energy required to hold water within the concrete matrix. The interlayer and gel products hold free water much more tightly compared to the capillary pores. As a result, when the paste dries, water is first lost from the capillary pores, then the adsorbed and gel-pore water and finally the interlayer water (Alexander & Beushausen, 2009). The relative pore sizes and connectivity are illustrated in Figure 2.26.

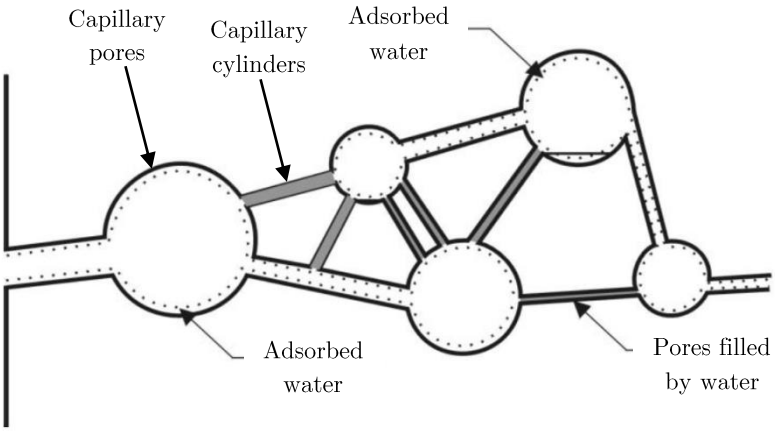

Figure 2.26: Water present in capillaries in equilibrium with a non-saturated atmosphere (Bertolini, 2004)

The effect of the relative humidity on the water content in concrete is illustrated in Figure 2.27. It is evident that purely adsorption of moisture occurs below a relative humidity of 40%. At a relative humidity higher than 40%, the capillary pores are also filled with water while adsorption continues. This illustrates the concept of moisture bonding energy discussed by Alexander and Beushausen (2009).

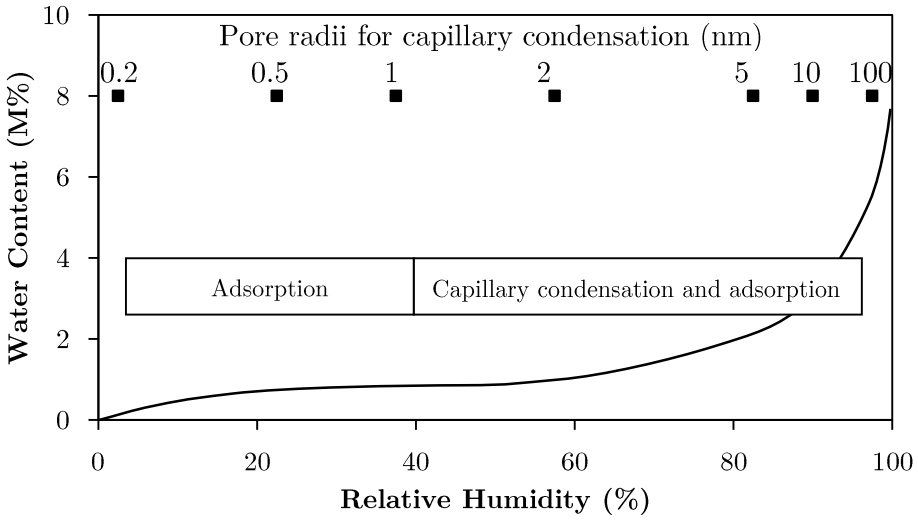

Figure 2.27: Typical sorption isotherm of concrete (after Hunkeler, 2005)

The moisture content of concrete structures in the marine environment is generally high (Gjørv *et al.*, 1986). The saturated condition of the concrete and interconnected nature of the pore structure directly affects the kinetics of the transport processes within concrete (Bertolini, 2004). Saturation of the pore structure will promote the ingress of chlorides by diffusion and other processes that occur in aqueous solutions. However, the low solubility of oxygen and carbon dioxide in water at standard temperatures will hinder their movement through the cover concrete. Consequently, saturated conditions will promote the transport of chlorides but may hinder the ingress of critical concentrations of oxygen. As a result, cycles of wetting and drying appear to be the most severe

conditions whereby sufficient amounts of oxygen are available without significantly reducing the transport of moisture and chlorides.

2.7.2.3 Uptake of moisture

Capillary suction and diffusion allow the infiltration of moisture under cyclic wetting and drying. Capillary suction is naturally more effective in dry concrete (low moisture content), as shown in Figure 2.28. Furthermore, it is evident from Figure 2.28 that the water uptake coefficient increases as the w/b ratio increases. This is expected due to the decrease in gel pores with respect to the capillary pores. As a result, capillary pores will be filled relatively rapidly in concrete with a high w/b ratio.

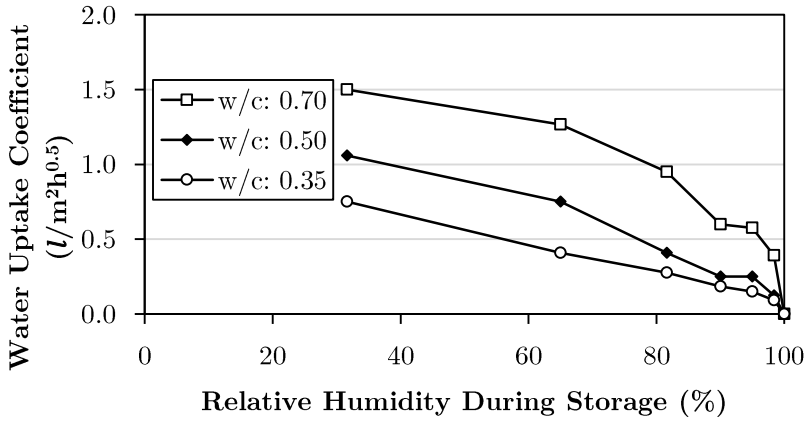

Figure 2.28: Water uptake coefficient for various storage conditions (after Hunkeler, 2005)

The relatively high moisture content leads to a high degree of saturation and an associated low electrical resistivity. There is an abundance of moisture and capacity to transfer hydroxyl ions in the corrosion process. As a result, the diffusion of oxygen becomes the controlling parameter on the corrosion rate in the marine environment (Gjørv *et al.*, 1986). The penetration of oxygen and carbon dioxide is limited and thus hinders the progress of chloride and carbonation induced corrosion. This is due to the decreased solubility of oxygen and carbon dioxide in water, discussed further in Section 2.7.3 (Hunkeler, 2005).

2.7.2.4 Influence on corrosion rate

The moisture content is a critical component in corrosion under cyclic wetting and drying. Dry or saturated conditions both tend to stunt corrosion, while moisture contents between these two extremes will be conducive to the development of corrosion. Concrete free from moisture will not corrode since the presence of water is an integral component to the development of corrosion. Without the presence of water there is no electrolyte to carry the current between the anode and the cathode. On the other hand, saturated concrete does not allow sufficient oxygen to penetrate through the concrete and assist the corrosion process. As a result, the two extremes of moisture content are desired for limiting corrosion.

When concrete is in equilibrium with the atmosphere, the moisture content can be directly correlated to the relative humidity (Bertolini *et al.*, 2013). However, in the marine environment

concrete is exposed to cycles of wetting and drying and this is only relevant to the exterior surface. This phenomenon is governed by the fact that concrete absorbs water faster than it loses it and, as a result, the moisture content at the reinforcement will be higher than the equilibrium level with the atmosphere. The effect of the external relative humidity on the corrosion rate is illustrated in Figure 2.29.

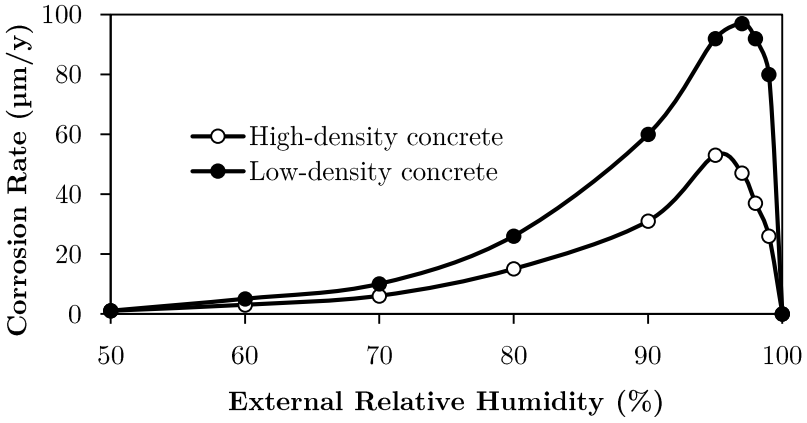

Figure 2.29: Corrosion rate of concrete as a function of external relative humidity (after Bertolini *et al.*, 2013)

2.7.2.5 Effect on the diffusion of oxygen

The relative humidity (RH) can be directly related to the moisture content but allows for easier measurements. The RH and moisture content generally control the ingress of oxygen and carbon dioxide into the concrete cover. The diffusion coefficient of oxygen decreases as the RH increases, as illustrated in Figure 2.30.

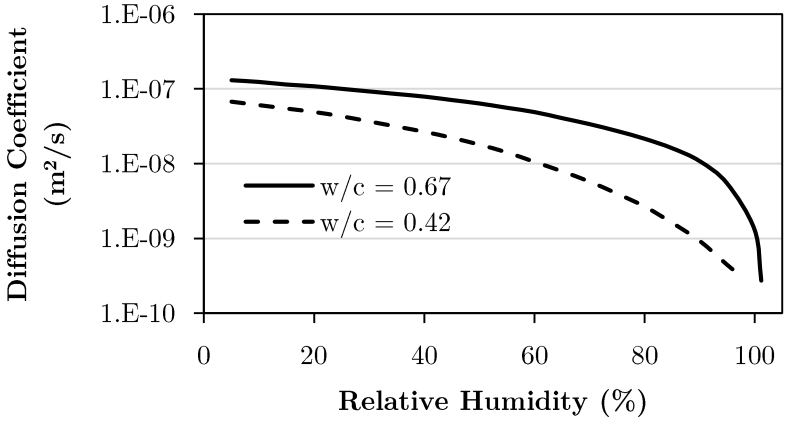

Figure 2.30: Effect of relative humidity on the diffusion coefficient of oxygen (after Bentur *et al.*, 1997)

2.7.2.6 Electrical resistivity

The electrical resistivity is a measure of the ability of a material to resist the transfer of charge. It is a geometry independent property that relates an applied voltage to a resulting current multiplied

by a cell constant (Hornbostel *et al.*, 2013). It is generally accepted that the corrosion rate is inversely proportional to the resistivity.

According to Raupach (1996), the corrosion rate is controlled by the concrete electrical resistivity once corrosion of the reinforcing steel has been initiated. The electrical resistivity is primarily dependent on the moisture condition of the concrete, permeability and interconnectivity of the pore structure, as well as the concentration of the ionic species in the pore structure (Heckroodt, 2002).

The electrical resistivity can be measured by applying an alternating current and measuring the potential difference. This is commonly implemented using a portable probe for site and laboratory work. The most commonly used probe is a four-point Wenner probe with guideline values for the susceptibility to corrosion shown in Table 2.5 (Heckroodt, 2002).

Table 2.5: Likelihood of corrosion based on concrete resistivity (Heckroodt, 2002)

Resistivity (kΩ-cm)	Likely corrosion rate for given corrosive conditions
<12	High
12-20	Moderate
>20	Low

2.7.3 Effect of oxygen availability

As discussed briefly in Section 1.1, Raupach (1996) describes an equivalent electric circuit to illustrate the resistance of the various components in the corrosion of reinforcing steel (see Figure 1.2). Since the reduction of oxygen occurs at the cathode, this component will be the limiting factor in oxygen deprived environments, to be considered in more detail in this section.

In submerged or saturated concrete, the presence of moisture is guaranteed and thus the corrosion rate is primarily controlled by the diffusion of dissolved oxygen through the concrete cover and, hence, the availability of oxygen for corrosion (Correia *et al.*, 2006). This assumption is based on the fundamental electrochemical reactions in the corrosion of steel, with the only possible cathodic reaction being the reduction of oxygen (Garcia *et al.*, 2002). The closest alternative cathodic reaction is the decomposition of water, which only occurs in corrosion pits where highly-negative potentials below -940 mV CSE can develop (Raupach, 1996). However, it has been reported that once corrosion has been initiated, the process will continue even if there is no presence of oxygen (Alonso *et al.*, 1998). Hence, the concept of the limiting cathodic reaction needs further clarification for the effects of oxygen availability.

Raupach (1996) indicates that the cathodic resistance (R_C) can be further subdivided into a component for the activation resistance of the cathode and for the resistance due to oxygen diffusion, shown in Eq. 2.13. The corrosion reaction will be controlled by limiting oxygen availability when the cathodic resistance (R_C) is significantly large that it controls the reaction process. The oxygen diffusion resistance (R_{C,O_2}) is generally an accepted component of the cathodic resistance, but the charge transfer or activation resistance ($R_{C,C}$) is not well understood in literature (Raupach, 1996).

$$R_C = R_{C,C} + R_{C,O_2} \quad \text{(Eq. 2.13)}$$

where: R_C is the cathodic resistance (cm^2/s), $R_{C,C}$ is the activation resistance of the cathodic reaction (charge transfer) and R_{C,O_2} is the oxygen diffusion resistance between the concrete and the steel surface.

The component of the cathodic resistance which governs how the reaction proceeds is primarily influenced by the surrounding ambient conditions. The diffusion resistance is large in long-term oxygen deprived conditions and becomes the controlling parameter. However, a similar consensus has not been achieved for concrete exposed to cyclic wetting and drying. As a result, Raupach (1996) completed experimental testing to quantify the effect of the cathodic resistance and provided four divisions based on the availability of oxygen:

- Permanently dry
- Short-term wetting
- Long-term wetting
- Permanently saturated

The cathodic resistance has distinctly different influences on the corrosion rate in each of these classifications, as illustrated in Figure 2.31. In permanently dry conditions (a), oxygen is readily available with the cathodic resistance unlikely to have any significant impact on the corrosion rate. However, exposure to moisture will directly affect the corrosion reaction. When concrete is exposed to short-term wetting (b), the primary influence is an increase in the conductivity. These conditions do not cause oxygen deprivation but do allow a substantial amount of moisture into the pore system. This will result in an increase in the short-term corrosion rate during the wetting period which will slowly revert to the corrosion rate level prior to wetting. The oxygen availability has a negligible effect on the corrosion rate and does not cause oxygen deprivation at the level of the steel. The increased initial corrosion rate can be attributed to the additional moisture in the system allowing hydroxyl ions to be transported with more ease.

Exposure to long-term wetting (c) can be characterised as subjecting reinforced concrete to sufficiently long water exposure to cause oxygen deprivation. This allows the lack of oxygen to have a significant impact on the corrosion rate. The corrosion rate will increase initially due to the elevated conductivity (similarly to short-term wetting) but then will decrease rapidly as the cathodic reaction slows down. At the end of the long-term wetting period the corrosion rate will revert to the original levels before wetting.

The final classification describes permanently submerged reinforced concrete (d). In this category it is evident that the corrosion rate follows a similar path to long-term wetting but the corrosion rate remains low under continued wetting. In this region the diffusion of oxygen will dominate how the corrosion reaction proceeds. Andrade *et al.* (1990) indicates that this is the only case (permanently submerged) where cathodic control can be implemented by limited oxygen availability.

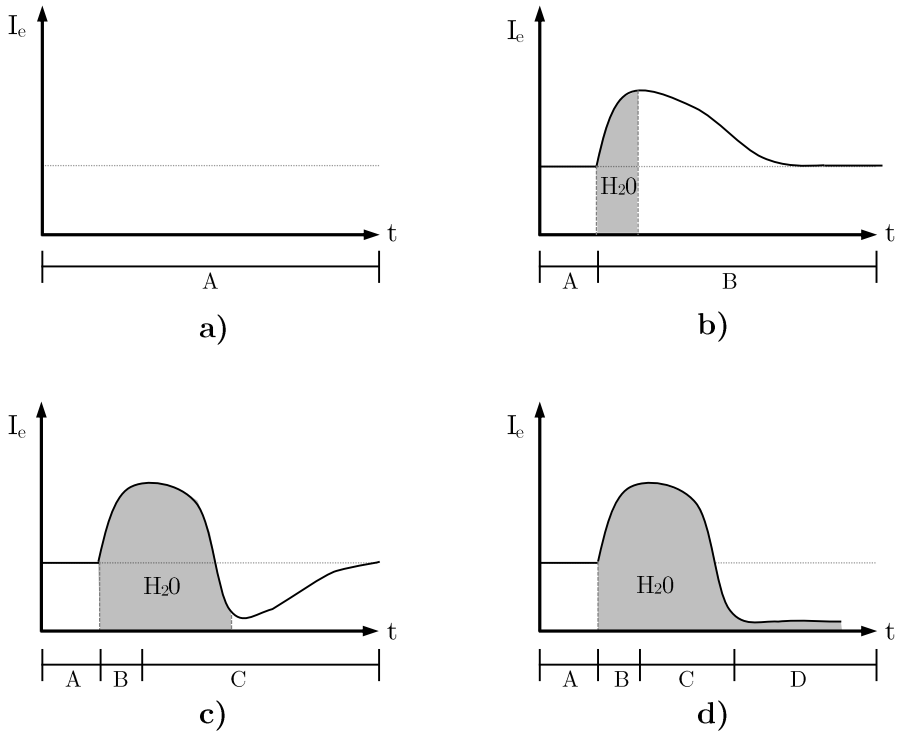

Figure 2.31: Corrosion rate of reinforced concrete that is a) permanently dry, b) exposed to short-term wetting, c) exposed to long-term wetting and d) permanently saturated (after Raupach, 1996a)

2.7.3.1 Diffusion resistance of oxygen

The diffusion, and thus availability, of oxygen is only of importance when the cover concrete is exposed to long-term or periodical saturation (Raupach, 1996). In dry concrete there is an abundance of oxygen and thus it is not a limiting parameter on the corrosion process. It is also worth noting the experimental work done by Correia *et al.* (2006) which showed that in fully saturated concrete, the oxygen transport is reduced and thus the oxygen concentration is reduced. This further emphasises the governing nature of the oxygen availability on the corrosion rate in submerged reinforced concrete.

The rate of diffusion of oxygen is primarily controlled by the concrete quality, permeability and the moisture content (Hunkeler, 2005). The pore saturation directly affects the rate of oxygen ingress since gases diffuse much more rapidly through open pores. The diffusion of oxygen in water is 4-5 orders of magnitude slower than diffusion through open pore (Bertolini, 2004). As a result, the diffusion of oxygen in concrete will be directly affected by the moisture content. The effective diffusion coefficient of oxygen in partially saturated concrete can be approximated using Eq. 2.14.

$$D(O_2, C) = \frac{D_L\left(\frac{D_L}{D_W} - W\frac{D_L}{D_W} + 3\right)}{2W\left(\frac{D_L}{D_W} - 1\right) + \frac{D_L}{D_W} + 2} \qquad \text{(Eq. 2.14)}$$

where: $D(O_2,C)$ is the oxygen diffusion coefficient in concrete (cm^2/s), D_L is the oxygen diffusion coefficient in dry concrete (cm^2/s), D_W is the oxygen diffusion coefficient in wet concrete (cm^2/s) and W is the water content of the concrete (vol. %).

Hunkeler (2005) used Eq. 2.14 to develop diffusion coefficient curves, shown in Figure 2.32, where it is evident that the porosity has a significant impact on the diffusion of oxygen at a lower relative humidity. However, the porosity has a less significant effect on the diffusion of oxygen at a relative humidity which borders on complete saturation of the pore space. These curves show good agreement with experimental results completed by various authors (Hunkeler, 2005).

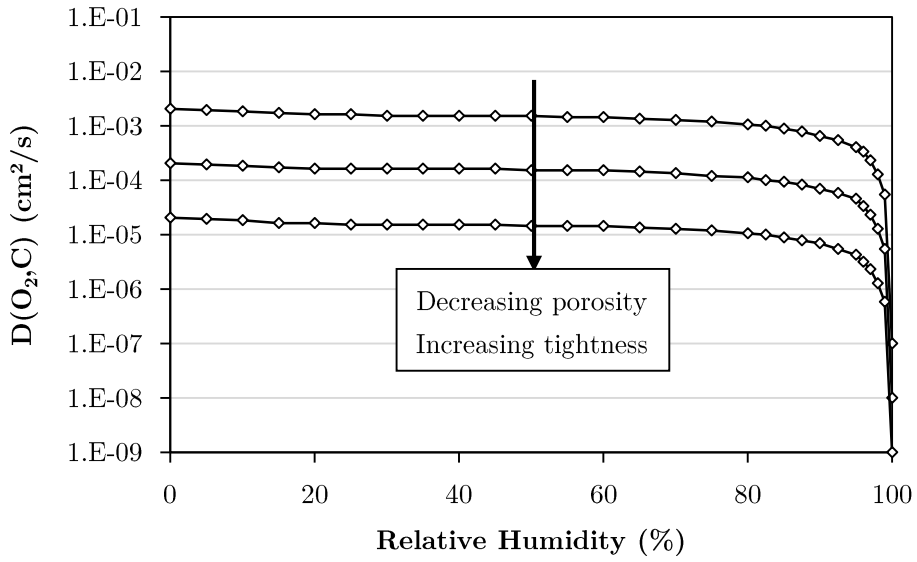

Figure 2.32: Influence of the relative humidity on the diffusion coefficient of oxygen (after Hunkeler, 2005)

2.7.3.2 Effect of ambient conditions

Oxygen may be present in its gaseous form or as dissolved oxygen. In submerged concrete there is only dissolved oxygen, which may not be sufficient to promote corrosion due to limited oxygen availability. This is a result of the increased humidity which is the primary controlling variable on the role of the oxygen availability on the corrosion rate (Andrade *et al.*, 1990). Consequently, the ambient conditions, more specifically the humidity, govern which cathodic resistance component will control the corrosion reaction (Raupach, 1996). The effect of the relative humidity on the diffusion of gases and ions through concrete is illustrated in Figure 2.33. The shape of the curves for the diffusion coefficients are primarily influenced by the sorption isotherm (Hunkeler, 2005)

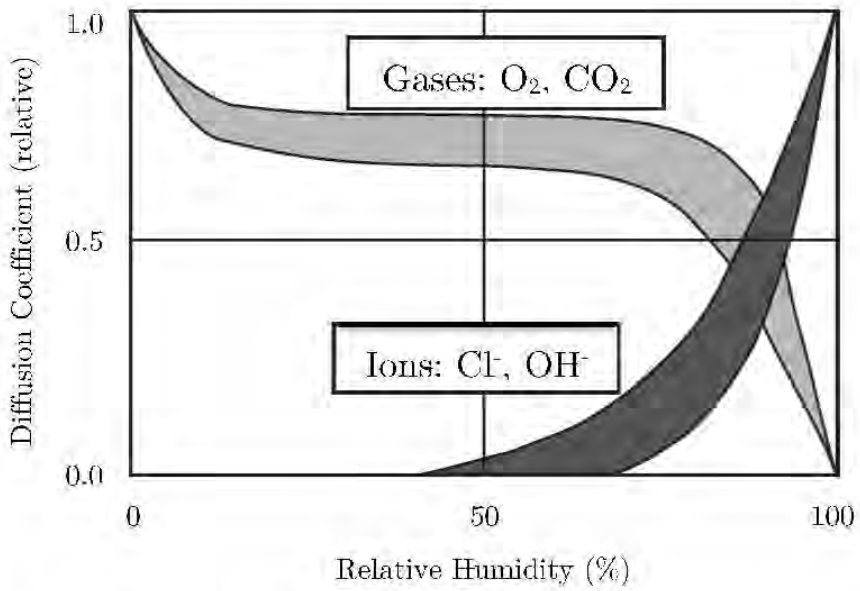

Figure 2.33: Schematic drawing showing the influence of the relative humidity on the diffusion coefficients of gases and ion (after Hunkeler, 2005)

It is critical to note the effect of permanent saturation on the corrosion potential of embedded reinforcing steel, illustrated in Figure 2.34. Under these specific experimental conditions, after approximately 28 days of complete immersion in water, Hunkeler (2005) noted a distinct drop in the potential. This drop was associated with the depletion of the available oxygen at the level of the reinforcement. With continued submersion the potential will remain at this low level, while the corrosion potential may significantly change if allowed to dry to the level of the reinforcing steel. It is worth noting that an assessment of the potential according to ASTM C876-09 (2009) would incorrectly classify the corrosion potential as severe.

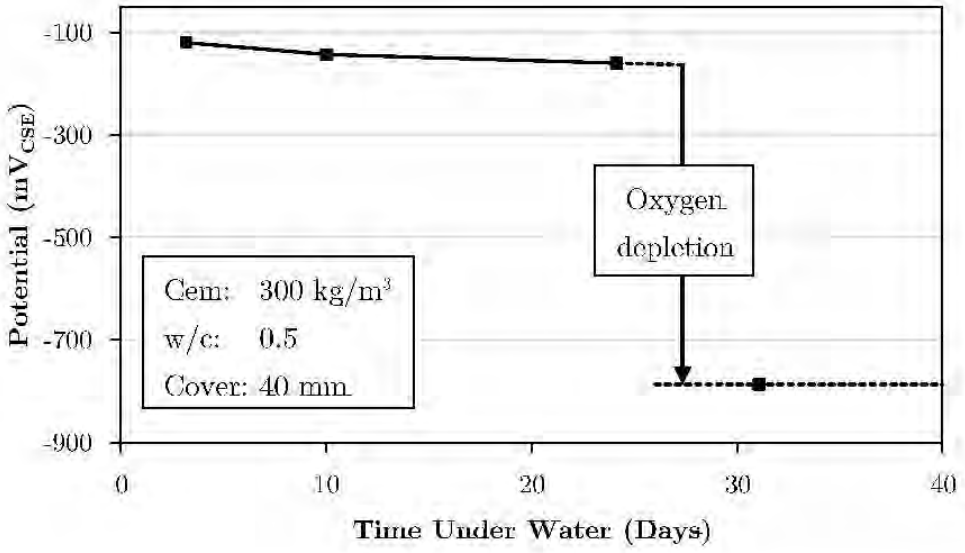

Figure 2.34: Corrosion potential of steel in concrete under complete immersion (after Hunkeler, 2005)

2.7.3.3 Reduction of oxygen

The reduction of oxygen is often simplified to a single equation showing the cathodic reaction to form hydroxides (Eq. 2.15).

$$O_2 + 2H_2O + 4e^- \rightarrow 4OH \qquad \text{(Eq. 2.15)}$$

This is, however, a simplification and in an alkaline solution this reaction will proceed in at least two steps. The production of hydrogen peroxide (H_2O_2) is formed as an intermediary product which is then reduced to form hydroxide ions (Eq. 2.16 and Eq. 2.17 below). The rate of hydrogen peroxide formation is probably governed by the simple ionization of the oxygen molecule.

$$O_2 + 2H_2O + 2e^- \rightarrow H_2O_2 + 2OH^- \qquad \text{(Eq. 2.16)}$$

$$H_2O_2 + 2e^- \rightarrow 2OH^- \qquad \text{(Eq. 2.17)}$$

The existence of this intermediary product (hydrogen peroxide) may explain the continued corrosion without the diffusion of oxygen to the reinforcing steel. Hydrogen peroxide adsorbed at the steel surface may continue the cathodic reaction without the presence of oxygen (Raupach, 1996).

2.7.3.4 Test methods for measuring oxygen availability

The reduction of oxygen is generally accepted as the only cathodic reaction in the corrosion of steel immersed in concrete (Garcia *et al.*, 2002; McCarter & Vennesland, 2004). Three methods exist for measuring the oxygen diffusion rate; namely mechanical driving forces, diffusion cell devices and electrochemical driving forces (Andrade *et al.*, 1990).

Mechanical driving forces provide an estimate of the diffusion of oxygen through concrete. The principles of gas permeability are applied by applying a pressure gradient and measuring the pressure decay. The resulting oxygen diffusion rates are typically greater than those experienced under natural conditions and could lead to erroneous conclusions (Garcia *et al.*, 2002). The primary shortfall of this testing method is that it does not adequately account for changes in the humidity (Andrade *et al.*, 1990)

Alternatively, diffusion cell devices allow natural diffusion processes to occur. These tests take much longer but typically provide a better estimate of the diffusion of oxygen in concrete. Diffusion cell devices are limited in their application requiring submerged conditions to accurately determine the rebar corrosion rate (Garcia *et al.*, 2002). However, it should be noted that in these submerged conditions it is not possible to determine the effect of the humidity on the corrosion rate.

The third method involves the application of electrochemical driving forces. This method requires that embedded metal is polarised at a potential where the reduction of oxygen is the primary reaction (Andrade *et al.*, 1990). Electrochemical driving forces have been regarded as the most accepted test method and have been implemented by various researchers to determine oxygen availability (Andrade *et al.*, 1990; McCarter & Vennesland, 2004; Correia & Salta, 2007; Correia *et al.*, 2006; Gjørv *et al.*, 1986). It is the most reliable method of measuring the oxygen availability at the rebar surface and its influence on the corrosion rate (Andrade *et al.*, 1990). Specimens can be

tested at various humidity conditions allowing for better simulation of real environmental exposure conditions.

2.7.4 Effect of the binder type

An appropriate binder type can assist in both delaying the initiation of corrosion and slowing down the corrosion rate. Supplementary cementitious materials (SCMs) cause a refinement of the pore structure which can slow down the penetration of chlorides. Furthermore, the binding capacity of certain cement extenders can reduce the amount of free chlorides and extend the time to corrosion initiation (discussed in more detail in Section 2.5.3). SCMs can also extend the duration of the propagation period by reducing the ease of transport of moisture and oxygen through the concrete (Polder, 1996). The inclusion of a SCM has been shown to increase the resistivity and thereby decrease the achievable corrosion rate (Thomas, 2013).

However, it should be noted that blends of fly ash and slag require extended curing durations to achieve the aforementioned benefits. This is due to the fact that SCMs result in the delayed formation of CSH and thus require extended periods of moist curing (Alexander & Mackechnie, 2003).

Scott (2004) showed that increasing the thickness of the cover concrete is more effective in limiting the corrosion rates where the corrosion reaction is governed by cathodic control (limited oxygen), which tends to occur in PC concrete. However, if SCMs are used the thickness of the cover concrete has less effect on the corrosion rate, while the corrosion rate will generally be controlled by the electrical resistivity (Scott, 2004).

2.7.4.1 Porosity and permeability

A key benefit of the inclusion of SCMs is a refinement of the pore structure. SCMs promote the formation of CSH gel which assists to develop a denser cement paste microstructure. A denser cement matrix will result in a reduction in the total porosity as well as a lower degree of interconnectivity between the pores.

Slag-bearing concretes have been shown to have similar overall porosity to Portland cement concrete. However, a slag bearing concrete will have a more refined pore structure characterised by an increase in the fine gel pores and a reduction in the connectivity of the capillary pores (Parrott, 1995). As a result, an improved permeability of slag bearing concrete can be expected despite no reduction in the overall porosity (Scott, 2004).

The inclusion of FA as a replacement for cement has been shown to increase the total porosity (Berry *et al.*, 1989 as cited in Scott, 2004). However, similarly to slag bearing concrete, the connectivity of the capillary pores is significantly reduced.

CSF is primarily used to increase the early strength development and to improve the permeability of concrete (Neville, 2004). CSF particles are typically 100 times smaller than Portland cement particles and are able to pack tighter on the surface of aggregates (Neville, 2004). This allows

the interfacial transition zone (ITZ) to develop improved permeability and provides greater resistance to the ingress of chlorides.

2.7.4.2 Oxygen and moisture transport

Davies (1954) completed one of the earliest studies on the effect of SCMs on the water permeability of concrete. It was found that replacing 30-50% of the binder with FA resulted in an increased permeability of concrete at 28 days. This trend was reversed at later ages with the FA blends producing significantly more permeable concrete in the long term (Thomas, 2013). An increase in the 28-day permeability can be justified by the delayed cementing reaction of the pozzolanic binder.

Table 2.6: Effect of fly ash on the permeability of concrete (after Thomas, 2013)

Source	Fly ash		Relative permeability	
	% by mass	w/cm	28 days	6 months
-	0	0.75	100	26
Chicago	30	0.70	220	5
	60	0.65	1410	2
Cleveland	30	0.70	320	5
	60	0.65	1880	7

The inclusion of CSF at various replacement levels has the effect of increasing the short-term permeability while decreasing the longer-term permeability, shown in Table 2.7. This testing was conducted by Hooton (1993) on paste samples with the high short-term permeability justified by the faster cementing reaction of the pozzolanic SCM.

Table 2.7: Effect of silica fume on water permeability (after Thomas, 2013)

Source	Coefficient of permeability ($\times 10^{-13}$ m/s)			
	7 days	28 days	91 days	182 days
100% Type V	6.3	3.8	1.3	0.3
10% Silica fume	10.0	0.9	0.6	0.4
20% Silica fume	6.3	<0.1	0.4	<0.1

2.7.4.3 Resistivity

Scott (2004) showed that the addition of SCMs substantially increases the resistivity. When SCMs are used the corrosion rate is generally controlled by the resistivity. Consequently, an increase in the resistivity will provide a beneficial limitation on the maximum achievable corrosion rate. Control of the corrosion rate through the resistivity is not likely in PC concrete where the cover depth and oxygen availability have a greater influence (Scott, 2004).

2.7.4.4 Corrosion rate

The effect of the binder type on the corrosion rate should be considered for the coupled effect on the transport of chlorides and the chloride threshold value. SCMs may lower the chloride threshold value but produce significantly denser concrete which slows the penetration of chlorides. As a result, Alonso *et al.* (2012) suggests that SCMs should be assessed by measuring the time required to initiate the

onset of corrosion. The effect of the binder type on the time to corrosion has previously been illustrated in Figure 2.7 and Figure 2.8.

Otieno (2014) investigated the effect of a number of parameters on the corrosion rate of steel embedded in concrete. These included laboratory and field specimens, most of which were cracked. However, for the relevance of this study, only the uncracked specimen results were assessed. In this work, Otieno (2014) found that, for a cover depth of 20 mm, replacing Portland cement with 50% GGBS or 30% FA resulted in a decrease in the average corrosion rate by a factor of approximately 3.

2.7.4.5 Suggested dosages

Polder (1996) suggests dosages of 25-30% for FA, 70% for slag and 8% for SF. Polder (1996) expresses some doubt about the use of SF due to the negative side effects of overdosing. These include lowering the pH of the pore solution and lowering the critical chloride content. Polder (1996) also identifies a flaw in the common assumption that an increase in strength can be linked to an increase in durability. A 5% replacement with SF has been shown to increase the compressive strength but does not always ensure improved concrete durability.

2.8 Corrosion Rate Testing Methods

2.8.1 Corrosion rate indicators

A combination of half-cell potential mapping, cover measurements and resistivity can provide an indication of the likelihood of corrosion. However, they do not provide a quantitative measure of the corrosion rate (ACI *et al.*, 2003). Nevertheless, they are useful indicators with details of their theory and application provided to follow. Additionally, corrosion rate monitoring is a specialist field and requires care when analysing and interpreting results. In comparison, these indicators are simple to implement and can be assessed using guideline values.

2.8.1.1 Resistivity

Discussed in Section 2.7.2.6, the electrical resistivity can provide an indication of corrosion potential where active corrosion conditions exist. The resistivity is mainly influenced by the temperature, relative humidity (internal and external), cover depth and the concrete permeability. The governing parameters, and hence the resistivity, provide an indication of the ease of transport for hydroxyl ions in concrete. As a result, the resistivity can be used as an indicator of corrosion in depassivated reinforced concrete.

Without built-in probes, the resistivity is commonly measured using a four-point Wenner probe. In this system four probes are brought into contact with the concrete surface with the outer two probes emitting an alternating current. The potential is then measured between the inner two proves and converted to a resistivity using Eq. 2.18.

$$\rho = 2R\pi x \qquad \text{(Eq. 2.18)}$$

where: ρ is the resistivity, R is the calculated resistance ($R=V/I$) and x is the probe spacing (shown in Figure 2.35).

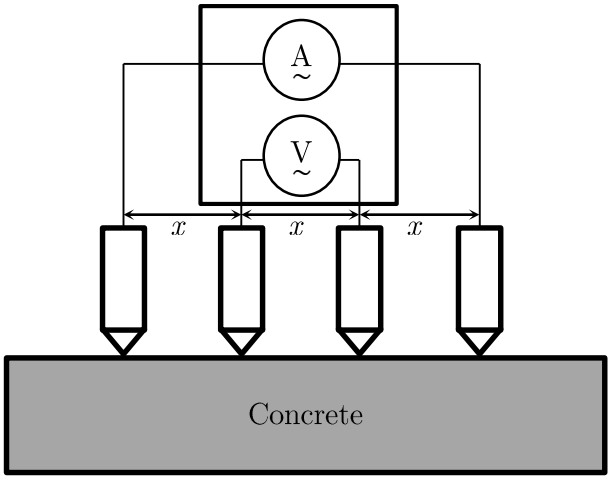

Figure 2.35: Four-point Wenner probe layout

2.8.1.2 Half-cell potential

Measuring half-cell potentials (HCPs) is a typical technique used to perform routine monitoring of reinforced concrete structures. An oversimplified interpretation of results is provided in Table 2.8 where the half-cell potential reading can be linked to a likelihood of corrosion. However, this method does not take into account rate effects and can thus be misleading (Berke *et al.*, 1994), discussed in more detail in Section 2.7.3.2.

Nevertheless, HCP measurements are beneficial in their relative ease in application and provide a short-term monitoring technique. As a result, half-cell potential measurements provide a suitable test method for in-situ reinforced concrete structures. However, the applicability of this technique is limited for experimental work on the corrosion rate of embedded reinforcing steel (due to the abovementioned inaccuracies). As a result, alternative measurement techniques have been developed. These include polarisation and electrochemical impedance techniques which have allowed for much more reliable indications of corrosion rates. Details of these testing methods can be found in Section 2.8.2.

Table 2.8: Interpretation of potential measurements (after Otieno, 2008; ASTM C876-09, 2009)

Cu/$CuSO_4$ Electrode	Ag/AgCl Electrode	Likelihood of corrosion
> -200 mV	> -106 mV	Low – 10% probability that corrosion is occurring
-200 to -350 mV	-106 to -256 mV	Intermediate– Corrosion of the reinforcing steel is uncertain
< -350 mV	< -256 mV	High – 90% Probability that corrosion is occurring
< -500 mV	< -406 mV	Severe – Likelihood of severe corrosion occurring

2.8.1.3 Cover mapping

Cover to reinforcement should be mapped in conjunction with HCP and resistivity measurements. A combination of all these measurements can be used to assess the state of corrosion and possible reasons for the corrosion propagation. The expectation is that numerous corrosion conditions are

brought about through insufficient cover and these locations can be identified with an appropriate cover survey.

2.8.2 Corrosion rate measurement technique

The corrosion rate of reinforced concrete can be measured through various testing methods; including destructive and non-destructive techniques. The electrochemical nature of corrosion allows the rate of corrosion to be determined by measuring the current flow between the anode and the cathode (Berke *et al.*, 1994). In the natural state of corrosion, the current flow between the anode and the cathode is balanced by an equally sized current flow in the opposite direction. Hence, the corrosion rate can be determined by monitoring the effects of a disturbance (perturbation) and accordingly estimating the corrosion rate.

There are a number of alternative methods available to assess corrosion of reinforcing steel. Some of these methods include gravimetric, galvanic current, electrochemical impedance spectroscopy, galvanostatic pulse transient analysis and electrochemical noise. However, the remainder of this section will focus on linear polarisation resistance (LPR) techniques with emphasis on the coulostatic technique. Nevertheless, the applicability of each of the abovementioned corrosion rate measurement techniques is illustrated in Table 2.9.

Table 2.9: Applicability of corrosion test methods (after ACI, 2003)

Method	Laboratory	Site surface	Site embedded	Site retro-fitted
Gravimetric	✓	×	×	×
Galvanic Current	✓	♦	✓	✓
LPR – Potentiostatic	✓	✓	✓	✓
LPR – Galvanostatic	✓	✓	✓	✓
Electrochemical Impedance Spectroscopy	✓	♦	✓	✓
Galvanostatic Pulse Transient Analysis	✓	♦	♦	♦
Electrochemical Noise	✓	♦	♦	♦

✓ Suitable for application

♦ Suitable for application in certain situations

× Not suitable for application on site

2.8.2.1 Linear polarisation resistance

The polarisation resistance (R_p) is essentially a quantification of the resistance of the system to the effects of corrosion (Berke *et al.*, 1994). The linear polarisation resistance (LPR) technique can be further subdivided into galvanostatic and potentiostatic. In the galvanostatic approach, a small potential shift (ΔE) is applied to the working electrode and the resulting current (ΔI) is measured between the working and counter electrode (ACI *et al.*, 2003). Alternatively, the LPR technique can be applied potentiostatically by applying a small current and measuring the associated potential shift. Monitoring the decay caused by the current or potential shift can then be converted to a corrosion current density using the Stern-Geary coefficient and Eq. 2.19.

$$i_{corr} = \frac{B\Delta I}{\Delta E} = 2.303 \cdot \frac{(\beta_a \times \beta_c)}{(\beta_a + \beta_c)} \cdot \frac{\Delta I}{\Delta E} = \frac{B}{R_p} \qquad \text{(Eq. 2.19)}$$

where: i_{corr} is the corrosion current, B is the Stern-Geary coefficient, ΔI is the change in current, ΔE is the change in potential, β_a is the anodic Tafel coefficient, β_c is the cathodic Tafel coefficient and R_p is the polarisation resistance.

The Stern-Geary coefficient (B) depends on the corrosion state of steel and varies between 13 and 52 mV. Commonly accepted values are 26 mV for active corrosion and 52 mV for passive conditions. This investigation focuses on active corrosion and thus a Stern-Geary coefficient of 26 mV was assumed throughout.

This corrosion rate monitoring technique was selected based on equipment availability and suitability for the experimental testing at hand. The steel-concrete interface has a slow response to an electrochemical perturbation and is ideally suited to measurements by the linear polarisation resistance method. A coulostatic technique was selected and is discussed in more detail in Section 2.8.2.2.

2.8.2.2 Coulostatic technique

The coulostatic technique is a LPR technique whereby the relaxation of the potential is measured after the application of a short duration charge (perturbation). This allows relatively rapid corrosion rate measurements with a required monitoring time of at least 30 seconds (Scott, 2004). The potential decay over time is monitored and can be related to the polarisation resistance through the double layer capacitance. This allows corrosion rates to be inferred from the rate of decay caused by a perturbation. A rapid decay of potential indicates a high corrosion current, whereas the decay will be much slower for low corrosion currents. A typical potential transient is illustrated in Figure 2.36 for both low and high corrosion cases.

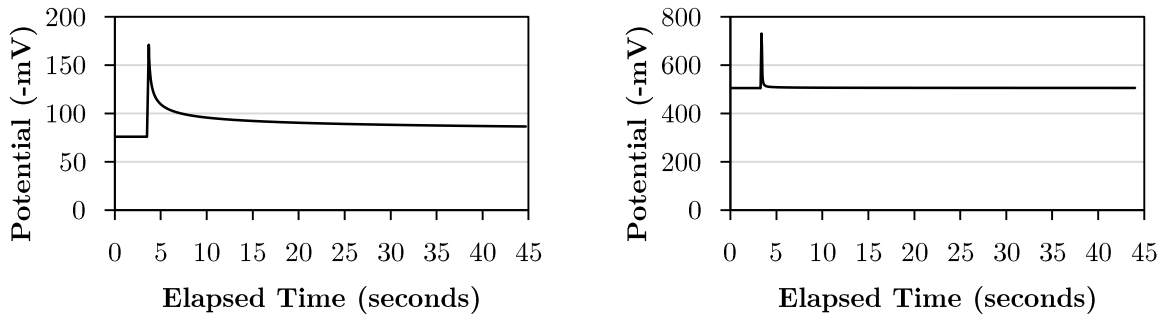

a) b)

Figure 2.36: Potential transient curves after the application of a perturbation showing a case of a) low corrosion current and b) high corrosion current

Glass (1995) investigated the effect of the perturbation duration on the shape of the relaxation transient, illustrated in Figure 2.37. Longer perturbation durations resulted in flatter curves with Scott (2004) suggesting that a pulse duration of 35 milliseconds differed only marginally from a pulse of 4.65 milliseconds. Consequently, and in line with previous studies, perturbation durations of 35 milliseconds were applied throughout (Scott, 2004; Otieno, 2008).

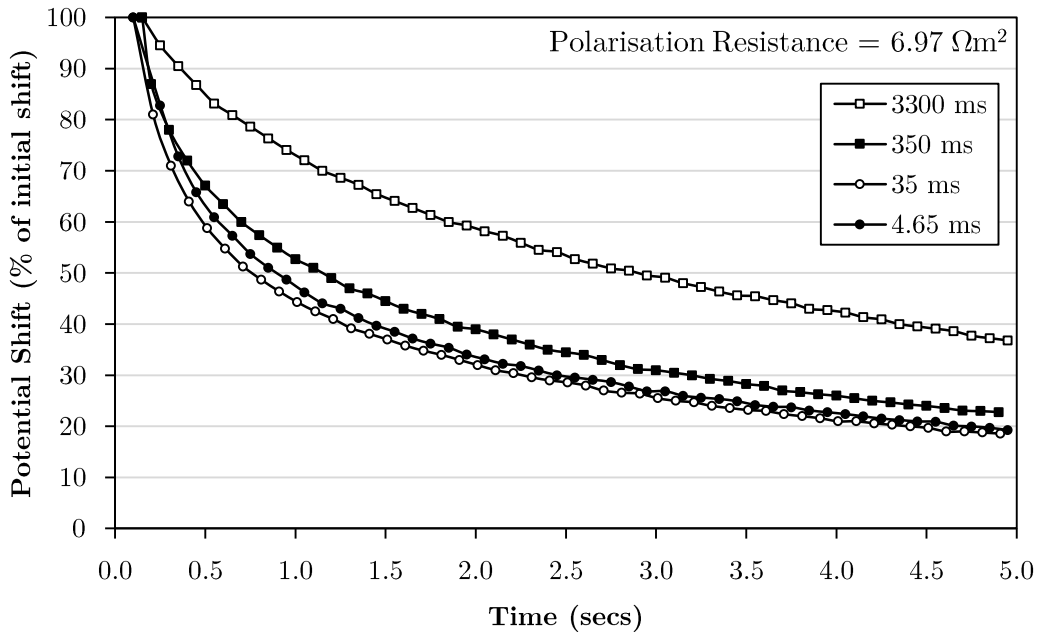

Figure 2.37: The effect of perturbation duration on the shape of the relaxation transient (after Glass, 1995)

The potential transients shown in Figure 2.36 can be mathematically described by Eq. 2.20. This equation is used to obtain case-specific time constants which, in combination with the capacitance, are used to determine the polarisation resistance. The capacitance is a measure of the applied current against the initial potential shift (Eq. 2.21). The polarisation resistance can then be determined using Eq. 2.22. The corrosion current can finally be determined by applying Eq. 2.19 to the measured polarisation resistance and applying a Stern-Geary coefficient of 26 for active corrosion conditions.

$$n_t = n_0 exp\left(\frac{-t}{\tau_c}\right) \qquad \text{(Eq. 2.20)}$$

where: n_t is the potential shift at time t, n_0 is the initial potential shift and τ_c is the time constant.

$$C = \frac{q_s}{n_0} \qquad \text{(Eq. 2.21)}$$

where: C is the capacitance, q_s is the applied current density and n_0 is the initial potential shift.

$$R_p = \frac{\tau_c}{C} \qquad \text{(Eq. 2.22)}$$

where: R_p is the polarisation resistance, τ_c is the time constant and C is the capacitance.

2.9 Summary

This chapter reviewed chloride-induced corrosion as a three-stage process; including initiation, propagation and acceleration. The transport mechanisms and fundamentals of corrosion were presented with respect to the initiation and propagation of corrosion. The chapter then focused on the acceleration phase of corrosion and presented general parameters affecting the corrosion rate, as well as an in-depth analysis of corrosion acceleration under cyclic wetting and drying. Typical

exposure conditions within the marine environment were also investigated for their influence on the corrosion of embedded reinforcing steel. A general overview of this literature is presented below.

Reinforced concrete structures in the marine environment are typically exposed to harsh conditions that lead to their deterioration, usually through reinforcement corrosion. The environmental exposure conditions vary depending on the location of the structure in the marine environment. Permanently saturated or permanently dry conditions typically stunt the progress of corrosion and are favourable in protecting embedded reinforcing steel. This is due to reinforcement corrosion requiring sufficient moisture and oxygen to proceed at an appreciable rate. Consequently, in permanently dry or permanently saturated conditions the corrosion rate will typically be slow irrespective of the chloride concentration.

On the other hand, exposure to cyclic wetting and drying leads to relatively rapid ingress of chlorides and the possibility of high corrosion rates. The ingress of chlorides under cyclic wetting and drying follows two predominant mechanisms of ingress. Drying of the concrete surface causes moisture to be removed from the pore spaces while chloride ions remain. This causes an increase in the surface chloride concentration with the transport of chlorides in this region governed by convection. Beyond this point normal diffusion mechanisms control the movement of chlorides. This phenomenon leads to relatively higher chloride concentrations when concrete is exposed to cyclic wetting and drying. As a result, relatively higher chloride concentrations are expected in the splash zone compared to the tidal zone; while the tidal zone is expected to have a higher chloride concentration that the submerged zone.

The thickness of the convection layer is also important when considering the availability of oxygen for corrosion under cyclic wetting and drying. Corrosion of reinforcing steel requires the availability of sufficient moisture and oxygen. Moisture is readily available in the marine environment; however, the availability of oxygen can be limited if the drying time is sufficiently short – resulting in a reduction in the thickness of the convection layer. Under normal conditions the reduction of oxygen is the only possible cathodic reaction and, as a result, the availability of oxygen at the level of the steel is of paramount importance when considering the progress of corrosion. The availability of oxygen can be significantly reduced if the drying time is sufficiently short to prevent the convection layer from progressing beyond the concrete cover. Consequently, the drying time is a fundamental parameter when considering corrosion under cyclic wetting and drying and should be considered in relation to the cover to the reinforcement and the concrete quality.

Nevertheless, the effect of oxygen availability under cyclic wetting and drying remains a contested topic with some researchers presenting contradictory interpretations. The multi-stage process for the reduction of oxygen has been cited as a primary source for discrepancies between respective studies. The formation of hydrogen peroxide as an intermediary product in the reduction of oxygen has been reported to allow corrosion to continue even when oxygen is no longer available. This process is not well understood with limited studies on the exact process of oxygen reduction. As a result, a generally accepted consensus has not been achieved on the effect of oxygen availability on the corrosion of embedded reinforcing steel.

Furthermore, researchers have applied a number of different exposure conditions and testing methods without much consistency between studies. Most of these studies are laboratory-based where researchers have applied a number of various techniques for exposing samples to cyclic wetting and drying and have also applied different measuring techniques. As a result, a fundamental understanding of the effect of oxygen on corrosion has not been developed.

Supplementary cementitious materials (SCMs) were investigated for their influence on active-state corrosion conditions. Fly ash, slag and silica fume were studied for their effects on the concrete properties pertinent to reinforcement corrosion. This primarily included examining their influence on the porosity and permeability of concrete and its influence on the resistivity, as well as ease of transport of oxygen and moisture. Each of the investigated SCMs has been reported to improve the permeability of concrete; however, fly ash has been shown to increase the overall porosity. This has generally resulted in slower transport of moisture and oxygen through the pore spaces when concrete exposed to cyclic wetting and drying. SCMs have also been investigated for their influence on the electrical resistivity of concrete. All of the abovementioned SCMs have been shown to increase the resistivity with respect to concrete containing only Portland cement as the binder. Consequently, reinforced concrete structures containing SCMs are expected to provide a significantly longer service life.

This literature review has been compiled in order to develop an appropriate laboratory-based experimental programme to investigate active corrosion conditions under cyclic wetting and drying. The effect of oxygen availability will be investigated by varying the drying time; while different w/b ratio and binder types will applied. The details for this experimental programme are presented in Chapter 3.

References

ACI Committee 222, 2001. Protection of metals in concrete against corrosion. *ACI222R-01.*

American Concrete Institute, Building Research Establishment, the Concrete Society & International Concrete Repair Institute. 2003. *Concrete repair manual.* Vol. 1. 2nd edition. 443-506.

Alexander M. & Beushausen, H. 2009. Deformation and volume change of hardened concrete. In *Fulton's concrete technology. 9th ed.* G. Owens, Eds. Cape Town: Cement & Concrete Institute. 111-154.

Alexander, M. G. & Mackechnie, J., 2003. Concrete mixes for durable marine structures. *Journal of the South African Institution of Civil Engineering*, 45(2): 20-25.

Alonso, C., Andrade, C. & Garcia, A. M., 1998. The role of oxygen in the kinetic of the corrosion of reinforcements. *Proceedings of Eurocorr'98.*

Alonso, M.C., Sanchez, M., Angst, U. & Garcia-Calvo, J.L. 2012. The effect of binder type on chloride threshold values for reinforced concrete. In: *Concrete Repair, Rehabilitation and Retrofitting III (ICCRRR).* M. Alexander, H. Beushausen, F. Dehn & P. Moyo, Eds. London: Taylor & Francis Group: 39-40.

ASTM C876-09. 2009. Standard test method for corrosion potentials of uncoated reinforcing steel in concrete. (ASTM C876-09). West Conshohocken, PA: ASTM International.

Andrade, C., Alonso, C. & Garcia, A. M., 1990. Oxygen availability in the corrosion of reinforcements. *Advances in Cement Research.* 11: 127-132.

Angst, U. & Vennesland, Ø. 2009. Critical chloride content in reinforced concrete – State of the art. In *Concrete Repair, Rehabilitation and Retrofitting II.* M. Alexander, H. Beushausen, F. Dehn & P. Moyo, Eds. London: Taylor & Francis Group. 311-317.

Arup, H. 1983. The mechanisms of protection of steel by concrete. In *Corrosion of reinforcement in concrete construction.* A.P. Crane, Eds. Ellis Horwood Limited: Society of chemical industry. 151-157.

Bakker, R.F.M, Van der Wegen, G. & Bijen, J.M. 1994. *Reinforced concrete: an assessment of the allowable chloride content.* Canmet: Nice.

Ballim, Y., Alexander M. & Beushausen, H. 2009. Durability of concrete. In *Fulton's concrete technology. 9th ed.* G. Owens, Eds. Cape Town: Cement & Concrete Institute. 155-188.

Bamforth, P.B. & Chapman-Andrews, J. 1994. Long term performance of RC elements under UK coastal conditions. *Proceedings from International conference on corrosion and corrosion protection of steel in concrete.* University of Sheffield, England. 139-156.

Bentur, A., Diamond, S. & Berke, N., 1997. *Steel Corrosion in Concrete: Fundamentals and Civil Engineering Practice.* London: E & FN Spon.

Berke, N.S., Hicks, M.C., Hoopes, R.J. & Tourney, P.J. 1994. Use of laboratory techniques to evaluate long-term durability of steel reinforced concrete exposed to chloride ingress. *American Concrete Institute.* Special publication: 299-330.

Berry, E., Hemmings, R., Langley, W. & Carette, G. 1989. Beneficiated fly ash: hydration, microstructure, and strength development in Portland cement systems. In: Fly ash, silica fume, slag, and natural pozzolans in concrete, proceedings third international conference. Trondheim, Norway. ACI, SP 114(1): 241-273.

Bertolini, L. et al., 2013. *Corrosion of Steel in Concrete.* Second ed. Weinham, Germany: Wiley-VCH.

Broomfield, J. P. 2007. *Corrosion of steel in concrete – understanding, investigation and repair.* 2nd ed. Oxford: Taylor & Francis Group.

Carino, N.J. 2004. Methods to evaluate corrosion of reinforcement. In *Handbook on nondestructive testing of concrete. 2nd ed.* V.M. Malhotra & N.J. Carino, Eds. Florida: CRC Press. 243-266.

Correia, M. J., Pereira, E. V., Salta, M. M. & Fonseca, I. T., 2006. Sensor for oxygen evaluation in concrete. *Cement and Concrete Composites.* 28: 226-232.

Correia, M. J. & Salta, M. M., 2007. Long term performance of a sensor for oxygen evaluation in concrete. *International RILEM Workshop on Integral Service Life Modelling of Concrete Structures.* 175-184.

Crank, J. 1975. *The mathematics of diffusion.* 2nd ed. Oxford: Clarendon Press.

Davies, R.E. 1954. Pozzolanic materials – with special reference to their use in concrete pipe. Technical memo. *American concrete pipe association.* Irving, TX.

Elsener, B. & Böhni, H. 1992. Potential mapping and corrosion of steel in concrete. *ASTM STP 1065.* N.S. Berke, V. Chaker & D. Whiting, Eds. Philadelphia: American society for testing and materials. 143-156.

European Standards. 2013. *Concrete Specification, performance, production and conformity.* (BS EN 206:2013).

Garcia, A. M., Andrade, C. & Alonso, C., 2002. Oxygen availability at the rebar surface and its relation with corrosion rate. *15th ICC: Frontiers in corrosion science and technologies.*

Ghods, P., Chini, M., Alizadeh, R. & Hoseini, M. 2005. The effect of different exposure conditions on the chloride diffusion into concrete in the Persian Gulf region. In Proceedings of the ConMAT conference. N. Banthia, Eds. Vancouver, Canada: University of British Columbia.

Glass, G.K. 1995. An assessment of the coulostatic method applied to the corrosion of steel in concrete. *Corrosion Science.* 37(4): 597-605.

Glass, G.K. & Beunfeld N.R. 1997. The presentation of the chloride threshold level for corrosion of steel in concrete. *Corrosion Science* 39: 1001-1013.

Gjørv, O. E., 1972. Durability of Concrete Structures in the Ocean Environment. *FIP Proceedings, Concrete Sea Structures.* 141.

Gjørv, O. E., Vennesland, Ø. & El-Busaidy, A. H., 1986. Diffusion of dissolved oxygen through concrete. *National Association of Corrosion Engineers.* 39-44.

Hearn, N., Hootton R.D. & Nokken, M.R. 2006. Pore structure, permeability, and penetration resistance characteristics of concrete. In *Significance of tests and properties of concrete and concrete-making materials.* J.F. Lamond & J.H. Pielert, Eds. West Conshohocken, PA: ASTM. 238-252.

Heckroodt, R. O., 2002. *Guide to deterioration and failure of building materials.* London: Thomas Telford Publising.

Hong, K. & Hooton, R. D., 1999. Effects of cyclic chloride exposure on penetration of concrete cover. *Cement and Concrete Research.* 29: 1379-1386.

Hooton, R.D. 1993. Influence of silica fume replacement of cement on physical properties and resistance to sulphate attack, freezing and thawing, and alkali-silica reactivity. *ACI Materials Journal.* 90(2): 143-151.

Hornbostel, K., Larsen, C.K. & Geiker, M.R. 2013. Relationship between concrete resistivity and corrosion rate- A literature review. *Cement & Concrete Composites.* Volume 39 (2013). 60-72.

Hunkeler, F., 2005. Corrosion in reinforced concrete: processes and mechanisms. In *Corrosion in reinforced concrete structures.* H. Bohni Eds. Abington Cambridge CBI A6H, England: Woodhead Publishing Limited. 1-45.

Mackechnie, J. R., 2001. *Predictions of reinforced concrete durability in the marine environment, Research Monograph No. 1 (Rev.),* South Africa: Dept of Civil Engineering, University of Cape Town.

Mancra, M., Vennesland, Ø. & Bertolini, L. 2008. Chloride threshold for rebar corrosion in concrete with addition of silica fume. *Corrosion Science.* 50 (2008). 554-560.

Mangat, P., Khatib, J. & Molloy, B., 1994. Microstructure, chloride diffusion and reinforcement corrosion in blended cement paste and concrete. *Cement and Concrete Composites.* 16: 73-81.

McCarter, W. J. & Vennesland, Ø., 2004. Sensor systems for use in reinforced concrete structures. *Construction and Building Materials.* 18: 351-358.

Mehta, P. K., 1991. *Concrete in the marine environment.* London: Elsevier Applied Science.

Miyazato, S. & Otsuki, N., 2010. Steel corrosion induced by chloride or carbonation in mortar with bending cracks or joints. *Journal of Advanced Concrete Technology,* 8(2): 135-144.

Neville, A.M. 2004. *Properties of concrete. 4th ed.* Essex, England: Longman Scientific & Technical.

Otieno, M.B. 2008. Corrosion propagation in cracked and uncracked concrete. *MSc Thesis.* University of Cape Town.

Otieno, M.B. 2014. The development of emperical chloride-induced corrosion rate prediction models for cracked and uncracked steel reinforced concret structures in the marine tidal zone. *PhD Thesis.* University of Cape Town.

Polder, R.B. 1996. The influence of blast furnace slag, fly ash and silica fume on corrosion of reinforced concrete in marine environment. *Heron.* 41 (4). 287-300.

Polder. R.B. 2005. Durability of marine concrete structures – field investigations and modelling. *Heron.* 50 (3). 133-153.

Poulsen, S.L. & Sørenson, H.E. 2012. Chloride threshold values – state of the art.

Pullar-Strecker, P. 2002. Concrete reinforcement corrosion: From assessment to repair decisions. *ICE Design and Practice Guide.* London: Thomas Telford.

Raupach, M., 1996. Investigations on the influence of oxygen on corrosion of steel in concrete - Part I. *Materials and Structures.* 29: 174-184.

Saleem, M., Shameem, N., Hussain, S.E. & Maslehuddin, M. 1996. Effect of moisture, chloride and sulphate contamination on the electrical resistivity of Portland cement concrete. *Construction and Building Materials.* 10(3): 209-214.

Schiessl, P. & Lay, S. 2005. Influence of concrete composition, In Corrosion in reinforced concrete structures. H Böhni, Eds. Cambridge, UK: Woodhead Publishing Limited.

Scott, A.N. 2004. The influence of binder type and cracking on reinforcing steel corrosion in concrete. PhD Thesis. University of Cape Town.

Siddique, R. & Khan, M.I. 2011. *Supplementary cementing materials.* Berlin, Germany: Springer. 108-110.

Stansbury, E.E. & Buchanan, R.A. 2000. *Fundamentals of electrochemical corrosion.* Materials Park, Ohio: ASM International.

Tang, L., Nilsson, L.O. & Basheer, P.A.M. 2011. *Resistance of concrete to chloride ingress: Testing and modelling.* Florida: CRC Press.

Tapan, M. 2007. Strength evaluation of deteriorated reinforced concrete bridge columns. PhD Thesis. Syracuse University.

Thomas, M. 2013. *Supplementary cement materials in concrete.* Boca Raton, FL: Taylor & Francis Group.

Tuutti, K. 1982. *Corrosion of steel in concrete.* Stockholm: Swedish Cement and Concrete Research Institute.

Zivica, V., 2003. Influence of w/c ratio on rate of chloride induced corrosion of steel reinforcement and its dependence on ambient temperature. *Bulletin of Materials Science,* 26(5). 471-475.

CHAPTER 3: EXPERIMENTAL METHODOLOGY

3.1 Introduction

This chapter presents details of the experimental component of this study. Specifications for the specimen details, manufacturing process, parameter variations and the exposure conditions are provided.

The purpose of the experimental work was to determine the effect of cyclic wetting and drying on the corrosion rate of steel embedded in concrete. This was determined through laboratory cast specimens of 6 different concrete mixtures exposed to 4 variations of cyclic wetting and drying. A summary of the experimental work is presented in Figure 3.1.

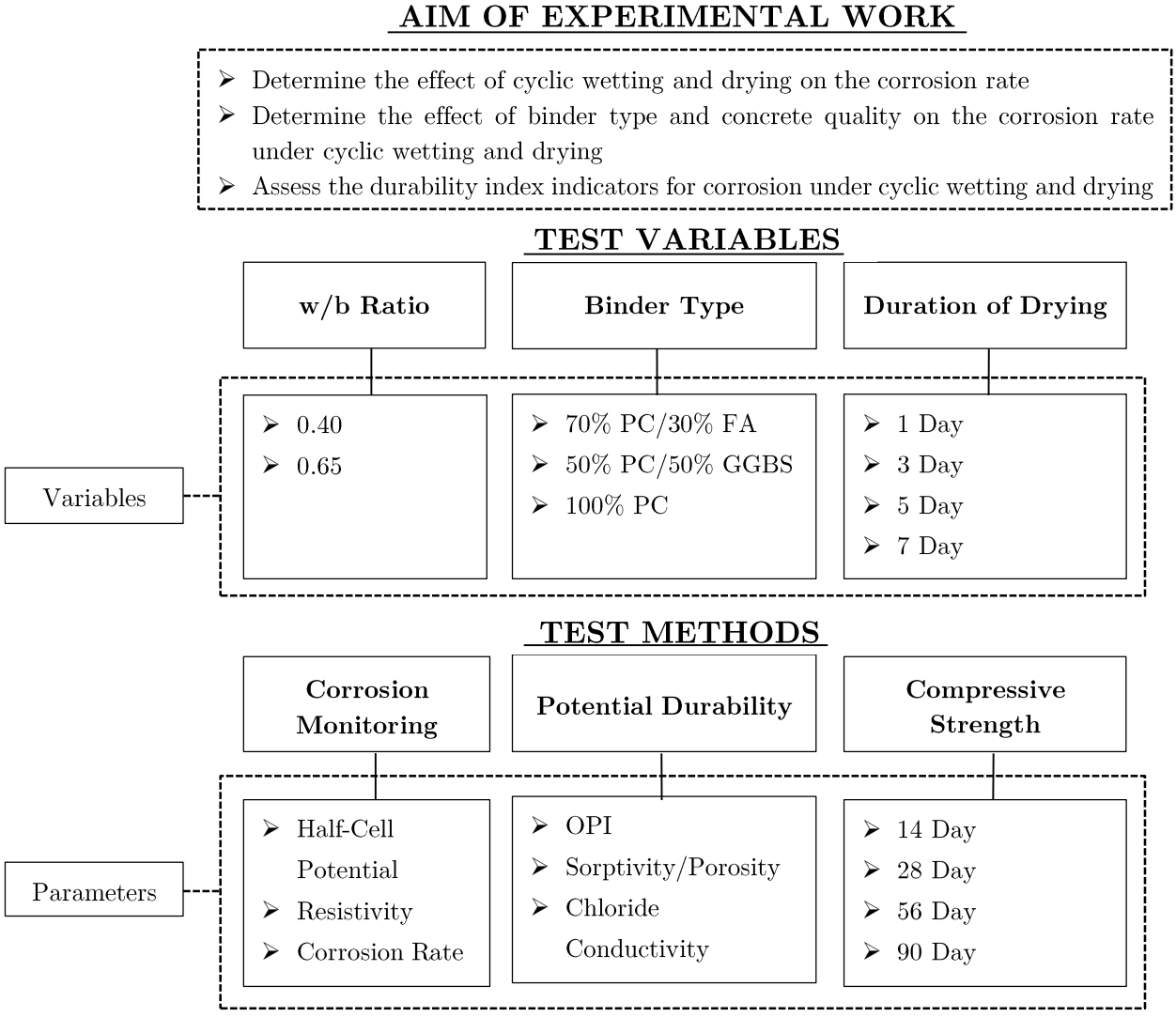

Figure 3.1: Overview of experimental work

3.2 Variables

The influence of the binder type, w/b ratio and duration of drying were investigated for their effects on the corrosion rate. The concrete cover and wetting duration remained constant throughout at 20 mm and 2 days, respectively. The 3 sets of variables (binder type, w/b ratio and duration of drying) applied in the experimental programme are detailed in Sections 3.2.1, 3.2.2 and 3.2.3.

3.2.1 Binder type

The use of supplementary cementitious materials to assist with corrosion prevention has been extensively investigated, *inter alia*, by Scott (2004). Thus it was deemed necessary to investigate whether these benefits are prevalent under conditions of cyclic wetting and drying. Furthermore, the commercially available cementitious products have changed substantially over the past few years and require the necessary investigations. This experimental work considered two supplementary cementitious materials. Ground granulated blastfurnace slag was used as a 50% replacement, while fly ash was used to replace 30% of Portland cement.

It is worth noting that material changes in the Western Cape of South Africa have resulted in the production of CEM II/A-L 52.5N as the cement containing the highest clinker content. This cement was used throughout as the Portland cement (PC); however, this includes approximately 9% ground limestone. As a result, the cement contains > 5% additional materials and is no longer a PC. Nevertheless, this cement will henceforth be referred to as PC and for all intents and purposes will likely perform like a PC. The oxide analysis for this cement is shown in Table 3.1 below.

Table 3.1: Typical oxide analysis for CEM II/A-L 52.5N (S. Crosswell, personal communication, January 16, 2015).

Constituent	Average % Composition
SiO_2	18.7
Al_2O_3	4.3
Fe_2O_3	2.9
Mn_2O_3	0.1
TiO_2	0.2
CaO	63.4
MgO	1.0
SO_3	2.2
K_2O	0.7
Na_2O	0.2
NaO equivalent	0.7

3.2.2 Water-binder ratio

Water-binder (w/b) ratios of 0.40 and 0.65 were selected in order to extract measureable differences in the corrosion rate based on the concrete quality and, as a result, the concrete durability. The w/b ratio is not intrinsically an indicator of durability, but varying the w/b ratio will modify the pore

structure which will have an impact on the transport mechanisms. The selection of the w/b ratios were also motivated by details in SANS 10100-2 (2013) and BS EN 206 (2013). These standards specify a maximum w/b ratio of 0.45 for reinforced concrete structures in the marine environment (specifically the submerged and the tidal and splash zone). As a result, the selected w/b ratios provide a representative from both ends of the spectrum, one which is below the suggested limit and one which is above the suggested limit.

3.2.3 Cycles of wetting and drying

The effects of cyclic wetting and drying were investigated through the implementation of 4 different cycles of wetting and drying, shown in Table 3.2.

Table 3.2: Cycles of wetting and drying

Wetting Time (days)	Drying Time (days)
2	1
2	3
2	5
2	7

The duration of the wetting period was fixed at 2 days while the drying time was varied. Saturation of concrete to a depth of 20 mm was expected within 1 day, however to ensure complete saturation a wetting period of 2 days was selected. A wetting period of 2 days also allowed a sufficient number of cycles of wetting and drying to be applied in the available time period. The wetting of concrete is generally a faster process than drying and thus a relatively shorter wetting period could be applied.

An estimation of the drying time was less obvious and an initial approximation was established from Parrott (1988). In his work it was found that a drying time of at least 1 day was required to detect a reduction in the relative humidity at 20 mm from the surface. As a result, a minimum of 1 day drying was selected and was varied up to 7 days to include a wide range of drying potential. This was an attempt to simulate the conditions hypothetically described by Raupach (1996) (discussed in Section 2.7.3) and varies the availability of oxygen at the level of reinforcement. 1 day drying cycles should theoretically imply saturated conditions, while 3, 5, and 7 days drying should implement different levels of drying to the level of the reinforcing steel.

3.3 Specimen Details

A total of 72 small prism specimens (100 x 100 x 242 mm) were cast of different concrete mixes, with a 10 mm diameter embedded steel working electrode with an exposed length of 200 mm (high yield reinforcing steel). A 10 mm diameter stainless steel rebar (316 Grade) was also embedded with a length of approximately 150 mm, to act as a counter electrode. The specimens were cast using 500 x 100 x 100 mm moulds with a 15 mm PVC divider inserted at the centre. The specimens were cast with the 20 mm cover provided at the bottom of the specimens by using spacer wheels, illustrated in Figure 3.2.

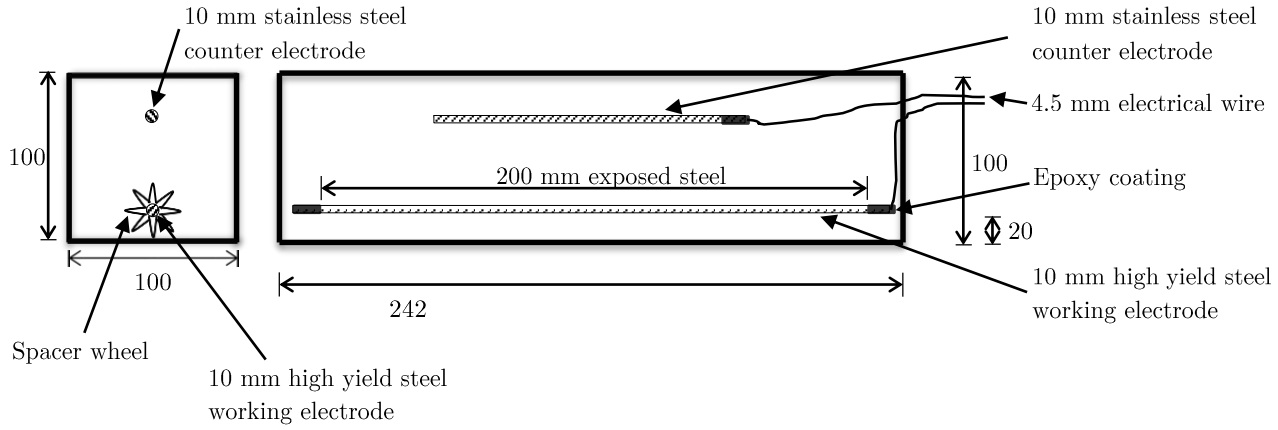

*Not Drawn to Scale

Figure 3.2: Specimen detailed cross-sections (dimensions in mm)

3.4 Manufacturing Process

The working electrodes are 10 mm diameter high yield steel cut to 230 mm in length and epoxy coated on both ends to ensure that 200 mm of steel was exposed. Electrical connectivity was provided to both the working and counter electrodes by drilling and inserting 4.5 mm copper wire. The counter electrodes are 10 mm diameter stainless steel 316 bars cut to 150 mm in length and epoxy coated on one end to protect the electrical connection. The epoxy coating and electrical connection are illustrated in Figure 3.3.

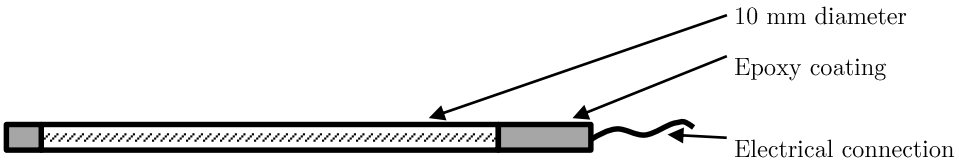

Figure 3.3: Preparation of high yield steel specimens (coated on both ends) and stainless steel (only coated to protect the electrical connection)

3.5 Mix Designs

The selection of 3 binder types and 2 w/b ratios required the casting of 6 different concrete mixes for experimental testing. The concrete mix designs were completed by following the procedure outlined in Addis and Goodman (2009) and the resulting mixes are shown in Table 3.3 for a 1 m^3 mix. The water content remained constant at 185 ℓ/m^3 throughout the mix designs, with the binder content adjusted to satisfy the required w/b ratios. A sieve analysis, fineness modulus and grading curve is presented in Appendix A for each aggregate type.

Table 3.3: Concrete mix designs

No.	w/b	Water	PC (CEM II/A-L 52.5N)	FA	GGBS	Greywacke (13.2 mm)	Greywacke Crusher Sand	Philippi Dune Sand	Superplasticiser*	
		[ℓ]	[kg]	[kg]	[kg]	[kg]	[kg]	[kg]	[mℓ]	[% weight of binder]
1	0.40	185	324	139	-	1029	285	428	250	0.06
2	0.65	185	199	85	-	1029	352	529	250	0.09
3	0.40	185	231	-	231	980	316	473	1000	0.23
4	0.65	185	142	-	142	980	378	568	400	0.15
5	0.40	185	463	-	-	980	321	482	1000	0.23
6	0.65	185	285	-	-	980	382	573	500	0.18

*new generation superplasticiser based on a modified polycarboxylate polymer (Density (20°C) – 1.050 ± 0.010; pH – 6.7 ± 2.0; Cl ions content < 0.10%; Na2O equivalent < 1.5%)

3.6 Casting and Curing

3.6.1 Casting

All the specimens were cast over a six day period. The FA and GGBS mixes were cast first in cognisance of the delayed strength development of these slower hydrating binders. Initial trial mixes showed that the FA mixes developed lower 28-day strengths, and were thus given preference in the casting order, followed by GGBS and then PC. The order of casting is shown in Table 3.4 with the mix descriptions and average measured slump. Mixes were cast in two 40 litre batches to fill 25 cubes (100 x 100 x 100 mm) and 12 prisms (242 x 100 x 100 mm) on each day.

Table 3.4: Order of concrete mix casting and measured slump

Day	w/b	Mix components	Slump (mm)
1	0.40	70 PC / 30 FA	75
2	0.65	70 PC / 30 FA	100
3	0.40	50 PC / 50 GGBS	80
4	0.65	50 PC / 50 GGBS	80
5	0.40	100 PC	85
6	0.65	100 PC	75

The contents for each mix were weighed using a scale accurate to the nearest 5 grams and batched according to the specifications for laboratory cast specimens in SANS5861-1 (2006). The mixes were cast under laboratory conditions, with a temperature of 20 ± 1°C and a RH of 60 ± 5%.

3.6.2 Curing

Immediately after casting, the specimens were covered with polyethylene sheeting and allowed to set for 24 hours. The specimens were then placed in the water curing bath at 22-25°C. The prisms were removed after 28 days, while the cubes remained in the curing tank until their respective dates for

testing. The water saturated cube specimens were tested for durability index values (potential durability) at 28 and 90 days, as well as compressive strength at 28, 56 and 90 days.

3.6.3 Cover measurements

After curing for 28 days the cover depth was measured using a commercial cover meter. This check was performed to ensure that the required cover thickness was achieved and was consistent throughout the sample sets. The results of the cover measurements are shown in Appendix B which identified one outlier to be excluded from further testing. This specimen was retained and used to measure the chloride content at a later stage. The specimen remained permanently submerged in NaCl solution and was monitored periodically for corrosion rate to assess the effect of permanent submersion.

3.7 Corrosion Activation

This investigation focused on the corrosion propagation and acceleration phases under the effects of cyclic wetting and drying of a 5% NaCl solution. As a result, and due to time constraints, it was necessary to impress a current to break down the gamma ferric oxide protective layer (γ-Fe_2O_3) and initiate active corrosion. The impressed current technique was selected for its ease of application and effectiveness, as illustrated by various authors (Austin, Lyons & Ing, 2004; Ahmad, 2009; El Maaddawy & Soudki, 2003) and discussed in Section 2.5.

Active corrosion conditions are usually assumed to commence at a current density of approximately 0.1 µA/cm^2. However, it was suggested that this threshold should be surpassed to avoid the specimens reverting to passive conditions upon removal of the charge (M.B. Otieno, personal communication, March 7, 2014). It was also deemed necessary to comply with the experimental limit of 200 µA/cm^2 developed by El Maaddawy & Soudki (2003). A current density of 10 µA/cm^2 was selected which falls well below the threshold value of 200 µA/cm^2.

After curing for 28 days, the specimens were removed from the curing tank and a current density of 10 µA/cm^2 was applied for a period of 6 hours. Based on Faraday's Law, this was expected to produce negligible mass loss (approximately 0.06 mg) with the current density two orders of magnitude greater than the theoretical active corrosion threshold. The specimens were then exposed to their respective cycles of wetting and drying with measurements commencing after 1 week of exposure.

The specimens were exposed to cyclic wetting and drying for a period of 5 weeks. There was no evidence of active corrosion during this 5 week period. Corrosion current densities were generally below the threshold value and HCP values were typically in the region of -50 to -100 mV, both indicative of passive conditions. As a result, a core specimen was extracted from one specimen to measure the chloride content. The surface 0-10 mm contained an average of 2.5% chlorides while the interior concrete did not contain any chlorides. As a result, it was evident that the impressed current was not effective to initiate active corrosion conditions. Consequently, it was deemed necessary to impress further current. Consultation was made with Otieno (2014) before impressing a current.

Otieno (2014) impressed a current density of between 475 and 9075 µA/cm², which is evidently over the suggested threshold (200 µA/cm²) to simulate natural corrosion. Calculations using Faraday's Law (discussed in Section 2.5) indicated a cross-sectional mass loss of between 0.04% and 0.70% for Otieno's (2014) testing. This mass loss was used as a guideline for selecting a revised current density and duration of the impressed current.

To counter for the continued passive conditions, at the end of the initial 5-week period an additional current of 10 mA was applied to a cross-sectional area of 62.8 cm². This equates to a current density of 160 µA/cm², which is significantly larger than the previous impressed current but still remains below the suggested threshold of 200 µA/cm². The duration for the impressed current was set as 5 days to limit the corrosion damage to less than 1%, as shown below.

$$M = \frac{ItA_w}{nF}$$

$$M = \frac{(10 \times 10^{-3}) \times 432000 \times 55}{2 \times 96485} \qquad \text{(Eq. 2.8)}$$

$$M = 1.23g$$

The total mass of exposed steel was 125.66 g, with 1.23 g of steel amounting to a mass loss percentage of 0.98%.

$$M_{loss} = \frac{M}{M_{total}}$$

$$M_{loss} = \frac{1.23}{125.66}$$

$$M_{loss} = 0.98\%$$

The corrosion rate measurements were resumed after the current was impressed. Further complications were raised after a few measurements were taken. It was evident that the method of impressing a current was only able to initiate corrosion in the first specimen in each set. The specimens were arranged in trays, as shown in Figure 3.4, and connected in series to a direct current power supply.

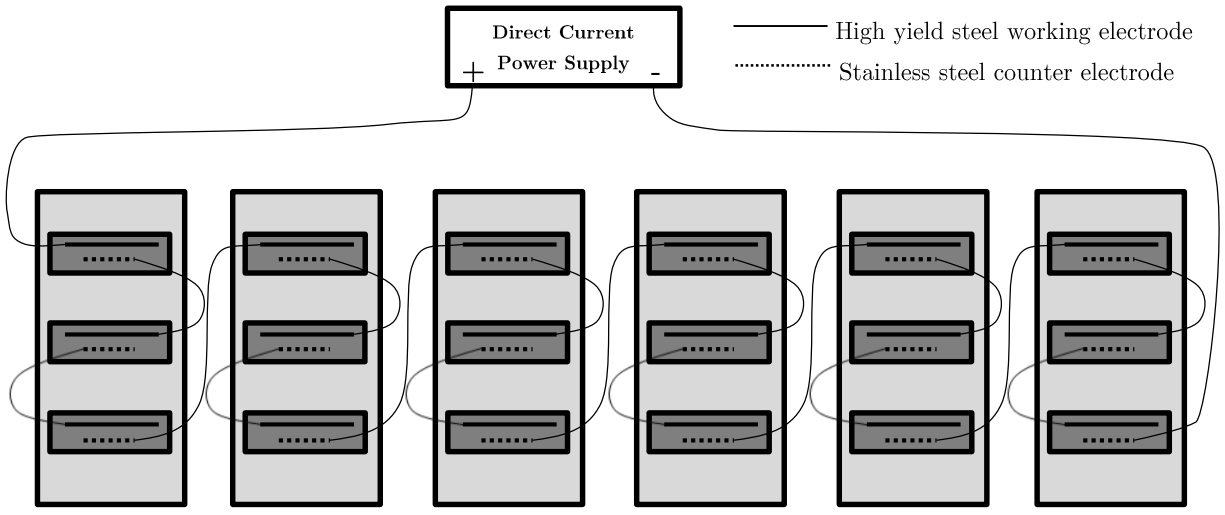

Figure 3.4: Initial schematic layout of specimens for impressed current (short circuit)

Each sample set of 3 small prisms was submerged in a single container of NaCl solution. This is most likely the source of the complication with the shared NaCl solution creating a short circuit. As a result, almost zero current was impressed into the 2nd and 3rd specimens of each set, while the 1st specimen in each set was actively corroding.

At this point it was deemed necessary to split the specimens into two distinct sample sets. The first specimen of each set would be considered separately, while a separate sample set would consist of the 2nd and 3rd specimens. This was necessary to account for the change in the condition of the specimens after an additional current was impressed. This limited the statistical confidence of the experimental work by limiting the number of repeat specimens; however, it did produce two separate sample sets for comparison. Henceforth, the two sample sets will be referred to as CR1 and CR2. CR1 included the 1st specimen in each set; while, CR2 included an average of the 2nd and 3rd specimens in each set.

It was noted that the specimens in CR1 were corroding at a very high corrosion rate (up to 27 $\mu A/cm^2$). As a result, a shorter duration current was selected for the CR2 specimens. An impressed current of 10 mA was applied for 3 days. This amounted to an expected percentage mass loss of 0.59% according to Faraday's Law. These specimens were connected in series whilst each submerged in its own container of NaCl solution, as shown in Figure 3.5. This prevented the possibility of a short circuit and allowed for the successful activation of corrosion.

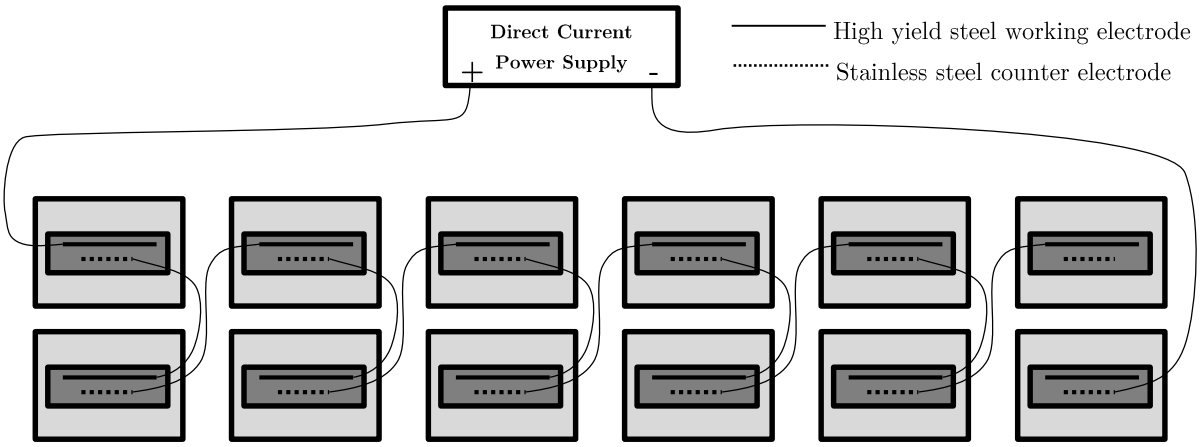

Figure 3.5: Final schematic layout of CR2 specimens for impressed current (isolated system)

3.8 Exposure Conditions

The durations for wetting and drying were specified in Section 3.2.3. The wetting period was implemented by submerging specimens in a 5% NaCl solution; while the specimens were stored on shelving during the drying cycle, shown in Figure 3.6. Drying cycles of various durations were applied using an environmental room set to 30°C and 50% RH with the achieved environmental conditions shown in Figure 3.7. On average the environmental room achieved a temperature of 30.1 ± 0.5°C and a relative humidity of 49.4 ± 3.6%. These conditions are similar to those applied by Scott (2004) to provide accelerated drying conditions.

Figure 3.6: Conditions for exposure to cyclic wetting and drying

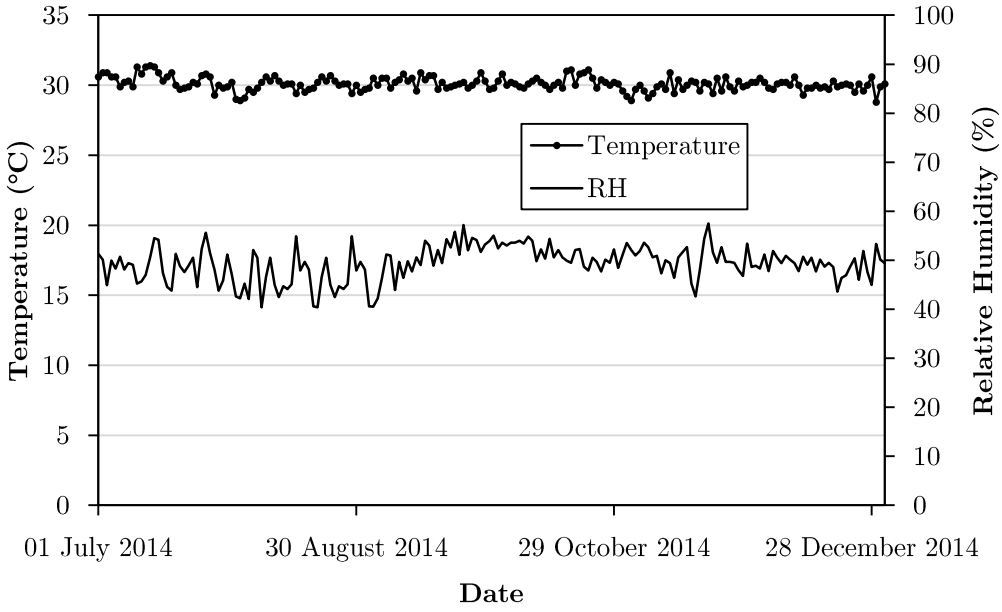

Figure 3.7: Measured environmental conditions with daily spot checks

3.9 Testing

3.9.1 Corrosion rate monitoring

Initially corrosion rate measurements were taken at the end of each cycle of wetting and at the end of each cycle of drying. Similar results were measured in both sets with a higher degree of scatter measured at the end of each drying period. The required laboratory time for both sets of measurements was deemed unnecessary and the measurements were reduced. As a result, corrosion rate measurements were only taken at the end of each cycle of wetting. Each set of measurements included half-cell potential, corrosion rate and concrete resistivity. The methods applied to obtain these results are discussed below.

3.9.1.1 Half-cell potential

Half-cell potential (HCP) readings were taken using a Ag/AgCl reference electrode, with the method of testing shown in Figure 3.8. The HCP was measured before the application of a perturbation for corrosion rate measurements.

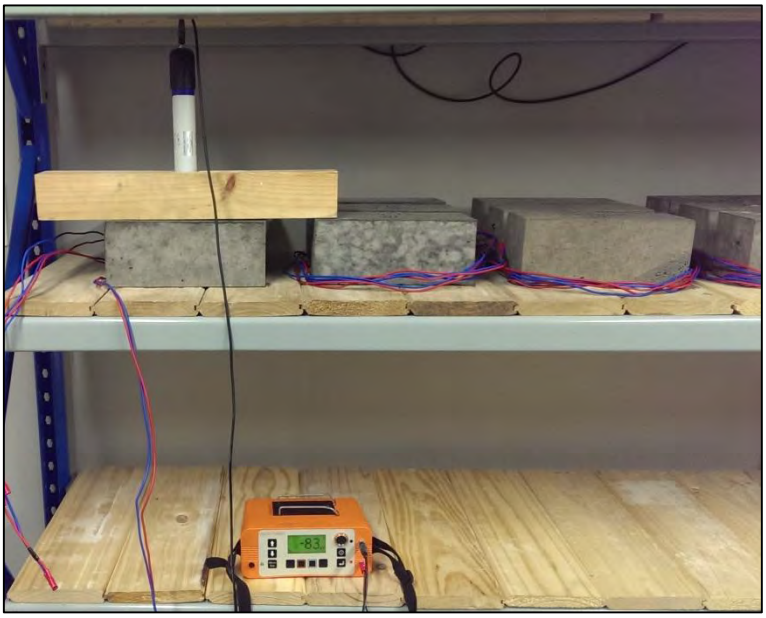

Figure 3.8: Half-cell potential test set-up

3.9.1.2 Corrosion rate

The coulostatic technique was applied to non-destructively measure the corrosion rate (method discussed in Section 2.8.2). A purpose-built pulse generator was used to apply the perturbation with the generator capable of sending an electrical pulse of 0–30 mA for a duration of 0–99 seconds. This was used in combination with a data logger and a Ag/AgCl reference electrode. The experimental test set-up is shown in Figure 3.9. The output from the data logger was then assessed to determine the effect of the perturbation and measure the corrosion rate by following the principles outline in Section 2.8.2.2.

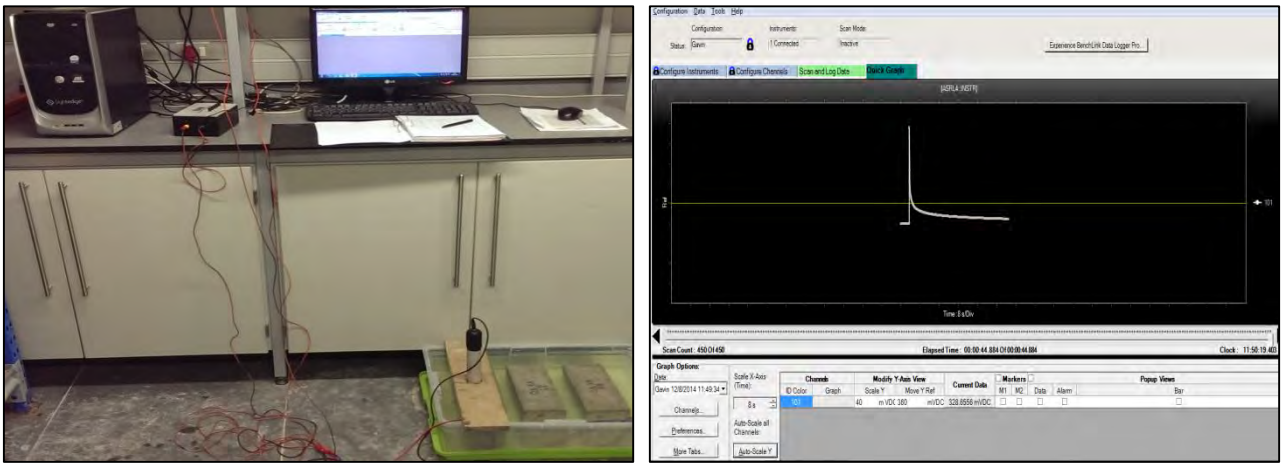

Figure 3.9: Coulostatic corrosion rate test set-up

3.9.1.3 Resistivity

Resistivity readings were taken using a four-point Wenner probe with probe spacing of 50 mm, shown in Figure 3.10. The probe spacing is more than sufficient for a maximum aggregate size of 13.2 mm.

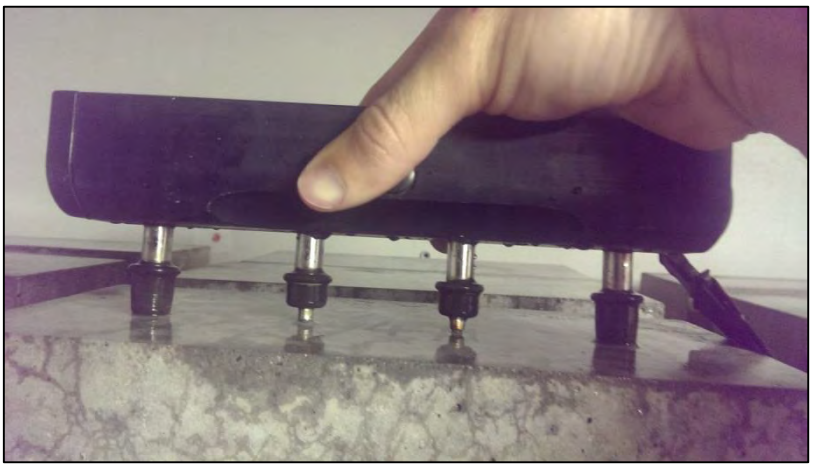

Figure 3.10: Four-point Wenner probe

3.9.2 Durability indicators

3.9.2.1 Durability Index tests

Companion cubes (100 x 100 x 100 mm) were cast from each mix in order to assess each batch in terms of potential durability. These test results can be used to justify or interpret observations during the experimental programme. Durability Index tests were conducted at 28 and 90 days. The Durability Index tests are outlined in the *Durability Index Testing: Procedure Manual* (Alexander, Ballim & Mackechnie, 2010) and include the following tests:

- Oxygen Permeability Index
- Sorptivity/Porosity Index
- Chloride Conductivity Index

3.9.2.2 Compressive strength

The compressive strengths of the various mixes were measured at 14, 28, 56 and 90 days. Cubes were crushed until failure and the compressive strength was calculated to the nearest 0.5 MPa, according to SANS 5863.

3.9.3 Chloride content

Upon completion of the monitoring phase of this experiment, the chloride content was measured at the level of the steel in each specimen. The chloride content was measured by extracting 20 mm diameter core samples and using chemical titration on a 10 mm thick slice which corresponds to a depth of 15-25 mm from the surface. The samples were then oven-dried at 50°C for 48 hours before pulverising to a fine powder. Chemical titration was conducted on the powder samples to measure the total chloride content. The chloride contents will be assessed in relation to the achieved corrosion rates, discussed in Chapter 4.

3.10 Closure

This chapter presented the experimental methodology applied to primarily assess the effect of cyclic wetting and drying on the corrosion rate of steel embedded in concrete. Exact details are provided for the specimen dimensions, method of preparation and manufacture, as well as the method of monitoring and testing.

The experimental testing includes 100 x 100 x 242 mm reinforced concrete specimens exposed to cyclic wetting and drying of a 5% NaCl solution. A 10 mm diameter high yield steel working electrode was embedded with a cover depth of 20 mm. Three binder types (100% PC, 70% PC/30% FA and 50% PC/50% GGBS) and two different w/b ratios (0.40 and 0.65) were used to assess the effect of the concrete quality.

An impressed current was applied to all of the specimens to initiate active corrosion conditions. Two sample sets were developed (CR1 and CR2) based on different degrees of corrosion caused by two durations of impressing a 10 mA current. After active corrosion conditions were achieved, the specimens were exposed to constant wetting of 2 days with varying drying times of 1, 3, 5 and 7 days. HCP, resistivity and corrosion rate measurements were taken at the end of each cycle of wetting. The CR1 specimens were monitored for 180 days, while CR2 was monitored for a period of 120 days. The results of the experimental testing are presented and discussed in Chapter 4. A summary timeline of the experimental programme is shown in Figure 3.11.

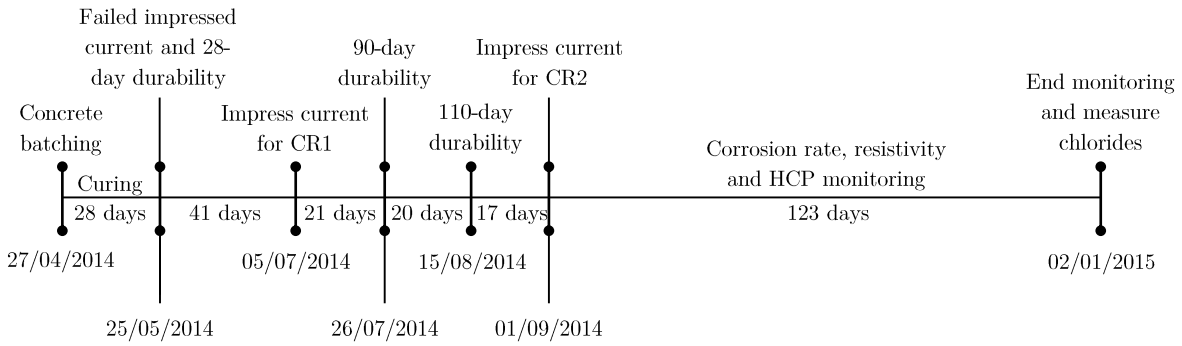

Figure 3.11: Timeline of experimental programme

References

Addis, B. & Goodman, J. 2009. Concrete mix design. In *Fulton's concrete technology. 9th ed.* G. Owens, Eds. Cape Town: Cement & Concrete Institute. 219-228.

Ahmad, S. 2009. Techniques for inducing accelerated corrosion of steel in concrete. *The Arabian journal for science and engineering.* 34(20): 95-104.

Alexander, M.G., Ballim, Y. & Mackechnie, J.R. 2010. *Durability index testing procedure manual (Ver 2.0, May 2010).* Department of Civil Engineering, University of Cape Town: Concrete Materials and Structural Integrity Research Unit.

Austin, S.A., Lyons, R. & Ing, M.J. 2004. Electrochemical behaviour of steel-reinforced concrete during accelerated corrosion testing. *Corrosion engineering.* 60(2): 203-212.

El Maaddawy, T.A. & Soudki, K.A. 2003. Effectiveness of impressed current technique to simulate corrosion of steel reinforcement in concrete. *Journal of materials in civil engineering.* 15(1): 41-47.

Glass, G.K. 1995. An assessment of the coulostatic method applied to the corrosion of steel in concrete. *Corrosion Science.* 37(4): 597-605.

Otieno, M.B. 2008. Corrosion propagation in cracked and uncracked concrete. *MSc. Thesis.* University of Cape Town.

Otieno, M.B. 2014. The development of emperical chloride-induced corrosion rate prediction models for cracked and uncracked steel reinforced concret structures in the marine tidal zone. *PhD Thesis.* University of Cape Town.

Parrott, L.J. 1988. Moisture profiles in drying concrete. *Advances in cement research.* 1(3): 164-170.

Scott, A.N. 2004. The influence of binder type and cracking on reinforcing steel corrosion in concrete. *Ph.D. Thesis.* University of Cape Town.

South African National Standards. 2013. *Code of practice - the structural use of concrete: Part 2: Materials and execution of work.* (SANS10100-2:2013). Pretoria: SANS Standards.

South African National Standards. 2006. *Concrete tests: Part 1: Mixing fresh concrete in the laboratory.* (SANS5861-1:2006). Pretoria: SANS Standards.

South African National Standards. 2006. *Concrete tests: Part 2: Sampling of freshly mixed concrete.* (SANS5861-2:2006). Pretoria: SANS Standards.

South African National Standards. 2006. *Concrete tests: Part 3: Making and curing of test specimens.* (SANS5861-3:2006). Pretoria: SANS Standards.

South African National Standards. 2006. *Concrete tests – Compressive strength of hardened concrete.* (SANS5863:2006). Pretoria: SANS Standards.

CHAPTER 4: RESULTS AND DISCUSSION

4.1 Introduction

This chapter presents results from the experimental testing phase of this research, with the detailed findings presented in the relevant Appendices. This includes initial observations, visual assessments and monitoring of the corrosion rate, half-cell potential and resistivity. Durability Index test results are also presented and discussed for their relevance to the investigation.

4.2 Durability Index Tests

Durability Index tests were completed at 28 and 90 days after casting. These tests were completed on companion cubes and provide an indication of the potential durability of the concrete mixes. This section presents a summary of the Durability Index results and analyses the mix properties for their suitability in the marine environment.

4.2.1 Oxygen Permeability Index

The Oxygen Permeability Index (OPI) results are given in Table 4.1, with the results presented visually in Figure 4.1. It is evident that the OPI results generally increased with age (i.e., permeability reduced), as expected with a refinement of the pore structure over time. Notably the 0.40 PC mix decreased slightly from 28 to 90 days. However, as evident in Figure 4.1, the standard error (SE) bars overlap and indicates no statistical significance between the two sets of data. Additionally, the PC mixes are expected to undergo a relatively faster hydration reaction, producing a denser matrix in a shorter period of time. As a result, the decrease in OPI for the 0.40 PC mix and the relatively small change in OPI for the 0.65 PC mixes are not a concern.

Table 4.1: 28 and 90-Day OPI results

Mix Designation	OPI (log scale)	
	28-Day	90-Day
0.40 FA	10.42	10.82
0.65 FA	10.11	10.36
0.40 GGBS	10.14	10.98
0.65 GGBS	10.04	10.31
0.40 PC	10.46	10.38
0.65 PC	10.11	10.29

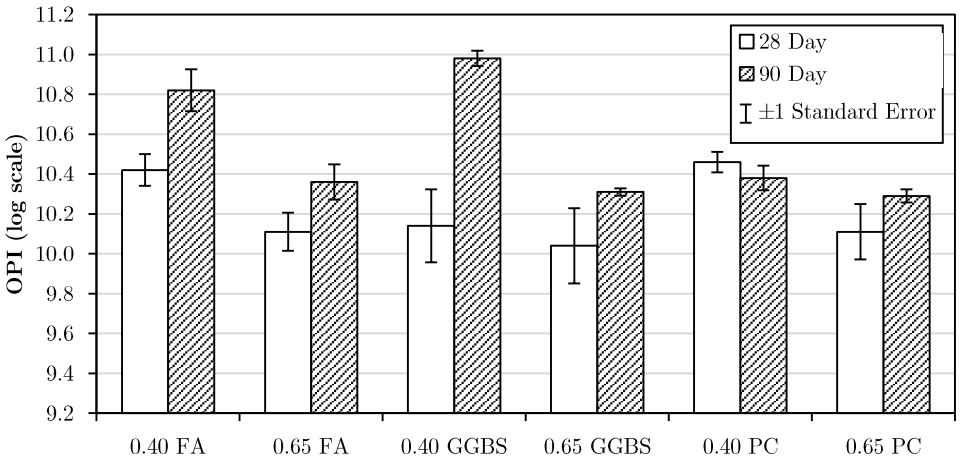

Figure 4.1: 28-Day and 90-Day OPI results

4.2.2 Chloride Conductivity Index

Table 4.2 presents the 28 and 90 day Chloride Conductivity Index (CCI) results, which are also illustrated in Figure 4.2. Upon completion of the 90-day Durability Index tests, it was evident that a component of the sample preparation technique had malfunctioned. An unexpected increase was measured in the CCI from 28 to 90 days. The continued hydration and pore refinement of concrete beyond 28 days should lead to a decrease in the Chloride Conductivity. Consequently the testing procedure was scrutinised and the oven drying phase was identified as the source of error.

Table 4.2: Chloride Conductivity Index results

Mix Designation	CCI (mS/cm)	
	28-Day	90-Day
0.40 FA	0.91	0.27
0.65 FA	0.89	1.36
0.40 GGBS	0.10	0.33
0.65 GGBS	0.41	0.91
0.40 PC	0.62	1.25
0.65 PC	1.29	2.10

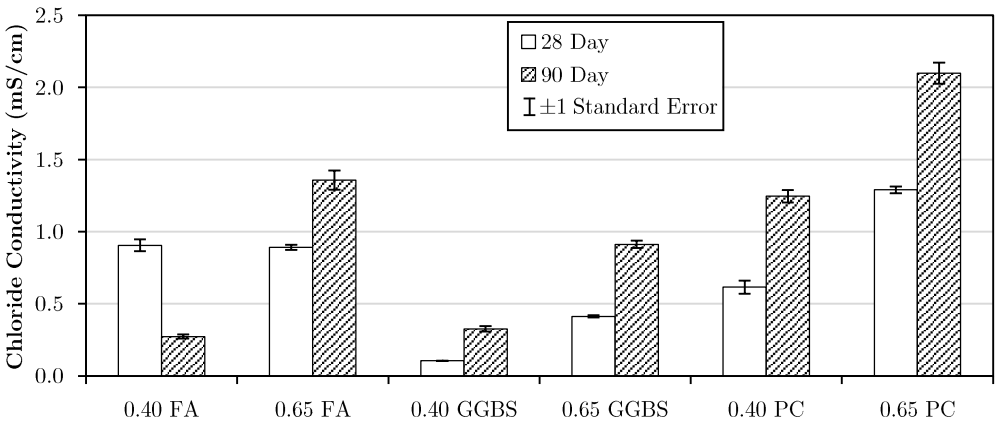

Figure 4.2: 28-Day and 90-Day Chloride Conductivity Index results

Samples must be oven-dried at 50°C for 7 days before testing (Alexander, Ballim & Mackechnie, 2010). These conditions were checked for the 28-day tests and satisfied the criteria. However, due to unforeseen circumstances, when conducting the 90-day tests the oven was no longer available. As a result, a different oven was used and set to the appropriate temperature of 50°C. The oven did not maintain this temperature and from independent measurements, it was found that the specimens were exposed to temperatures in the region of 70°C. The microstructure of concrete specimens can be damaged at this elevated temperature which explains the unexpected results. Pigeon *et al.* (1993) found that drying at 110°C caused a significant increase in the chloride ion permeability of concrete at w/b ratios of 0.45 and 0.35. Thus, the elevated temperature was likely the source of the error.

Consequently, the remaining companion cubes were tested for CCI at an age of 110 days. The results thereof are presented in Table 4.3 and shown graphically in Figure 4.3. It is evident that these CCI values are plausible and, albeit at a later stage, provide a better reflection of the concrete quality. The CCI of the slag-bearing concrete remained low and relatively unchanged from 28 to 110 days. The FA mixes made the most notable improvements in CCI from 28 to 110 days, decreasing by a factor of at least 2. When considering the PC mixes, it is worth noting the high CCI for the 0.65 PC mix. This remained relatively unchanged over the short period of time but such a high CCI is undesirable. It is also worth noting the high CCI values for the 0.40 PC, which are in the range of the 0.65 w/b ratio mixes which included SCMs.

Table 4.3: Adjusted Chloride Conductivity Index results

Mix Designation	CCI (mS/cm)	
	28-Day	110-Day
0.40 FA	0.91	0.27
0.65 FA	0.89	0.41
0.40 GGBS	0.10	0.13
0.65 GGBS	0.41	0.23
0.40 PC	0.62	0.39
0.65 PC	1.29	1.35

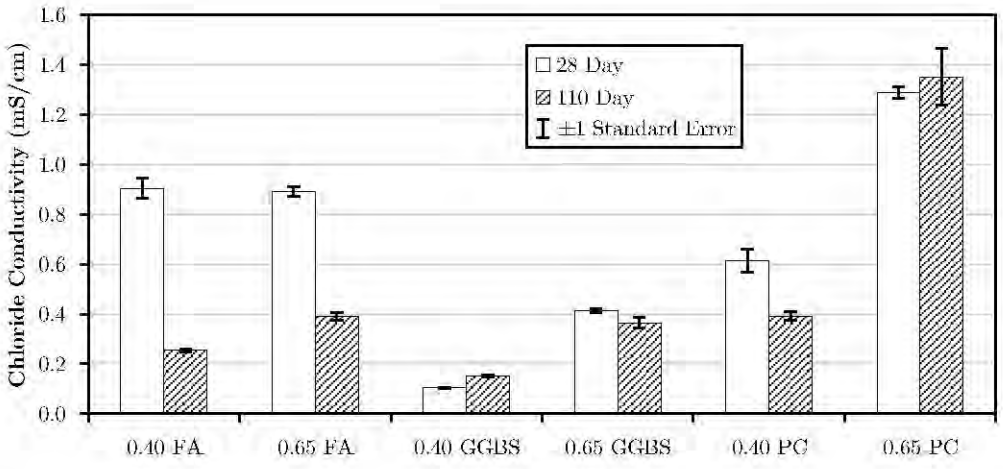

Figure 4.3: 28-Day and 110-Day Chloride Conductivity Index results

Oven drying the samples at 70°C, instead of 50°C, caused the Chloride Conductivity to increase by an average factor of 2.95. This is due to damage of the concrete pore structure and possible interconnection of the voids. This effect may be exaggerated by the continued hydration and refinement of the cement matrix for an additional 20 days; however, this would not account for a considerable variation. Consequently, the 110-day Chloride Conductivity results will be considered henceforth.

4.2.3 Water Sorptivity Index and Porosity

The 28 and 90-day Water Sorptivity Index (WSI) and porosity results are presented in Table 4.4. The incorrect oven-drying temperature caused similar problems in the porosity measurements. A general increase in the porosity was measured when comparing the 28 and 90 day measurements.

Table 4.4: Water Sorptivity Index and porosity results

Mix Designation	WSI (mm/hour$^{0.5}$)		Porosity (%)	
	28-Day	90-Day	28-Day	90-Day
0.40 FA	6.3	6.1	12.66	9.19
0.65 FA	8.7	6.9	10.93	11.82
0.40 GGBS	7.0	4.4	5.48	8.29
0.65 GGBS	7.3	4.7	11.04	12.02
0.40 PC	7.2	6.5	8.59	10.70
0.65 PC	8.6	7.8	10.62	11.76

Again, this is contrary to expectations with a refinement in the pore structure over time likely to decrease the porosity. However, insufficient companion cubes were available to redo both the sets of testing. Consequently, the CCI test was repeated and the porosity was estimated using the saturation of 5M NaCl solution. The 5M NaCl solution was assumed to have a relative density of 1.20 (Stanish, Alexander & Ballim, 2004) in calculating the porosity. This calculated porosity was then used to back-calculate a Water Sorptivity Index value based on the previously determined absorption gradients. This process of estimating the porosity, and hence sorptivity is described in more detail in Appendix D, with the results presented in Table 4.5 and shown graphically in Figure 4.4 and Figure 4.5.

Table 4.5: Adjusted Water Sorptivity Index and porosity results

Mix Designation	WSI (mm/hour$^{0.5}$)		Porosity (%)	
	28-Day	110-Day	28-Day	110-Day
0.40 FA	6.3	12.8	12.66	4.40
0.65 FA	8.7	10.7	10.93	7.56
0.40 GGBS	7.0	7.9	5.48	4.57
0.65 GGBS	7.3	6.6	11.04	8.53
0.40 PC	7.2	10.6	8.59	6.51
0.65 PC	8.6	9.0	10.62	10.19

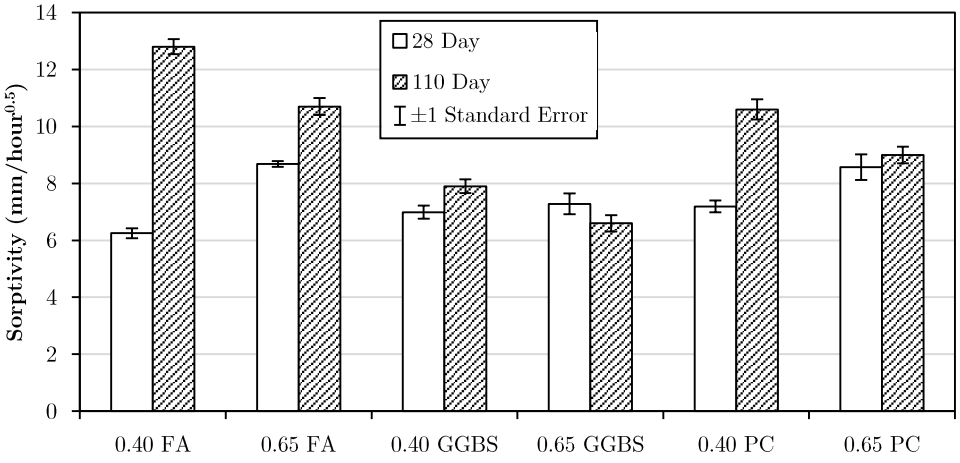

Figure 4.4: 28-Day and 110-Day sorptivity

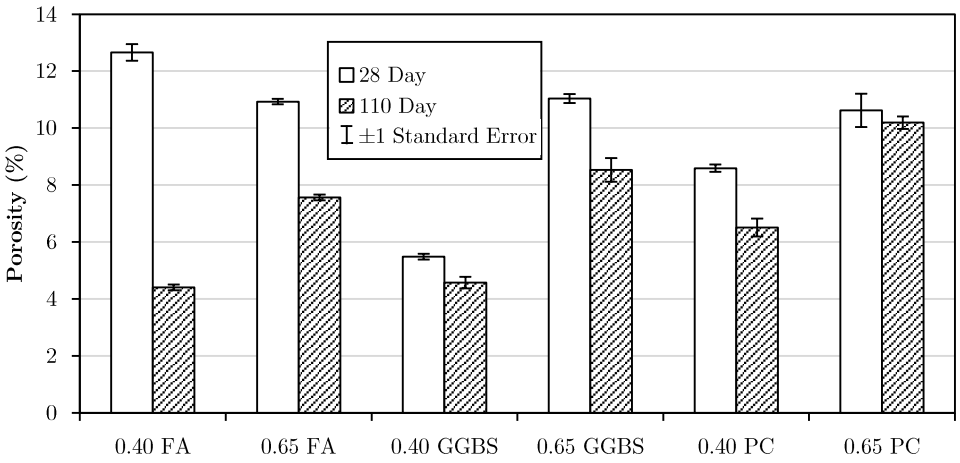

Figure 4.5: 28-Day and 110-Day porosity

The overall porosity generally decreased from 28 to 110 days. These porosity values are consistent with expectations of the relevant mixes. The porosity of the 0.40 FA and 0.40 GGBS are comparatively lower than the other mixes, with the 0.40 FA mix undergoing a drastic reduction in porosity from 28 to 110 days. However, the WSI results do not align themselves with expected values and show a general increase in the WSI from 28 to 110 days. The source of error is most likely from an accumulation of errors in the back-calculation and a major reduction in the porosity from 28 to 110 days, with a reduction in porosity causing higher WSI values (porosity is in the denominator for WSI calculations). As a result, the WSI results will not be considered in the subsequent analysis.

4.2.4 Synopsis of durability indices

The durability indices can generally be assessed according to Table 4.6. As evident in Table 4.1, all of the 6 mixes obtained OPI values greater than 10.0 for both 28 and 90 days. All the concrete mixes can thus be classified as 'excellent' quality, with the 0.40 FA and 0.40 GGBS achieving the highest OPI values.

Table 4.6: Durability index indicator values

Quality Rating	OPI (log scale)	Sorptivity ($mm/h^{0.5}$)	Chloride Conductivity (mS/cm)
Excellent	> 10.0	< 6	< 0.75
Good	9.5 – 10.0	6 -10	0.75 – 1.50
Poor	9.0 – 9.5	10 – 15	1.50 – 2.50
Very Poor	< 9.0	> 15	> 2.50

The sorptivity values generally increased from 28 to 110 days. This was unexpected and likely due to the unorthodox back-calculation of the 110 day sorptivity values. Hence, further analysis of the sorptivity will only include the 28 day results. As expected with a refinement of the pore structure over time, the porosity generally decreased with age throughout. Also, from Figure 4.6 it is evident that a rough trend exists between the OPI results and the porosity. Furthermore, it is worth noting that the significantly lower porosity values (0.40 FA and 0.40 GGBS) correspond with higher OPI values.

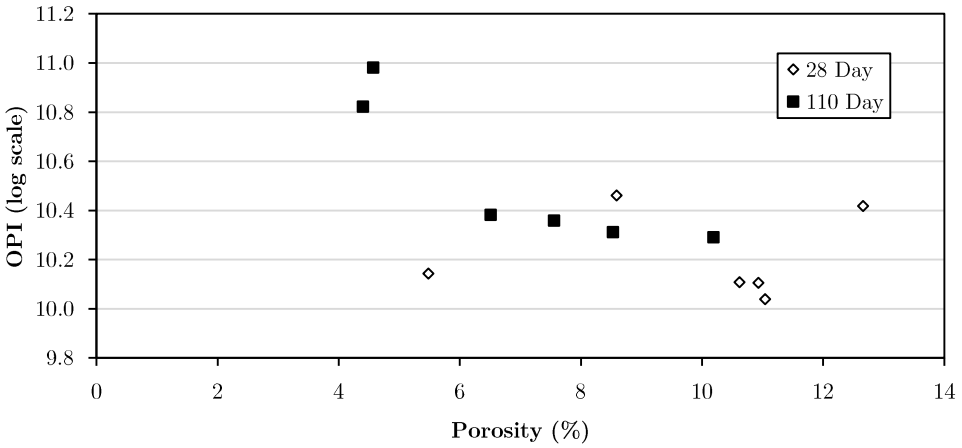

Figure 4.6: OPI vs Porosity at 28 and 110 days

In terms of the CCI, only the 0.65 PC did not receive an 'excellent' rating. With a 110 day CCI value of 1.35, this mix can be qualified as 'good' but appears significantly less suitable in the marine environment than the other investigated mixes. The abovementioned factors will be considered in Section 4.4 when assessing the corrosion rate of the respective mixes and the impact of the durability index parameters.

4.3 Early-Age Corrosion Rate (first 5 weeks)

This phase of monitoring covers the specimens during the first 5 weeks of cyclic wetting and drying (before active corrosion conditions were achieved). The observations were made before the successful activation of corrosion and thus include measurements conducted on all the specimens (CR1 and CR2), and are reported as an average of 3 readings.

4.3.1 Passive corrosion conditions

4.3.1.1 Corrosion rate and HCP

The corrosion rates measured in the first 5 weeks of monitoring fall within the passive state (HCP > -256 mV and i_{corr} < 0.1 µA/cm²) for the FA and PC mixes. The early-age corrosion rates were highly variable with the duration of wetting and drying having no noticeable effect on the corrosion rate. In Figure 4.7 it is evident that for the 0.40 FA specimens the corrosion rate generally remained below the threshold value during this 5 week period.

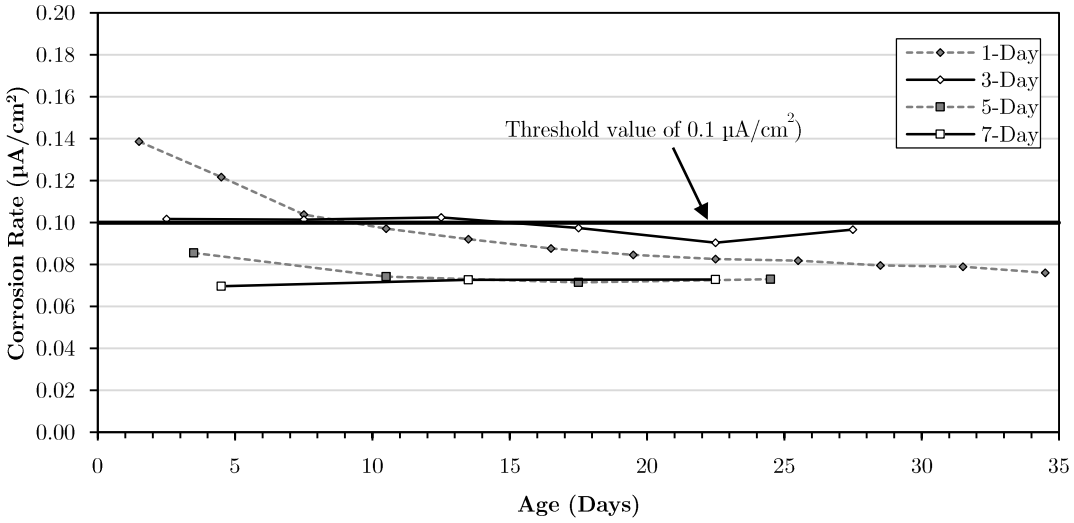

Figure 4.7: Early-age corrosion rate monitoring of 0.40 FA

During this initial phase, it was apparent that the specimens were passive due to the low corrosion rates and relatively high HCP values (less negative). The impressed current technique applied was not able to activate corrosion, with the cycles of wetting and drying of 5% NaCl solution having no noticeable impact on the corrosion rate. The HCP readings were generally greater than -100 mV, which is well above the commonly accepted HCP threshold value of -256 mV and indicates a low probability that corrosion is occurring (ASTM C876-09, 2009). Moreover, the corrosion rates were generally between 0.06 and 0.14 µA/cm², as illustrated in Figure 4.7 for 0.40 FA. The relatively low corrosion rates (Table 4.7) and HCP (Table 4.8) readings of the FA and PC mixes indicated that the specimens were in a passive state of corrosion.

Table 4.7: Average corrosion rates for the first 5 weeks (as a function of drying time)

Mix Designation	Average corrosion rate for the first 5 weeks (µA/cm²)			
	1-Day	3-Day	5-Day	7-Day
0.40 FA	0.10	0.10	0.10	0.08
0.65 FA	0.09	0.15	0.10	0.07
0.40 GGBS	0.65	0.52	0.36	0.43
0.65 GGBS	1.17	0.86	0.88	1.33
0.40 PC	0.11	0.08	0.08	0.13
0.65 PC	0.12	0.10	0.08	0.08

Table 4.8: Average HCP measurement for the first 5 weeks (as a function of drying time)

Mix Designation	Average HCP measurement for the first 5 weeks (mV)			
	1-Day	3-Day	5-Day	7-Day
0.40 FA	-38	-66	-68	-114
0.65 FA	-33	-105	-106	-54
0.40 GGBS	-444	-353	-387	-272
0.65 GGBS	-499	-414	-470	-243
0.40 PC	-72	-35	-71	-181
0.65 PC	-61	-42	-48	-50

This phase did, however, highlight the effect of sulphides and thiosulphates on the early-age passive state corrosion rate of slag-bearing concrete. In Table 4.7 and Table 4.8 it is evident that the GGBS specimens appear to be actively corroding. Figure 4.8 and Figure 4.9 present corrosion rate measurements for the 0.40 GGBS and 0.65 GGBS specimens, respectively. From these figures it is evident that the slag-bearing specimens showed corrosion rates of between 0.3-1.5 $\mu A/cm^2$. Scott (2004) and Otieno (2008) also measured high early-age corrosion rates in slag-bearing concretes; however, the measured corrosion rates in the current experiments are significantly higher. Scott (2004) also found that the passive state corrosion rates in slag-bearing concretes were not limited by the concrete resistivity. Additionally, Scott (2004) found that the negative effect of sulphides and thiosulphates ceased after approximately 6 weeks when a passive protective layer had formed to protect the steel. Scott (2004) inferred that the corrosion rates reduced after the formation of a passive protective layer and the sulphides and thiosulphates ceased to have a significant effect on the corrosion rate.

Nevertheless, the short duration of monitoring and the apparent scatter in the data do not show a clear trend on the effect of the drying duration on this early-age corrosion rate. No conclusive trends were visible based on the duration of the cycle of drying.

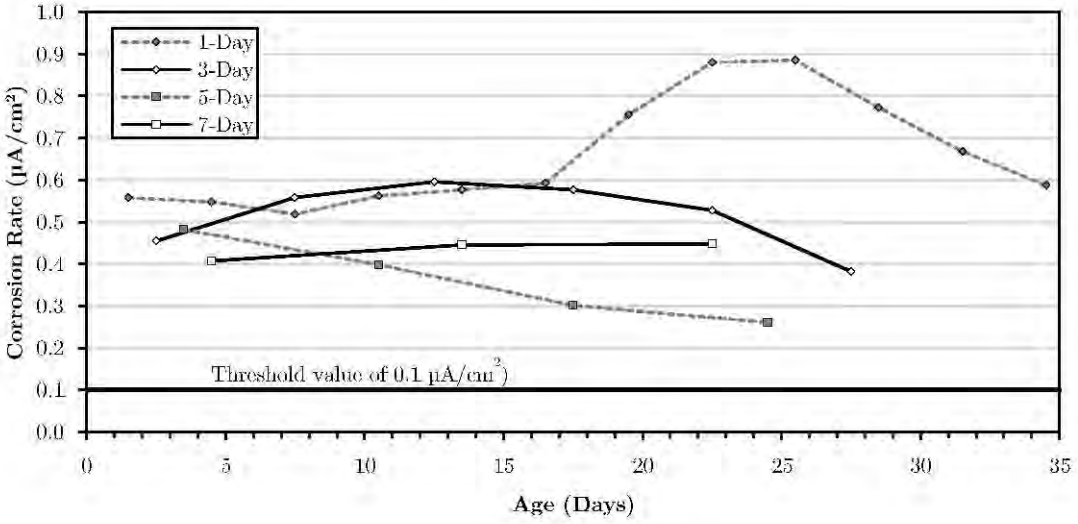

Figure 4.8: Early-age corrosion rate monitoring of 0.40 GGBS

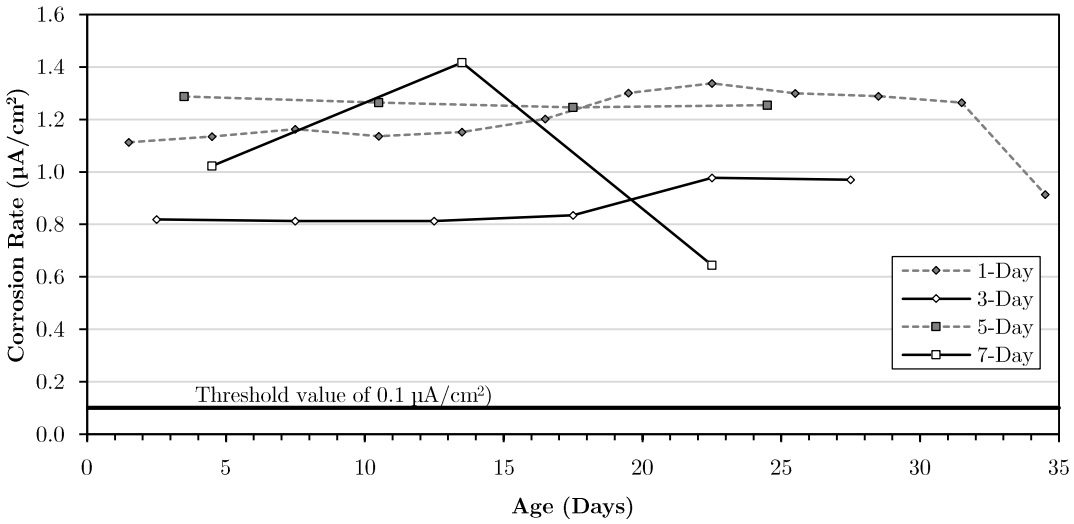

Figure 4.9: Early-age corrosion rate monitoring of 0.65 GGBS

The inclusion of slag as a SCM in concrete introduces sulphides and thiosulphates into the mix. These constituents have oxygen reducing characteristics and hence lower the dissolved oxygen concentration at the level of the steel (Scott, 2004). Without sufficient oxygen the steel is unable to develop its natural protective layer which is essentially a small amount of corrosion product coating the steel surface. This effect causes relatively high early-age corrosion rates in slag-bearing concretes. Otieno (2008) noted that the corrosion rate in specimens containing Corex slag reverted to passive corrosion rate conditions after 6 weeks. This is likely due to the oxidation of the majority of the sulphides and thiosulphates allowing a sufficient amount of dissolved oxygen to be available at the steel surface.

4.3.1.2 Chloride content

The cover measurements identified an outlier specimen which had a cover of 35 mm. This specimen was not included in the monitoring phase of this experiment. However, the specimen was used to provide an indication of the chloride content in the specimens. At the end of the initial 5-week period, a 20 mm diameter core sample was extracted from the 0.65 GGBS 1-3 (specimen number 3 exposed to cycles of 1-day wetting) specimen and the total chloride content was measured by chemical titration. As mentioned in Section 3.7, the surface chloride content was 2.5%; however, chlorides were not present at the level of the steel (20 mm deep). Consequently, an insufficient quantity of chlorides was available at the steel surface to activate chloride-induced corrosion, thus indicating that the impressed current technique had not successfully driven chlorides to the level of the steel in both CR1 and CR2.

4.3.2 Active corrosion conditions

4.3.2.1 CR1 visual assessment

A current of 10 mA was impressed into the CR1 specimens for 5 days. The condition of the specimens was noted immediately after removal of the current. In Figure 4.10 it is evident that predominantly one specimen from each tray showed evidence of corrosion product on the concrete surface. In each

case these are specimens from the 1st set and make up sample set CR1. The pictures in Figure 4.11 show close-ups of the rust staining in all of the CR1 specimens.

Figure 4.10: Specimens at the end of the impressed current

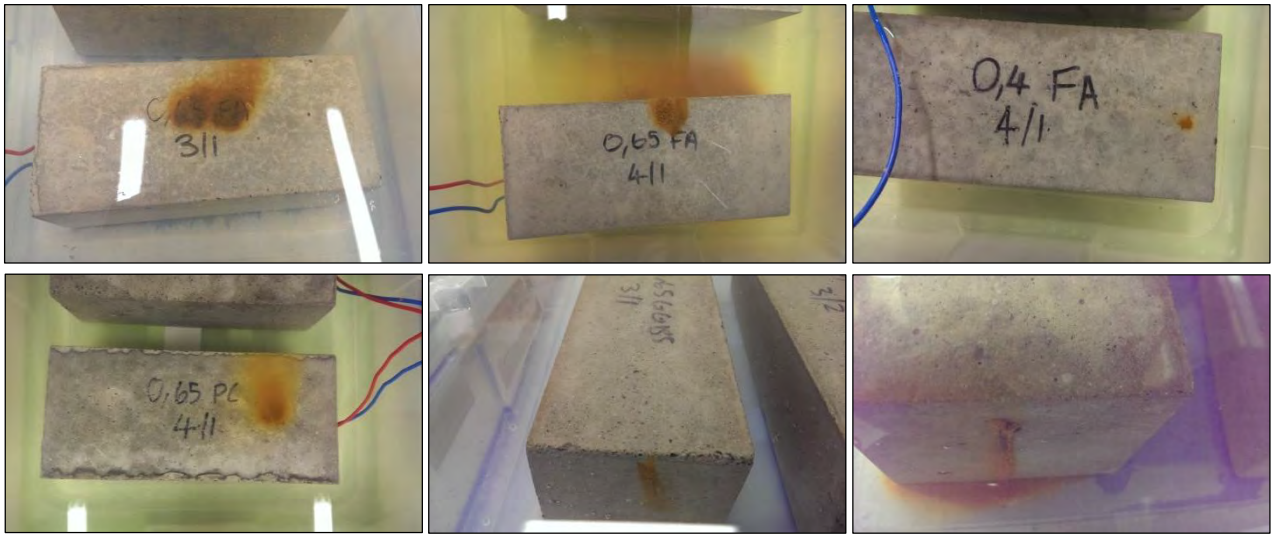

Figure 4.11: Corrosion product on selected specimens from CR1 (brown rust stains)

4.3.2.2 CR2 visual assessment

As indicated in Section 3.7 and shown in Figure 3.11, the specimens in CR2 were exposed to another impressed current of 10 mA for 3 days – with each specimen isolated in its own container of NaCl solution. The resulting impressed current was sufficient to cause active corrosion in all of the CR2 specimens and the chloride content was once again checked on the faulty specimen (which had already been excluded from the sample set). It should be noted that the increased cover depth would have an effect on the distribution of chlorides in the specimens and thus merely provided an indication of the chloride content. In Figure 4.12, it is evident that sufficient chlorides were now present at the level of the steel once active corrosion conditions had been achieved.

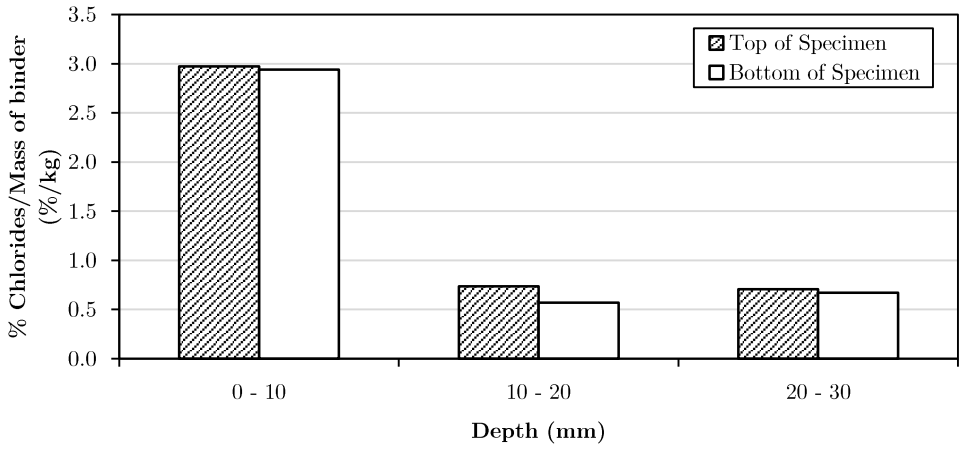

Figure 4.12: Chloride content of 0.65 GGBS 1-3

4.4 Corrosion Monitoring under Cyclic Wetting and Drying

Sections 4.4.1 to 4.4.5 discuss the results for measurements taken while implementing the various cycles of wetting and drying. The results are presented for both sets of samples and are calculated as a two-point moving average. Conclusions thereof in Chapter 5 will assess the collective findings of both sets of measurements.

For ease of reference, Figure 4.13 presents a summary timeline of the experimental programme highlighting the start and end dates for monitoring (detailed timeline presented in Figure 3.11). As mentioned previously, the CR1 specimens included approximately 180 days of monitoring while the CR2 specimens were monitored for approximately 120 days. The CR1 specimens were exposed to an impressed current of 10 mA for 5 days, while the CR2 specimens were exposed to an impressed current of 10 mA for 3 days. The shortened duration for the impressed current caused a significant reduction in the achieved corrosion rates, with the CR2 specimens providing better correlations to expected corrosion rates in practice. Additionally the CR2 sample set includes two specimens for each data point and thus improves the reliability of the results. The CR1 sample set provides some insight while the CR2 sample set will be considered as the primary source of discussion.

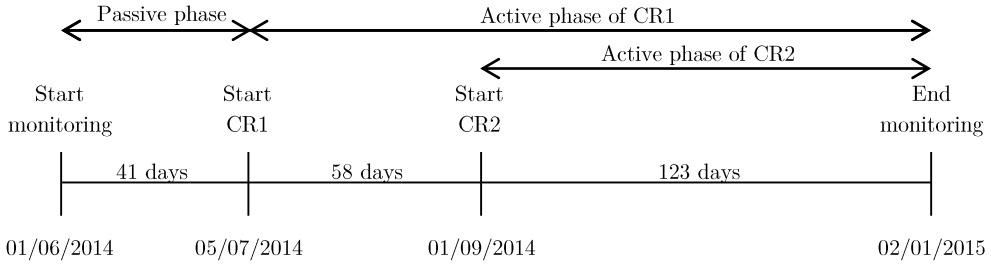

Figure 4.13: Summary timeline for monitoring of CR1 and CR2 data sets

4.4.1 Effect of the drying duration on the corrosion rate

The oxygen availability, i.e. the dissolved oxygen content, was not directly measured in the current experimental work. However, this work will make reference to an inferred oxygen availability in the

sense that, from the theoretical background presented in Chapter 2, active corrosion will be assumed to indicate a sufficient availability of oxygen, while passive or low corrosion rates will assume the opposite. The oxygen availability will be affected by the duration of drying and thus sufficiently short drying durations have the potential to limit the availability of oxygen. During the experimental testing, four variations of drying time were applied which will vary the availability of oxygen for corrosion. Hence, unless otherwise specified, any further reference to oxygen availability implies an inferred oxygen availability based on the implemented cycles of wetting and drying.

Figure 4.14 to Figure 4.19 illustrate the corrosion rate measurements for each combination of binder type and w/b ratio (CR1 and CR2). These figures illustrate the effect of the drying duration on the corrosion rate (enlarged versions can be found in Appendix E). The drying duration is illustrated on each figure as the primary variable (e.g. '1-Day' indicates cycles of 2 days wetting and 1 day drying).

4.4.1.1 CR1

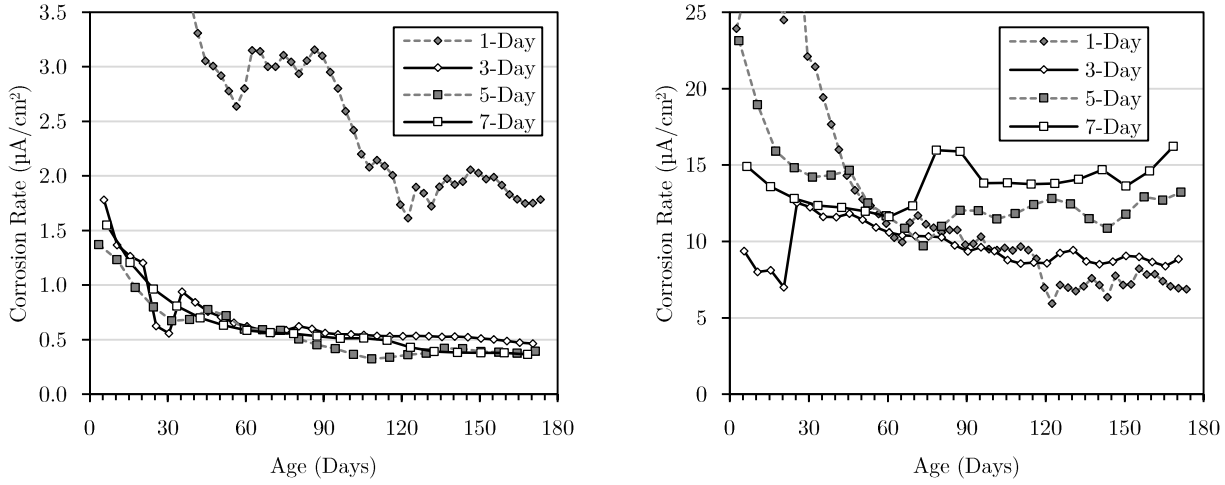

Figure 4.14: CR1 corrosion rate for a) 0.40 FA and b) 0.65 FA

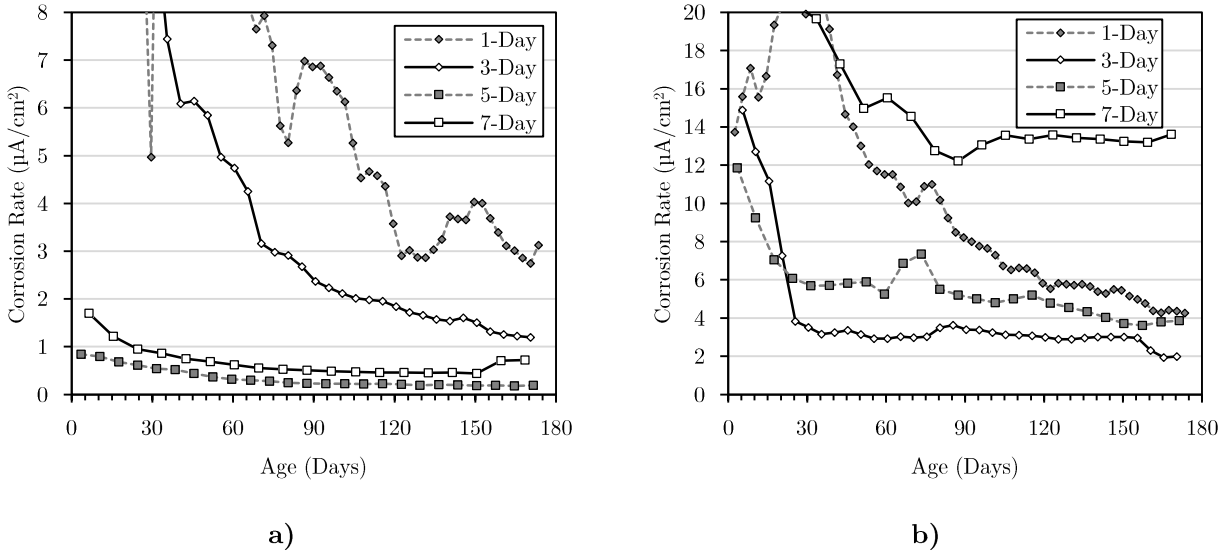

Figure 4.15: CR1 corrosion rate for a) 0.40 GGBS and b) 0.65 GGBS

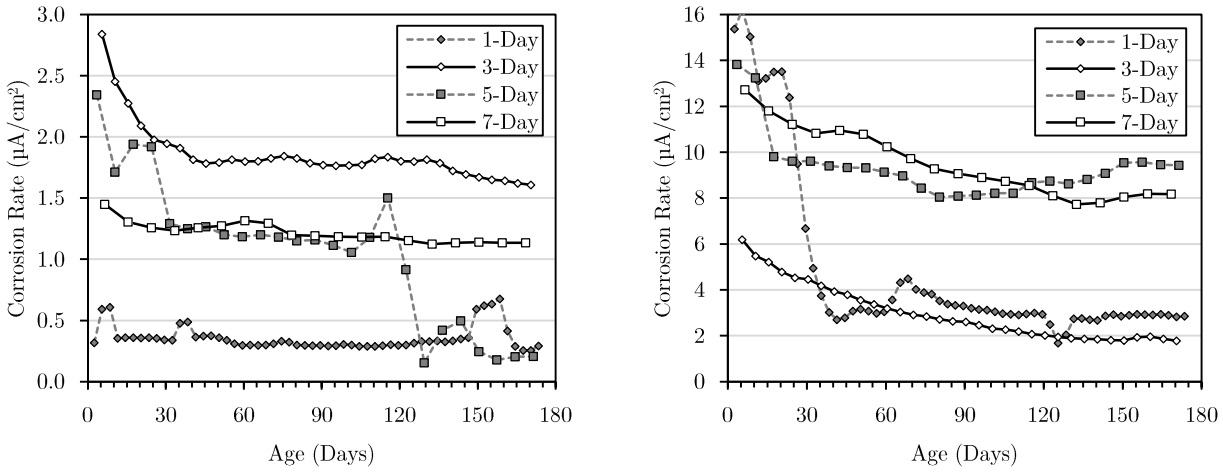

Figure 4.16: CR1 corrosion rate for a) 0.40 PC and b) 0.65 PC

4.4.1.2 CR2

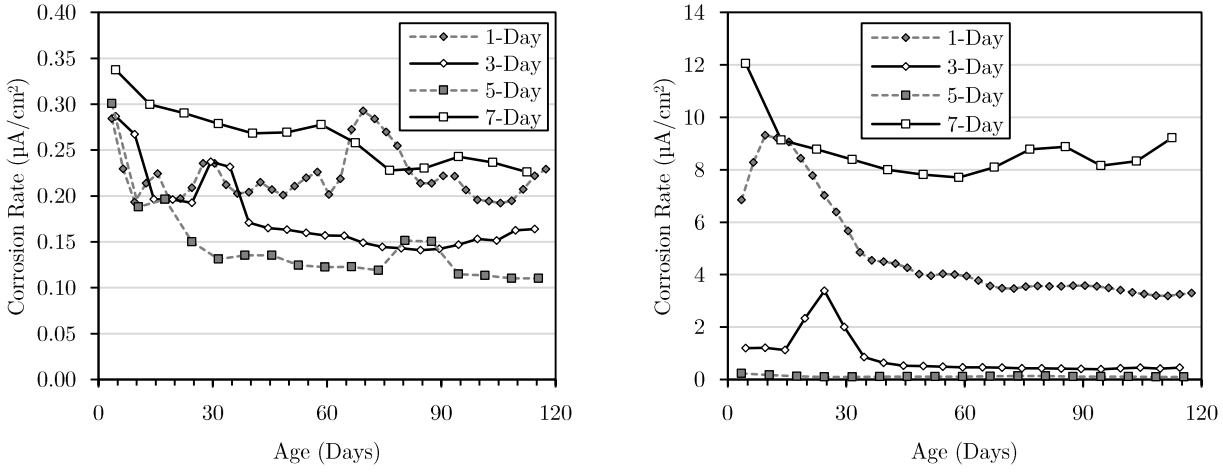

Figure 4.17: CR2 corrosion rate for a) 0.40 FA and b) 0.65 FA

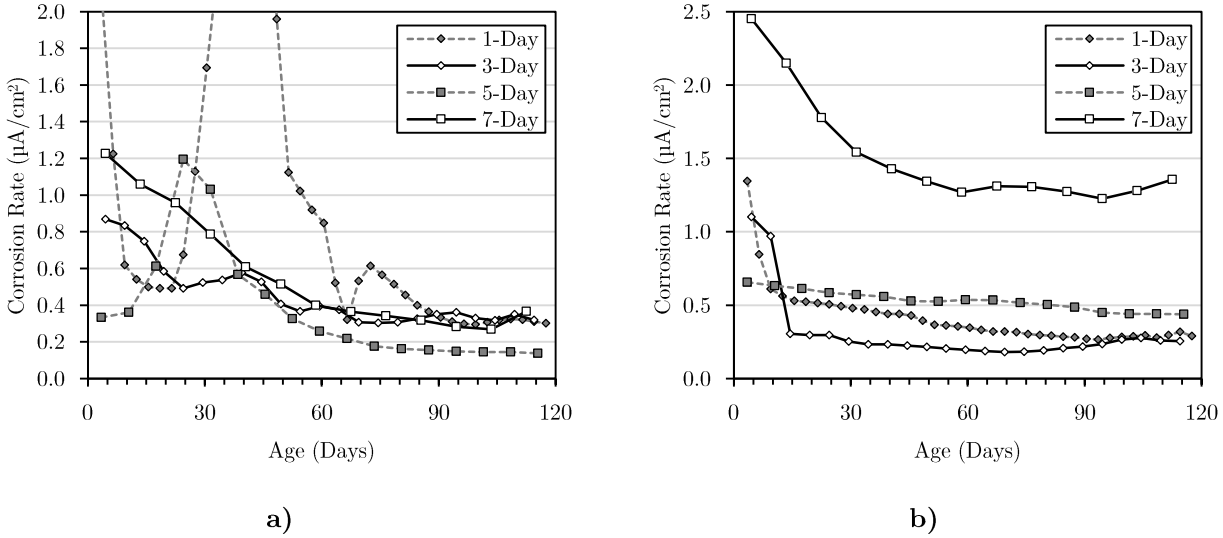

Figure 4.18: CR2 corrosion rate for a) 0.40 GGBS and b) 0.65 GGBS

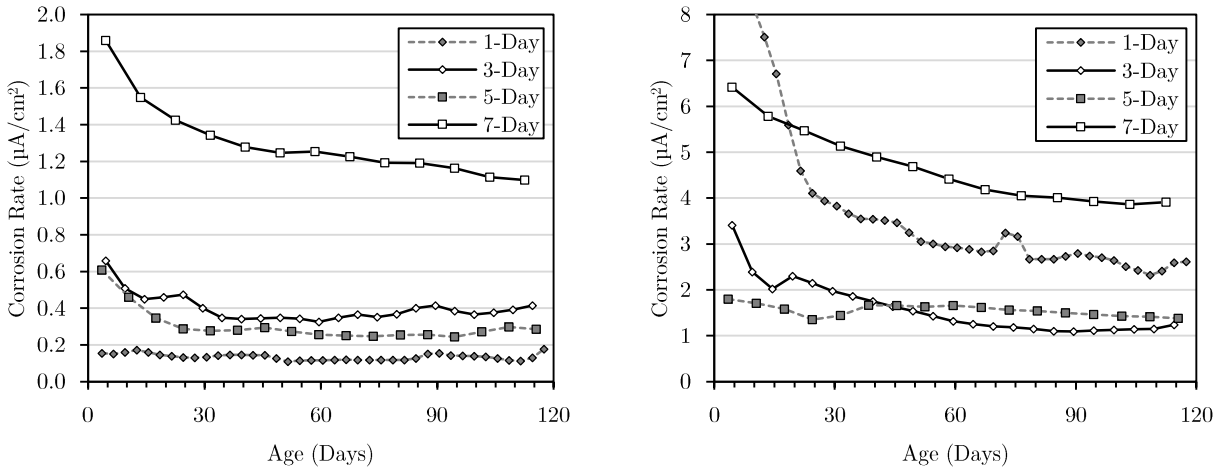

Figure 4.19: CR2 corrosion rate for a) 0.40 PC and b) 0.65 PC

From Figure 4.14 to Figure 4.16 it is evident that the CR1 specimens went through an initial period of high corrosion rates, which decreased relatively rapidly in the first few weeks of monitoring. The specimens were not able to naturally maintain these high corrosion rates and the corrosion rates decreased until more stable, consistent corrosion rates were achieved. The CR2 specimens (shown in Figure 4.17 to Figure 4.19) were impressed with a shorter duration current and thus lower initial corrosion rates were measured and the specimens required a shorter time to achieve naturally sustainable corrosion rates.

4.4.1.3 Discussion

Existing studies on the depth of drying in concrete are scarce. As mentioned in Section 2.7.2, an indication of the moisture content is normally derived from measuring the internal relative humidity with purpose-built relative humidity probes. However, to the author's knowledge there are no existing studies investigating the change in relative humidity with depth under exposure to multiple cycles of wetting and drying. Parrott (1988) completed relative humidity testing under extended drying durations of 1 cycle of wetting and drying. Parrott (1988) makes reference to a proposed equation for the relative humidity as a function of the depth into concrete. Equation 4.1 has been used to plot Figure 4.20, which shows the internal relative humidity under the exposure conditions applied in this research (rha = 50%, t = 1, 3, 5 and 7 days).

$$RH = 100 - (1 - e^{-At})(100 - rha) \qquad \text{(Eq. 4.1)}$$

where: RH is the relative humidity (%), rha is the ambient relative humidity (%), t is the drying time (days), $A = 1.42/(d + 0.01)^2$ and d is the depth from the exposed surface (mm).

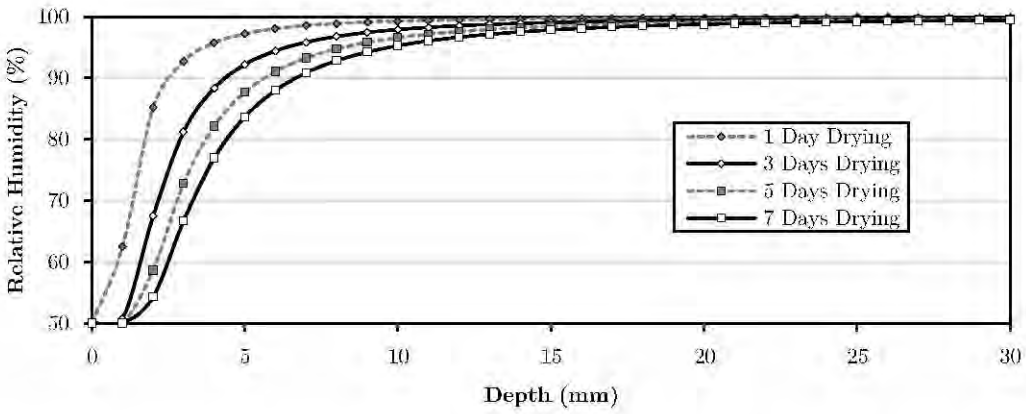

Figure 4.20: Internal relative humidity as a function of depth into concrete (50% external RH) (Parrott, 1988)

From this figure, it is apparent that at a depth of 20 mm the internal RH appears almost unchanged (max. 99.8% RH and min. 98.8% RH). However, the degree of saturation does decrease exponentially with a reduction in RH (as illustrated in Figure 2.25) and may cause a more substantial change in the moisture condition. Also, Figure 4.20 does not take into account the effect of the binder type and the w/b ratio. A denser matrix with reduced permeability will limit the transport of moisture and oxygen, which is not accounted for in Figure 4.20. Consequently, the applicability of this figure to the study at hand will be limited. The figure may only apply to certain binder types and w/b ratios, which was not specified by Parrott (1988).

The corrosion rate plots in Figure 4.14 to Figure 4.19 show that most of the specimens are in a high state of active corrosion. The drying duration appears to have no significant impact on the corrosion rate for a w/b ratio of 0.40 which would be expected if the drying followed the progress shown in Figure 4.20. However, at a w/b ratio of 0.65 the impact of the varied drying duration is apparent. The figures show a general trend of an increase in the corrosion rate as the drying duration is increased. The expectation is that the higher permeability associated with a w/b ratio of 0.65 allowed the concrete to dry out more rapidly resulting in a more open pore structure for oxygen ingress and thus an increased supply of oxygen. The effect of the increased w/b ratio on the durability indices of the concrete is assessed in Table 4.9. From this table it is evident that the increase in the w/b ratio has caused a significant decrease in the concrete potential durability.

Table 4.9: Change in 28-Day durability index properties from a w/b ratio of 0.40 to 0.65

Binder Type	Change in k*	Change in WSI	Change in Porosity
FA	+ 110%	+ 40%	- 15%
GGBS	+ 30%	+ 5%	+ 100%
PC	+ 155%	+ 20%	+ 25%

*OPI is measured on a log scale, hence k (coefficient of permeability) is analysed

The durability indices generally show that an increase in the w/b ratio adversely affects the concrete properties that allow moisture and oxygen movement through concrete. Quantifying the effect of these properties on the drying time was not possible; however, a general assumption is that the decreased potential durability properties will lead to faster drying to the level of the steel. This provides justification for the noticeable impact of the drying duration on the corrosion rate in the 0.65 w/b specimens, while the drying duration had no noticeable impact on the 0.40 w/b specimens. More extensive variation in the w/b ratio would be required to provide some sort of quantification and to develop a threshold value which is likely somewhere between 0.40 and 0.65 (for a cover depth of 20 mm).

The FA mixes present one notable exception in Table 4.9 for the change in porosity. However, in Figure 4.5 the 28 day porosity measurements appear overstated for the 0.40 FA mix and is unlikely a realistic reflection of the 28 day porosity. For a similar mix (containing 30% FA), Angelucci (2013) measured a 28 day porosity of 8.4%, compared to a porosity of 12.7% measured in this study. In comparison the 0.65 FA specimens achieved a 10.9% porosity which compares more appropriately with a porosity of 8.4% for the 0.40 FA mix. Consequently, this entry should be considered as an outlier, with the general trend showing a decrease in concrete durability with an increase in w/b ratio.

The corrosion rate in the PC mixes is expected to be controlled by the resistance of the cathode (availability of oxygen). As a result, the PC mixes should be more susceptible to the cycles of wetting and drying and should show a distinct fall in the corrosion rate if the drying time is significantly reduced. However, based on previous studies by Otieno (2008) and Scott (2004), it was unexpected that the corrosion rate in the 0.65 FA and 0.65 GGBS would be affected significantly by the drying duration, since it is primarily controlled by the concrete resistivity. Specimens containing these binder types are expected to be resistivity controlled. However, these specimens showed clear distinctions in the corrosion rates without a noticeable change in the resistivity.

As a result, one 0.65 GGBS specimen was submerged for a period of 50 days to investigate the controlling effect of the oxygen availability. The effect on the corrosion rate is shown in Figure 4.21. It is evident that the submerged conditions were insufficient to stifle corrosion in the GGBS specimen. This is likely due to the controlling effects of the concrete resistivity which was in the region of 25-35 kOhm-cm before immersion. In GGBS and FA specimens, the resistivity and oxygen availability appear to have a combined effect on the corrosion rate, with limited oxygen availability alone not able to stifle corrosion. It is expected that the resistivity has a primary controlling effect and the oxygen availability acts as a secondary effect influencing the rate of corrosion. However, the combination and interaction of these factors was not investigated further.

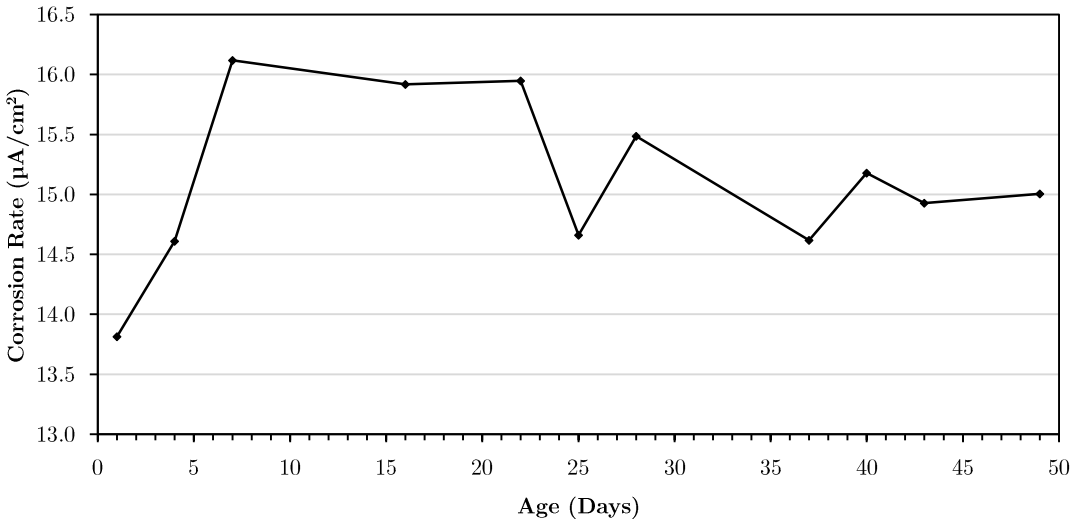

Figure 4.21: Corrosion rate of one 0.65 GGBS specimen submerged for 50 days

It is apparent from the figures to follow (Figure 4.22 to Figure 4.25) that varying the drying time caused no consistent or significant trend on its influence on the corrosion rate in the 0.40 GGBS and 0.40 FA specimens; while, the corrosion rate in the 0.40 PC specimens generally decreased with a reduction in the drying time. The effect of the drying duration on the 0.40 w/b ratio specimens is illustrated in Figure 4.22 to Figure 4.25. The effect of limiting the oxygen availability on the 0.40 PC specimens is evident by comparing the relative corrosion rates in these figures. It is evident that at longer drying times the 0.40 PC specimens performed the worst; while the 0.40 PC specimens performed the best for the shortest applied drying time (1-Day).

4.4.1.4 CR1

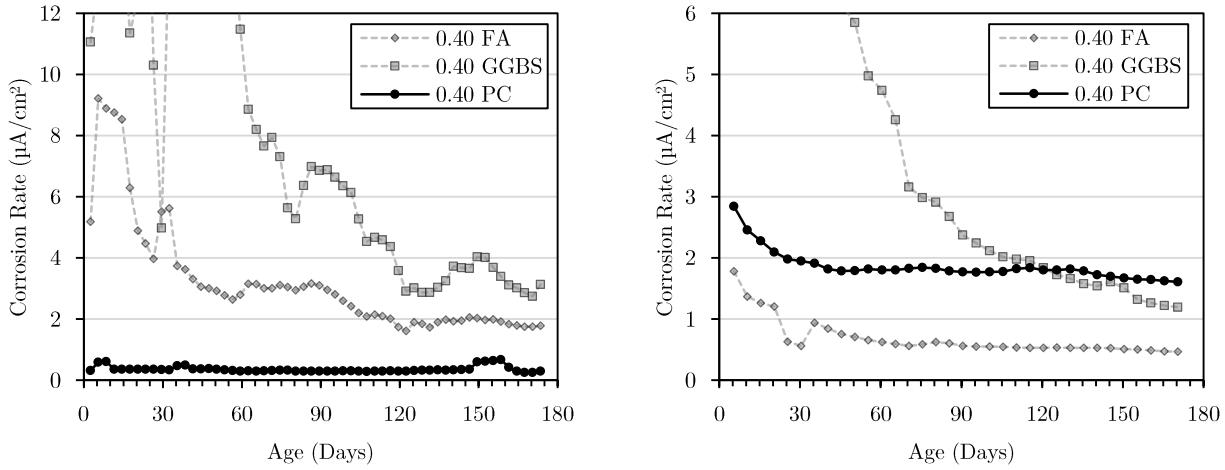

Figure 4.22: CR1 corrosion rate for a) 1-Day and b) 3-Day drying cycles

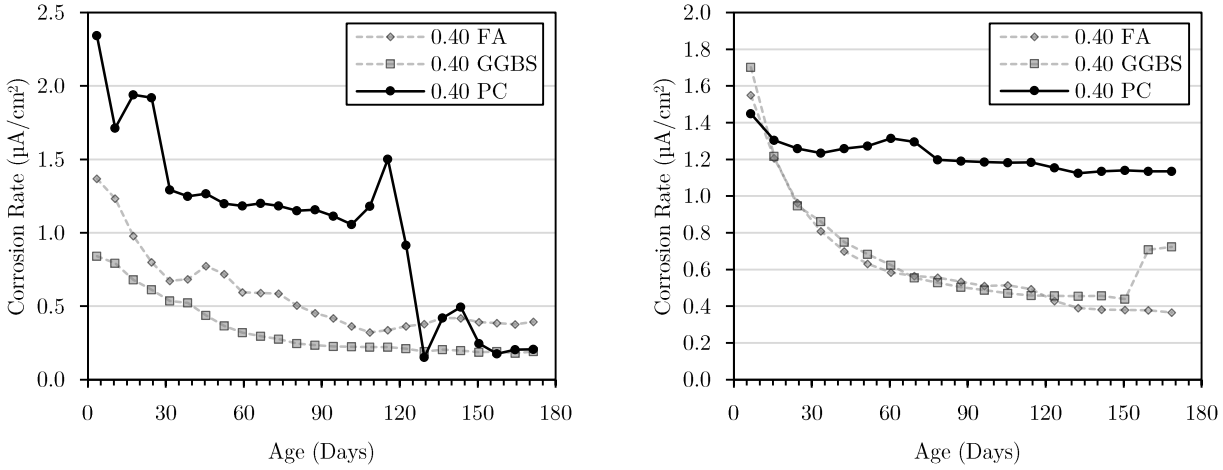

Figure 4.23: CR1 corrosion rate for a) 5-Day and b) 7-Day drying cycles

4.4.1.5 CR2

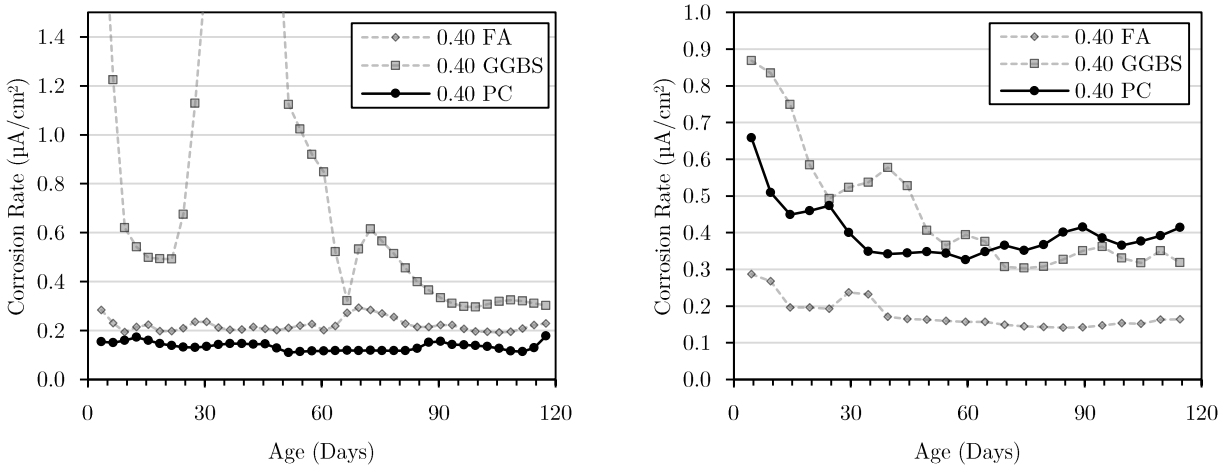

Figure 4.24: CR2 corrosion rate for a) 1-Day and b) 3-Day drying cycles

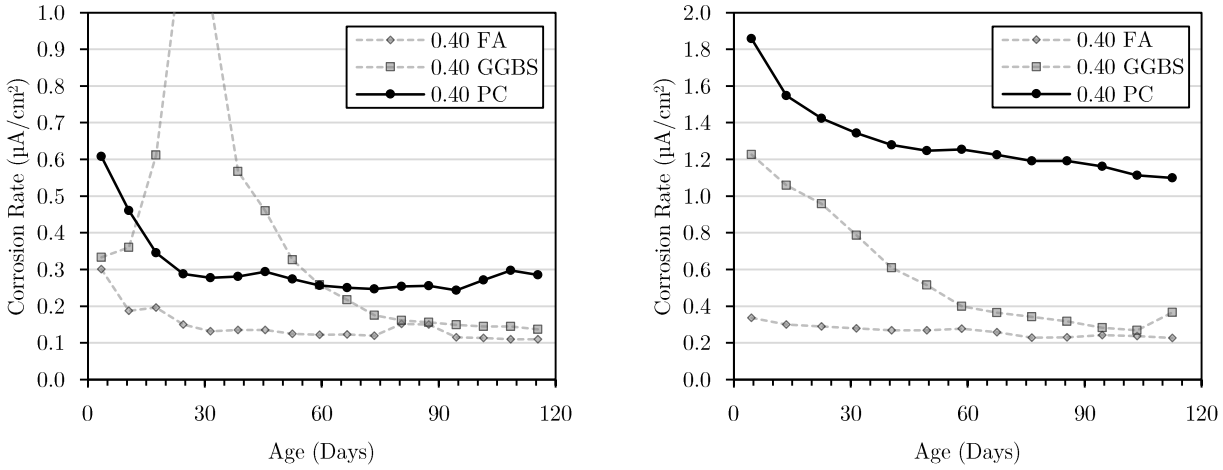

Figure 4.25: CR2 corrosion rate for a) 5-Day and b) 7-Day drying cycles

The effect of the inferred limited oxygen availability on the corrosion rate in the 0.65 PC specimens is presented in Figure 4.26 and Figure 4.27. These figures present the corrosion rate measurements normalised against their Day 1 value. As a result, these figures present a proportional rate of decline in the corrosion rate. It is evident that the drying time had a noticeable impact on the rate of decline of corrosion with the shorter duration drying times causing more rapid declines in the corrosion rate.

In most cases (except primarily the 7-Day drying specimens) the corrosion rate appears to reduce near the 20 day mark (indicated on Figure 4.26 and Figure 4.27). Hunkeler (2005) presented a threshold immersion time of 28 days after which oxygen within concrete had become depleted. However, the time required for oxygen depletion at the level of the reinforcement will vary depending on the concrete properties and the exposure conditions. It is unlikely that submerged conditions have been achieved in the 0.65 PC mix since the corrosion rates have not reverted to passive conditions (which was the case for the 0.40 PC mix in the CR2 sample set – Figure 4.19). However, these figures do illustrate the controlling effect of limited oxygen availability on the corrosion rate in PC concrete but the indicated 20-day marks are unlikely locations of oxygen depletion due to the continued active corrosion conditions.

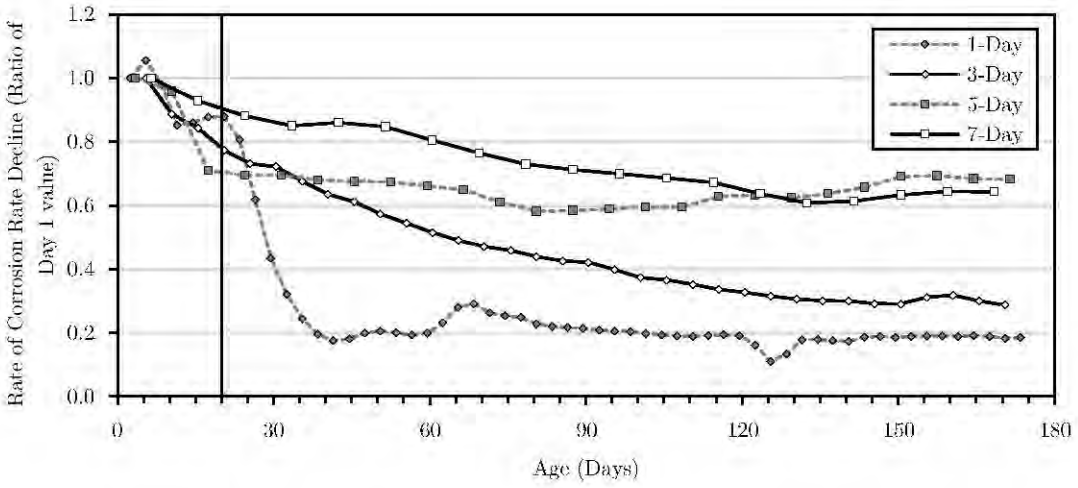

Figure 4.26: CR1 rate of decline in corrosion rate of 0.65 PC

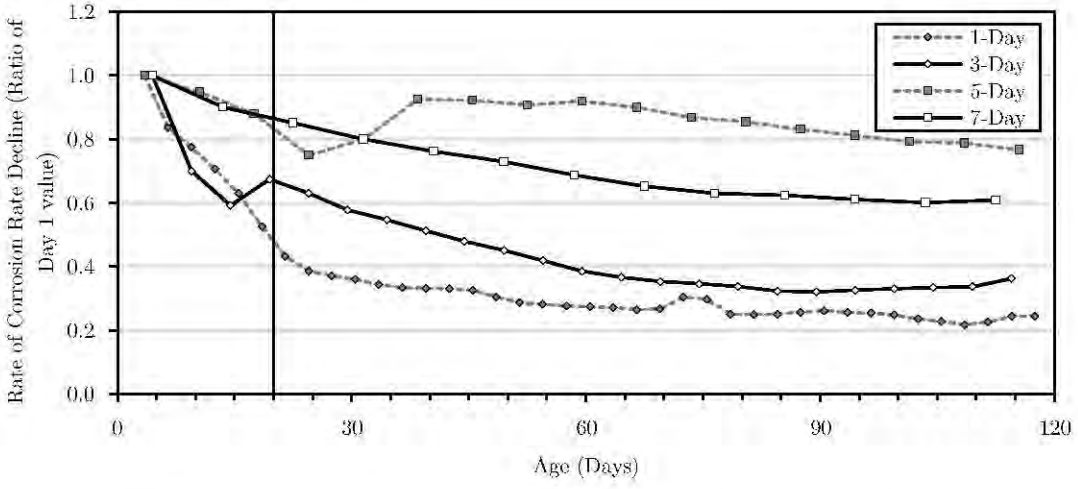

Figure 4.27: CR2 rate of decline in corrosion rate of 0.65 PC

Similar trends are not visible in the 0.40 PC mixes shown in Figure 4.28 and Figure 4.29. The decline in the corrosion rate is less rapid and there is no apparent trend in the effect of the drying duration. This is likely due to the denser cement matrix and slower transport of oxygen and moisture in the 0.40 PC mixes. Additionally, the 0.40 PC specimens were either corroding at a low rate (CR1) or remained in passive state (CR2), with corrosion rates between 0.10 and 0.35 $\mu A/cm^2$. No significant decrease in the corrosion rate was possible from these low values. Hence, the figures for the 0.40 PC specimens do not present a fair comparison of the rate of decline in the corrosion rate with respect to the 0.65 PC specimens.

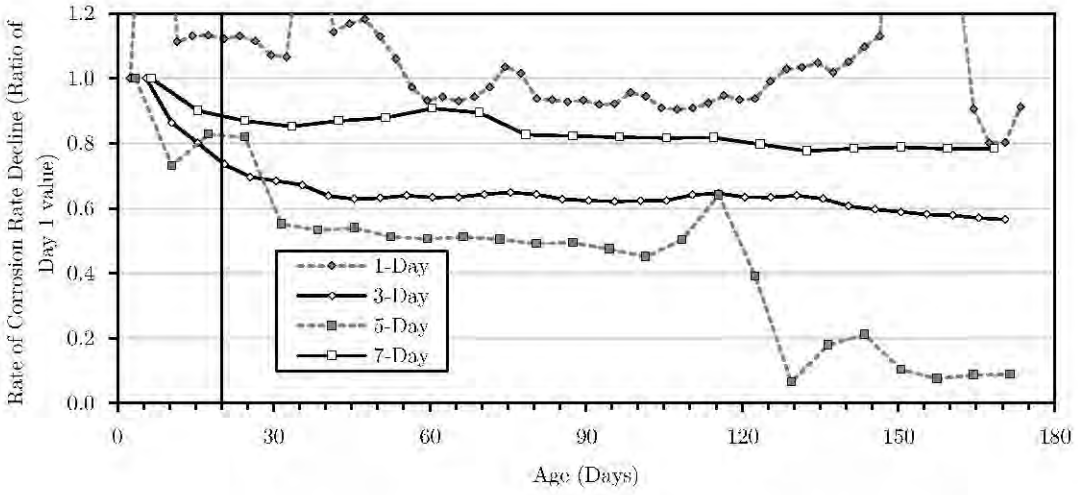

Figure 4.28: CR1 rate of decline in corrosion rate of 0.40 PC

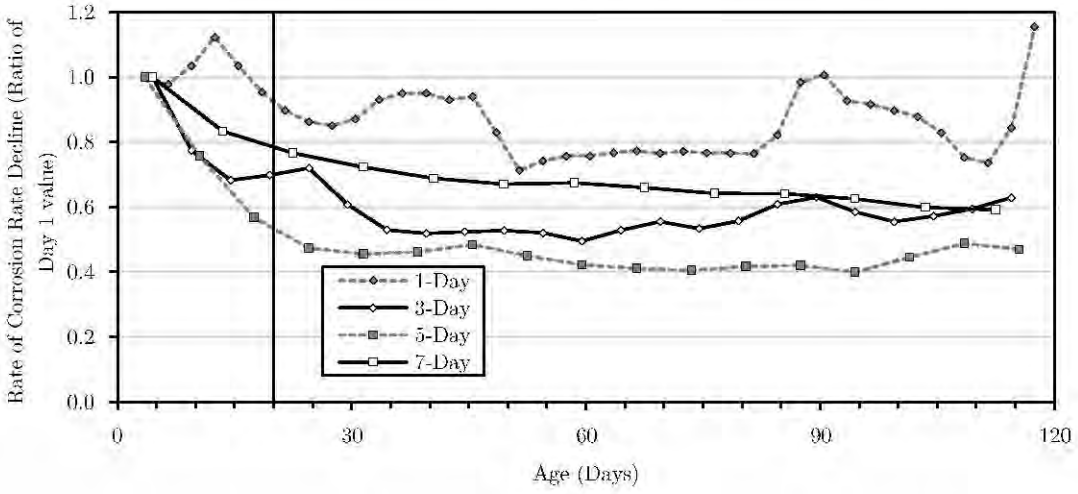

Figure 4.29: CR2 rate of decline in corrosion rate of 0.40 PC

The consequence of this finding cannot be fully realised without moisture profile measurements and modelling. This is beyond the scope of this study and the timeframe at hand. However, this work does show to a certain extent that the tidal zone may not provide the perceived severity of exposure conditions. Drying to the level of the steel, and hence corrosion, can be prevented if sufficient cover thickness and concrete quality is provided. With a w/b ratio of 0.40, the CR2 PC mixes reverted to

passive conditions when exposed to 1-Day drying (shown in Figure 4.24a). Consequently, it is fair to assume that the passive conditions arise from an inferred limited oxygen availability (cathodic control) and similar conditions could be possible in the marine tidal zone. Drying to the level of the steel is primarily controlled by the concrete cover thickness and the concrete quality. Hence these factors must be considered in combination to prevent drying to the level of the steel. This concept is illustrated in Figure 4.30, where two alternatives are presented for limiting the depth of the convection layer, and hence the depth of drying, with a description of the schematic provided in the subsequent paragraph.

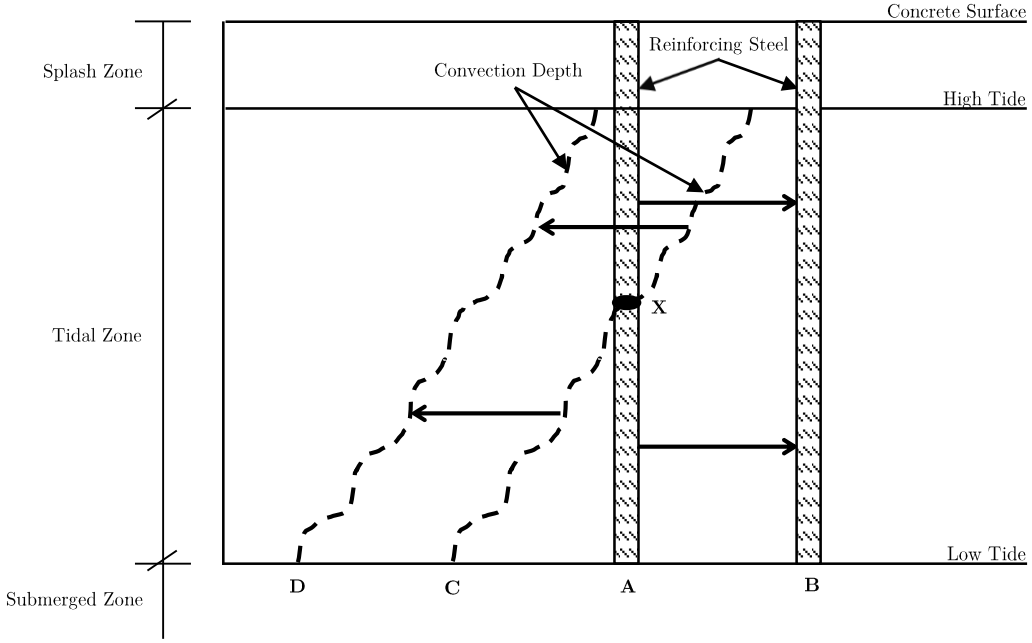

Figure 4.30: Hypothetical convection zone depth depending on the cover thickness and concrete quality

When exposed to cyclic wetting and drying in the marine environment, the cover depth should ideally be sufficiently deep or the convection zone should be sufficiently shallow to prevent drying to the level of the steel. This is illustrated in Figure 4.30 and can be described as follows:

- If the steel is at position A and the convection zone is represented by C – this scenario would present differential drying where only the steel above point X will feel the effects of cyclic wetting and drying. Limited corrosion activity can be expected below this point (X) due to an inadequate supply of oxygen. Below this threshold point PC mixes are expected to perform better; while PC mixes are unfavourable when the embedded reinforcing steel is exposed to the effects of cyclic wetting and drying.
- This knowledge can be used to achieve oxygen deprived conditions throughout the tidal zone by either increasing the cover depth (from A to B) or by improving the concrete quality (shifting the drying depth from C to D). This would negate the effects of cyclic wetting and drying on the corrosion of the embedded reinforcing steel by stifling the supply of oxygen. Reinforced concrete in the tidal zone would theoretically perform as if it were permanently submerged.

4.4.2 Effect of the binder type and w/b on the corrosion rate

This section focuses on the effect of varying the w/b ratio, and the inclusion of FA and GGBS. The early-age effect of GGBS on the corrosion rate has already been discussed in Section 4.3.1.1 and thus the effect of sulphides and thiosulphates will not be discussed further in this section. The corrosion rate measurements highlighting the binder type as the primary variable are shown in Figure 4.31 to Figure 4.34 (enlarged versions can be found in Appendix E).

4.4.2.1 CR1

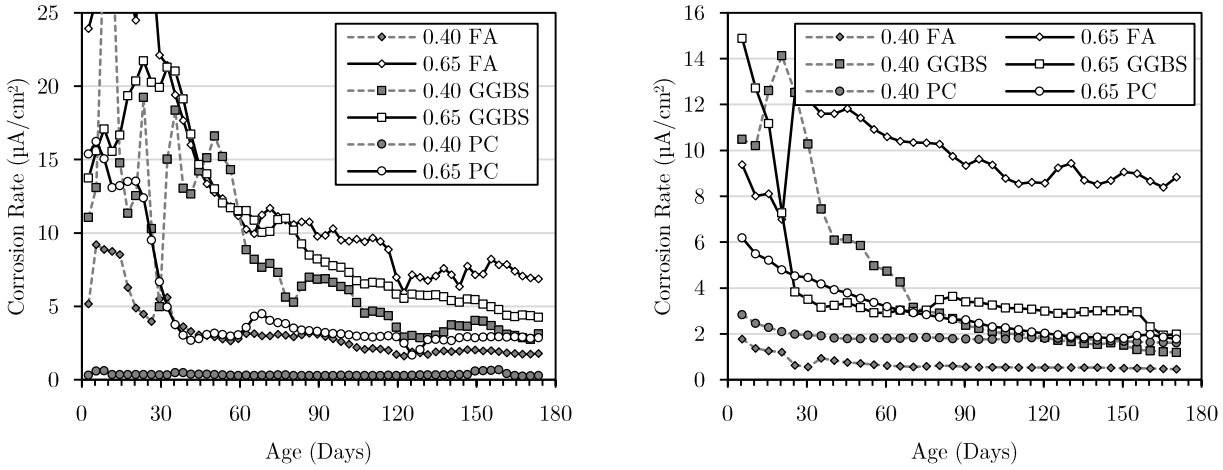

a) b)

Figure 4.31: CR1 corrosion rate for a) 1-Day and b) 3-Day drying cycles

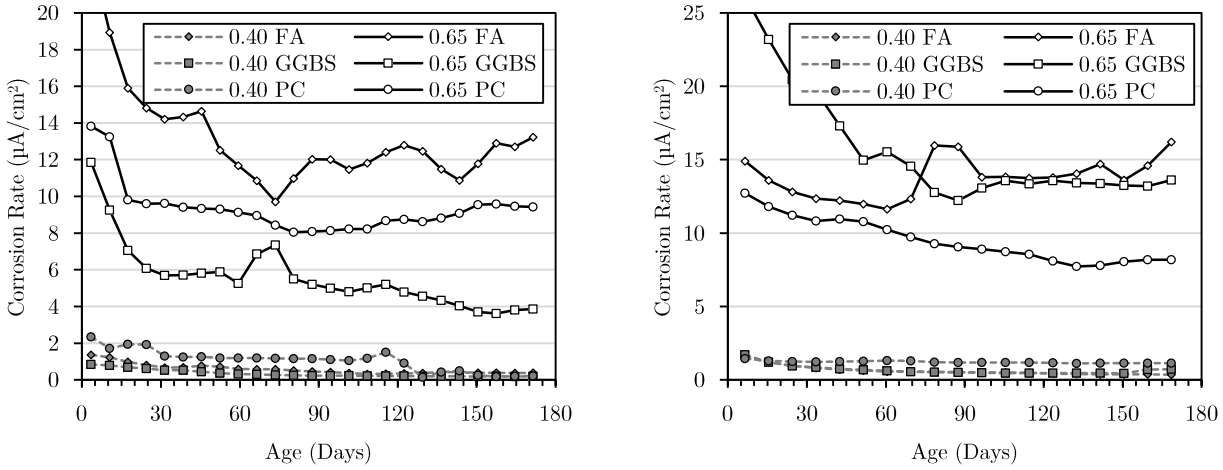

a) b)

Figure 4.32: CR1 corrosion rate for a) 5-Day and b) 7-Day drying cycles

4.4.2.2 CR2

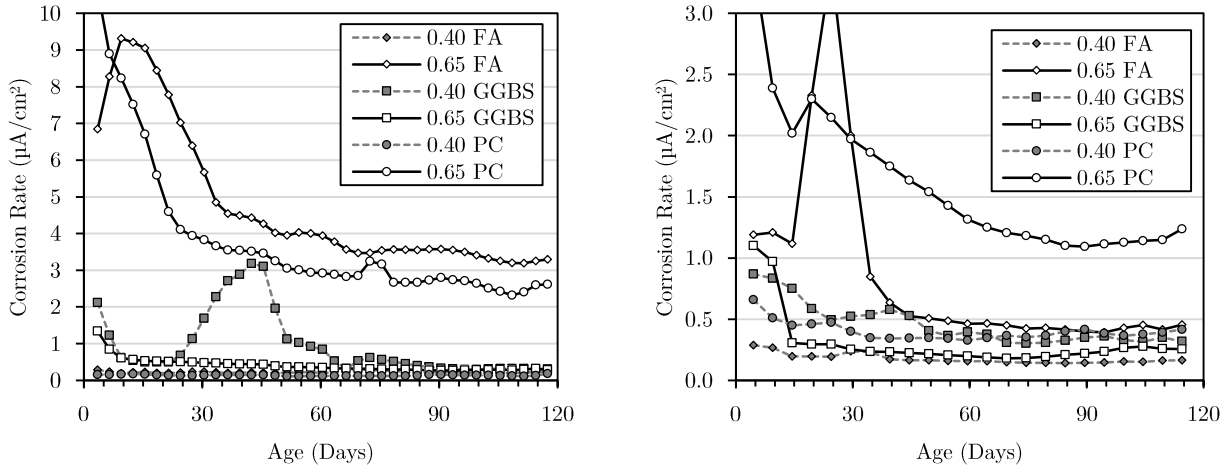

a) b)

Figure 4.33: CR2 corrosion rate for a) 1-Day and b) 3-Day drying cycles

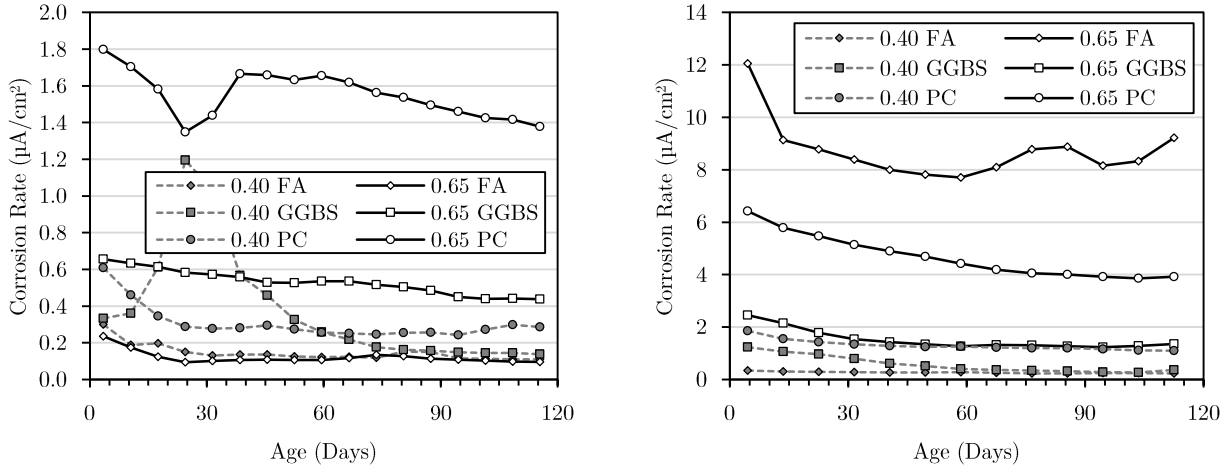

a) b)

Figure 4.34: CR2 corrosion rate for a) 5-Day and b) 7-Day drying cycles

4.4.2.3 Discussion

As discussed in Section 2.7.3, a number of opposing views have been presented in the literature on the effect of limited oxygen availability on the corrosion rate of embedded reinforcing steel. A key finding of this research is that under 1-Day cycles of drying the CR2 0.40 PC specimens remained in a passive state, while the respective FA and GGBS mixes were actively corroding (Figure 4.34a). Justification for this phenomenon can most sensibly be sought in the inferred limiting oxygen availability at the level of the steel. The effect of limited oxygen availability on stifling the corrosion rate in PC mixes was also reported by Scott (2004).

Figure 4.35 and Figure 4.36 show the correlation between the 1-day and 7-day corrosion rate measurements throughout the monitoring phase. A stark contrast between the CR1 and CR2 results is evident in these figures, with the CR1 results not following the expected trends. The CR1 results reflect a different regime of corrosion due to the high initial corrosion rates and extended settling

period before relatively stable corrosion rates were achieved. These figures consider the entire monitoring phase and thus the results will be affected by this initial period. As a result, the CR2 results will be considered for this analysis going forward.

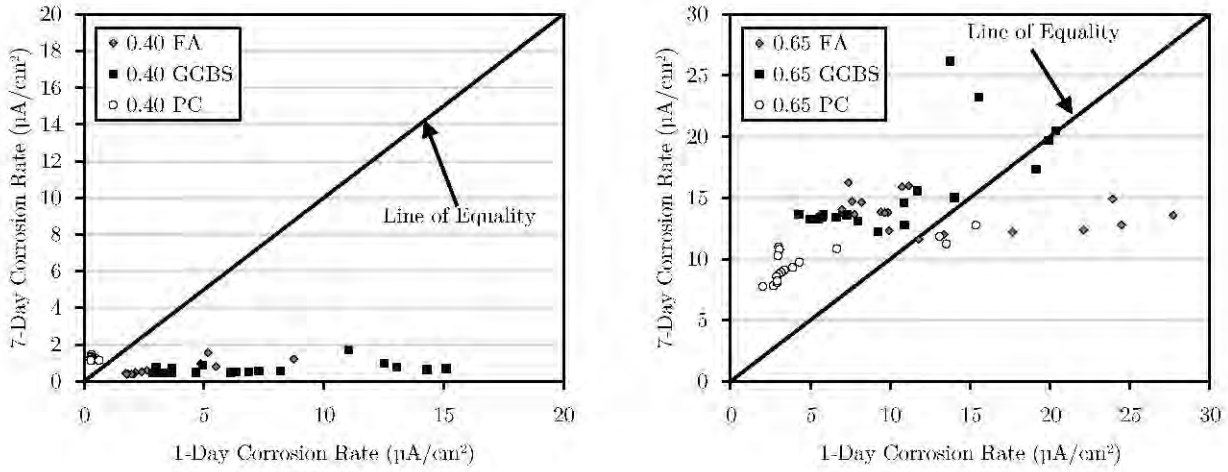

a) b)

Figure 4.35: CR1 7-Day vs. 1-Day corrosion rate for w/b ratio of a) 0.40 and b) 0.65

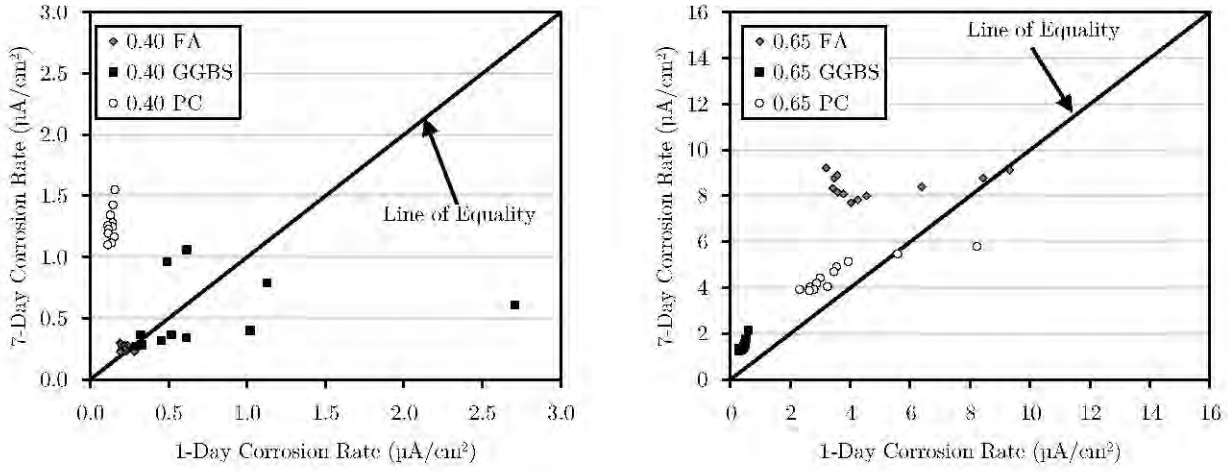

a) b)

Figure 4.36: CR2 7-Day vs. 1-Day corrosion rate for w/b ratio of a) 0.40 and b) 0.65

In the CR2 sample set the corrosion rate for the 0.40 GGBS and 0.40 FA specimens appears almost unchanged when the drying duration was extended from 1 day to 7 days Figure 4.36(a). This is evident by the data points falling along the line of equality. In contrast the 0.40 PC specimens fall to the left of the line of equality and show a general increase in the corrosion rate as the drying time is extended. A similar pattern is not evident for the 0.65 w/b ratio specimens which show a general shift to the left from the line of equality, irrespective of the binder type. The shift in the corrosion rate is likely to originate from an increased oxygen availability in the 0.65 w/b ratio specimens. However, the oxygen availability was not expected to alter the corrosion rate in the FA and GGBS specimens due to the higher resistivity of concrete controlling the corrosion rate.

The aforementioned points are further reinforced when considering Figure 4.37 and Figure 4.38. These figures only show the data entries collected after 90 days – thus eliminating the noise from the initial stages of high corrosion. Considerably less scatter is evident, highlighting the influence of the drying time on the corrosion rate.

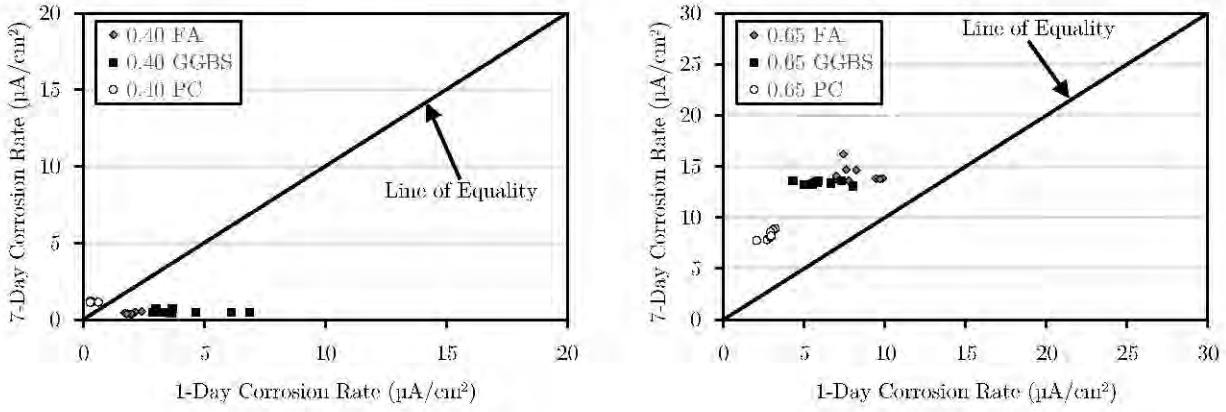

a) b)

Figure 4.37: CR1 7-Day vs. 1-Day corrosion rate for w/b ratio of a) 0.40 and b) 0.65 (data entries collected after 90 days only)

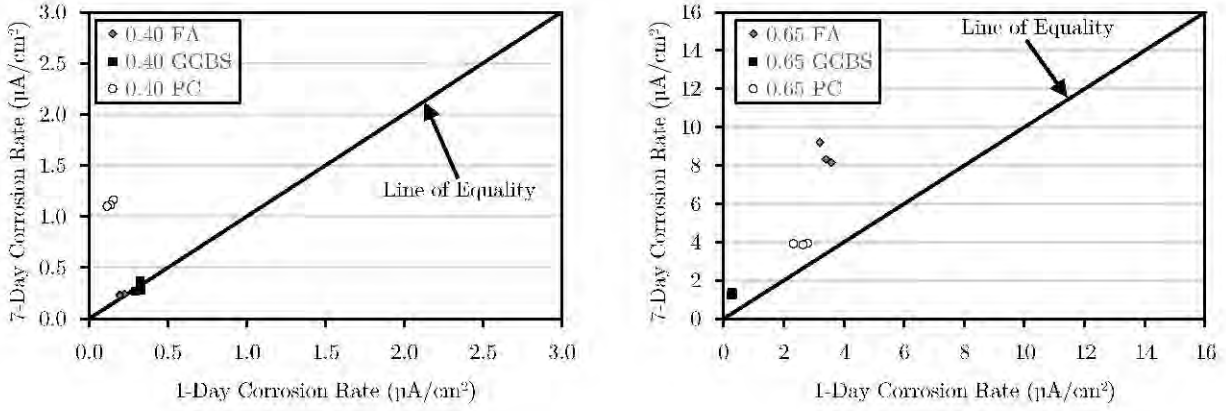

a) b)

Figure 4.38: CR2 7-Day vs. 1-Day corrosion rate for w/b ratio of a) 0.40 and b) 0.65 (data entries collected after 90 days only)

As a result of the uncertainty, a mixed effects model for a continuous response was fitted to the data to assess the combined effect of the binder type and the w/b ratio. A mixed effects model for a continuous response takes into account a multi-factorial analysis while considering a time component. It is a two-sided linear formula object describing both the fixed-effects and random-effects. The fixed-effects take into account the expected relationships between the variables if the experiment were to be repeated; while, the random effects take into account the individual properties inherent in the specific sample chosen (from a population of samples). If the experiment were to be repeated,

the sample chosen from the population would be different and thus these random effects would be different.

The data was statistically analysed using this model to assess the predominant factors influencing the corrosion rate and was selected to adequately account for the initial 'settling' period for the corrosion rate. This model was applied through a simplified additive model using the following equation:

$$Corrosion\ Rate = \beta_0 + \beta_1\ (Age) + \beta_2\ (Binder\ type) + \beta_3\left({}^{w}/_{b}\ ratio\right) + \beta_4\ (Drying\ time) \quad \text{(Eq. 4.2)}$$

The model showed that the w/b ratio played a more significant role in controlling the corrosion rate compared to the binder type. The change in w/b ratio was found to have a p-value of ≈ 0.05, indicating a low correlation and hence a significant difference between a w/b ratio of 0.40 and 0.65 at the 5% significance level. However, the binder type was found to be non-significant at the 10% level (p-value > 0.1). Hence, it is evident that controlling the corrosion rate will be governed primarily by the w/b ratio.

Table 4.10: Mixed-effects model coefficients

Factor		CR2			
		Value	**Standard Error**	**t-value**	**p-value**
β_0		1.463	0.847	1.727	0.085
β_1		-0.009	0.003	-3.421	0.001
β_2	FA	0.000	0.000	0.000	0.000
	GGBS	-0.977	0.711	-1.374	0.187
	PC	-0.301	0.711	-0.423	0.677
β_3	0.40	0.000	0.000	0.000	0.000
	0.65	1.091	0.580	1.880	0.077
β_4	1-Day	0.000	0.000	0.000	0.000
	3-Day	-0.202	0.815	-0.248	0.808
	5-Day	-0.009	0.817	-0.011	0.991
	7-Day	1.763	0.821	2.147	0.047

Additionally, it was found that for a w/b ratio of 0.40 the effect of the binder type was non-significant. Hence, at a w/b ratio of 0.40, the embedded reinforcing is expected to corrode at the same rate irrespective of the binder type. However, the GGBS was found to perform much better at a w/b ratio of 0.65, compared to the FA and PC. No significant difference was found between the performance of the FA and PC mixes at a w/b ratio of 0.65. The relative performances of the binder types at a w/b ratio of 0.65 are illustrated below.

$$GGBS > PC \approx FA \quad \text{(Eq. 4.3)}$$

4.4.3 Resistivity as a corrosion rate indicator

The concrete resistivity limits the flow of ions from the anode to the cathode. This is a fundamental component of chloride-induced reinforcement corrosion and can control the progress of corrosion (resistivity control). Scott (2004) found, *inter alia*, that the resistivity does not control the corrosion rate under passive conditions, irrespective of the binder type. He also found that the concrete resistivity was not rate controlling in PC concrete; whereas the resistivity governed the corrosion rate in concretes containing FA and GGBS.

In the research at hand, resistivity measurements were taken at the end of each cycle of wetting. As a result, pore spaces were filled with NaCl solution which provided a path for current flow and generally resulted in lower resistivity measurements (higher conductivity). As a result, variations in the resistivity will be smaller than commonly expected for in-situ concrete structures. However, the resistivity guidelines presented in Table 2.5 (Section 2.7.2.6) assume that conditions are "favourable for corrosion" (Heckroodt, 2002). In the marine environment these conditions must imply that a sufficient chloride content and moisture is available. Hence, the relevance of this table can be assessed as an indicator of the likelihood of corrosion.

The resistivity measurements remained largely unchanged throughout the monitoring period, but in some cases the resistivity increased slightly over time. This is likely due to continued hydration during the timeframe of monitoring. Full resistivity plots for each binder type are included in Appendix G, with a selection of specific plots presented in this section. Figure 4.39 to Figure 4.42 show the CR1 and CR2 resistivity plots for the 1 and 7-Day drying cycles.

4.4.3.1 CR1

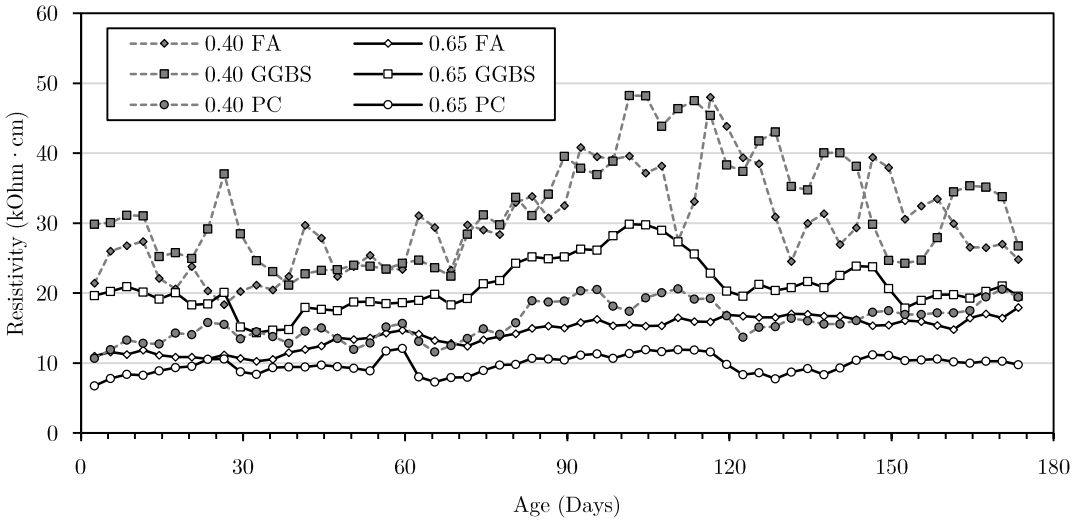

Figure 4.39: CR1 resistivity measurements for 1-Day drying cycles

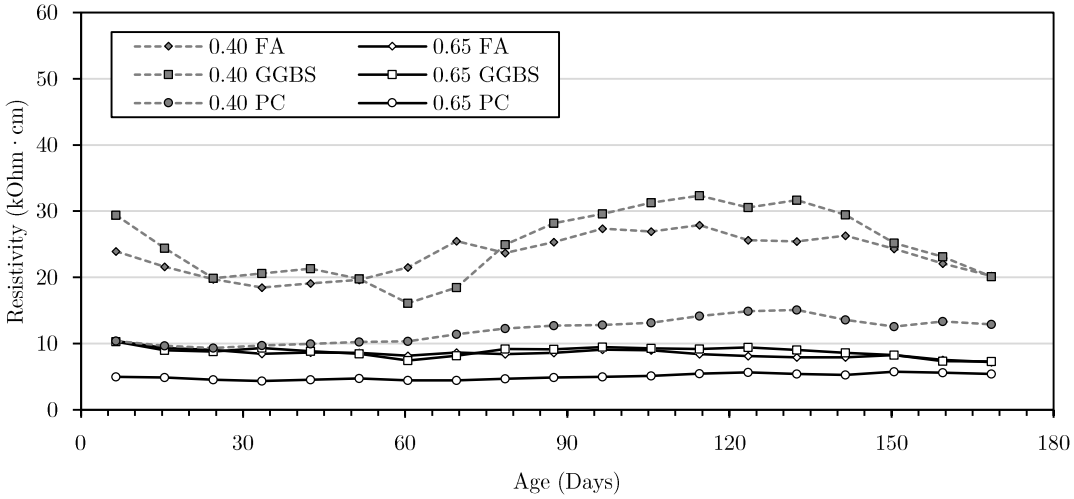

Figure 4.40: CR1 resistivity measurements for 7-Day drying cycles

4.4.3.2 CR2

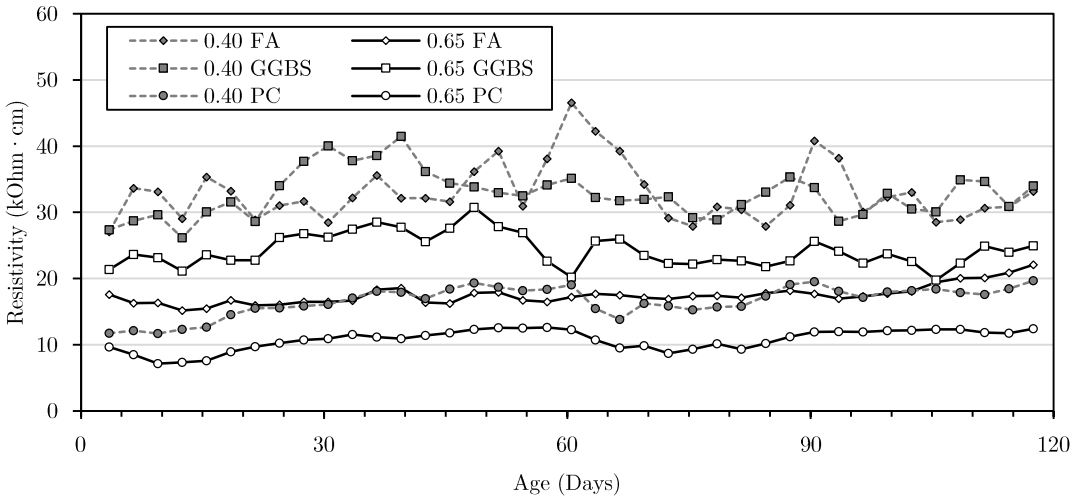

Figure 4.41: CR2 resistivity measurements for 1-Day drying cycles

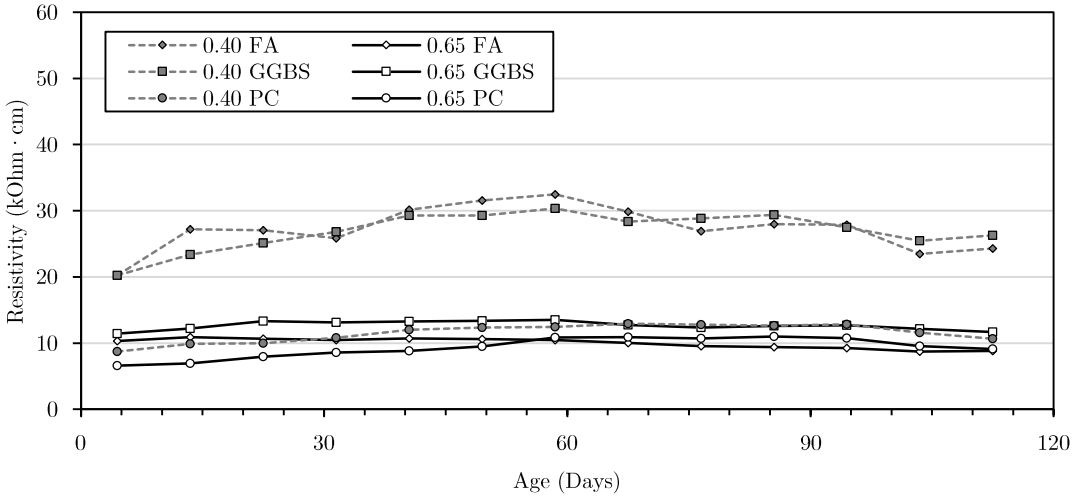

Figure 4.42: CR2 resistivity measurements for 7-Day drying cycles

From these plots it is evident that the resistivity measurements are comparatively higher when the drying duration was shortened, which is counter-intuitive. A shortened drying duration can also be linked to higher variability in the resistivity measurements. This can be seen by comparing the scatter in Figure 4.39 to the more regular resistivity measurements in Figure 4.40 (also visible when comparing Figure 4.41 to Figure 4.42). It is important to note that the PC mixes obtained relatively low resistivity values irrespective of the drying time. The PC mixes generally attained resistivity values of 5-15 kOhm-cm which are generally indicative of medium to high corrosion potential.

In these figures it is evident that the 0.40 FA and 0.40 GGBS mixes achieved the highest resistivity values. It is also evident that the resistivity generally decreased with an increase in drying time. This is likely due to the continued hydration of the binder or the deposition of chlorides from multiple cycles of wetting and drying. The continued hydration of the binder will cause a further reduction in the pore size and interconnectivity, with an associated increase in the resistivity. The shorter duration drying cycles will allow for better curing and hence a higher resistivity as the drying duration is shortened.

An alternative approach is to consider an increase in chloride deposition as the drying time is increased. A longer drying time will cause a higher component of chloride deposition in the convection zone. The subsequent wetting of the same 5% NaCl solution will result in the development of a higher chloride concentration. This will have the effect of increasing the conductivity, and conversely decreasing the resistivity. The effect of the drying time on the resistivity is presented in Figure 4.43 and Figure 4.44 which consider the average resistivity over the entire monitoring period.

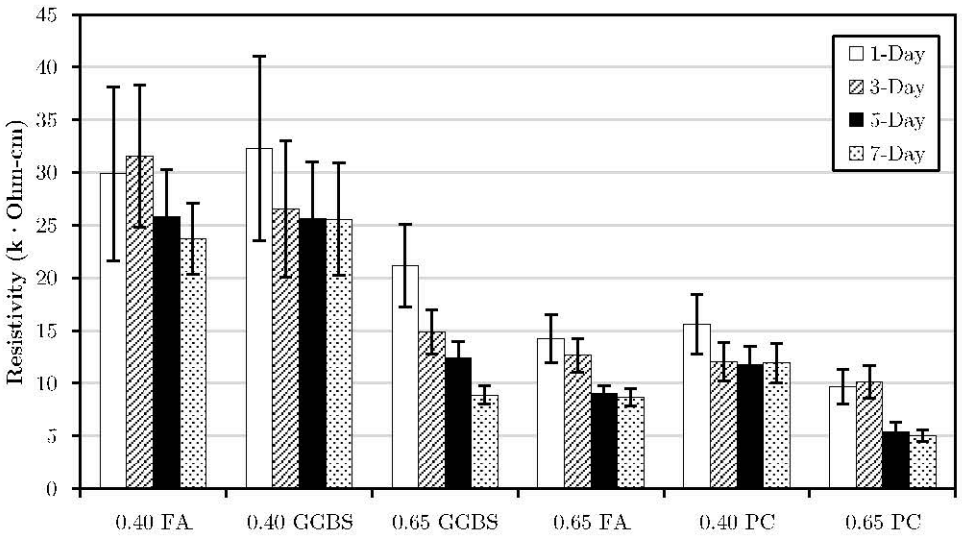

Figure 4.43: CR1 overall average resistivity values (presented with 1 standard deviation)

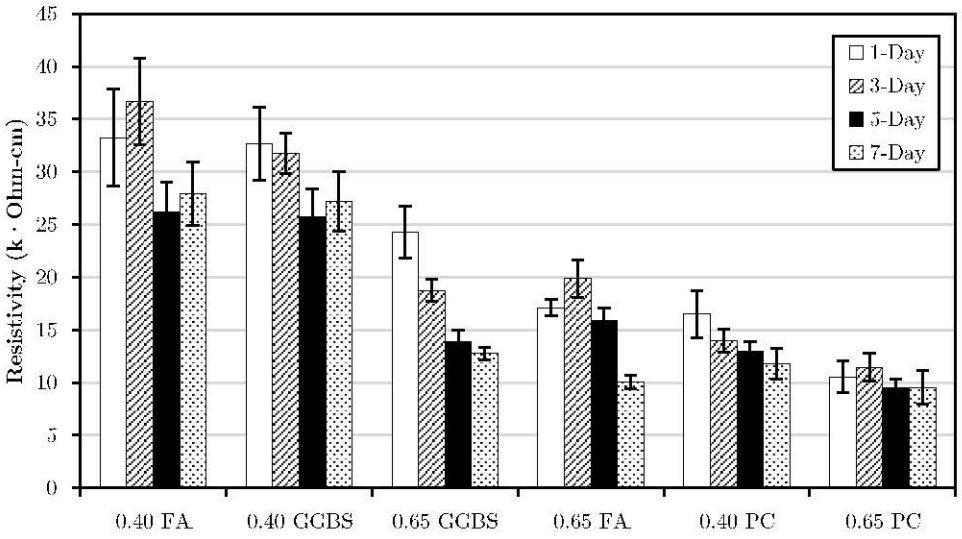

Figure 4.44: CR2 overall average resistivity values (presented with 1 standard deviation)

Irrespective of the drying time, the corrosion rate for the 0.40 GGBS and 0.40 FA mixes remained low. These two mixes obtained comparatively higher resistivity values throughout the monitoring period. Scott (2004) cited resistivity control as the source for limited corrosion activity in concretes containing FA and GGBS and is likely the reason for the reduced corrosion rate in these specimens. However, at a higher w/b ratio the effect of resistivity control does not appear to be significant. As discussed in Section 4.4.1, the 0.65 GGBS and 0.65 FA mixes are corroding at a relatively high rate and changes in the corrosion rate were not associated with changes in the resistivity.

Figure 4.45 to Figure 4.48 consider the whole monitoring phase and illustrate the correlation between the corrosion rate and the resistivity for the FA and GGBS mixes. Once again it is apparent that there is far less scatter in the data when the drying duration was extended. However, a few additional features are evident in these figures. At a resistivity above 20 kOhm-cm, the corrosion rate is assumed to be low (according to Table 2.5). Above this resistivity value the corrosion rate remained generally unchanged with small fluctuations in the resistivity. This is evident in the 0.40 w/b ratio specimens where the data points are aligned horizontally, and indicates resistivity control of the corrosion rate. However, for the 0.65 w/b ratio specimens the corrosion rate appears to fluctuate without a noticeable change in the resistivity. This indicates that a factor other than the resistivity is governing how the corrosion rate proceeds. It is likely that the oxygen availability and resistivity have a combined effect on the corrosion rate in the specimens containing FA and GGBS.

4.4.3.3 CR1

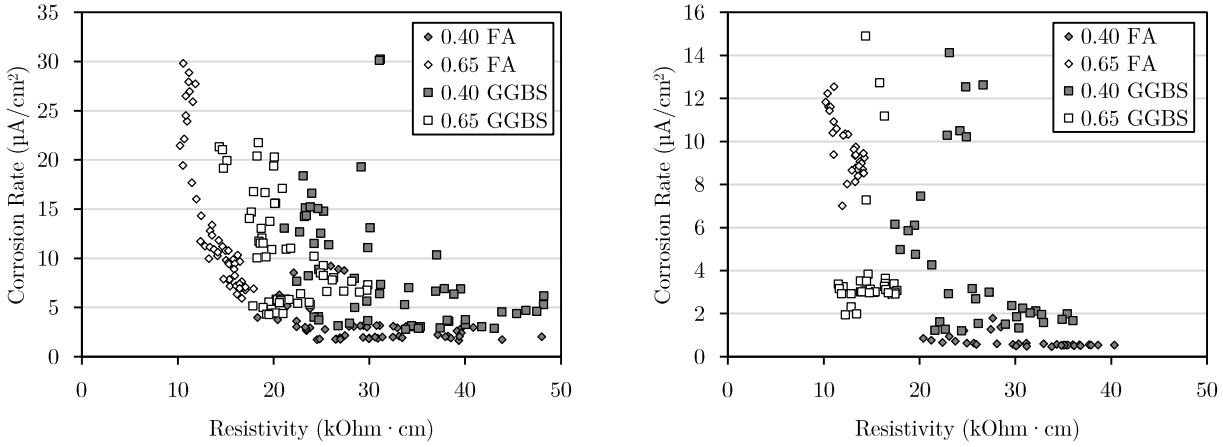

Figure 4.45: CR1 corrosion rate vs resistivity for a) 1-Day and b) 3-Day drying cycles

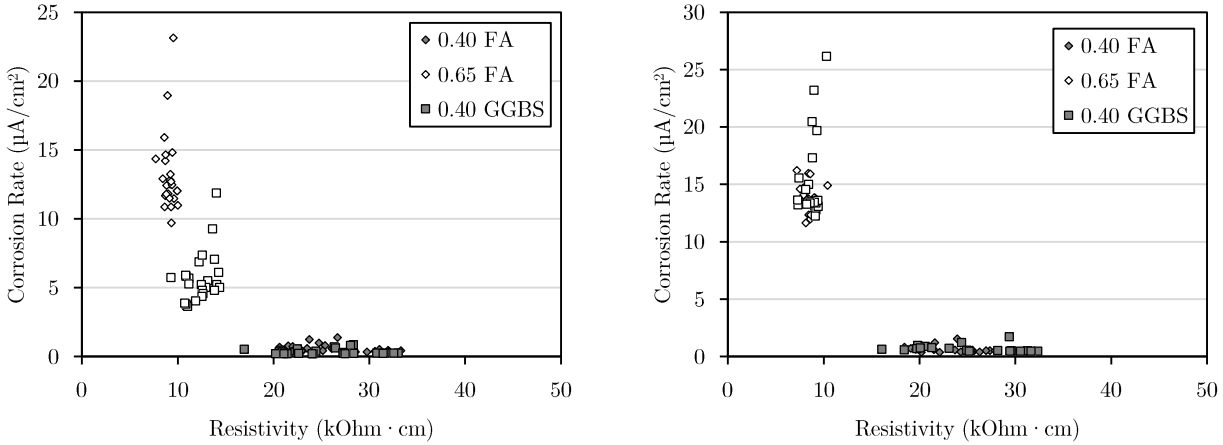

Figure 4.46: CR1 corrosion rate vs resistivity for a) 5-Day and b) 7-Day drying cycles

4.4.3.4 CR2

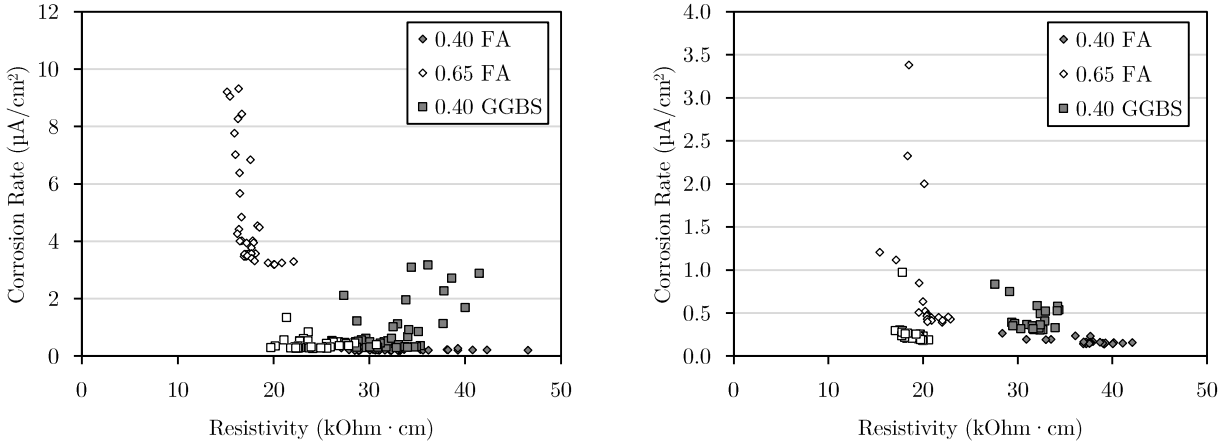

Figure 4.47: CR2 corrosion rate vs resistivity for a) 1-Day and b) 3-Day drying cycles

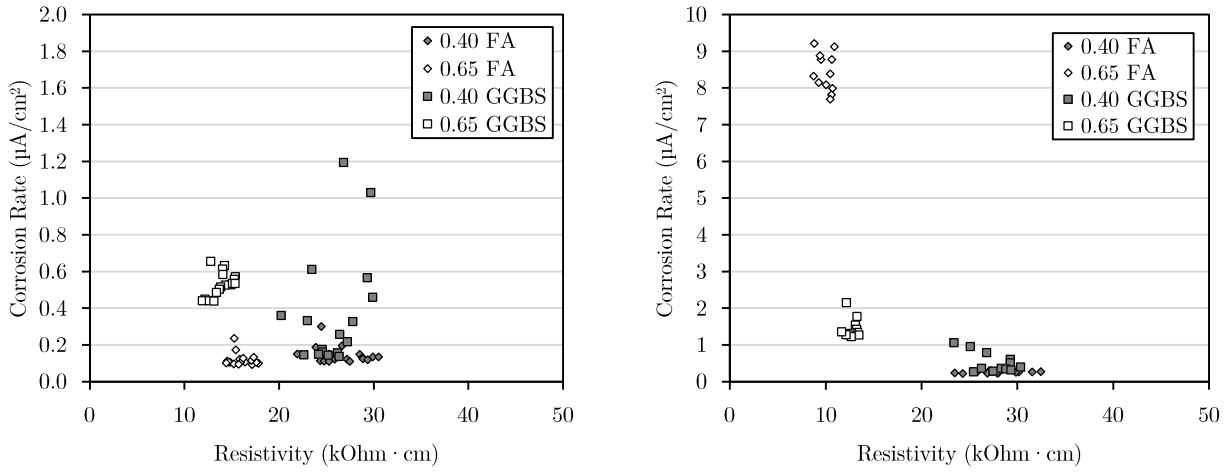

Figure 4.48: CR2 corrosion rate vs resistivity for a) 5-Day and b) 7-Day drying cycles

4.4.4 HCP as a corrosion rate indicator

As discussed in Section 2.8.1.2, the HCP provides a rough indication of the likelihood of corrosion. The relevance of this test method will be investigated by comparing the HCP values and the measured corrosion rates. It is worth noting that ASTM C876-09 (2009) states that there is a 90% likelihood of corrosion below a HCP (Ag/AgCl) value of -256 mV. Additionally, below -406 mV the corrosion rate can be considered severe.

4.4.4.1 CR1

Figure 4.49 presents the measured HCP and corrosion rates for CR1. This figure shows a wide spread in both corrosion rates and HCP values, although it is apparent that high HCP values generally correspond with high corrosion rates. However, the use of HCP measurements is generally not relevant for excessively corroding reinforcing steel since the technique only provides an indication of the likelihood of corrosion. Rodriguez *et al.* (1994) consider corrosion rates in excess of 1.0 µA/cm² as high, while Clear (1989) expects corrosion damage to be visible within 2 years at a corrosion rate greater than 10.0 µA/cm². At these high corrosion rates it is likely that corrosion damage will be visible and measuring the HCP would not provide any additional information since it does not provide any measure of the rate of corrosion. The HCP and corresponding corrosion rates are presented in Figure 4.49, Figure 4.50 and Figure 4.51, which consider each data point over the whole period of monitoring. All the data points were considered in these plots to assess the applicability of the HCP measurements at all states of corrosion. It is worth noting that a reasonable correlation between the HCP and the corrosion rate is apparent in Figure 4.49. Furthermore, the threshold values of -256 mV and -406 mV appear to be justified.

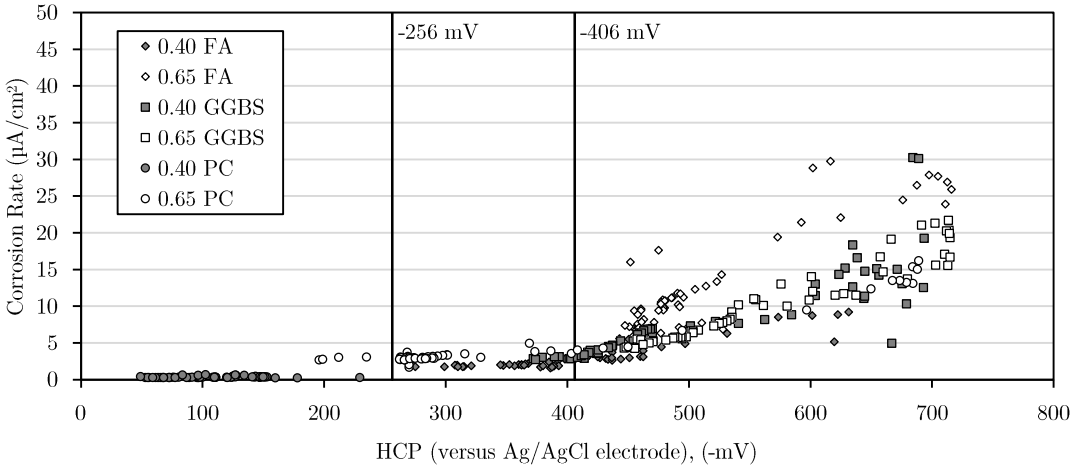

Figure 4.49: CR1 HCP vs corrosion rate, showing threshold values

In light of the information provided above, Figure 4.50 shows an excerpt of data showing only measurements with a corrosion rate in the range of 0-10 µA/cm². There is a reasonable scatter in the data but it generally shows an increase in the corrosion rate above the indicated threshold value of -256 mV. However, in this sample set a number of the specimens are in a severe state of corrosion and fall outside of the presented range in Figure 4.50.

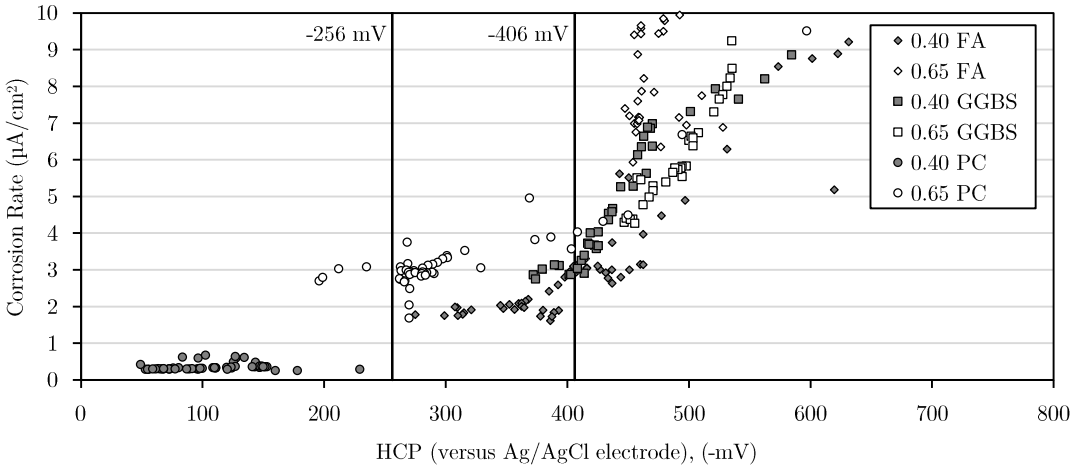

Figure 4.50: CR1 HCP vs corrosion rate (mild corrosion range), showing threshold values

4.4.4.2 CR2

Figure 4.51 presents the measured HCP and corrosion rates for CR2. Once again the threshold values of -256 mV and -406 mV are apparent and relatively distinct changes in the corrosion rate magnitude are evident beyond these points. The CR2 sample set presents less severe corrosion rates and shows a clear picture of the relevance of the HCP. The CR1 specimens are mostly undergoing severe active corrosion; while the CR2 specimens are more likely in the range of expectations from in-situ reinforced concrete structures in the marine environment. As a result, the CR1 specimens are generally corroding beyond the severe threshold value of -406 mV; while the CR2 specimens are corroding more mildly with HCP values generally below the -406 mV threshold value. It is clear to see that

the HCP is a good indicator of corrosion activity and the existing threshold values generally apply to all the investigated concrete mixes.

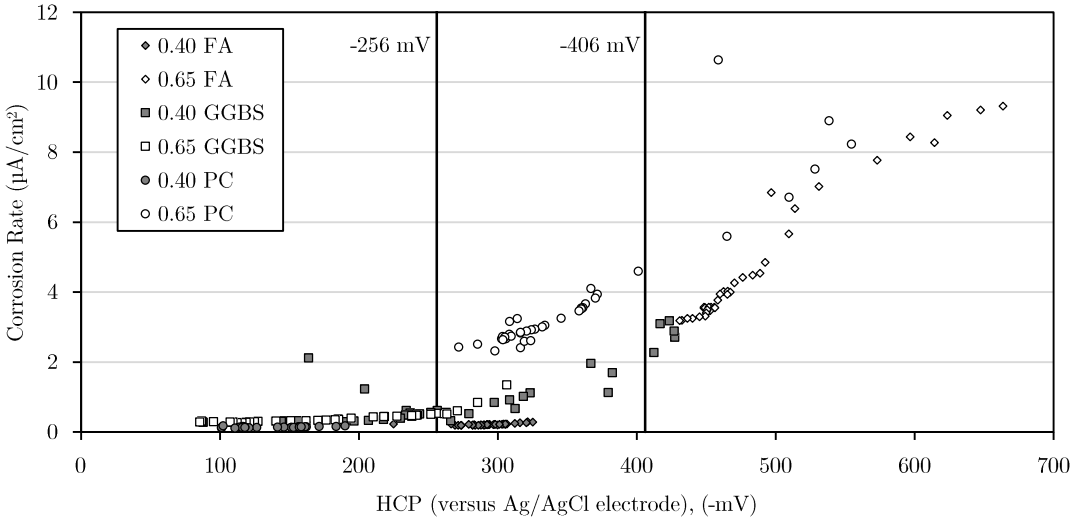

Figure 4.51: CR2 HCP vs corrosion rate, showing threshold values

4.4.5 Effect of the chloride concentration

The total chloride concentration was measured by chemical titration of core samples extracted from each specimen at the end of the monitoring phase. After extraction of the core samples, a number of the remaining specimens were broken to expose the embedded reinforcing steel. It was evident that corrosion was generally occurring on the steel face nearest to the concrete surface, with minimal corrosion product below the steel, as shown in Figure 4.52. Consequently, it was deemed more suitable to measure the chlorides around the top surface of the steel. Accordingly, a 10 mm thick core slice was taken at a depth of 15-25 mm from the surface (even though the steel occupied a depth of 20-30 mm).

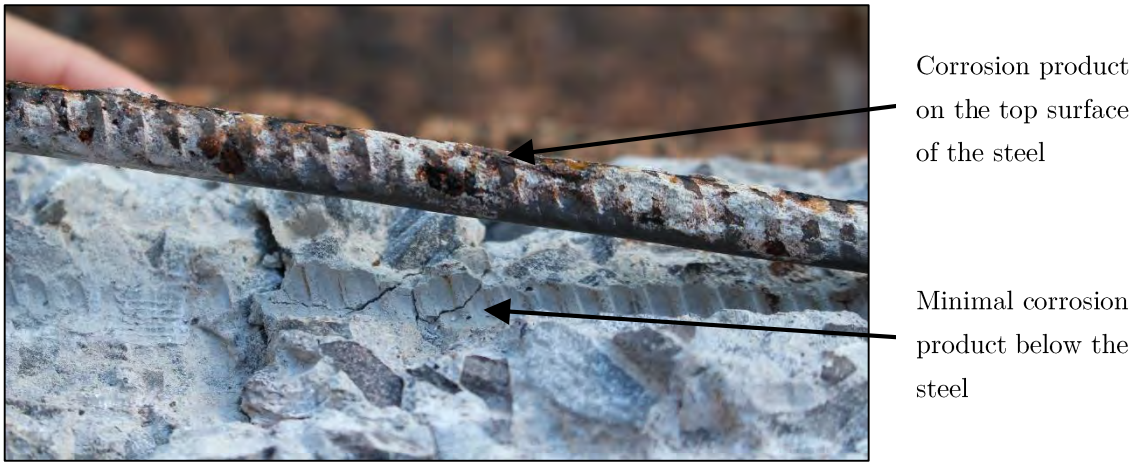

Figure 4.52: Visible corrosion damage with no corrosion product on the bottom surface of the embedded steel

The chloride content did not meet the expectation of an increase in chloride content with an increase in drying time (due to chloride deposition). Figure 4.53 shows how the chloride content varied in each mix depending on the drying time. The data appears random with the 0.65 w/b ratio specimens generally having higher chloride concentrations.

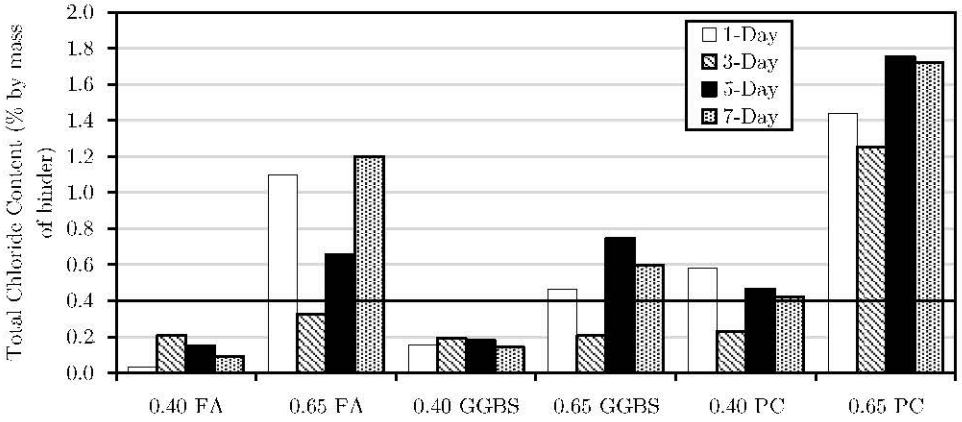

Figure 4.53: Average chloride content at 15-25 mm depth, expressed as a factor of drying time

From Figure 4.53 it is evident that a number of the specimens have not surpassed the generally accepted threshold chloride content of 0.40% by mass of binder. However, this threshold value can vary quite widely depending on the selected binder type and w/b ratio. As presented previously in Figure 2.11, the chloride threshold value can vary by as much as an order of magnitude and has been reported to be as low as 0.1% in some cases. As a result, a chloride content below 0.4% cannot be used to justify passive corrosion conditions and requires further analysis.

The chloride contents were then assessed according to the final measured corrosion rates. The correlations are shown in Figure 4.54 and Figure 4.55 for a w/b ratio of 0.40 and 0.65, respectively. The generalised threshold values of 0.4% chloride content by mass of binder and 0.1 $\mu A/cm^2$ have been included in these figures.

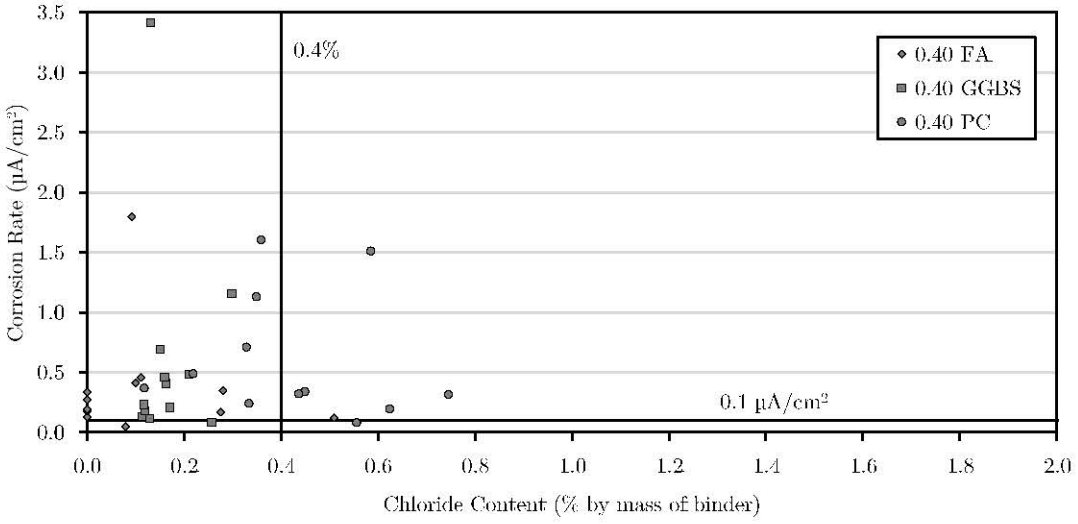

Figure 4.54: Measured chloride contents and corrosion rates for specimens with a w/b ratio of 0.40

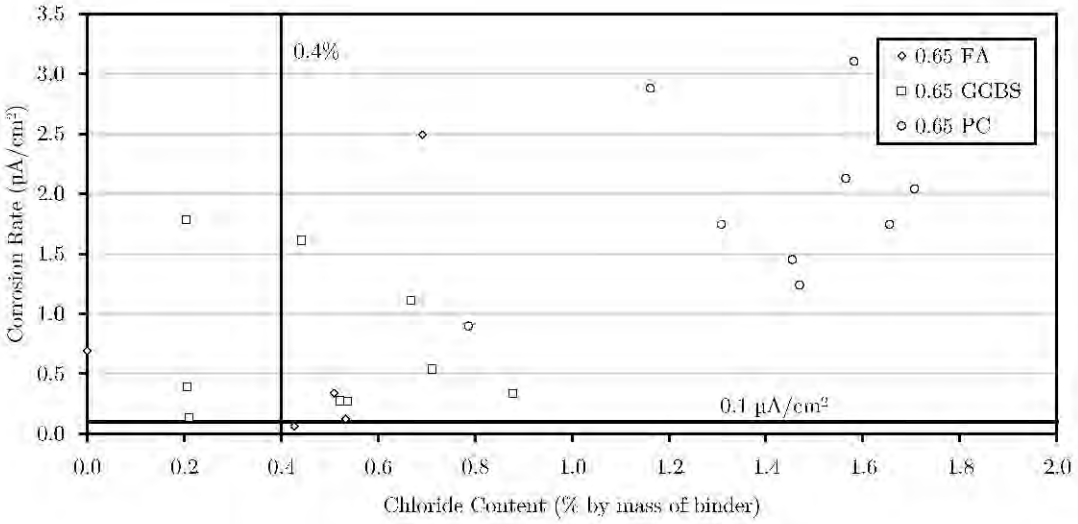

Figure 4.55: Measured chloride contents and corrosion rates for specimens with a w/b ratio of 0.65

The chloride contents are comparatively low in the 0.40 w/b ratio specimens but also appear to be corroding without exceeding the threshold chloride content of 0.4% by weight of binder. In comparison, the 0.65 w/b ratio specimens generally exceed both the active corrosion threshold values (chloride content and corrosion rate). The progress of corrosion irrespective of the chloride concentration was unexpected for the 0.40 w/b ratio specimens.

Figure 4.56 and Figure 4.57 differentiate between the two sample sets, CR1 and CR2. From these figures it is evident that the CR1 specimens are corroding at a higher rate without a considerable increase in the chloride concentration. These results generally show a large scatter in results and in isolation would not provide a suitable indicator of corrosion potential.

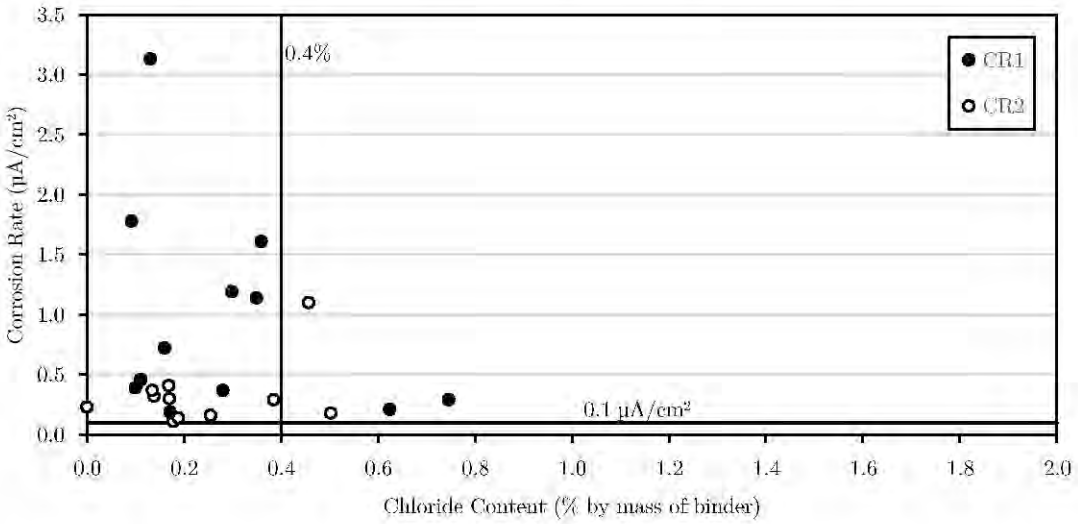

Figure 4.56: CR1 vs CR2 correlation of chloride content and corrosion rate for a w/b ratio of 0.40

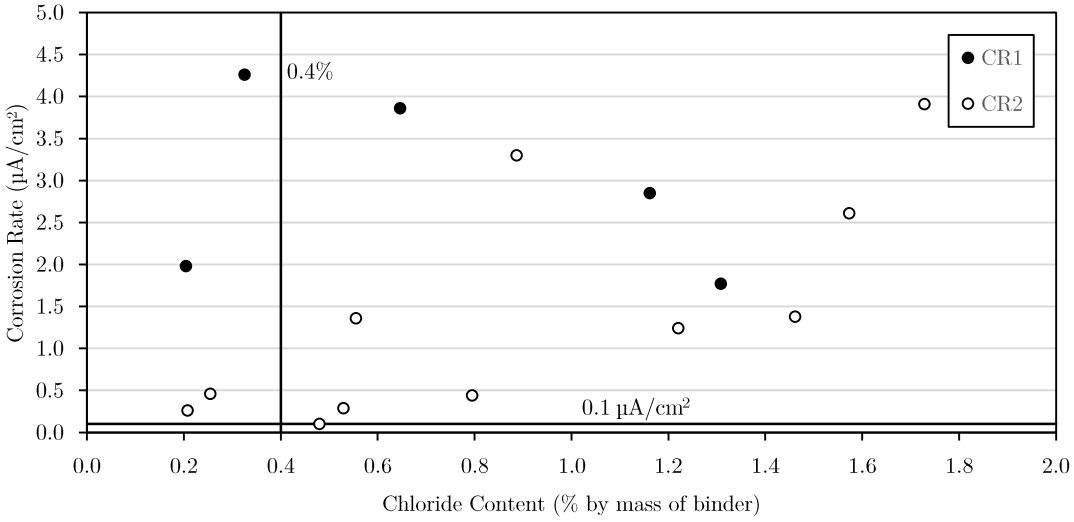

Figure 4.57: CR1 vs CR2 correlation of chloride content and corrosion rate for a w/b ratio of 0.65

Finally, the Chloride Conductivity Index test was assessed for its relevance in predicting corrosion potential based on chloride concentrations. Figure 4.58 shows a relatively good correlation between the measured 110-day CCI values and the final chloride contents. This is a very interesting finding and reinforces the relevance of the Durability Index tests.

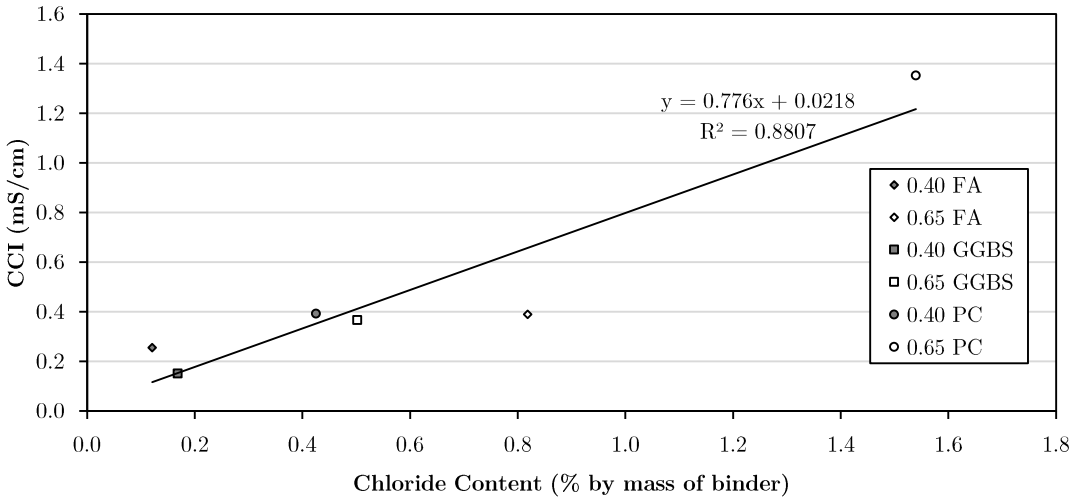

Figure 4.58: 110-Day Chloride Conductivity Index vs chloride content

4.5 Closure

The primary function of this experimental work was to investigate the influence of different cycles of wetting and drying on the corrosion rate of steel embedded in concrete. The applied cycles of wetting and drying were found to have a negligible impact on the corrosion rate when the w/b ratio was 0.40. Furthermore, at a w/b ratio of 0.40, no substantial difference was found between the performance of the various binder types. A statistical model was applied to measure any potential differences, with the w/b ratio dominating the progress of corrosion. However, a different scenario

was evident when the w/b ratio was increased to 0.65. At the increased w/b ratio, the reinforced concrete appeared more susceptible to changes in exposure conditions and binder type.

An increase in the w/b ratio from 0.40 to 0.65 caused a substantial increase in the corrosion rate. Furthermore, at a w/b ratio of 0.65, the applied cycles of wetting and drying were able to influence the corrosion rate. It was noted that an increase in drying time generally caused an increase in the corrosion rate. No noticeable difference was detected between 1 and 3-Day drying, however the corrosion rate increased when the drying time was increased to 5 and 7-Days (more substantially at 7-Day drying).

The change in corrosion rate was attributed to an inferred change in supply of oxygen. In the PC specimens the oxygen availability was the primary controlling factor and allowed the corrosion rate to be controlled by the supply of oxygen. Sufficiently short cycles of drying were able to effectively stifle corrosion by preventing drying to the level of the steel. This was only achieved in the 0.40 PC specimens where the improved concrete quality required longer drying times to the level of the steel. On the other hand, the corrosion rate increased rapidly as the drying time and w/b ratio were increased.

Interestingly, the oxygen availability did influence the corrosion rate in the 0.65 FA and 0.65 GGBS specimens. The corrosion rate for these binder types was expected to be controlled by the concrete resistivity; however, the oxygen availability caused a secondary effect. Limiting the oxygen availability was not able to stifle the corrosion; however, an increased supply of oxygen was able to increase the corrosion rate. Consequently, it is evident that the concrete resistivity governs whether or not corrosion will proceed, but the oxygen availability can affect the rate of corrosion.

In the FA and GGBS mixes the resistivity measurements provided a useful indicator for the corrosion potential when assessed according to Heckroodt's (2002) guidelines. The resistivity measurements were not as useful for the PC mixes where generally low resistivity values were measured, indicating a high corrosion potential in most cases. Furthermore, the PC corrosion rates were shown not to be governed by the resistivity and thus the resistivity did not provide a good indicator of corrosion potential in the PC concretes. On the other hand, the half-cell potential measurements provided a more useful indicator irrespective of the binder type and w/b ratio. The HCP potential results compared favourably with the guidelines provided in ASTM C876-09 (2009) and substantiate the indicated threshold values.

Throughout the experimental findings the applicability of the Durability Indices were substantiated. The Durability Index tests indicate that the binder type has less of a controlling effect than the w/b ratio on the transport of moisture and oxygen in concrete. The benefits of including FA and GGBS are however evident when comparing the CCI values, with the CCI decreasing considerably with the inclusion of FA or GGBS. The OPI and WSI provided useful indicators to explain the perceived drying times within concrete; while a useful correlation was found between the CCI values and the final chloride concentrations. Overall these indicators appear to provide a succinct laboratory-based indicator system for the potential to resist reinforcement corrosion under cyclic wetting and drying.

References

Angelucci, M. 2013. The influence of mix design parameters and compressive strength on durability indices. *MSc. Thesis*. University of Cape Town.

ASTM C876-09. 2009. Standard test method for corrosion potentials of uncoated reinforcing steel in concrete. (ASTM C876-09). West Conshohocken, PA: ASTM International.

Clear, K.C. 1989. Measuring rate of corrosion of steel in field concrete structures. *Transportation Research Record*. 1211: 28-37.

Heckroodt, R. O., 2002. *Guide to deterioration and failure of building materials.* London: Thomas Telford Publising.

Otieno, M.B. 2008. Corrosion propagation in cracked and uncracked concrete. *MSc. Thesis*. University of Cape Town.

Parrott, L.J. 1988. Moisture profiles in drying concrete. *Advances in cement research*. 1(3): 164-170.

Scott, A.N. 2004. The influence of binder type and cracking on reinforcing steel corrosion in concrete. *Ph.D. Thesis*. University of Cape Town.

Rodriguez, P., Ramirez, E. & Bonzalez, J.A. 1994, Methods for studying corrosion in reinforced concrete. *Magazine of Concrete Research*. 45(167): 81-90.

Stanish, K., Alexander, M.G. & Ballim, Y. 2004. Durability index interlaboratory test results – statistical analysis of variance. University of Cape Town and University of the Witwatersrand.

CHAPTER 5: GENERAL DISCUSSION, CONCLUSIONS AND RECOMMENDATIONS

5.1 General Discussion

The experimental findings in this research illustrate the complex nature of reinforcement corrosion under cyclic wetting and drying. The corrosion system appears to respond differently depending on the applied cycles of wetting and drying. This topic is not widely covered in literature, and seems previously to have been overlooked by researchers investigating corrosion under cyclic wetting and drying. Existing studies in this field tend to apply only one cycle of wetting and drying and ignore the duration of the cycles as an influencing parameter on the corrosion rate. While previous results may still provide useful insight, it is important to realise that it may not present the full picture, and consequently the results need to be interpreted carefully.

In the study at hand, varying the duration of the drying cycle had different impacts on the corrosion rate for the different binder types and w/b ratios. No consistent or significant trends were visible on the influence of the applied drying times when a w/b ratio of 0.40 was used, irrespective of the binder type. However, the drying time had a noticeable influence on the corrosion rate when the w/b ratio was increased to 0.65. Furthermore, at this higher w/b ratio, the binder type also influenced the corrosion rate, showing the complex and interconnected nature of reinforcement corrosion under cyclic wetting and drying. The primary parameters influencing the corrosion rate were found to be the w/b ratio, binder type, the cover depth (not experimentally investigated in this study) and the duration of the cycles of wetting and drying. If the w/b ratio, binder type and cover depth are appropriately selected, the effect of the cycles of wetting and drying may become negligible. Negating the effects of exposure to cyclic wetting and drying will be beneficial to reduce the likelihood of corrosion, but this must be considered when designing a suitable experimental programme.

It is imperative to select an appropriate wetting and drying regime for any testing undertaken, since different binders/systems respond differently for any given regime. This is evident by the applied wetting and drying regimes having negligible influence on the corrosion rate at a w/b ratio of 0.40, compared to a noticeable impact on the corrosion rate at a w/b ratio of 0.65 (both at a cover of 20 mm). An entirely different picture could emerge from selecting another wetting and drying regime and, hence, it appears necessary to implement more than one wetting and drying regime to establish conclusive results. The process to select an appropriate wetting and drying cycle should primarily consider a combination of the w/b ratio, binder type and the cover depth. The cycles of wetting and drying must be appropriately selected to highlight the desired effects on the corrosion rate, without biasing the findings. Longer drying times will allow the concrete to dry out further, allowing exposure to deeper underlying steel or investigations incorporating high quality concretes.

Conversely, shorter drying times can be used to investigate the corrosion rate when low cover depths or low quality concrete is used. These factors should be considered carefully when designing an experimental programme to investigate corrosion under cyclic wetting and drying and, depending on the required results, may require the implementation of multiple different cycles of wetting and drying.

Taking into account these findings, it is evident that this field of study has not yet been adequately investigated. Corrosion under cyclic wetting and drying still requires extensive research to properly characterise the influencing parameters. Suitable literature is not readily available and what exists does not consider a number of fundamental parameters, such as selecting an appropriate wetting and drying regime. Varying the drying duration in this study has inferred that the oxygen availability can be a controlling factor when considering reinforcement corrosion under cyclic wetting and drying. This will depend on a number of factors, including the moisture content, resistivity, chloride content, concrete quality (w/b ratio and binder type) and the concrete cover thickness. The chloride content does not provide a good indicator of the potential for corrosion, as shown in previous studies and reaffirmed in this one. However, the chloride content is a fundamental component of reinforcement corrosion in the marine environment and cannot be neglected. Nevertheless, considering the remaining factors, it is evident that this field requires a multi-factorial study of reinforcement corrosion to properly characterise the influencing parameters on reinforced corrosion under exposure to cyclic wetting and drying.

Nevertheless, there exists a crucial interaction between the saturation of concrete and the availability of oxygen, which appears previously to have been neglected. Limited oxygen availability has allowed PC mixes to perform beneficially in the marine environment despite the expected lower resistivity and higher chlorides in PC concretes. In the testing at hand, the 0.40 PC specimens compared favourably to the 0.40 FA and the 0.40 GGBS specimens, even though the FA and GGBS specimens yielded considerably higher resistivity values. This idea supports the concept of limiting corrosion activity through cathodic control of PC concrete. This provides suitable justification for the unexpectedly low corrosion damage visible in the tidal zone in Namibia. This case study identified the need for this research and a suitable conclusion was derived from this research.

A simpler approach for limiting the progress of corrosion has been presented in this research. Figure 4.30, reproduced as Figure 5.1, illustrates a key component of reinforcement corrosion under cyclic wetting and drying. This figure demonstrates the relationship between the drying depth in concrete and the concrete cover depth, which can be optimised to prevent drying to the level of the reinforcement. The influence of the moisture content, resistivity, chloride content and oxygen availability can be reduced if an appropriate concrete quality and cover thickness is selected. Drying to the level of the steel can be prevented to ensure that the effects of cyclic wetting and drying do not impact the embedded reinforcing steel, or at least the impact is limited. As a result, corrosion of embedded reinforcing steel can be controlled through two primary parameters – the concrete quality and the cover thickness.

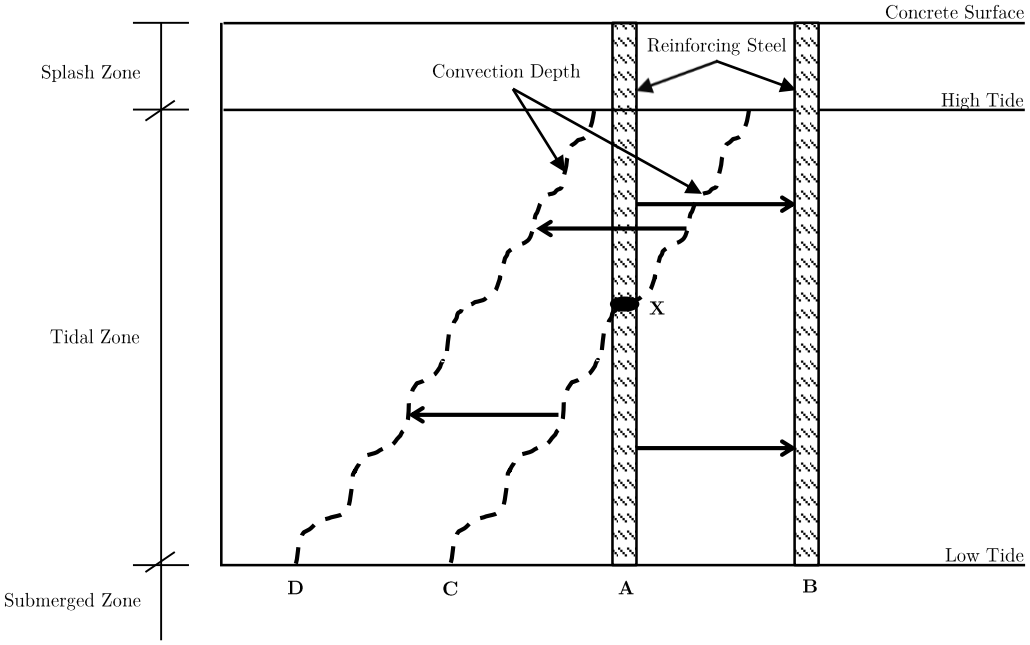

Figure 5.1: Hypothetical convection zone depth depending on the cover thickness and concrete quality

This concept of controlling the corrosion rate by limiting the drying to the level of the steel has the potential to minimise the influence of cyclic wetting and drying on the corrosion rate. This would allow generic marine environment classifications to be stipulated for the construction of reinforced concrete structures in the marine tidal, splash and submerged zones. However, this concept requires an extensive experimental programme to verify these expectations and may require modelling and experimental results of drying times in concrete and specimens exposed to in-situ marine environment conditions.

5.2 Conclusions

This section provides conclusions on the key findings presented in Chapter 4. The conclusions will draw on findings from both sample sets and provide relevant correlations to the literature provided. Recommendations will be formulated from the combined conclusions and possible future studies will be suggested.

5.2.1 Effect of the drying time on the early-age corrosion rate

Monitoring of the specimens in a passive state for the first 5 weeks highlighted the effect of the sulphides and thiosulphates on the early-age corrosion rate of slag-bearing concretes. The applied cycles of wetting and drying had no apparent effect on the early-age corrosion rate measurements. Additionally, the early-age corrosion rates in the GGBS specimens did not appear to be controlled by the w/b ratio or the concrete resistivity. During this time the FA and PC specimens remained in a passive state of corrosion.

5.2.2 Effect of the drying time on the corrosion rate

The experimental work at hand illustrated that corrosion of embedded reinforcing steel can be effectively reduced by limiting the availability of oxygen. The control of corrosion hinges on providing sufficient concrete quality and adequate cover thickness. There is likely a trade-off between concrete quality and cover thickness that will provide similar protection to the reinforcing steel. If these parameters are appropriately optimised the expected harsh conditions in the marine tidal zone can be minimised. The cover concrete may not dry to the level of the steel if sufficient concrete quality and cover thickness are provided. As a result, reinforced concrete in the marine tidal zone can perform as if it was permanently submerged which allows the corrosion rate to be effectively reduced.

Cycles of 2 days wetting and 1 day drying were able to maintain the CR1 0.40 PC corrosion rates and prevent active corrosion conditions in the CR2 0.40 PC sample set. The 0.40 PC specimens performed similarly to the 0.40 FA and 0.40 GGBS. Contrary to most perceptions, this showed the possibility of using plain PC concrete in submerged reinforced concrete structures despite the reduced potential durability properties of PC concrete, although as a general rule, blended binder concrete are still preferable. However, when the w/b ratio was increased to 0.65, the corrosion rate increased markedly when exposed to longer drying durations. Increasing the w/b ratio from 0.40 to 0.65 highlighted the controlling effect of the inferred oxygen availability.

The cycles of wetting and drying chosen for this work identified the controlling effect of the oxygen availability on the corrosion rate in PC concretes. It was also revealed that at a higher w/b ratio (0.65) the oxygen availability played a major role in the progress of corrosion in the FA and GGBS mixes. However, the oxygen availability did not play a comparable role in the FA and GGBS mixes when the w/b ratio was reduced to 0.40. Consequently, the rate controlling parameters for corrosion appear to be the oxygen availability and the concrete resistivity. The results show that the drying time can have a primary influence on the corrosion rate in PC concrete and a secondary influence on FA and GGBS mixes.

5.2.3 Effect of the binder type and w/b ratio on the corrosion rate

The results of this experimental work suggest that the corrosion rate can be effectively controlled by limiting the w/b ratio alone; while the benefits of including FA and GGBS for exposure to cyclic wetting and drying appear to be overstated under certain conditions. However, it has to be recognised that blended cements do provide an additional safeguard to protect the embedded reinforcing steel. This added protection cannot be neglected, but when blended cements are not available, the use of plain PC concrete can be considered at a sufficiently low w/b ratio. In this research, the benefit of including FA and GGBS was noted for a w/b ratio of 0.65, but the European Standard EN 206 (2013) stipulates a maximum w/b ratio of 0.45 for the marine tidal and splash zone.

The PC mixes performed well at a w/b ratio of 0.40 when compared to the 0.40 FA and 0.40 GGBS mixes. This is likely due to the controlling effect of the oxygen availability on the corrosion rate in the PC mixes. However at a w/b ratio of 0.65, the PC mixes performed considerably

worse, especially as the drying time was extended to 7 days. As a result, oxygen deprived conditions are required in order for plain PC concrete to be suitable in the marine tidal and splash zone.

The use of plain PC concrete in the marine tidal and splash zone will require an increase in steel protection through a combination of cover thickness and concrete quality. It is expected that either the concrete quality or cover thickness could be reduced if FA or GGBS was incorporated in the mix. At a w/b ratio of 0.65 the inclusion of GGBS was found to be beneficial with the 0.65 GGBS outperforming both the 0.65 FA and the 0.65 PC.

5.2.4 Effect of the chloride concentration on the corrosion rate

The chloride concentration had a more significant effect on the corrosion rate at a w/b ratio of 0.65 compared to a w/b ratio of 0.40. The corrosion rate generally increased with an increase in chloride concentration for a w/b ratio of 0.65. However, for a w/b ratio of 0.40 the chloride concentration appeared to have negligible influence. The specimens were actively corroding without the chloride concentration surpassing the generally accepted threshold chloride content of 0.4% by mass of binder. This was an unexpected finding and requires further investigation.

5.2.5 Suitability of corrosion rate indicators

5.2.5.1 Durability Index tests

The Durability Index tests provided useful quantifications of the concrete quality. These values also correlated well with their intended functions. Changes in the OPI and WSI values were able to identify changes in the w/b ratio and hence the concrete quality. These parameters were identified as key factors when assessing the quality of concrete for the marine tidal zone. It is expected that the OPI and WSI values provide a good indication of the required drying time to the level of the steel.

The CCI values were able to distinguish between changes in the w/b ratio, but also changes in the binder type. The PC mixes obtained higher CCI values compared to the FA and GGBS mixes. Also, these CCI values correlated well with the measured chloride concentrations irrespective of the w/b ratio and binder type.

5.2.5.2 Resistivity

The resistivity guidelines provided by Heckroodt (2002), and presented in Table 2.5, were shown to apply relatively well for the FA and GGBS specimens. However, the table provided does not allow any distinction for the binder type. Furthermore, as identified by Scott (2004), the resistivity was not rate controlling in the PC concretes and thus these guidelines were no longer applicable. Likewise this research identified that changes in the resistivity of the PC mixes did not correspond with changes in the corrosion rate.

The FA and GGBS specimens generally obtained resistivity values in the region of 20-40 kOhm-cm; while the PC concrete specimens generally obtained resistivity values in the region of 5-15 kOhm-cm. The resistivity measurements for the PC were all indicative of high corrosion potential which further illustrated the limited value of resistivity measurements for PC concrete. It

is also worth noting that the shorter duration cycles of drying led to higher resistivity values, which also had a higher degree of variability. The change in resistivity was justified by various degrees of chloride deposition and curing, depending on the drying duration. It is expected that an increase in the drying time caused an increase in the chloride deposition, which provided a better connection for the pore spaces and lowered the resistivity. Furthermore, the shorter duration drying cycles allowed for better curing of the specimens and thus increased the resistivity in the specimens exposed to shorter drying durations. Hence, in both cases the specimens exposed to shorter durations of drying will measure higher resistivity values.

5.2.5.3 Half-cell potential

Half-cell potential measurements provided a relatively good indication of the condition of the embedded reinforcing steel. A good correlation was found between corrosion rate measurements and the HCP values. The measurements also highlighted the threshold values presented in ASTM C876-09 (2009). These include threshold values of -256 mV (Ag/AgCl) for mild corrosion and -406 mV (Ag/AgCl) for severe corrosion. A good correlation was found for both these threshold values irrespective of the binder type and w/b ratio.

5.2.6 The impressed current technique

A novel contribution of this research was to present a clear description of the procedure for implementing the impressed current technique. The sources cited in this research provide a number of small pieces to this puzzle, which was only solved through a trial-and-error approach in implementation. Future difficulties in accelerating corrosion will hopefully be avoided by consulting the brief guideline to the impressed current technique, provided in Appendix H. The impressed current technique appears to give reasonably good results when applied correctly. In the CR1 sample set, the current was likely impressed for too long with unexpectedly high corrosion rates measured. However, the CR2 specimens were impressed with a shorter duration current and achieved more reasonable initial corrosion rates. The CR2 results also presented more consistent findings and were generally considered to provide a better representation of natural corrosion conditions.

5.3 Recommendations

Based on the findings included in Chapter 4 and 5, the following recommendations should be considered for future work and possible implementation into practice.

5.3.1 Binder type and w/b ratio

The European Standards EN 206 (2013) do not suggest specific binder types in the marine environment and only prescribe a maximum w/b ratio. There appears to be some merit in this approach with no noticeable benefit measured for the inclusion of FA or GGBS (at a w/b ratio of 0.40 and a cover depth of 20 mm). However, this requires that continuously submerged conditions are implemented and drying to the level of the steel is prevented. Ensuring that these conditions are achieved will require more accurate modelling of drying times in concrete. It is expected that including FA or GGBS will allow the concrete quality or cover depth to be decreased; however

further research is required to develop accurate guidelines and specifications for the binder type and w/b ratio taking into account the concrete cover depth.

5.3.2 Modelling drying times

A major shortfall of the existing knowledge is a clear understanding of the required drying times for concrete exposed to multiple cycles of wetting and drying. This is a fundamental parameter that has shown the potential to effectively limit corrosion but has not been sufficiently investigated. Modelling of drying times based on concrete quality and cover depth should be investigated coupled with experimental work to establish suitable requirements for the marine tidal zone. These models could be included in performance-based design of reinforced concrete structures. With sufficiently accurate drying models the appropriate binder type and w/b ratio could be optimised to minimise the likelihood of corrosion.

5.3.3 Corrosion rate indicators

The resistivity and HCP guidelines show promising results and should be considered as good indicators of corrosion potential. The threshold values should be considered as valid for both the resistivity and the HCP guidelines; however, resistivity measurements are generally low in plain PC concretes and a change in corrosion rate cannot be recognised by measuring the resistivity. HCP measurements show good correlations to the corrosion rate and may provide more useful information than previously expected. The relevance of these corrosion rate indicators should be investigated further for in-situ reinforced concrete structures.

5.3.4 Further experimental work

These findings should serve as a preliminary study into the controlling effects of the resistivity and an inferred oxygen availability on the corrosion rate under cyclic wetting and drying. A number of shortfalls are evident in the presented experimental programme and should be addressed by researchers going forward.

5.3.4.1 Correlation to in-situ corrosion measurements

The experimental work at hand is only relevant to the applied laboratory exposure conditions. Further testing should aim to correlate these findings with in-situ reinforced concrete structures exposed directly to the marine environment. This knowledge could allow for better performance-based design of reinforced concrete structures in the marine environment.

5.3.4.2 Further laboratory experiments

Any further experimental work following a similar experimental programme should include a baseline sample set that is permanently submerged. This will allow the influence of the drying time to be more effectively analysed allowing for more accurate comparisons to permanently submerged specimens.

Additionally, a major contribution to this field of study would be to correlate cycles of wetting and drying to a supply of oxygen at the level of the steel. The inferred oxygen availability in this

study requires verification by direct measurements. Combining measurements of the supply of oxygen and relevant drying models will allow for more accurate conclusions on the direct effect of the oxygen availability on the corrosion rate under cyclic wetting and drying.

5.3.4.3 Impressed current technique

The impressed current technique was hugely problematic and imposed a limitation on the experimental work with the samples divided into two separate data sets. Consequently, the number of repeat specimens was reduced which limits the accuracy of the results. Future studies will hopefully take due cognisance of these findings and avoid future problems with the impressed current technique.

APPENDICES

Appendix A: Laboratory Mix Designs

A.1: Sieve analysis

A.1.1: Fine aggregate

Table A.1: Sieve analysis for Philippi Dune Sand

Sieve Size	Mass retained	% Mass retained	Cumulative % mass retained	Cumulative % mass passing
[µm]	[g]	[%]	[%]	[%]
4750	0.0	0.0	0.0	100.0
2360	0.1	0.0	0.0	100.0
1180	1.5	0.3	0.3	99.7
600	44.9	8.5	8.8	91.2
300	280.8	53.0	61.8	38.2
150	191.7	36.2	98.0	2.0
75	9.3	1.8	99.8	0.2
< 75	1.3	0.2	100.0	0.0
Sample size: 529.5 g				
Fineness Modulus = 1.69				

Table A.2: Sieve analysis for Greywacke Crusher Sand

Sieve Size	Mass retained	% Mass retained	Cumulative % mass retained	Cumulative % mass passing
[µm]	[g]	[%]	[%]	[%]
4750	4.8	0.9	0.9	99.1
2360	139.7	27.3	28.3	71.7
1180	135.2	26.5	54.7	45.3
600	87.5	17.1	71.8	28.2
300	51.5	10.1	81.9	18.1
150	34.6	6.8	88.7	11.3
75	26.1	5.1	93.8	6.2
< 75	31.5	6.2	100.0	0.0
Sample size: 511.1 g				
Fineness Modulus = 3.26				

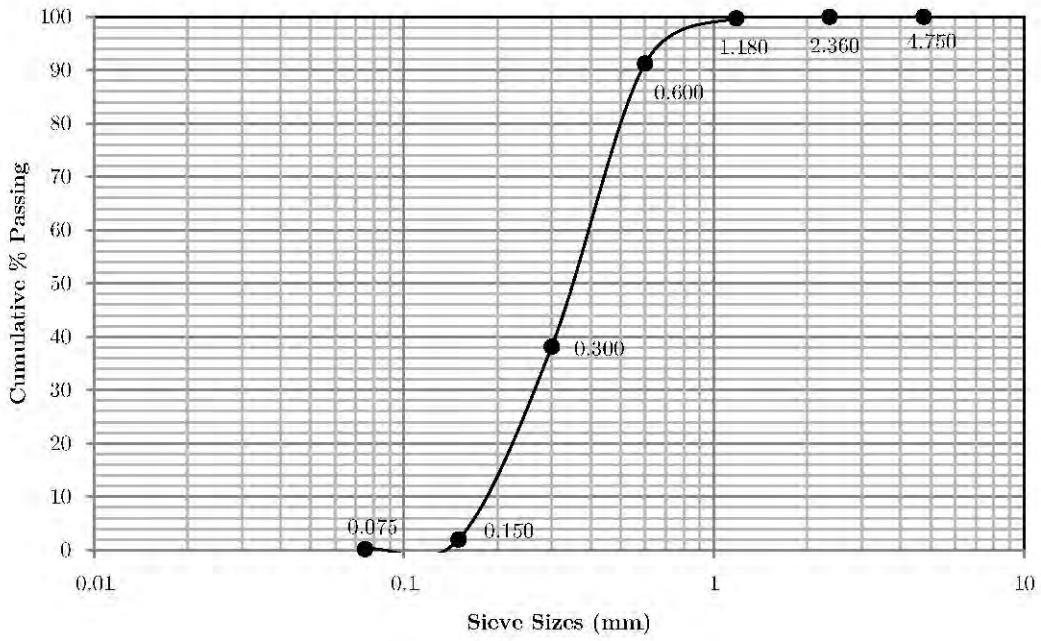

Figure A.1: Fine aggregate grading curve for Philippi Dune Sand

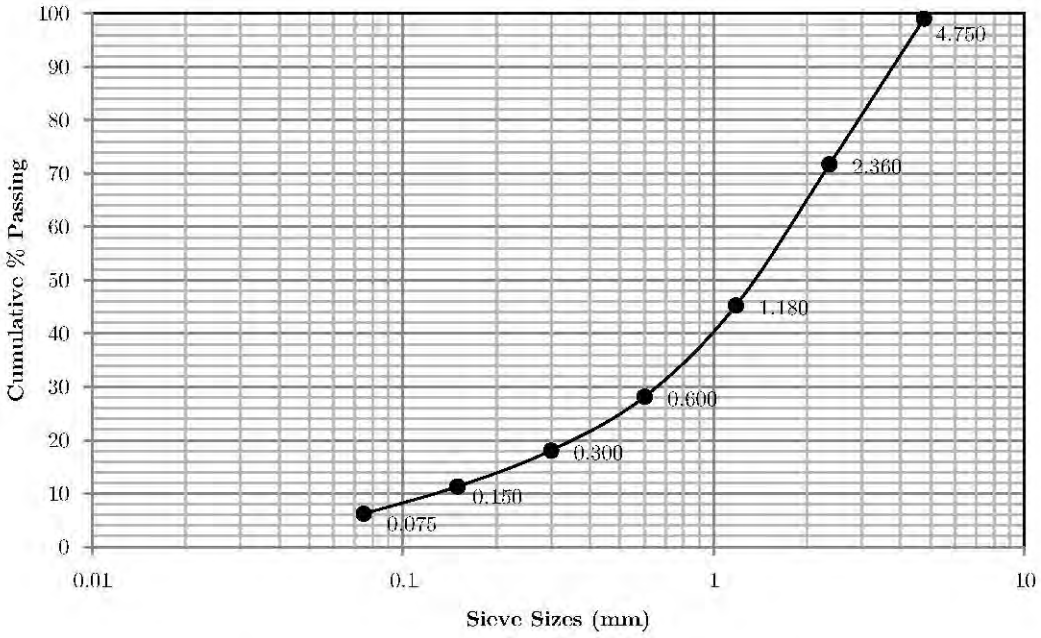

Figure A.2: Fine aggregate grading curve for Crusher Sand

A.1.1: Coarse aggregate

Table A.3: Sieve analysis for 13.2 mm Greywacke

Sieve Size	Mass retained	% Mass retained	Cumulative % mass retained	Cumulative % mass passing
[mm]	[g]	[%]	[%]	[%]
19.00	0.0	0.0	0.0	100.0
13.20	156.6	7.8	7.8	92.2
9.50	897.7	44.9	52.7	47.3
6.70	718.6	35.9	88.6	11.4
4.75	165.4	8.3	96.9	3.1
2.0	56.6	2.8	99.7	0.3
< 2.00	4.9	0.2	100.0	0.0
Sample size: 2000.2 g				

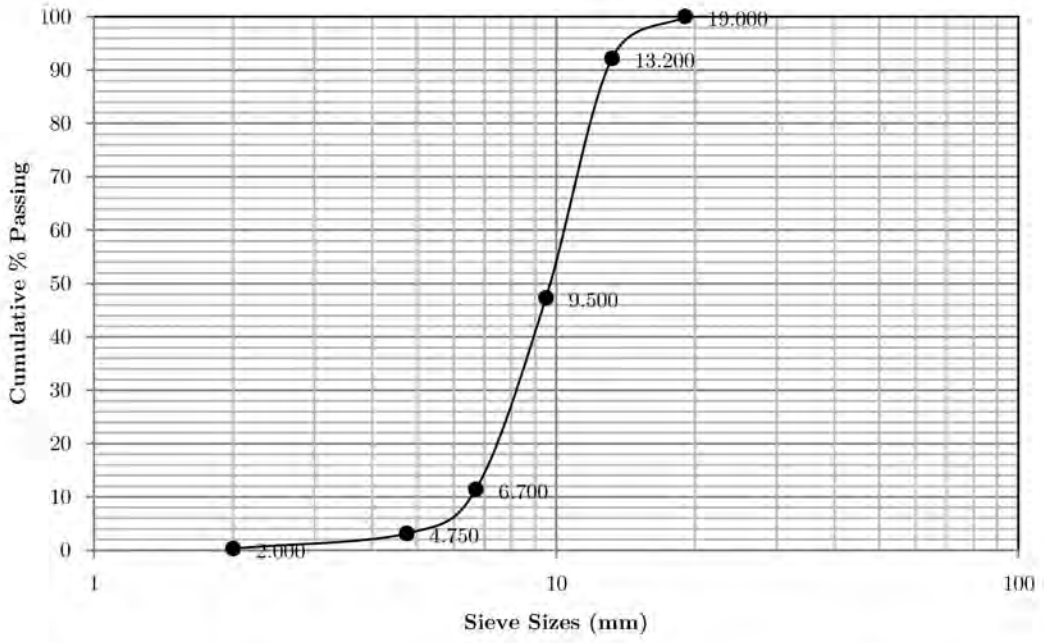

Figure A.3: Coarse aggregate grading curve for 13.2 mm Greywacke

Appendix B: Cover Measurements

B.1: Cover measurements

A commercial covermeter was used to measure the achieved cover to the reinforcing steel in each specimen. This may be used to justify variations in corrosion rate based on slight variations in the cover thickness. Table B.1 below illustrates what cover was actually achieved in the specimens. One outlier was identified and is highlighted in the table below.

Table B.1: Measured cover to reinforcement

Mix Designation	1 Day [mm]	3 Day [mm]	5 Day [mm]	7 Day [mm]
0.40 FA	19	19	20	19
	20	19	20	19
	19	19	22	19
0.65 FA	19	19	20	19
	19	20	19	19
	19	20	19	19
0.40 GGBS	20	19	21	19
	19	20	22	21
	21	21	20	18
0.65 GGBS	19	21	21	19
	22	23	19	22
	35	21	22	21
0.40 PC	20	20	20	21
	19	20	19	24
	20	20	20	19
0.65 PC	23	20	19	22
	25	20	21	20
	20	23	20	24

Appendix C: Compressive Strength

The compressive strength of each mix was measured at 14, 28, 56 and 90 days. The compressive strength results complied with SANS 5863 (2006), where the range/average must be less than 15%. Results are presented in Table C.1 with the strength development shown in Figure C.1 and Figure C.2.

Table C.1: Compressive strength results

Mix Designation	Compressive strength	Range/Average	Density
	[MPa]	[%]	[kg/m^3]
0.40 FA	47.0	6.6	2395
	52.0	1.0	2375
	59.5	5.7	2378
	69.0	4.1	2395
0.65 FA	21.5	5.1	2400
	26.5	1.9	2380
	33.0	7.6	2385
	36.5	3.8	2400
0.40 GGBS	53.5	6.3	2380
	63.5	5.8	2410
	68.5	5.8	2420
	72.5	5.0	2395
0.65 GGBS	21.5	1.4	2345
	27.0	4.9	2315
	31.5	13.3	2320
	35.0	2.9	2330
0.40 PC	56.5	6.2	2440
	61.0	2.0	2415
	66.5	4.2	2440
	66.5	5.4	2435
0.65 PC	32.0	1.9	2345
	35.5	3.9	2360
	38.5	6.8	2345
	40.0	7.5	2355

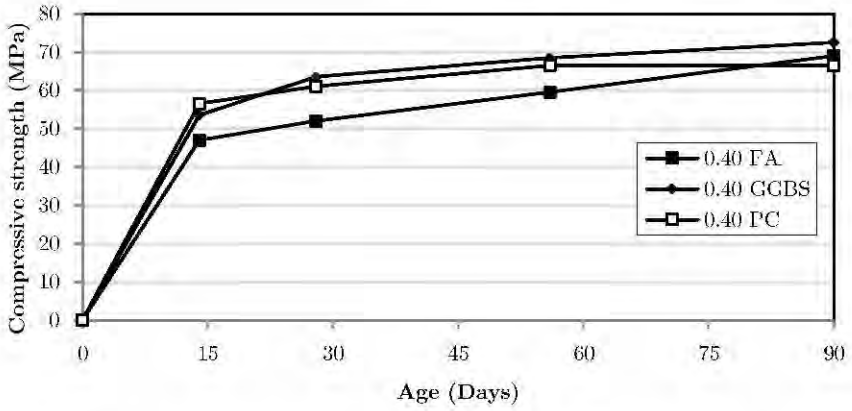

Figure C.1: Compressive strength development for w/b = 0.40

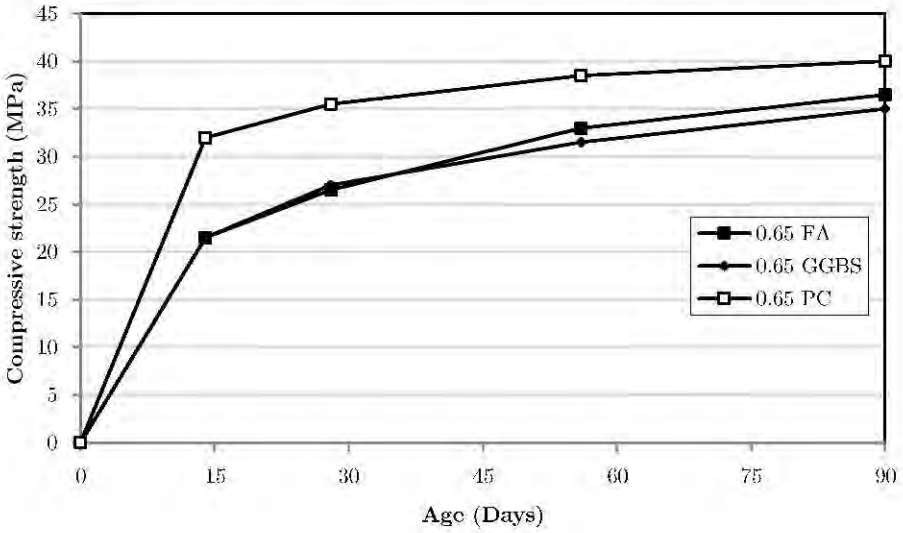

Figure C.2: Compressive strength development for w/b = 0.65

Appendix D: Porosity and Sorptivity Calculations

D.1: Porosity

Sample calculations are presented for the 0.65 FA specimens to give an indication of the process for determining the porosity and sorptivity. The porosity was determined through processing of data obtained from concrete discs saturated with 5M NaCl solution. The density of the solution was assumed to be 1.20 g/mm^3 for calculations using Eq. D.1.

$$Porosity = \frac{M_s - M_d}{V \times \rho_{sw}} \quad \text{(Eq. D.1)}$$

where: M_s is the saturated mass (g), M_d is the dry mass (g), V is the volume (mm^3) and ρ_{sw} is the density of 5M NaCl solution (1200 g/mm^3).

In each case four specimens were tested and the porosity presented as the average, shown in Table D.1. Sample calculations are provided for the 0.65 FA mix and presented in detail for specimen number 1.

$$Porosity\ (0.65\ FA, 1) = \frac{M_s - M_d}{V \times \rho_{sw}} \quad \text{(Eq. D.1)}$$

$$Porosity\ (0.65\ FA, 1) = \frac{249.74 - 240.34}{103 \times 1.20}$$

$$Porosity\ (0.65\ FA, 1) = 7.61\%$$

Table D.1: Processed porosity data for 0.65 FA

0.65 FA							
No.	**Diameter**	**Thickness**	**Dry Mass**	**Saturated Mass**	**Mass Change**	**Total Volume**	**Porosity**
	[mm]	**[mm]**	[g]	[g]	[g]	**[mm^3]**	[%]
1	68.35	28.05	240.34	249.74	9.40	103	7.61
2	68.50	28.90	244.91	254.69	9.78	107	7.65
3	68.35	28.18	242.40	251.56	9.16	103	7.38
4	68.40	28.35	243.45	252.96	9.51	104	7.61
						Average:	**7.56**

The same procedure was followed for all the mixes, with the combined results presented in Table D.2.

Table D.2: Porosity determination for each mix (average)

Mix	Diameter	Thickness	Dry Mass	Saturated Mass	Mass Change	Total Volume	Porosity
	[mm]	[mm]	[g]	[g]	[g]	[mm^3]	[%]
0.40 FA	68.35	28.62	240.60	246.14	5.54	105.02	4.40
0.65 FA	68.40	28.37	242.78	252.24	9.46	104.25	7.56
0.40 GGBS	68.42	28.36	237.25	242.96	5.72	104.25	4.57
0.65 GGBS	68.43	28.12	233.30	243.88	10.59	103.39	8.53
0.40 PC	68.46	28.11	244.25	252.34	8.09	103.47	6.51
0.65 PC	68.50	28.45	236.75	249.57	12.82	104.85	10.19

D.2: Sorptivity

As mentioned in Section 4.2.3, the sorptivity values were calculated using the 110 day NaCl saturated porosity and the previously determined moisture absorption gradients. The porosity was fixed based on Table D.2 with the saturated mass adjusted accordingly. Consequently, for the 0.65 FA specimens the porosity was set to 7.56% and the saturated mass adjusted accordingly.

Table D.3: 0.65 FA specimen details

Measurement	Specimen 1	Specimen 2	Specimen 3	Specimen 4	Average
Diameter (mm)	68.50	68.40	68.65	68.40	68.49
Thickness (mm)	29.98	30.73	30.50	30.20	30.35
Porosity (%)	7.56	7.56	7.56	7.56	7.56

Table D.4: Adjusted saturation masses for 0.65 FA specimens

Time (min)	Mass (g)				
	Specimen 1	Specimen 2	Specimen 3	Specimen 4	Average
0	253.69	257.39	257.44	252.45	255.24
3	254.46	258.15	258.21	253.24	256.02
5	254.67	258.38	258.39	253.45	256.22
7	254.83	258.56	258.53	253.62	256.39
9	254.99	258.69	258.67	253.73	256.52
12	255.14	258.88	258.81	253.93	256.69
16	255.33	259.10	259.03	254.13	256.90
20	255.52	259.32	259.21	254.35	257.10
25	255.71	259.51	259.38	254.49	257.27
Saturation	**262.04**	**265.93**	**265.97**	**260.84**	**263.70**

The values in Table D.3 were then used to determine the mass gain as a function of the square root of time. These results are presented in Table D.5.

Table D.5: Adjusted mass gain for 0.65 FA specimens

Square Root Time ($hours^{0.5}$)	Mass (g)				
	Specimen 1	Specimen 2	Specimen 3	Specimen 4	Average
0.224	0.77	0.76	0.77	0.79	0.77
0.289	0.98	0.99	0.95	1.00	0.98
0.342	1.14	1.17	1.09	1.17	1.14
0.387	1.30	1.30	1.23	1.28	1.28
0.447	1.45	1.49	1.37	1.48	1.45
0.516	1.64	1.71	1.59	1.68	1.66
0.577	1.83	1.93	1.77	1.90	1.86
0.645	2.02	2.12	1.94	2.04	2.03
Gradient	**2.938**	**3.218**	**2.798**	**3.006**	**2.990**
Correlation Factor	**0.9994**	**0.9997**	**0.9996**	**0.9990**	**0.9994**

These moisture absorption gradients were then used in combination with the porosity to determine the sorptivity. This process followed the instructions outline in Alexander, Ballim & Mackechnie (2010) and used Eq. D.2 below.

$$S = \frac{Fd}{M_{sv} - M_{s0}} \qquad \text{(Eq. D.2)}$$

$$S\,(0.65\,FA, 1) = \frac{2.9378 \times 29.98}{262.04 - 253.69}$$

$$S\,(0.65\,FA, 1) = 10.5\,mm/hour^{0.5}$$

The same process was applied to all of the specimens with Table D.6 presenting a summary table of the sorptivity values.

Table D.6: Summary table of sorptivity values

Measurement	0.40 FA	0.65 FA	0.40 GGBS	0.65 GGBS	0.40 PC	0.65 PC
Diameter (mm)	68.36	68.49	68.35	6841	68.33	68.38
Thickness (mm)	29.81	30.35	30.52	30.33	30.33	29.86
Porosity (%)	4.40	7.56	4.57	8.53	6.51	10.19
Dry Mass (g)	251.98	255.24	258.47	245.43	256.52	249.50
Saturated Mass (g)	256.79	263.70	263.59	254.94	263.76	260.67
Gradient	2.071	2.990	1.332	2.062	2.532	3.368
Correlation Factor	0.9978	0.9994	0.9962	0.9988	0.9993	0.9997
Sorptivity	**12.8**	**10.7**	**7.9**	**6.6**	**10.6**	**9.0**

Appendix E: Corrosion Rate Measurements

E.1: Early-age corrosion rate

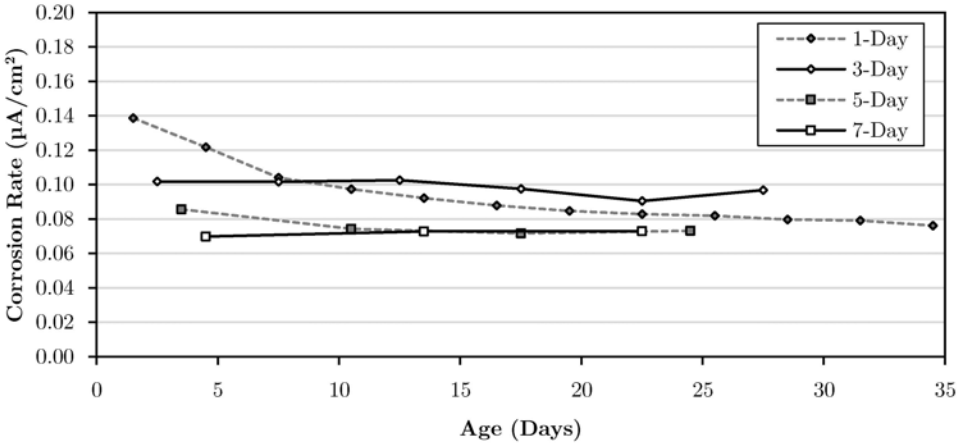

Figure E.1: Early-age corrosion rate for 0.40 FA

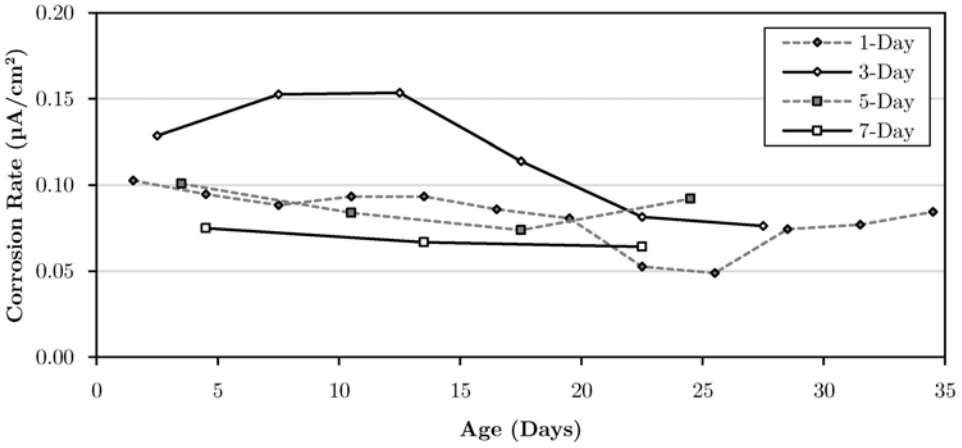

Figure E.2: Early-age corrosion rate for 0.65 FA

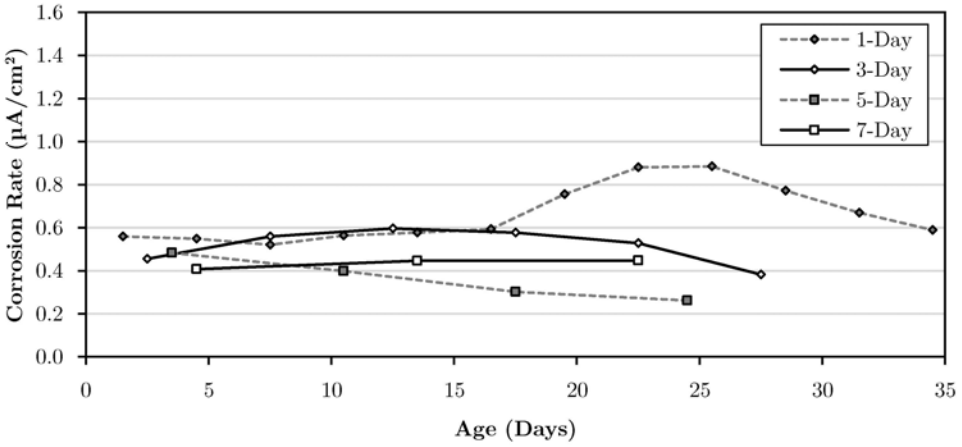

Figure E.3: Early-age corrosion rate for 0.40 GGBS

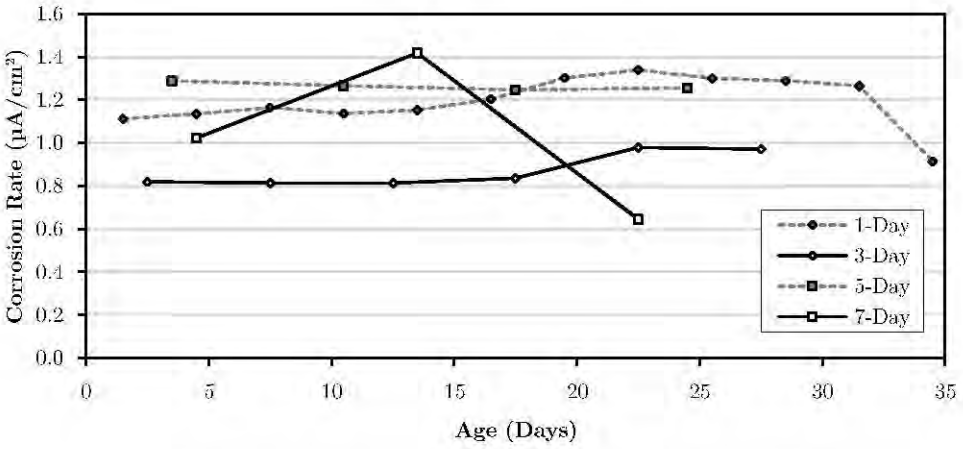

Figure E.4: Early-age corrosion rate for 0.65 GGBS

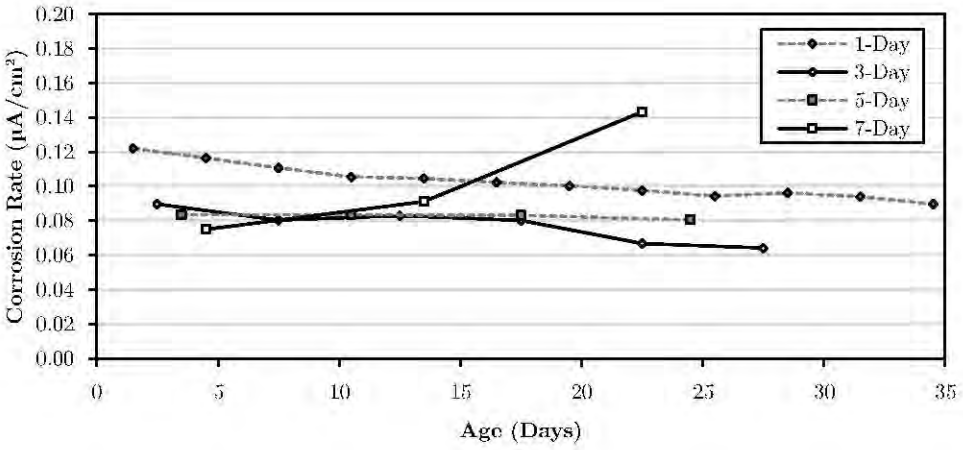

Figure E.5: Early-age corrosion rate for 0.40 PC

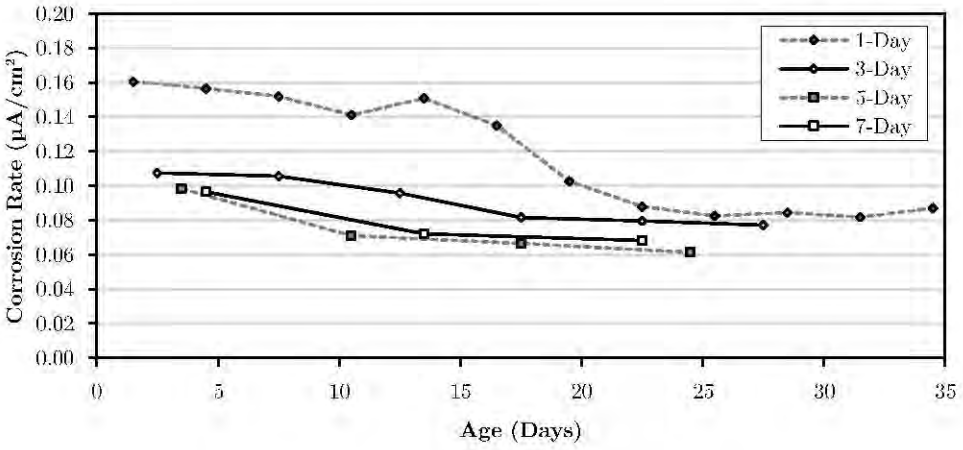

Figure E.6: Early-age corrosion rate for 0.65 PC

E.2: Corrosion rate measurements for CR1

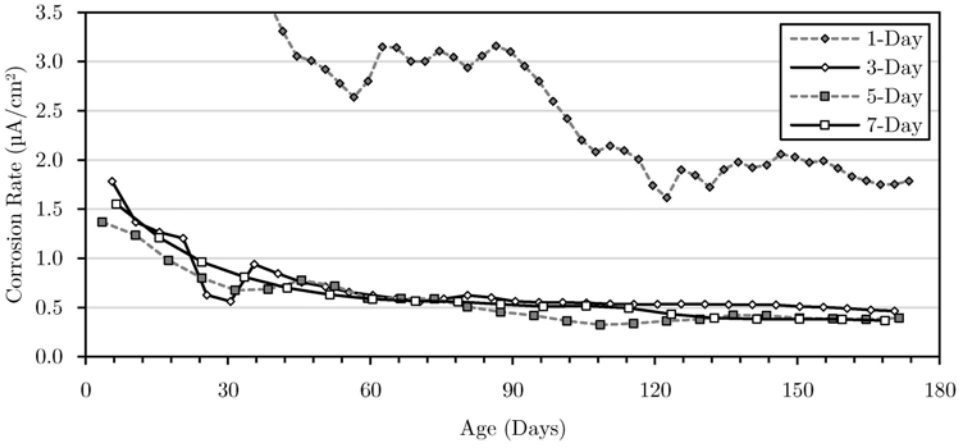

Figure E.7: CR1 corrosion rate measurements for 0.40 FA

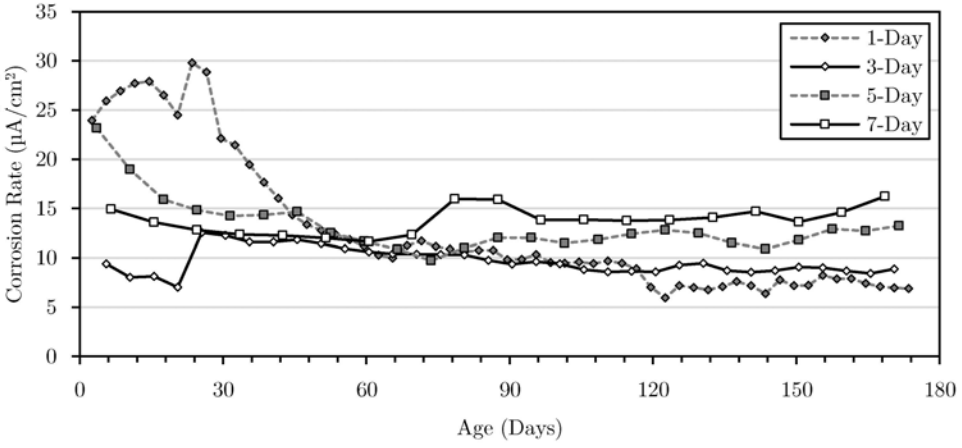

Figure E.8: CR1 corrosion rate measurements for 0.65 FA

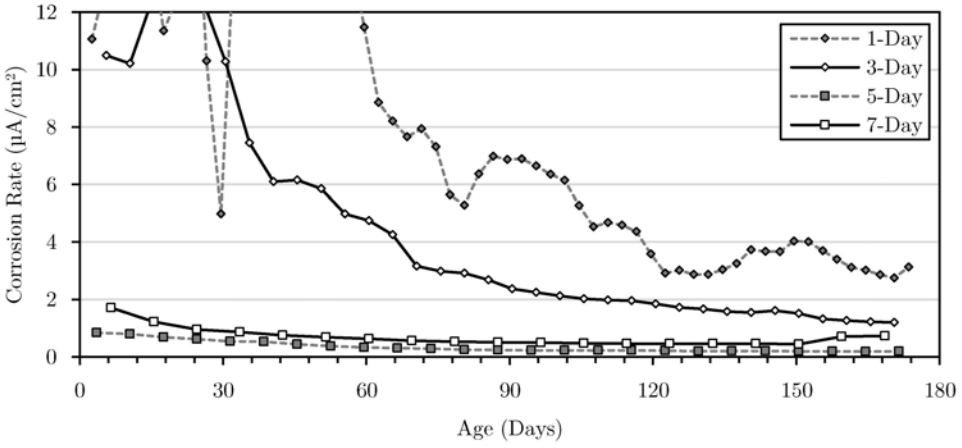

Figure E.9: CR1 corrosion rate measurements for 0.40 GGBS

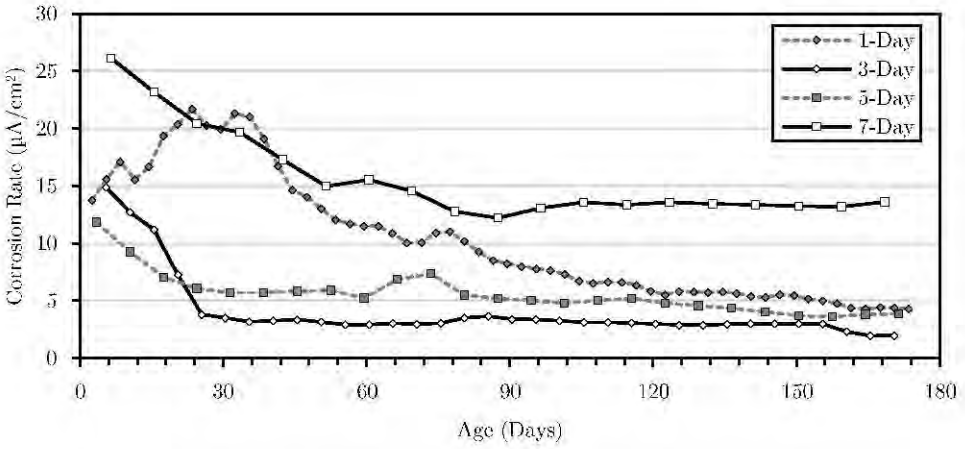

Figure E.10: CR1 corrosion rate measurements for 0.65 GGBS

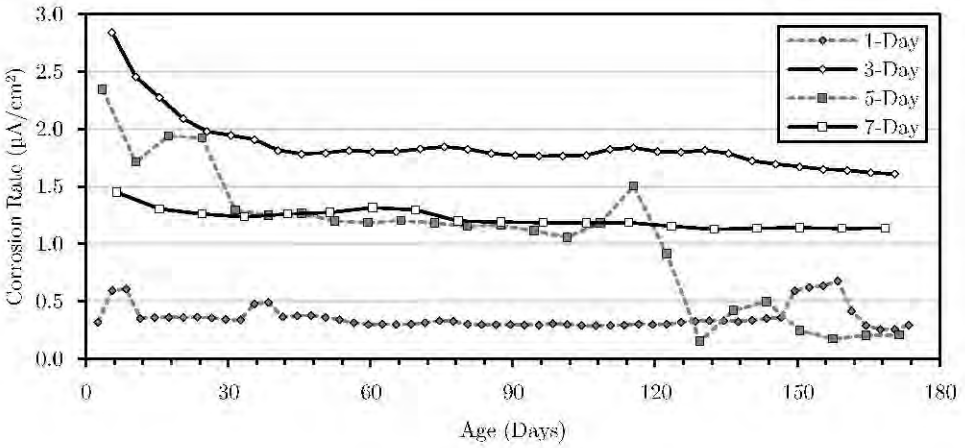

Figure E.11: CR1 corrosion rate measurements for 0.40 PC

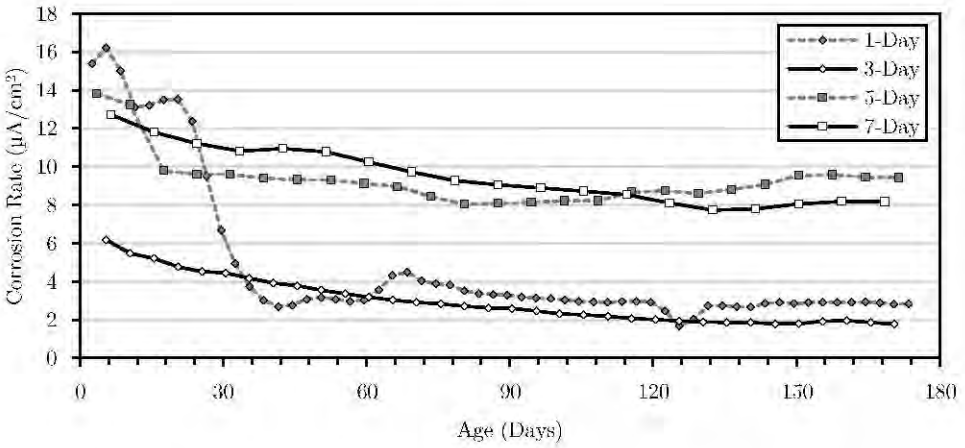

Figure E.12: CR1 corrosion rate measurements for 0.65 PC

E.3: Corrosion rate measurements for CR2

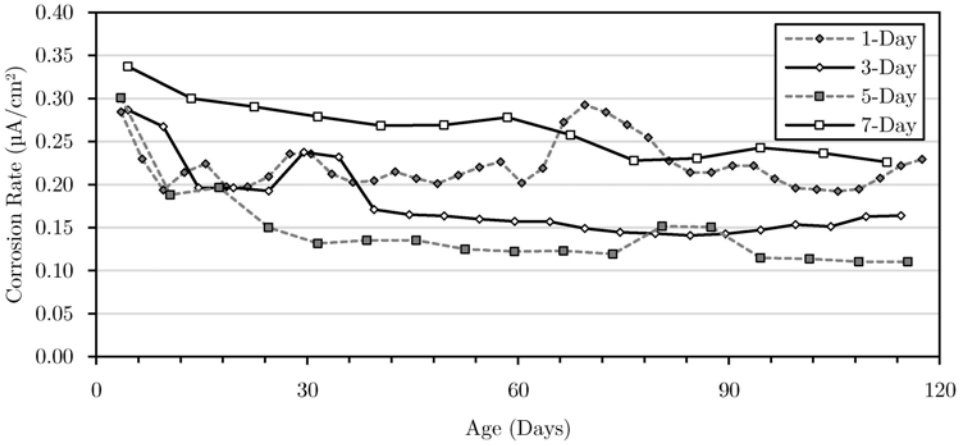

Figure E.13: CR2 corrosion rate measurements for 0.40 FA

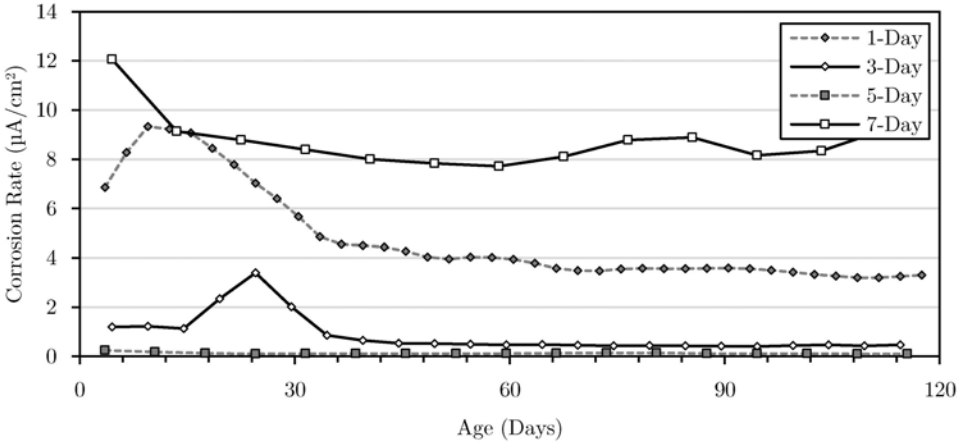

Figure E.14: CR2 corrosion rate measurements for 0.65 FA

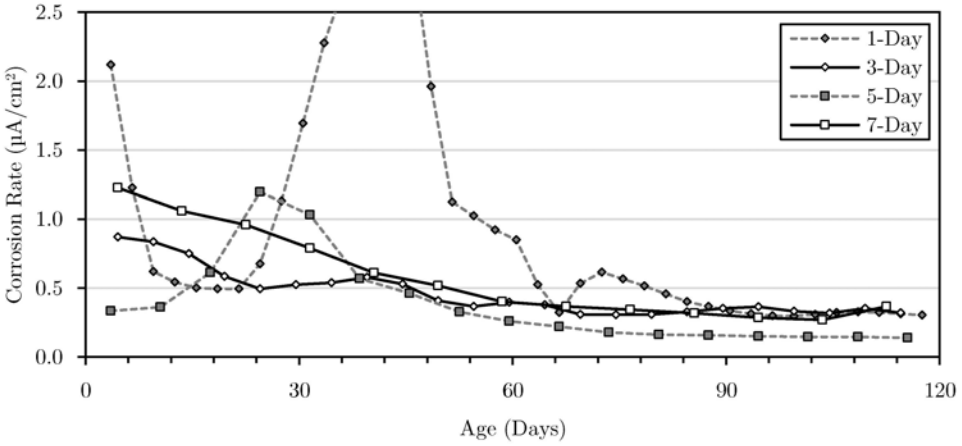

Figure E.15: CR2 corrosion rate measurements for 0.40 GGBS

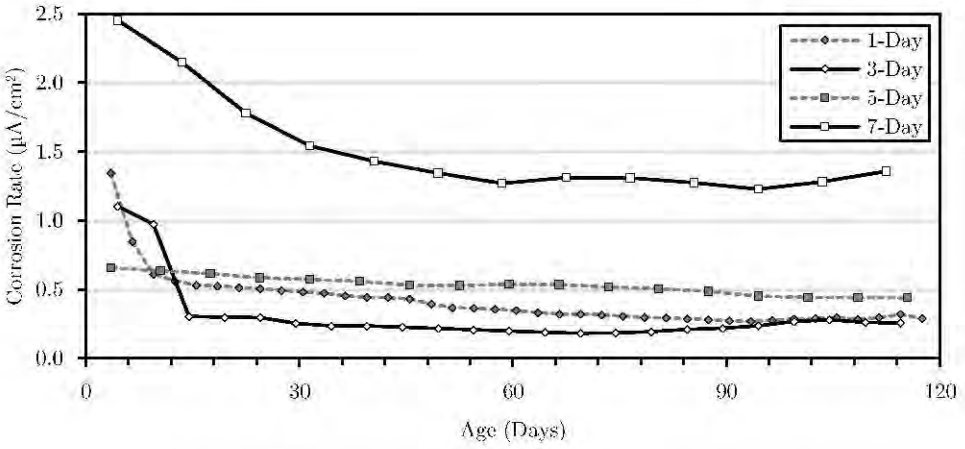

Figure E.16: CR2 corrosion rate measurements for 0.65 GGBS

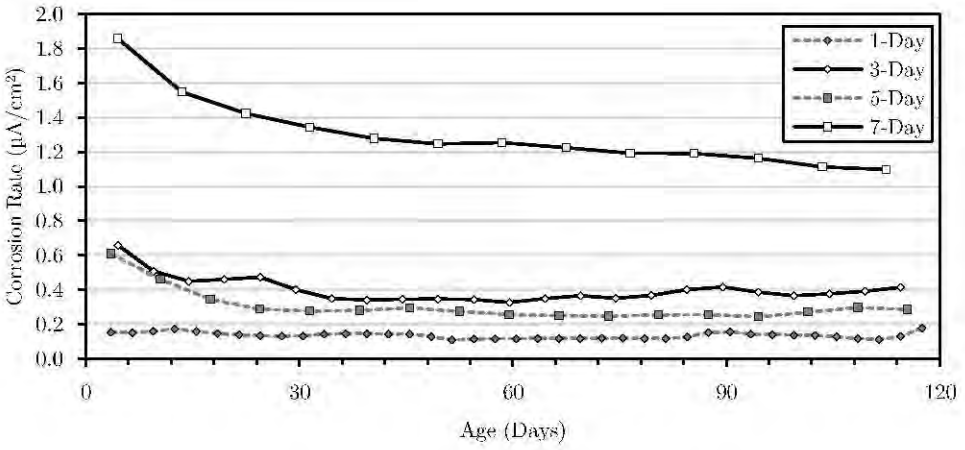

Figure E.17: CR2 corrosion rate measurements for 0.40 PC

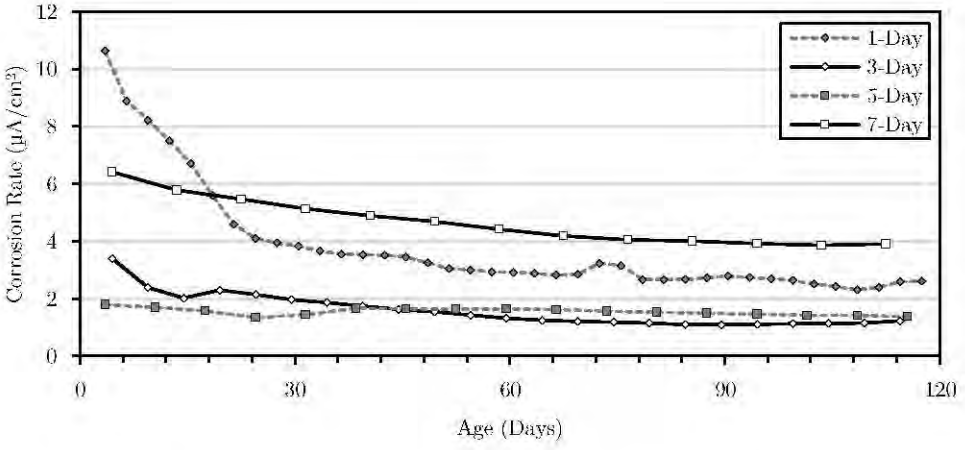

Figure E.18: CR2 corrosion rate measurements for 0.65 PC

Appendix F: HCP Measurements

F.1: HCP measurements for CR1

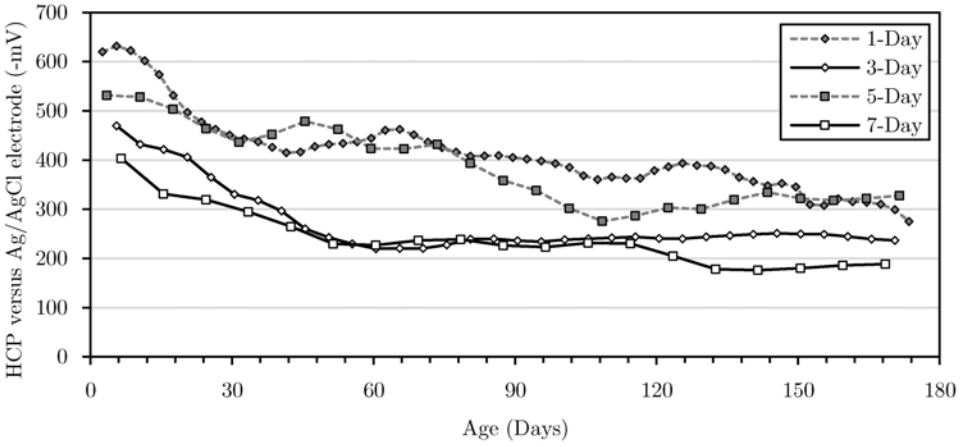

Figure F.1: CR1 half-cell potential measurements for 0.40 FA

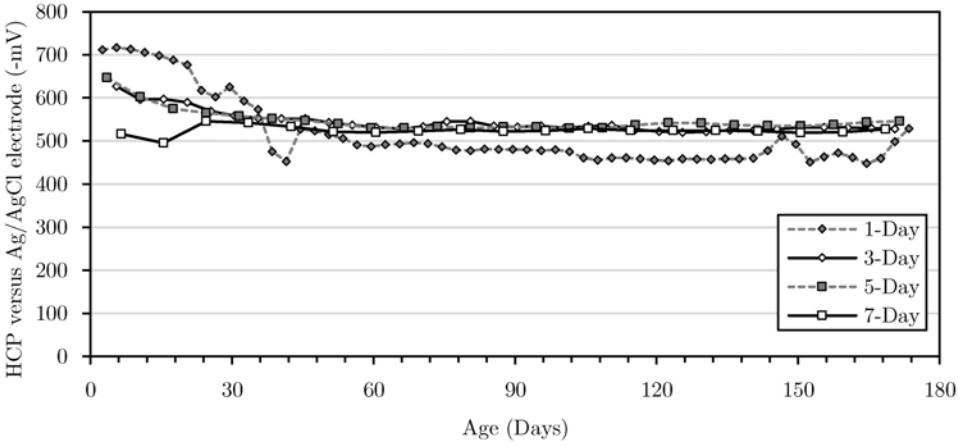

Figure F.2: CR1 half-cell potential measurements for 0.65 FA

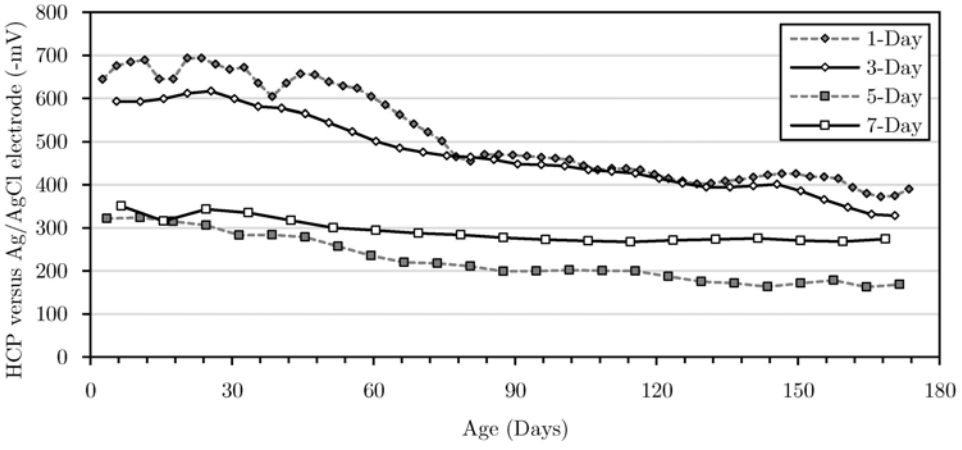

Figure F.3: CR1 half-cell potential measurements for 0.40 GGBS

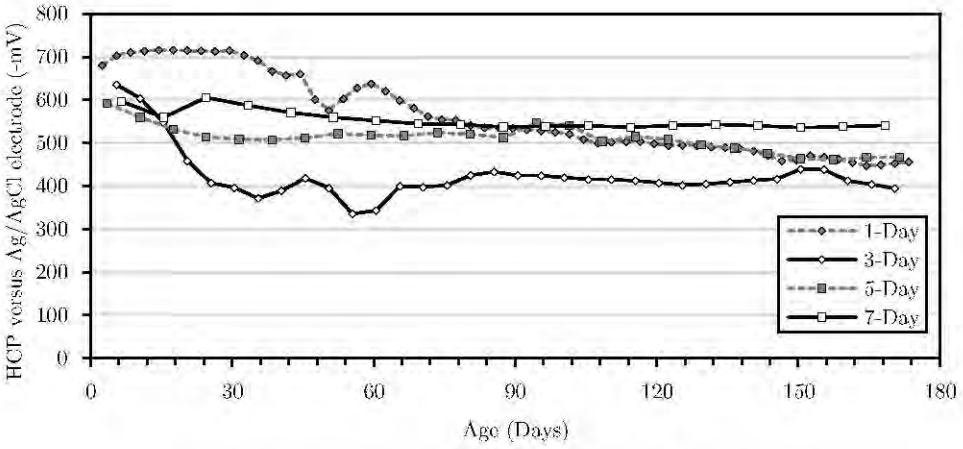

Figure F.4: CR1 half-cell potential measurements for 0.65 GGBS

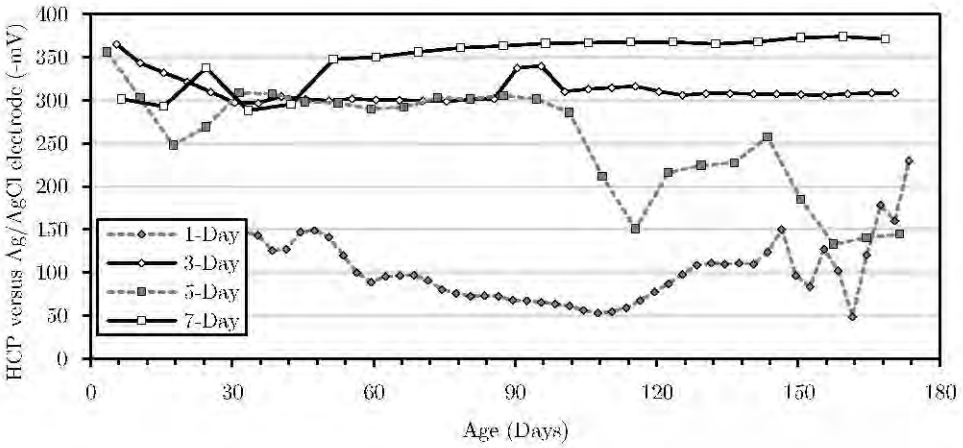

Figure F.5: CR1 half-cell potential measurements for 0.40 PC

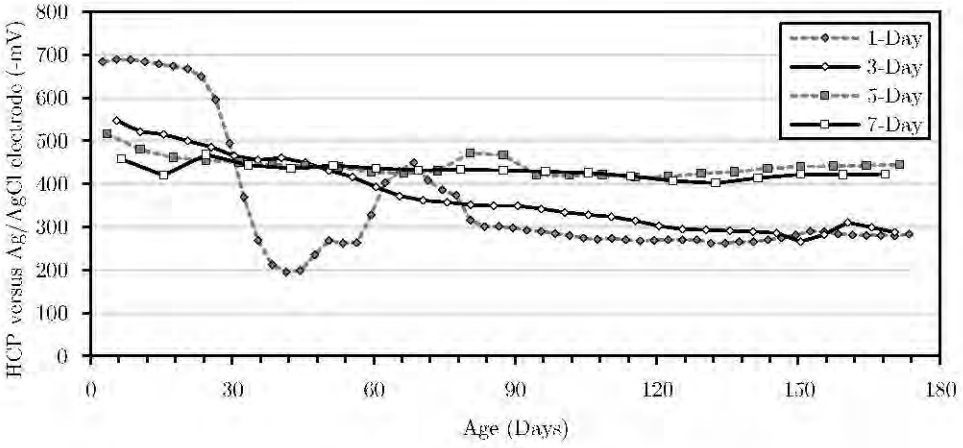

Figure F.6: CR1 half-cell potential measurements for 0.65 PC

F.2: HCP measurements for CR2

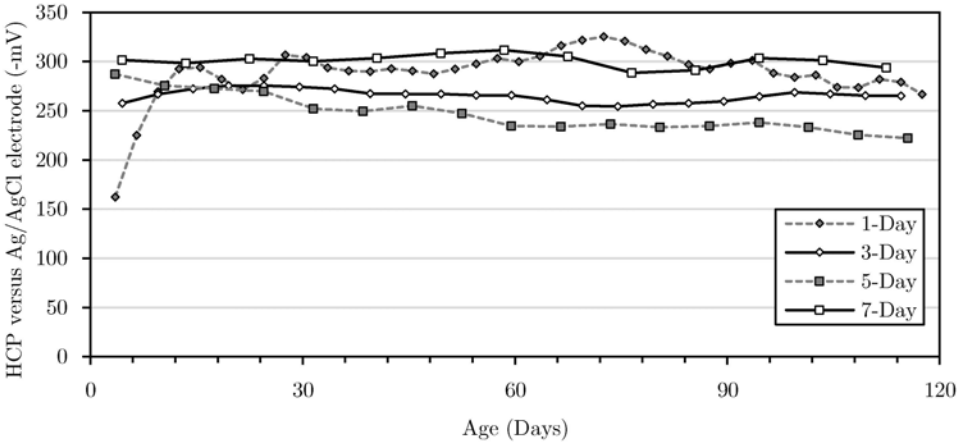

Figure F.7: CR2 half-cell potential measurements for 0.40 FA

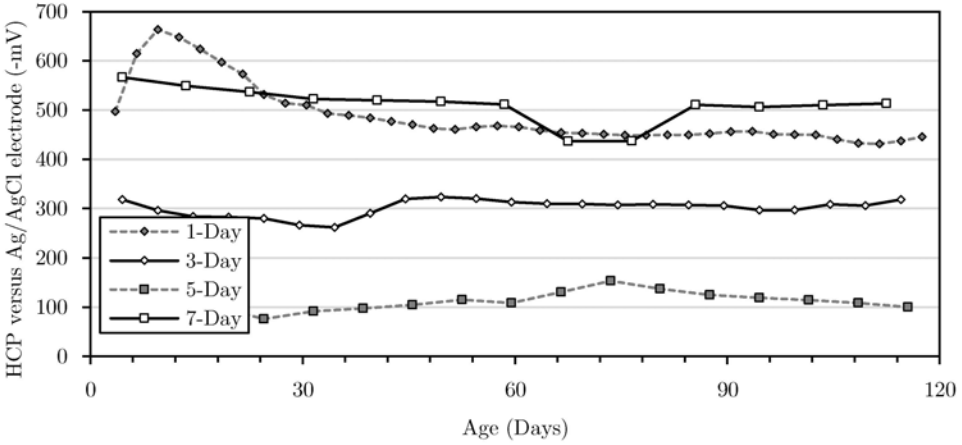

Figure F.8: CR2 half-cell potential measurements for 0.65 FA

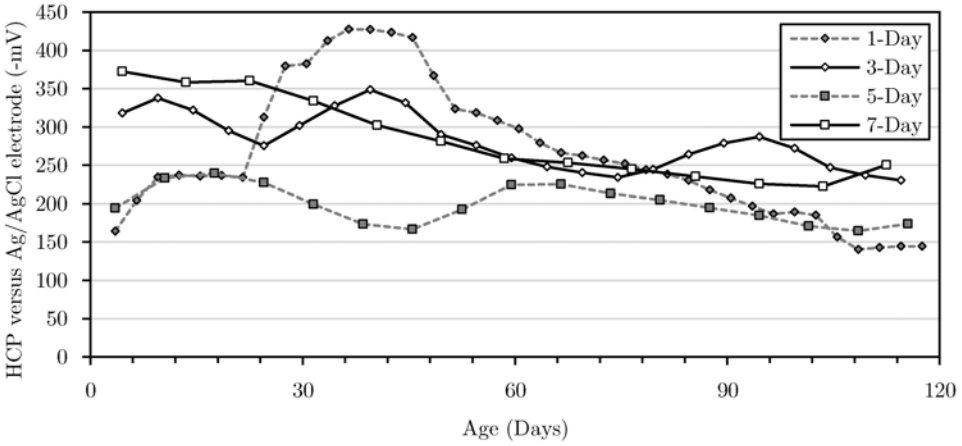

Figure F.9: CR2 half-cell potential measurements for 0.40 GGBS

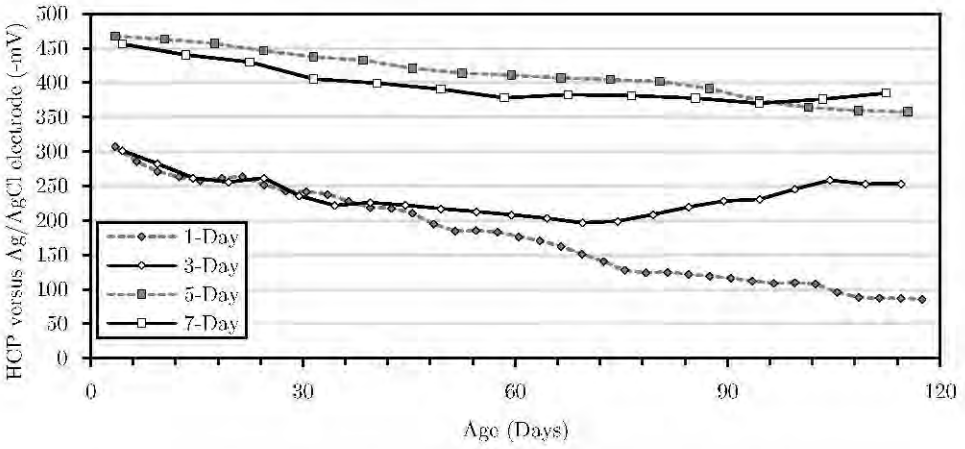

Figure F.10: CR2 half-cell potential measurements for 0.65 GGBS

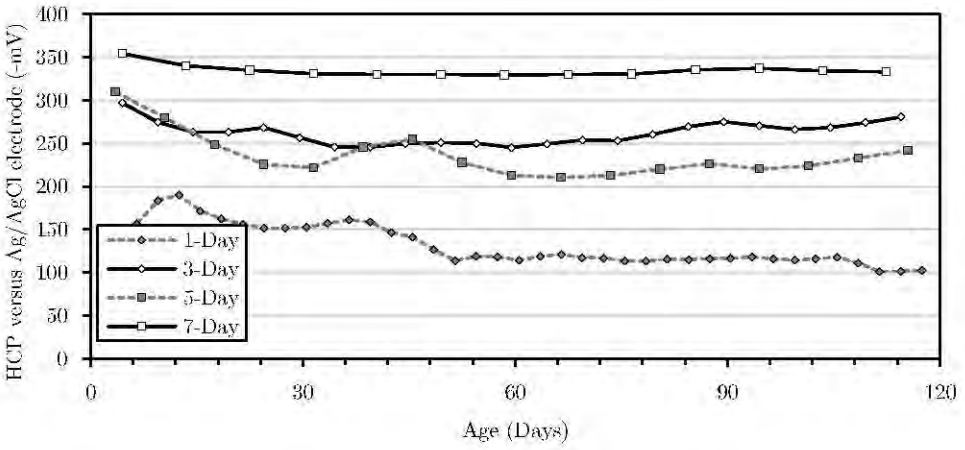

Figure F.11: CR2 half-cell potential measurements for 0.40 PC

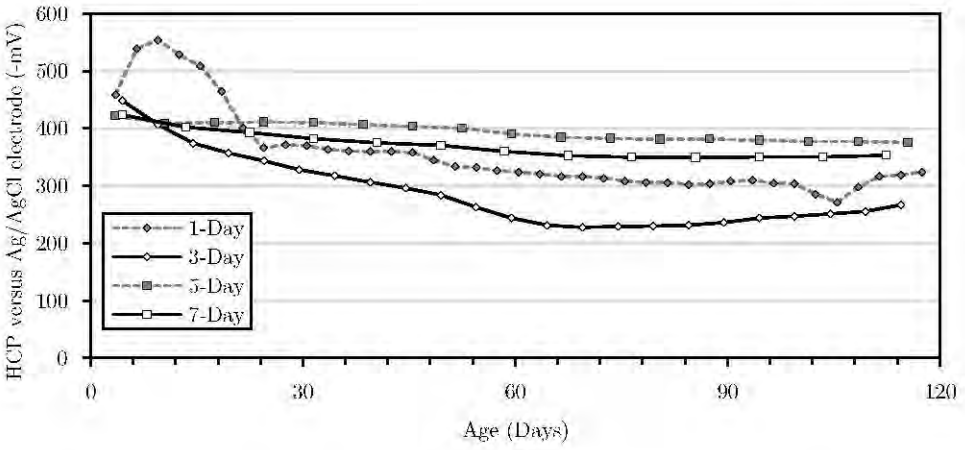

Figure F.12: CR2 half-cell potential measurements for 0.65 PC

Appendix G: Resistivity Measurements

G.1: Resistivity measurements for CR1

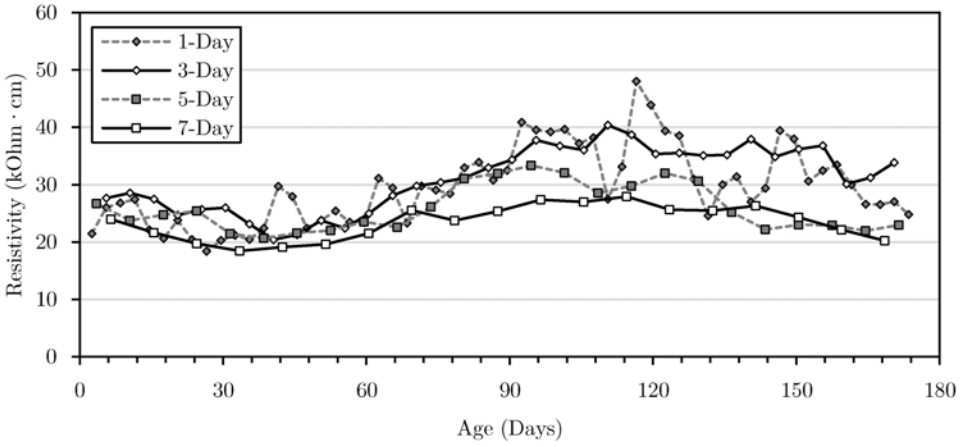

Figure G.1: CR1 resistivity measurements for 0.40 FA

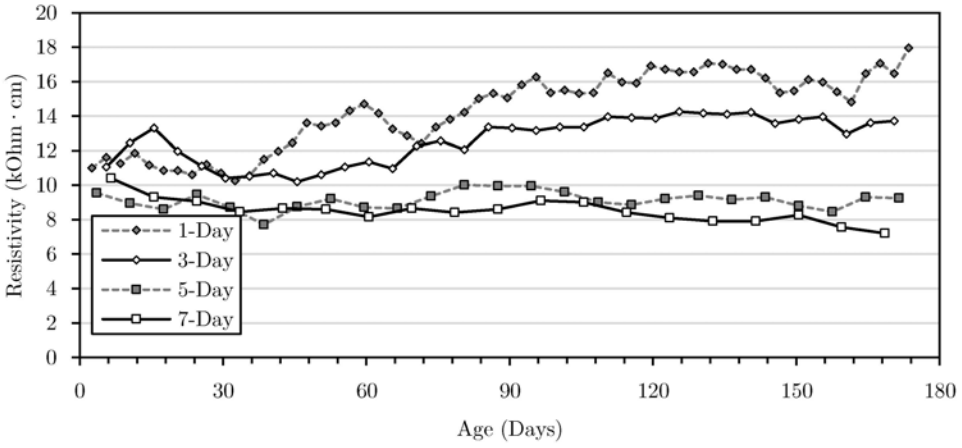

Figure G.2: CR1 resistivity measurements for 0.65 FA

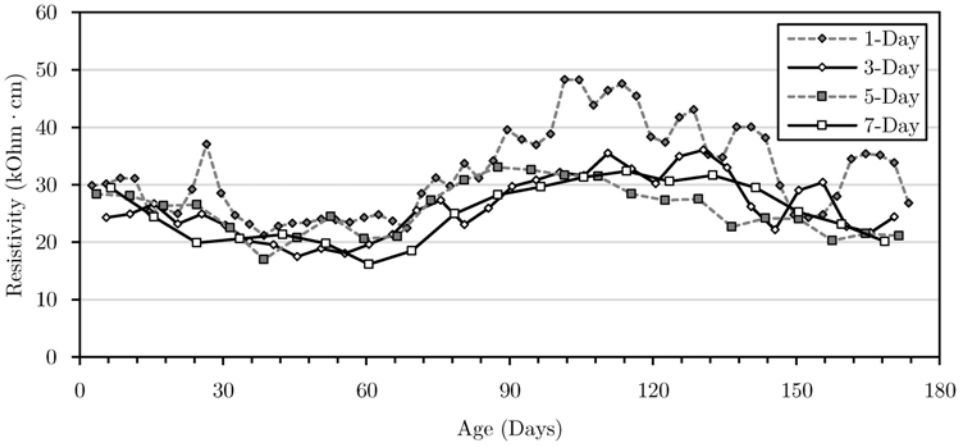

Figure G.3: CR1 resistivity measurements for 0.40 GGBS

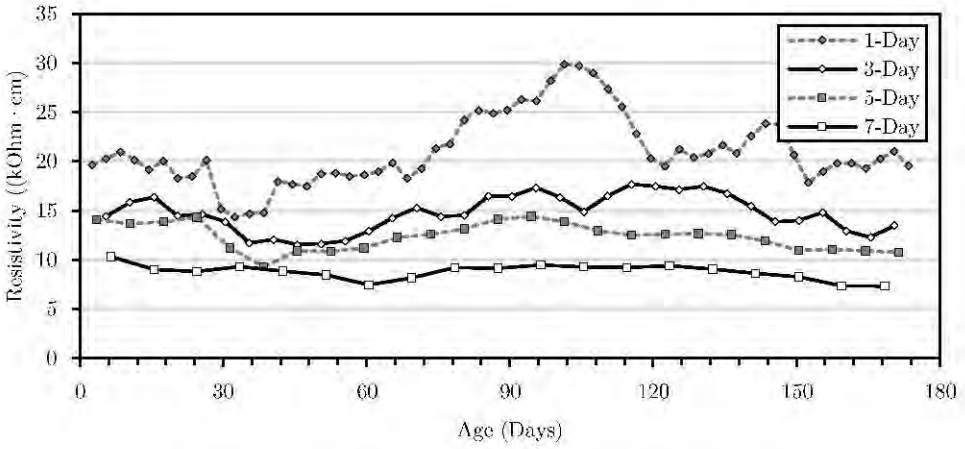

Figure G.4: CR1 resistivity measurements for 0.65 GGBS

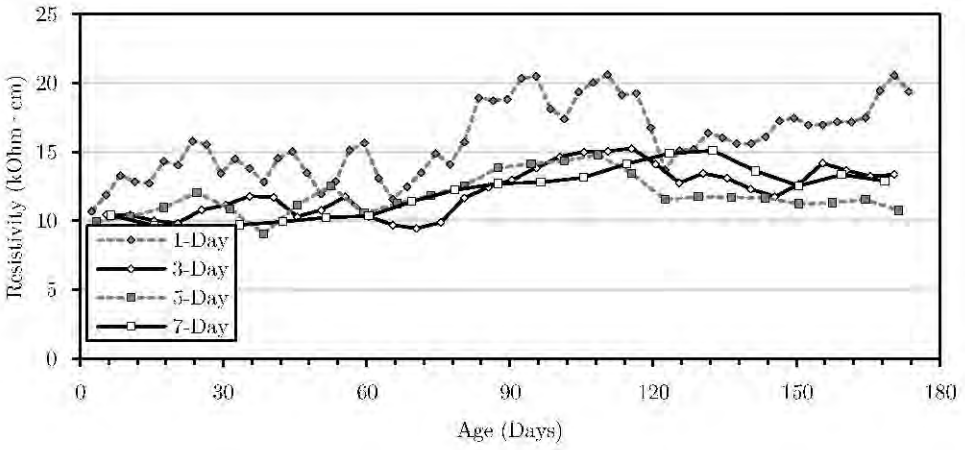

Figure G.5: CR1 resistivity measurements for 0.40 PC

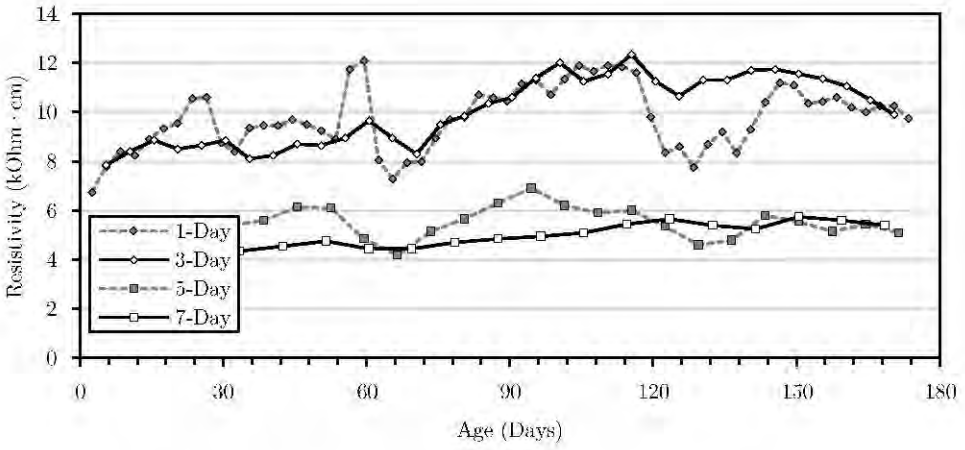

Figure G.6: CR1 resistivity measurements for 0.65 PC

G.1: Resistivity measurements for CR2

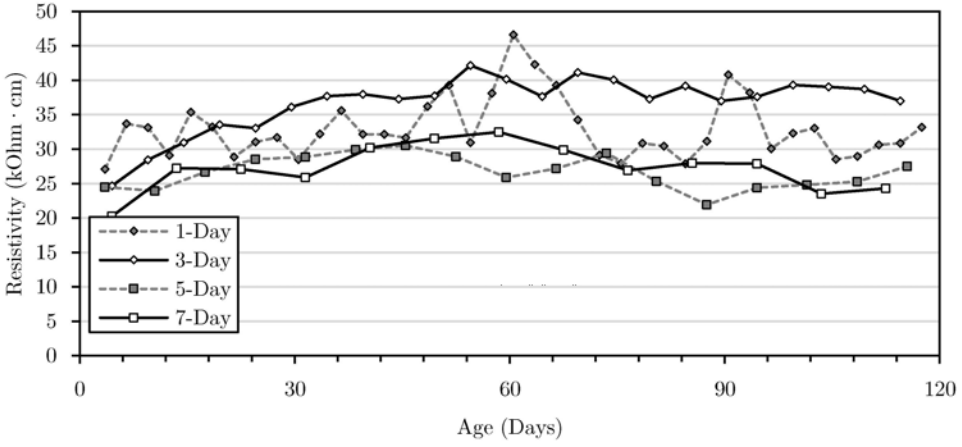

Figure G.7: CR2 resistivity measurements for 0.40 FA

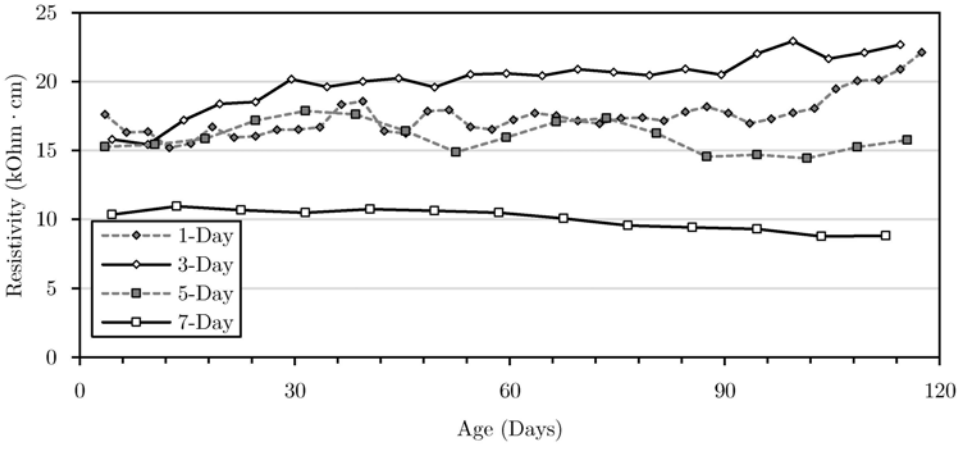

Figure G.8: CR2 resistivity measurements for 0.65 FA

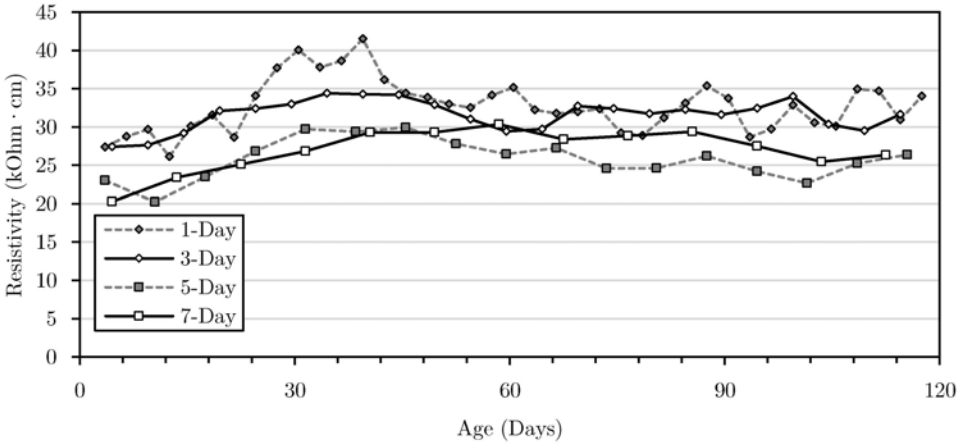

Figure G.9: CR2 resistivity measurements for 0.40 GGBS

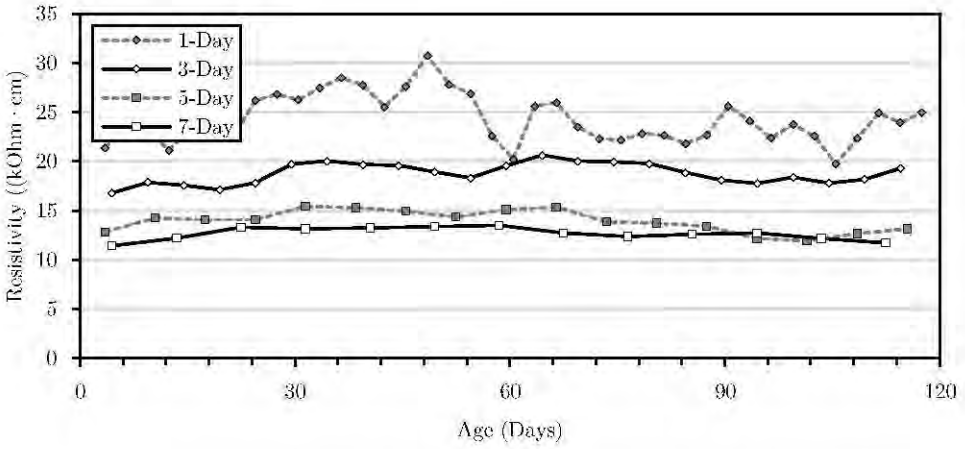

Figure G.10: CR2 resistivity measurements for 0.65 GGBS

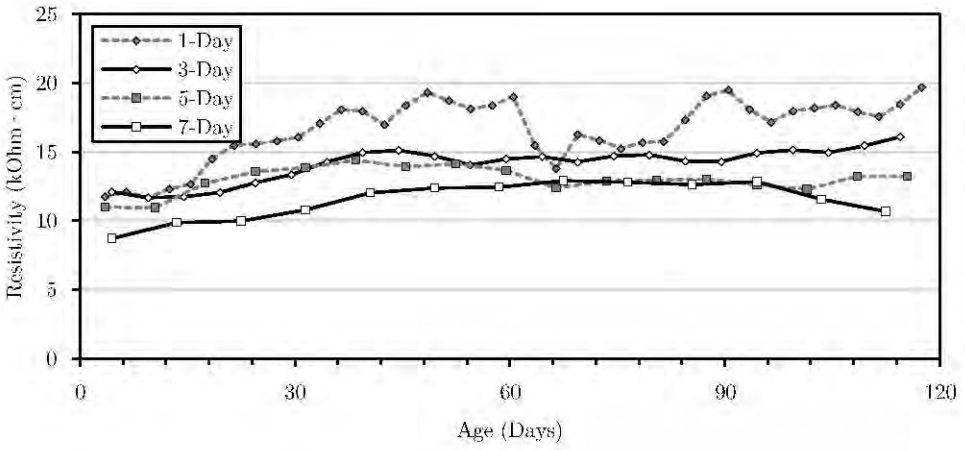

Figure G.11: CR2 resistivity measurements for 0.40 PC

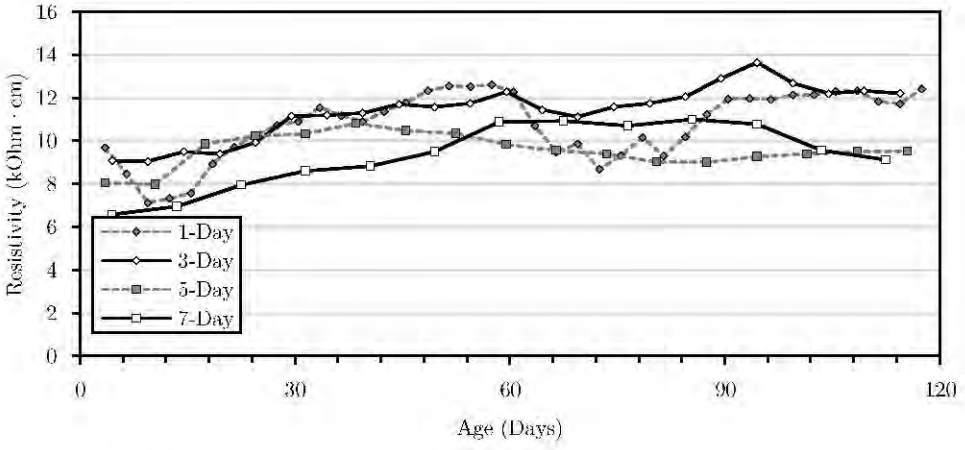

Figure G.12: CR2 resistivity measurements for 0.65 PC

Appendix H: Guide to the Impressed Current Technique

The impressed current technique is not covered extensively in literature, without any clear guidelines provided on its implementation. This appendix aims to provide a brief overview on the required processes to induce active corrosion conditions through the impressed current technique.

The first requirement is to select an appropriate current density based primarily on the required corrosion damage, the concrete quality and the embedded steel cross-sectional area. El Maaddawy and Soudki (2003) suggest that the applied current density should not exceed 200 $\mu A/cm^2$ to ensure that natural corrosion conditions are simulated. The duration of the impressed current can be increased if high corrosion currents are required. The current must be impressed by connecting a direct current power supply to the embedded steel. The negative terminal must be connected to the steel and the positive terminal connected to a counter electrode. The applied current should be checked by including a multimeter in the circuit.

In most cases, testing will require repeat specimens and they should be connected in series. Some literature suggests that the specimens should not be submerged, and rather ponded with a NaCl solution, although the relevance of this is unclear. Each specimen requires its own source of NaCl solution and should be isolated completely from its adjacent specimens. The specimens should be connected as illustrated in Figure H.1.

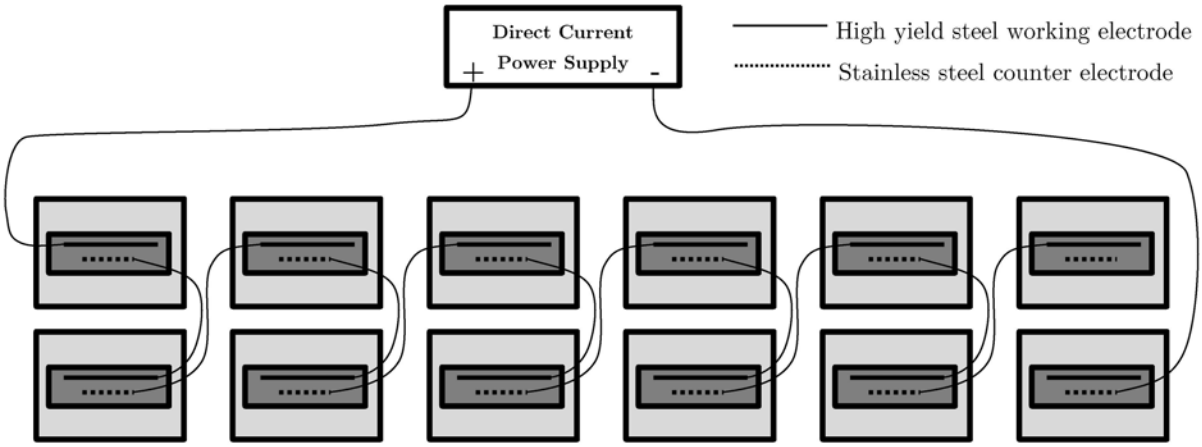

Figure H.1: Schematic layout of specimens for impressed current (isolated system)

The half-cell potential can be measured within the first few hours of removing the current to ensure the effectiveness of the system. The half-cell potential values after impressing the current should be high and will generally decrease in the first few days. An expected decrease in the corrosion rate after removal of the current should be taken into account when selecting an appropriate current density.

Appendix I: EBE Faculty Assessment of Ethics in Research Projects

EBE Faculty: Assessment of Ethics in Research Projects

Any person planning to undertake research in the Faculty of Engineering and the Built Environment at the University of Cape Town is required to complete this form before collecting or analysing data. When completed it should be submitted to the supervisor (where applicable) and from there to the Head of Department. If any of the questions below have been answered YES, and the applicant is NOT a fourth year student, the Head should forward this form for approval by the Faculty EIR committee: submit to Ms Zulpha Geyer (Zulpha.Geyer@uct.ac.za; Chem Eng Building, Ph 021 650 4791). Students must include a copy of the completed form with the thesis when it is submitted for examination.

Name of Principal Researcher/Student: Gavin Golden Department: Civil Engineering

If a Student: Degree: Master of Science in Engineering Supervisor: Prof. Mark Alexander

If a Research Contract indicate source of funding/sponsorship: NRF

Research Project Title: The effect of cyclic wetting and drying on the corrosion rate of steel in reinforced concrete

Overview of ethics issues in your research project:

Question 1: Is there a possibility that your research could cause harm to a third party (i.e. a person not involved in your project)?	YES	NO
Question 2: Is your research making use of human subjects as sources of data? If your answer is YES, please complete Addendum 2.	YES	NO
Question 3: Does your research involve the participation of or provision of services to communities? If your answer is YES, please complete Addendum 3.	YES	NO
Question 4: If your research is sponsored, is there any potential for conflicts of interest? If your answer is YES, please complete Addendum 4.	YES	NO

If you have answered YES to any of the above questions, please append a copy of your research proposal, as well as any interview schedules or questionnaires (Addendum 1) and please complete further addenda as appropriate.

I hereby undertake to carry out my research in such a way that

- there is no apparent legal objection to the nature or the method of research; and
- the research will not compromise staff or students or the other responsibilities of the University;
- the stated objective will be achieved, and the findings will have a high degree of validity;
- limitations and alternative interpretations will be considered;
- the findings could be subject to peer review and publicly available; and
- I will comply with the conventions of copyright and avoid any practice that would constitute plagiarism.

Signed by:

	Full name and signature	Date
Principal Researcher/Student:	GAVIN GOLDEN 	21/01/2014

This application is approved by:

Supervisor (if applicable):	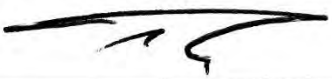	21/01/2014
HOD (or delegated nominee): Final authority for all assessments with NO to all questions and for all undergraduate research.	PP 	31/01/14
Chair : Faculty EIR Committee For applicants other than undergraduate students who have answered YES to any of the above questions.		